Advanced Biofilm and Aerobic Granulation Technologies for Water and Wastewater Treatment

Yewei Sun

Dissertation Submitted to the Faculty of Virginia Polytechnic Institute and State University

In Partial Fulfillment of the Requirements for the Degree of

Doctor of Philosophy

In

Civil Engineering

Zhi-Wu (Drew) Wang

Amy Pruden-Bagchi

Danmeng Shuai

Wendell Khunjar

March 12th, 2020

Manassas, VA

Keyword: Biofilm, Aerobic Granular Sludge, Biologically Active Filtration, Wastewater Treatment, Potable Water Reuse, Stormwater Treatment, Mathematical Modeling

Advanced Biofilm and Aerobic Granulation Technologies for Waterad Wastewater Treatment

Yewei Sun

Abstract (academic)

Attached growth biological processes offer advantages over traditional water purification technologies through high biomass retention, easy sludge-water separation, multiple multispecies synergies in proximity, resilience to shock loading, low space requirements, and reactor operational flexibility. Traditionally, attached growth refers to biofilms that require abiotic carrying media for bacteria to attach and grow on. While biofilms have been broadly applied in wastewater treatment, its potential for potable reuse or stormwater treatment has not been well studied. The treatment trains of pre-ozonation followed by biologically active filtration (ozone-BAF) is an advanced biofilm technology for potable reuse that can generate high-quality potable water at reduced energy and chemical demands by removing pollutant through three different pathways: oxidation, adsorption, and biodegradation. However, these pathways can result in both desirable and undesirable effects, and the mechanism behind it is still unclear. To understand the mechanisms of various pollutant removal, parallel performance comparisons of ozone-BAF treatment trains with spent and regenerated granular activated carbon (GAC), along with a range of pre-oxidant ozone doses were performed. Another common issue of BAF is the headloss buildup during its operation, which has become a significant energy and maintenance burden at many utilities. Thus, a mathematical model was developed to predict BAF headloss buildup in response to organic removal and nitrification. For stormwater treatment, the feasibility of using biofilms for stormwater biological nitrogen removal (BNR) is still largely unknown, as very limited research effort has been dedicated to this aspect. Thus, a mathematical model was developed to evaluate the potential of using BNR techniques for stormwater nitrogen removal. Aerobic granules are an even more advanced attached growth process, which eliminates the need for abiotic carrying media. So far, aerobic granular sludge is only formed in sequential batch reactors but not in a continuous flow system. Therefore, continuous flow aerobic granulation from traditional activated sludge was investigated and, for the first time, successfully achieved in continuous flow plug-flow bioreactors fed with real municipal wastewater. Besides, the role and critical value of an essential operational parameter, feast/famine ratio, for continuous flow aerobic granulation were determined.

Advanced Biofilm and Aerobic Granulation Technologies for Water and Wastewater Treatment

Yewei Sun

Abstract (general audience)

Water scarcity and increasing water demand caused by urban population growth and climate change is a reality throughout the world. Thus, process intensification of the current water and wastewater technologies is gaining increasing attention globally. Comparing to traditional water purification technologies, attached growth biological processes offers advantages such as high biomass retention, easy sludge-water separation, multiple multispecies synergies in proximity, resilience to shock loading, small footprint requirement, and reactor operational flexibility. Traditionally, attached growth refers to biofilms that require abiotic carrying media for bacteria to attach and grow on. While biofilms have been broadly applied in wastewater treatment, its potential for potable reuse or stormwater treatment has not been well studied. For potable reuse, the treatment trains of pre-ozonation followed by biologically active filtration (ozone-BAF) is an advanced biofilm technology that can generate high-quality potable water at reduced energy and chemical demands by removing pollutant through different pathways. However, the mechanism behind it is still unclear. To understand the mechanisms of various pollutant removal, parallel performance comparisons of ozone-BAF treatment trains operated with different operational conditions were performed in this dissertation. Another common issue of BAF is the headloss buildup during its operation, which has become a significant energy and maintenance burden at many utilities. Thus, a mathematical model was developed to predict the headloss buildup during BAF operation. For stormwater treatment, the feasibility of using biofilms for stormwater biological nitrogen removal (BNR) is still largely unknown, as very limited research effort has been dedicated to this aspect. Thus, a mathematical model was developed to evaluate the potential of using BNR technique for stormwater. Aerobic granules are an even more advanced attached growth process. However, aerobic granular sludge is so far only formed in sequential batch reactors which are incompatible with the continuous flow nature of most wastewater treatment plants. Therefore, aerobic granulation from traditional activated sludge was investigated and, for the first time, successfully achieved in continuous flow plug-flow bioreactors fed with real municipal wastewater. Besides, the role of an essential operational parameter, feast/famine ratio, for continuous flow aerobic granulation was determined.

Acknowledgments

Time flies! Looking back at my four-year Ph.D. journey, I feel grateful for being helped by so many kind people. I would not be able to get where I am without having their encouragement and endorsement.

I would first like to thank my advisor, Dr. Zhi-Wu Wang, for offering me the opportunity of this Ph.D. study and for all the support and guidance on the research and life of mine in Northern Virginia. I did not have much research experience prior to my Ph.D. application. Dr. Wang still gave me the opportunity to join his team because his discerning eyes found that my expertise in computer programing could potentially become a very useful academic tool for my Ph.D. study. During the four years of my Ph.D. study, he helped me a lot with my research by his expertise and gave me many opportunities to build connections with utilities and consulting firms in Northern Virginia. I further appreciate his patience in his thorough revision of my manuscripts, and I could not have published these papers in well-respected journals without his help. I would further like to thank all my committee members, including Dr. Amy Pruden, Dr. Danmeng Shuai, and Dr. Wendell Khunjar, for their willingness to serve on my committee and for all the helpful feedback they provided. Special thanks go to Dr. Khunjar for providing me constructive suggestions and experimental data for BAF model development. Besides, it is his recommendation that led to my upcoming employment opportunity with Hazen & Sawyer upon my graduation. I would also like to thank Dr. Zhen He for serving on my committee during the first three-year of my Ph.D. study and for all his outstanding suggestions and comments to my research.

Next, I would like to thank my parents. I feel fortunate for having their unconditional love and financial support for my life and Ph.D. study. Although they are far away in China, our minds and hearts are connected. Whenever I felt down or depressed about my research projects, my parents would give me a video call and they always have their own trick to cheer me up. Although they cannot help me with my research, their words and advice always make me feel energetic and have a positive attitude toward challenges in my life.

I would also like to thank my fellow classmates and lab mates who assisted me during my four years of Ph.D. study. Firstly, I would like to thank Dian Zhang for being a great lab mate. As the

first two Ph.D. students in Dr. Wang's Sustainable Environment Research Laboratory (SERL), we have overcome so many challenges together and witnessed the growth of SERL during the past four years. Secondly, I would like to thank Zhaohui An for being a great roommate and lab mate. We lived and worked together during the past two years, and he is indeed an interesting and kind-hearted person. He always offered to help me take care of my reactors in my absence. Besides, I would like to thank all the other SERLers, including Tim Kent, Jie Lin, Parita Shah, Jiefu Wang, and Hao Luo. I will definitely miss the time we spent together.

I would like to thank the staff of UOSA and OWML for their assistance to me during the past four years. Mrs. Barbara Angelotti has been a great manager of OWML for providing us a comfortable and organized working environment. Mrs. Marilyn Stull, Mrs. Alicia Tingen, and Mrs. Mimi Miller have offered me great help in the process of orders and returns on lab equipment and materials. Ms. Dongmei Wang and Mr. Curt Eskridge also kindly assisted me in learning how to use equipment in the lab and resolve the issues I encountered. Since all my reactors are operated in UOSA and I spent most of my time there during the past two years, I would further like to thank Mr. Bob Angelotti, Mr. Matt Brooks, and all the other UOSA lab staff for their generous assistance and help on my reactor design and fabrication, as well as sample analysis.

I would also like to thank funding agencies and sponsors who generously supported my research and study, including Upper Occoquan Service Authority, Thomas J. Grizzard Jr. Graduate Fellowship Foundation, Edna Bailey Sussman Foundation, 4-VA, Virginia Water Environment Association, American Water Works Association, and Virginia Tech Institute for Critical Technology and Applied Science. Special thanks go to Dr. Thomas J. Grizzard, Jr., the founder of OWML. I miss you so much!

All my accomplishments today should be attributed to the love and strong support of all the aforementioned people and organizations. I hope I can make all of you feel proud in the future.

Go Hokies!

Publication List

Journal Papers (*represent co-first author)

1. **Sun Y.W.***, Vaidya R.*, Khunjar W.O., Rosenfeldt E.J., Selbes M. Wilson C., Bott C.B., Titcomb M., and Wang Z.W. (2019) Mathematical modeling of biologically active filtration (BAF) for potable water production applications, **Water Research**, 115128
2. **Sun Y.W.**, Angelotti B., Wang Z.W. (2019) Continuous-flow aerobic granulation in plug-flow bioreactors fed with real domestic wastewater, **Science of The Total Environment**, 688 (20): 762-770
3. Kent T.R., **Sun Y.W.**, An Z.H., Bott C.B., Wang Z.W. (2019) Mechanistic understanding of the NOB suppression by free ammonia inhibition in continuous flow aerobic granulation bioreactors, **Environment International**, 131: 105005
4. Li X.J.*, **Sun Y.W.***, Wang Z.W., He Z. (2019) Theoretical understanding of the optimum conditions for a mainstream granular nitritation-anammox reactor coupled with anaerobic pretreatment, **Science of The Total Environment**, 669 (15): 683-691
5. Yu D., **Sun Y.W.**, Wang W.J., O'Keefe S.F., Neilson A.P., Feng H., Wang Z.W., Huang H.B., (2019) Recovery of protein hydrolysates from brewer's spent grain using enzyme and ultrasonication, **International Journal of Food Science and Technology** doi:10.1111/ijfs.14314
6. **Sun Y.W.**, Angelotti B., Brooks M., Dowbiggin B., Evans P.J., Devins B., and Wang Z.W. (2018) A pilot-scale investigation of disinfection by-product precursor and trace organic removal mechanisms in ozone-biologically activated carbon treatment for potable reuse, **Chemosphere**, 210:539-549
7. **Sun Y.W.**, Zhang D., and Wang Z.W. (2017) The potential of using biological nitrogen removal technique for stormwater treatment, **Ecological Engineering**, 106: 482-495
8. Wang Z.W., Xu F.Q, Manchala, K.R., **Sun Y.W.**, and Li Y.B. (2016) Fractal-like kinetics of the solid-state anaerobic digestion, **Waste Management**, 53: 55-61
9. An Z.H., Kent T.R., **Sun Y.W.**, Bott C.B., Wang Z.W. (2020) Free ammonia resistance of NOB developed in aerobic granular sludge cultivated in continuous upflow airlift reactors performing partial nitritation, **Water Research** (under review)
10. Zhang D., **Sun Y.W.**, Angelotti B., and Wang Z.W. (2020) Understanding the dewaterability of aerobic granular sludge formed in continuous flow bioreactors treating real domestic

wastewater: is it really better than the dewaterability of activated sludge? **Science of The Total Environment** (under review)

11. **Sun Y.W.**, Angelotti B., Brooks M., Wang Z.W. (2020) Feast/famine condition is a prerequisite for continuous flow aerobic granulation (in preparation)
12. **Sun Y.W.**, Angelotti B., Brooks M., Wang Z.W. (2020) Evolution of sludge characteristics from feast to famine conditions in continuous flow aerobic granulation (in preparation)

Book Chapters

13. Manchala K.R, **Sun Y.W.**, Zhang D. and Wang Z.W. (2017) Anaerobic digestion modeling. In: "Advances in Bioenergy 2", Elsevier, Amsterdam, The Netherlands.

Conference Talk/Oral Presentations

14. **Sun Y.W.**, Khunjar W., Rosenfeldt K., Selbes M., Vaidya R., Wilson C., Bott C.B., Wang Z.W., (2019) Mathematical modeling of biofiltration for potable water reuse, **WEFTEC 2019**, Illinois, Chicago, USA, September 23-25 **(Featured Speaker)**
15. **Sun Y.W.**, Angelotti B., Brooks M., Willoughby A., Fleischer E., Gallagher T, Constantine T., Wang Z.W. (2019) Effect of feast/famine and settling velocity based selection pressure on continuous flow aerobic granulation, **WEFTEC 2019**, Illinois, Chicago, USA, September 23-25
16. **Sun Y.W.**, Khunjar W., Rosenfeldt K., Selbes M., Vaidya R., Wilson C., Bott C.B., Wang Z.W., (2018) Mathematical modeling of deep-bed biofiltration to describe contaminant control and headloss development, **WEFTEC 2018**, New Orleans, Louisiana, USA, October 1-3
17. Rosenfeldt K., **Sun Y.W.**, Khunjar W., Selbes M., Vaidya R., Wilson C., Bott C.B., Wang Z.W., (2018) Mathematical modeling of deep-bed biofiltration to describe contaminant control and headloss development, **WaterJAM 2018**, Virginia Beach, Virginia, USA, September 10-13
18. **Sun Y.W.**, Angelotti R., Brooks M., Dowbiggin W., Evans P.J., Devins B.R., and Wang Z.W. (2017) Roles of Ozone Oxidation, Adsorption and Biodegradation in the Removal of Disinfection By-Products and Emerging Contaminants in Pilot-Scale Ozone BAC Contactors Applied for Potable Reuse, **WEFTEC 2017**, Chicago, Illinois, October 1-4
19. **Sun Y.W.**, and Wang Z.W. (2017) Biological Nitrogen Removal Potential of Stormwater, **WaterJAM 2017**, Hampton, Virginia, USA, September 11-14

20. **Sun, Y.W.**, Angelotti, B., Evans, P., Brooks, M., Wang, Z.W. (2017) Pilot-scale investigation of ozone-enhanced biofiltration using spent and regenerated granular activated carbon media for potable reuse, **254th ACS National Meeting**, Washington, DC, USA, August 20-24
21. **Sun, Y.W.**, Angelotti, B., Brooks, M., Dowbiggin, B., Evans, P., Devins, B., Wang, Z.W. (2017) The role of ozone oxidation, adsorption and biodegradation in the removal of disinfection by-product precursors and emerging contaminants in pilot-scale ozone BAC contactors applied for potable reuse, **The 23rd International Ozone Association World Congress, National Harbor**, Maryland, USA, August 13-17
22. **Sun, Y.W.**, Wang, Z.W. (2017) Biological nitrogen removal of stormwater runoff, **ASABE 2017 Annual International Meeting**, Spokane, Washington, USA, July 16-19
23. **Sun Y.W.**, Wang Z.W. (2017) The Potential of Using Biological Nitrogen Removal Technique for Stormwater Treatment, **CWEA Stormwater 2017 Spring Seminar**, Linthicum, Maryland, USA, May 18

Conference Posters/Abstracts

24. **Sun Y.W.**, Vaidya R., Khunjar W.O., Rosenfeldt E.J., Selbes M. Wilson C., Bott C.B., Titcomb M., and Wang Z.W. (2019) Mathematical modeling of biologically active filtration (BAF) for potable water production applications, **WaterJAM 2019**, Virginia Beach, Virginia, USA, September 9-12 **(Fresh Idea Poster Competition 1st Place)**
25. **Sun Y.W.**, Angelotti B., Wang Z.W. (2019) Continuous-flow aerobic granulation in plug-flow bioreactors fed with real domestic wastewater, **WaterJAM 2019**, Virginia Beach, Virginia, USA, September 9-12
26. **Sun Y.W.**, Angelotti B., Brooks M., Wang, Z.W. (2019) Pilot-scale evaluation of the effects of settling velocity-based selection and feast/famine conditions on continuous flow aerobic granulation in real municipal wastewater, **AEESP 2019**, Tempe, Arizona, USA, May 14-16
27. Sun, Y.W., Angelotti, B., Evans, P., Wang, Z.W. (2017) Pilot-scale investigation of ozone-enhanced biofiltration using spent and regenerated granular activated carbon media for potable reuse, **AEESP 2017**, Ann Arbor, Michigan, USA, June 19-22

Table of Contents

List of Figures

List of Tables

Chapter 1 Introduction

1.1 Background

Attached growth biological processes are advantageous for aqueous pollutant removal in view of their high biomass retention, easy solid-water separation, multispecies synergy in proximity, resilience to shock loading, low footprint requirements, and reactor operational flexibility (Gao et al., 2011; Hasebe et al., 2017; Sehar et al., 2016). Traditionally, attached growth refers to biofilms which requires abiotic carrying media for bacteria to attach and grow on. While biofilms have been broadly applied in wastewater treatment, its potential for potable reuse or stormwater treatment has not been well studied.

For potable reuse, the treatment trains of pre-ozonation followed by biologically active filtration (ozone-BAF) is an advanced biofilm technology because it has the potential to generate high quality potable water at reduced energy and chemical demands (Schimmoller et al., 2014). The mechanism of pollutant removal in such treatment trains can be largely attributed to three pathways: oxidation via ozonation, adsorption via filtration media, and biodegradation via attached biofilm (Basu et al., 2016). However, one of the current issues is that these pathways can result in both desirable and undesirable effects (Gunten, 2003). For example, during ozonation, while some pollutants are oxidized and removed, some other undesirable byproducts such as trihalomethanes (THMs) and haloacetic acids (HAAs) can be formed as a result of oxidation (Richardson et al., 1999). The headloss buildup due to the biofilm growth and particle deposition during ozone-BAF operation is another challenge because it substantially increases backwash frequency as well as the energy consumption of BAF (Moore et al., 2001; Slavik et al., 2013; Snowball, 2006) and reduces the water productivity (Adams et al., 1989; Simpson, 2008).

For stormwater treatment, most existing nitrogen removal mechanisms, e.g., plant uptake or soil adsorption, can only temporarily store or relocate nitrogen pollutants (Valero et al., 2010), while biofilms can simultaneously provide both the aerobic and anoxic environments required by biological nitrogen removal (BNR) which allows for permanent nitrogen removal by transforming

nitrogen pollutants into harmless nitrogen gas through nitrification, denitrification and/or anammox (Cao, 2008). However, the potential of using biofilms for stormwater nitrogen removal is still largely unknown, as very limited research effort has been dedicated to this aspect. Besides, stormwater is characterized by its low organic and nitrogen strength, as well as high dissolved oxygen content, which poses multiple challenges to effective BNR.

Aerobic granules are an even more advanced attached growth process over biofilms because using aerobic granules eliminate the need of abiotic carrying media and thus can retain even higher concentration of biological catalyst for further enhanced high-rate wastewater treatment (Morgenroth et al., 1997). However, it is noteworthy that the application of aerobic granulation technique is still only limited to sequential batch reactors (SBRs) after its about twenty years of development (Kent et al., 2018; Pronk et al., 2015), which is inconsistent with the continuous flow nature of the majority of existing domestic wastewater treatment plants (WWTPs). Continuous flow reactors (CFRs) provide advantages over SBRs in terms of simple process operation and control while accommodating larger treatment capacities (Chen et al., 2017; Juang et al., 2010; Kent et al., 2018; Li et al., 2016). Hence, the development of a continuous flow aerobic granulation technique is highly desired for promoting the application of aerobic granular sludge in large-scale WWTPs (Kent et al., 2018).

Therefore, this dissertation is aimed to explore the potential of harnessing biofilms for potable reuse and stormwater treatment, as well as the possibility of forming aerobic granules in continuous flow bioreactors treating real domestic wastewater.

1.2 Outline

This dissertation has in total six (6) chapters. The overarching goal of all the studies is to address the current challenges for the applications of attached growth biological processes (biofilm and aerobic granulation) in the advanced water and wastewater treatment industry.

The first specific aim (**SA1)** of this dissertation is to identify the pathway of pollutant removal in ozone-BAF treatment trains applied for in-direct potable reuse. Although ozone-BAF has been

broadly applied in the systems for potable reuse of municipal wastewater, the mechanisms of various pollutant removal remain largely unknown. This pilot study was designed to understand the roles of different pathways, namely oxidation, adsorption, and biodegradation, in the removal or formation of 5 disinfection by-product precursors and over 70 trace organics for ozone-BAF treatment trains via parallel performance comparisons of spent and regenerated granular activated carbon (GAC), along with a range of pre-oxidant ozone doses.

The second specific aim (**SA2)** of this dissertation is to establish and validate a mathematical modeling framework to mechanistically interpret and predict the physical, chemical, and biological performance of BAF. During BAF operation, because of the continuous growth of biofilm, the porosity inside the BAF will decrease with time, leading to headloss buildup. A common industrial practice for limiting biofilm overgrowth on BAF media surfaces is to initiate backwash whenever the headloss builds up to a threshold value. However, since it is hard to predict headloss accumulation in BAF bed, backwashes are usually triggered empirically, which can be a significant energy and maintenance burden at many full-scale facilities. In this study, a modeling framework was established and validated to simulate BAF headloss buildup in response to organic removal and nitrification. This model considered not only the biofilm growth on the BAF media but also the particle deposition in the BAF bed.

The third specific aim (**SA3)** of this dissertation is to evaluate the potential of harnessing soil biofilms for biological nitrogen removal of stormwater with a theoretical mathematical model developed and verified with accumulated stormwater data. BNR can provide permanent elimination of nitrogen pollutants by conversion to nitrogen gas. However, few studies have explored the potential of BNR for stormwater because stormwater is characterized by its low organic and nitrogen strength as well as high dissolved oxygen content, which poses multiple challenges to effective BNR. In this study, mathematical model was developed to evaluate the potential of using BNR technique for the removal of nitrogen from stormwater.

The fourth specific aim (**SA4)** of this dissertation is to achieve successful aerobic granulation from traditional activated sludge in continuous flow plug-flow bioreactors fed with real municipal wastewater. Aerobic granular sludge holds promise to intensify municipal wastewater treatment

plant. However, aerobic granular sludge is so far only formed in sequential batch reactors which are incompatible with the continuous flow nature of most WWTPs. Therefore, this study was performed to explore the feasibility of achieving successful aerobic granulation in continuous flow biological processes broadly used in modern wastewater treatment plants.

The fifth specific aim (**SA5)** of this dissertation is to understand the essential role of feast/famine conditions for continuous flow aerobic granulation (SA5). Aerobic granules cannot be formed without periodic feast/famine condition alternation, and a proper feast/famine ratio was found important for successful aerobic granulation. This study investigated the variation of sludge properties such as particle size, circularity, settleability, specific gravity, zone settling velocity, and extracellular polymeric substance contents in continuous-flow plug-flow reactors with different feast/famine ratios intending to infer the cause-effect correlations between the feast/famine ratios and continuous flow aerobic granulation.

1.3 Attribution

Each coauthor is duly credited for his or her contribution to this work, both in their sharing of ideas and technical expertise.

Zhi-Wu (Drew) Wang, Ph.D., Professor of Civil and Environmental Engineering (Principal Investigator)
Department of Civil and Environmental Engineering, Virginia Polytechnic Institute and State University, Manassas, VA 20110

Coauthor of Chapter 2, 3, 4, 5, 6

Bob Angelotti, Deputy Executive Director of Technical Services
Upper Occoquan Service Authority, Centreville, VA 20121

Coauthor of Chapter 2, 5, 6

Matt Brooks, Process Control Engineer
Upper Occoquan Service Authority, Centreville, VA 20121

Coauthor of Chapter 2, 5, 6

Patrick J. Evans, Ph.D., Vice President
CDM Smith, Bellevue, WA 98007

Coauthor of Chapter 2

Bill Dowbiggin, Engineer
CDM Smith, Raleigh, NC 27612

Coauthor of Chapter 2

Bradford Devins, Engineer
CDM Smith, Raleigh, NC 27612

Coauthor of Chapter 2

Ramola Vaidya
Department of Civil and Environmental Engineering, Virginia Polytechnic Institute and State University, Blacksburg, VA 24061

Coauthor of Chapter 3

Wendell O. Khunjar, Ph.D., Director of Wastewater Innovation
Hazen and Sawyer, Fairfax, VA 22030

Coauthor of Chapter 3

Erik J. Rosenfeldt, Ph.D., Director of Drinking Water Process Technology
Hazen and Sawyer, Fairfax, VA 22030

Coauthor of Chapter 3

Meric Selbes, Ph.D., Senior Principal Scientist
Hazen and Sawyer, Fairfax, VA 22030

Coauthor of Chapter 3

Christopher Wilson, Ph.D., Chief of Process Engineering and Research
Hampton Roads Sanitation District, Virginia Beach, VA 23455

Coauthor of Chapter 3

Charles B. Bott, Ph.D., Director of Water Technology and Research (Chief Technical Officer)
Hampton Roads Sanitation District, Virginia Beach, VA 23455

Coauthor of Chapter 3

Mark Titcomb, Facilities Engineer
Newport News Waterworks, Newport News, VA 23606

Coauthor of Chapter 3

Dian Zhang
Department of Civil and Environmental Engineering, Virginia Polytechnic Institute and State University, Manassas, VA 20110

Coauthor of Chapter 4

1.4 References

Adams, J. Q., and Clark, R. M. (1989). Cost estimates for GAC treatment systems. *Journal - American Water Works Association, 81*(1), 35-42.

Cao, Y. S. (2008). *Biological nitrogen removal activated sludge process in warm climates: full-scale process investigation, scaled-down laboratory experimentation and mathematical modelling*. London: IWA Pub.

Gao, D., Liu, L., Liang, H., and Wu, W. M. (2011). Aerobic granular sludge: characterization, mechanism of granulation and application to wastewater treatment. *Critical Reviews in Biotechnology, 31*(2), 137-152.

Gunten, v. (2003). Ozonation of drinking water: Part I. Oxidation kinetics and product formation. *Water Res, 37*(7), 1443-1467.

Hasebe, Y., Meguro, H., Kanai, Y., Eguchi, M., Osaka, T., and Tsuneda, S. (2017). High-rate nitrification of electronic industry wastewater by using nitrifying granules. *Water Sci Technol, 76*(11), 3171-3180.

Kent, T. R., Bott, C. B., and Wang, Z. W. (2018). State of the art of aerobic granulation in continuous flow bioreactors. *Biotechnol. Adv., 36*(4), 1139-1166.

Moore, R., Quarmby, J., and Stephenson, T. (2001). The effects of media size on the performance of biological aerated filters. *Water Res, 35*(10), 2514-2522.

Morgenroth, E., Sherden, T., Van Loosdrecht, M., Heijnen, J., and Wilderer, P. (1997). Aerobic granular sludge in a sequencing batch reactor. *Water Res, 31*(12), 3191-3194.

Pronk, M., De Kreuk, M., De Bruin, B., Kamminga, P., Kleerebezem, R. v., and Van Loosdrecht, M. (2015). Full scale performance of the aerobic granular sludge process for sewage treatment. *Water Res, 84*, 207-217.

Schimmoller, L., and Foundation, W. (2014). *Fit for purpose water: The cost of overtreating reclaimed water*: WateReuse Research Foundation.

Sehar, S., and Naz, I. (2016). Role of the biofilms in wastewater treatment. *Microbial biofilms-importance and applications*, 121-144.

Simpson, D. R. (2008). Biofilm processes in biologically active carbon water purification. *Water Res, 42*(12), 2839-2848.

Slavik, I., Jehmlich, A., and Uhl, W. (2013). Impact of backwashing procedures on deep bed filtration productivity in drinking water treatment. *Water Res, 47*(16), 6348-6357.

Snowball, M. (2006). Water treatment: Reducing backwash with air scouring. *Filtration & separation, 43*(10), 39-40.

Valero, M. A. C., Read, L. F., Mara, D. D., Newton, R. J., Curtis, T. P., and Davenport, R. J. (2010). Nitrification-denitrification in waste stabilisation ponds: a mechanism for permanent nitrogen removal in maturation ponds. *Water Sci Technol, 61*(5), 1137-1146.

Chapter 2 A Pilot-Scale Investigation of Disinfection By-product Precursors and Trace Organic Removal Mechanisms in Ozone-Biologically Active Filtration for Potable Reuse

(This chapter has been published as "Sun, Y.W., Angelotti, B., Brooks, M., Dowbiggin, B., Evans, P. J., Devins, B., and Wang, Z. W. (2018). A pilot-scale investigation of disinfection by-product precursors and trace organic removal mechanisms in ozone-biologically activated carbon treatment for potable reuse. Chemosphere, 210, 539-549")

2.1 Abstract

Although granular activated carbon (GAC) has been broadly applied in ozone-biologically active filtration (O_3/BAF) systems for potable reuse of municipal wastewater, the mechanisms of various pollutant removal remain largely unknown as the regenerated GAC develops microbial populations resulting in BAF but loses significant adsorption capacity as it becomes spent GAC. Therefore, pilot-scale parallel performance comparisons of spent and regenerated GAC, along with a range of pre-oxidant ozone doses, were used to shed light on the mechanisms responsible for the removal of various types of treatment byproduct precursors and trace organic compounds. It was confirmed from this pilot-study that ozone alone can effectively degrade chlorinated trihalomethane (THM) and haloacetic acid (HAA) precursors, chloramine-reactive N-nitrosodimethylamine (NDMA) precursors, and 29 PPCPs. In contrast, biodegradation by microbial population on spent or regenerated GAC can remove NDMA and 22 PPCPs, while the adsorption by regenerated GAC can remove chlorinated THM and HAA precursors, PFAS, flame retardants, and 27 PPCPs. The results of this pilot study are intended to provide those interested in potable reuse with an example of the simultaneous removal capabilities and mechanisms that can be anticipated for treating a complex mixture of organics present in real municipal wastewater effluent.

2.2 Keywords

Ozonation; BAF; GAC; Potable water reuse; DBPs

2.3 Introduction

Water scarcity and increasing water demand caused by urban population growth is a reality throughout the world (Nagel, 2015). Communities with limited water supply realized that using their drinking water only once and then discarding it couldn't meet their daily water demand. Hence, potable water reuse is gaining increasing attention across the U.S. and globally (EPA, 2012). Potable water reuse relies on advanced purification technology to treat wastewater into high-quality water that can fulfill state and federal drinking water standards, so that it can then be reused by blending it with other raw source waters entering drinking water treatment plants or to blend directly into the potable water distribution system. Ozone and BAF using granular activated carbon (GAC) media is an advanced water purification technology broadly applied because of the numerous benefits it provides (Pharand et al., 2015). Ozone acts as an oxidant to degrade organic matter in the water to form more biodegradable organic molecules that can be mineralized through subsequent BAF (Volk and Lechevallier, 2002). The ozone BAF process holds promise to reduce the formation of some regulated disinfection byproducts (DBPs) (Yan et al., 2010) and emerging contaminants including nitrosamines, perfluoro alkyl acids and sulfonate substances (PFASs), flame retardants, as well as pharmaceuticals and personal care products (PPCPs) (Benitez et al., 2009; Huang et al., 2016; Lin et al., 2012; Rodriguez et al., 2013). These advantages can also increase the bio-stability of finished water, and reduce regrowth within distribution systems (Yan et al., 2010).

The mechanism of organic matter removal in treatment trains using ozone-BAF can be largely attributed to three major pathways: oxidation, adsorption, and biodegradation (Basu et al., 2016). It should be realized that water pollutants and their precursors can be removed through different pathways, and thus can result in both desirable and undesirable effects (Gunten, 2003). For example, during ozonation, while some pollutants are oxidized and degraded, some other undesirable byproducts such as bromate and brominated trihalomethanes (THMs) and haloacetic acids (HAAs) can be formed as a result of oxidation (Richardson et al., 1999). This problem can become even more prominent when higher ozone exposures are needed (Rennecker et al., 1999). Consequently, the role of each pathway in the removal or formation of different pollutants should

be understood to minimize undesirable consequences while achieving improved treatment performance.

Although numerous research projects have been carried out to study the performance of pilot-scale ozone-BAF (Farré et al., 2011; Griffini et al., 1999; Li et al., 2017; Liao et al., 2014; McKie et al., 2015; Rittmann et al., 2002; Sundaram et al., 2014; Zhang et al., 2017), very few have looked into the difference between using spent and regenerated GAC as a BAF media. Spent GAC used for water purification for an extended period typically contains little adsorption capacity. However, as a result of its prolonged use an extensive biofilm forms on the media surface. In contrast, regenerated GAC, which has been thermally regenerated from spent GAC, is similar to virgin GAC in its adsorption capacity and has zero initial biological activity (Liu and Wagner, 1985). Thermal regeneration of GAC requires high energy input (Liu and Wagner, 1985), and regenerated GAC will eventually become spent GAC after prolonged usage (Akcay et al., 2016). Therefore, it is prudent to compare the performance difference between these two types of activated carbon and identify the most cost effective means of utilizing GAC for the water reuse industry. More importantly, such a comparison may clarify the respective contribution of physical adsorption and biological degradation on the removal of pollutants or their precursors. Also, pairing spent and regenerated GAC with various pre-ozonation doses helps identify the importance of oxidation on adsorption and degradation performance. Hence, a pilot-scale test using pre-ozonation followed by spent or regenerated GAC filtration can provide meaningful insights from both theoretical and practical perspectives. One of the outcomes of this study was to estimate the significance of oxidation, adsorption and bio-degradation for handling DBPs (including THMs, HAAs, and nitrosamines) as well as three groups of other unregulated contaminants (six PFASs, two flame retardants, and 66 PPCPs). This study investigated such water quality aspects for the tertiary treated multi-media filter effluent from an advanced potable reuse plant in the U.S.

2.4 Material and Methods

2.4.1 Experimental setup

Eight pilot-scale biofilters were continuously operated for over 12 months at the Upper Occoquan Service Authority (UOSA) water reclamation plant in Centreville, VA, USA. Results from six of those eight biofilters were used in this manuscript with key operating conditions for those six biofilters described in Table 2.1. The ozone dose for each biofilter was controlled at relatively constant ozone-to-dissolved organic carbon (DOC) ratios ranging from 0 to 1.1 mg O_3 mg^{-1} DOC (0 to 4.5 mg L^{-1} ozone dose). The spent and regenerated GAC (Calgon, F300-GAC, Pittsburgh, PA USA) was obtained from full-scale water reclamation processes. Regenerated GAC was obtained from UOSA's GAC regeneration furnace and spent GAC was collected from a carbon contactor that had been in service for about three years. The pilot plant influent was pumped from the full-scale granular, multi-media filter effluent channel. Prior to granular media filtration, wastewater received treatment through UOSA's primary, secondary, high-lime and recarbonation processes. This water was firstly pumped to an equalization tank to provide constant hydraulic head to the gravity fed pilot ozone contactors before water flowed to the downstream biofilters. Biofilters were operated at an empty bed contact time (EBCT) of 23 minutes. The inner diameter and height of each biofilter was 10 cm and 610 cm, respectively. The pilot biofilter underdrain consisted of a plastic nozzle surrounded by a 20 cm deep support layer of gravel. Active biofilter media was comprised of approximately 305 cm height of either spent or regenerated GAC. Ozone was generated by electrical discharge in an ozone generator (IN USA, AC-Series Ozone Generator, Norwood, MA USA) fed with oxygen gas, and introduced into the ozone contactors using 20-µm fine bubble stainless steel diffusers (Ozone Solutions, SD-6, Hull, IA USA). Using a measured average influent DOC concentration of 4.17 mg L^{-1} and field verified ozone transfer efficiency of 95%, ozone transfer doses of 1.3, 2.6, and 4.5 mg L^{-1} were applied to achieve the 0.33, 0.65, and 1.1 mg O_3 mg^{-1} DOC ratios listed in Table 2.. The pilot columns were backwashed approximately every two to three weeks to control head loss and maintain biofilm quality.

The 12-month study consisted of two six-month phases. During phase 1, the study focused on ozone byproduct formations (NDMA), and the removal of Safe Drinking Water Act (SDWA) regulated DBP precursors. The removal efficiency of a number of unregulated trace organic compounds was also investigated during phase 1. These included nitrosamines, PFASs, flame retardants, and a variety of PPCPs. Although PFASs were monitored during phase 1, no PFASs were detected during the first three months due to elevated analytical method detection limits

(MDL). After the fourth month of pilot operation revised analytical methods were employed to lower the MDL for PFASs by an order of magnitude. During phase 2, the pilot treatment trains ran for another six months to investigate the effect of ozone on NDMA formation, and long-term overall performance of the ozone BAF treatment trains in the removal of PPCPs. For this reason, this research focused on the evaluation of regulated DBP precursors (THMs, HAAs), nitrosamines, and flame retardants based on the data from the first six months of the pilot study. Data from the fourth to the sixth month of operation were used to evaluate PFASs. Evaluation of NDMA formation and precursor removal was based on the last six-month of data, after the biofilters adequately grew a biofilm population that was acclimated to biodegradation of NDMA. Data from the entire 12-month operating period were used to assess performance with respect to PPCP removal.

2.4.2 Sample analysis

Samples were collected at different locations across the treatment trains, including effluent from the equalization tank (pilot influent), ozone contactor effluents, and GAC effluents. Samples were analyzed using the methods and instruments listed in Table 2.2. Briefly, ozone dose was analyzed using an ozone analyzer (IN USA, Mini-Hicon Ozone Analyzer, Norwood, MA USA). DOC and pH were analyzed by using Standard Methods (APAH et al., 2005). Concentrations of bromide, bromate, PFASs, and nitrosamine concentrations were determined according to EPA methods (Telliard et al., 1999). The formation of THMs and HAAs were analyzed by using both Standard Methods and EPA methods (APAH et al., 2005; Telliard et al., 1999) in conjunction with a simulation of UOSA's chlorine contact basin which consisted of a free chlorine residual maintained around 1 mg L^{-1} for one hour at 25 ^{o}C. The technique of fluorescence excitation-emission matrix (FEEM, Horiba Scientific, Aqualog-UV-800-C, Edison, NJ USA) has been widely used to characterize dissolved organic matter in water and soil (Chen et al., 2003). FEEM collects a series of emission spectra from samples over a range of excitation wavelengths. Previous literature reported the use of FEEM to analyze the effect of ozonation on the removal of humic-like and fulvic-like substances (Swietlik and Sikorska, 2004; Zhang et al., 2008; Liu et al., 2011). Nitrosamine formation was assessed using a system distribution simulation method adapted from EPA to simulate the local potable distribution system. This method involved the application of 3

mg L^{-1} residual chloramine and then incubation for 24 hours at 25 ^{o}C followed by nitrosamines analysis using EPA method 521 (Telliard et al., 1999). Flame retardants and PPCPs were analyzed using methods equivalent to Underwriters Laboratory Methods L200 and L221 (now Eurofins Eaton Analytical, Indiana, USA) (Table 2.2).

2.4.3 Pollutant removal pathway

The performance of treatment trains listed in Table 2.1 were compared to each other to infer the contributions of ozone oxidation, adsorption, and biodegradation on pollutant removal during the ozone BAF process. For example, some insight into the role that ozone oxidation can have on pollutant degradation may be gathered by looking at a comparison of treatment trains with varying ozone doses while also looking at the type of GAC (spent or regenerated GAC). Likewise, the role of biodegradation and adsorption can be inferred from the performance difference between treatment trains using spent versus regenerated GAC but at the same or zero ozone doses.

2.5 Results and Discussion

This study analyzed the roles of ozone oxidation, adsorption, and biodegradation on the removal of DBPs and their precursors as well as trace organics. While the major focus of this study is on the chlorinated THMs and HAAs formation and the removal of NDMA, as well as 6 PFAS, 2 flame retardants, and 66 PPCPs, the effects of ozone dose on bromide, bromate, and brominated THMs and HAAs formation were also studied but not emphasized in this work.

2.5.1 Bromate formation

Bromide, is commonly found in natural water along with chloride but in smaller quantities (World Health Organization, 2009). Bromide is a precursor to bromate during ozonation and bromate is a Safe Drinking Water Act (SDWA) regulated constituent. Concentrations of bromide in fresh water typically range from trace amounts to about 0.5 mg L^{-1} (World Health Organization, 2009). Figure 2.1 shows that the pilot influent contained an average of about 90 μg L^{-1} bromide. The chemical transformation of bromide to bromate and other DBPs can be described by Eqs. 2.1 to 2.4 (Siddiqui,

1992). Briefly, ozone first oxidizes bromide (Br^-) to hypobromide (OBr^-) as expressed in Eq. 2.1. Then, hypobromide (OBr^-) can be further oxidized to bromate (BrO_3^-) with more ozone addition (Eq. 2.2). Meanwhile, OBr^- can associate with a hydrogen ion to form hypobromous acid (HOBr) in a reversible equilibrium (Eq. 2.3). When DOC is present, it can react with HOBr to form total organic brominated compounds (TOBr) as described in Eq. 2.4.

$$O_3 + Br^- \rightarrow O_2 + OBr^- \quad \textbf{(2.1)}$$

$$O_3 + OBr^- \rightarrow 2O_2 + BrO_3^- \quad \textbf{(2.2)}$$

$$H^+ + OBr^- \leftrightarrow HOBr \quad \textbf{(2.3)}$$

$$HOBr + DOC \rightarrow TOBr \quad \textbf{(2.4)}$$

As predicted by Eqs. 2.1 and 2.2, bromate formation increased as ozone:DOC increased and became detectable in effluent from spent GAC reactors when ozone dose was greater than 0.65 mg O_3 mg^{-1} DOC (Figure 2.1). It should be noted that the drinking water maximum contaminant level (MCL) was not exceeded until ozone dose became as high as 1.1 mg O_3 mg^{-1} DOC, suggesting that keeping ozone dose lower than 1.1 mg O_3 mg^{-1} DOC is beneficial to limit bromate formation.

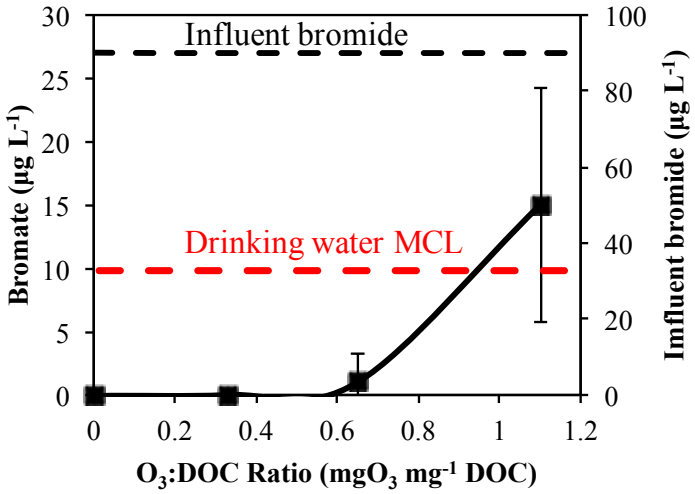

Figure 2.1 Influent bromide and effluent bromate concentrations of spent GAC treatment trains operated at various ozone:DOC ratios

2.5.2 Brominated THM and HAA formation

THMs are chemical compounds in which three of the four hydrogen atoms of methane are substituted by halogen atoms. HAAs are carboxylic acids in which a halogen atom takes the place of a hydrogen atom in acetic acid. THM and HAAs are groups of compounds that have MCLs regulated by the SDWA. Brominated THMs and HAAs can be formed as DBPs during ozonation in the presence of bromide and organic matter contained in the water being ozonated (Siddiqui, 1992). Typical brominated THMs and HAAs include bromoform ($CHBr_3$), chlorodibromomethane ($CHClBr_2$), and dibromoacetic acid ($C_2H_2Br_2O_2$) (Chang et al., 2001). Figure 2.2 shows the formation of $CHBr_3$ and $C_2H_2Br_2O_2$ resulting from different ozone:DOC ratios. It was observed that the formation of both brominated DBPs initially increased and then decreased as the ozone:DOC ratio increased. The apparent mechanism appears to be when ozone:DOC ratio was low, the resulting OBr^- concentration formed is also low due to insufficient ozone in solution (Eq. 2.1). This in turn results in limited HOBr concentrations formed in accordance with the ionization equilibrium between HOBr and OBr^- in Eq. 2.3. As a consequence, and in waters containing significant DOC, the formation of TOBr is limited by low concentrations of HOBr which can be seen in Eq. 2.4. However, at ozone:DOC ratios above 0.65 there is enough ozone available to further oxidize OBr^- to BrO_3^- (Eq. 2.2) making OBr^- less available to be ionized to HOBr. Thus, a higher ozone:DOC ratio tends to result in a lower OBr^- concentration which in turn limits HOBr formation (Eq. 2.3) and then reduces the formation of brominated organics, TOBr (Eq. 2.4).

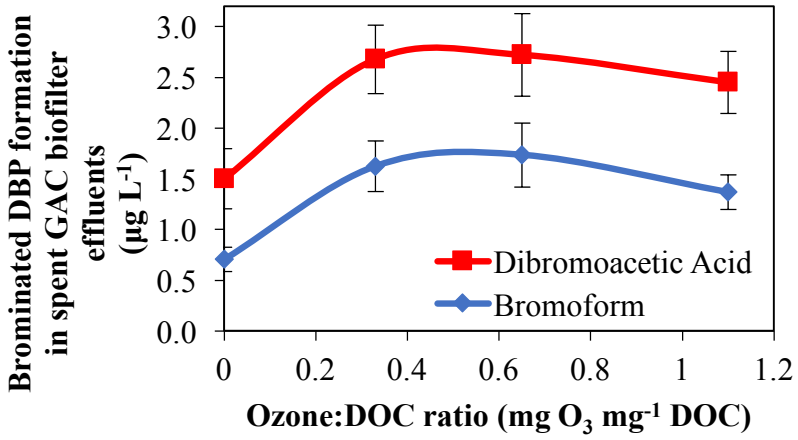

Figure 2.2 Profiles of dibromoacetic acid and bromoform formations in the effluent of spent GAC treatment trains operated at various ozone:DOC ratios

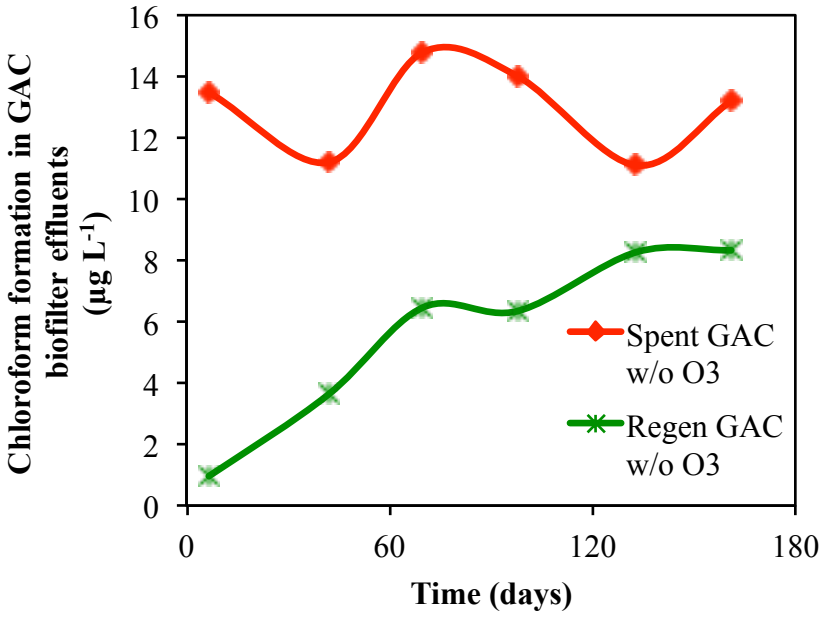

Figure 2.3 Effluent chloroform formation in treatment trains without (w/o) ozonation

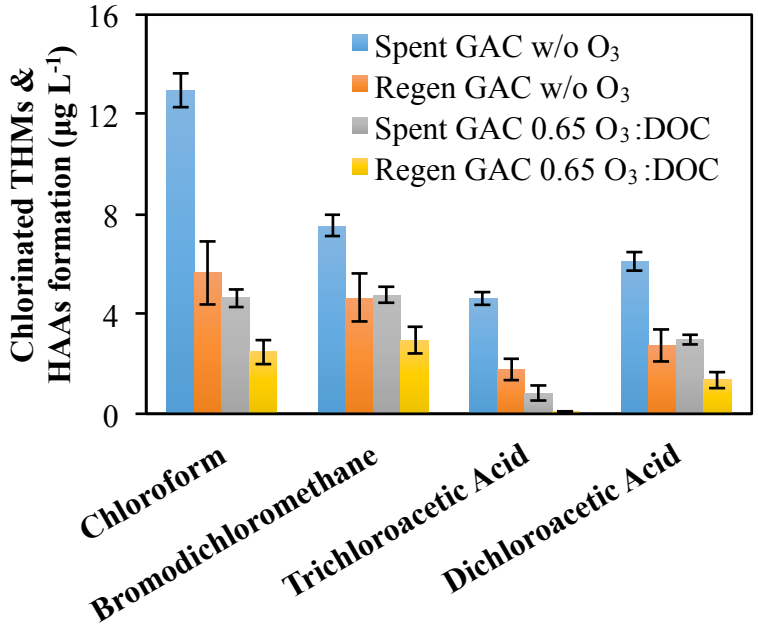

Figure 2.4 Chlorinated THMs and HAAs formations in the effluent of spent and regenerated GAC treatment trains with or without ozonation during the first 5 months

2.5.3 Chlorinated THM and HAA formation

Chlorinated THMs and HAAs are defined as the THMs and HAAs that incorporate only chlorine or more chlorine than other halogens. Unlike brominated counterparts, chlorinated THMs and HAAs are mainly formed during chlorination, which is a common final disinfection step in many water and wastewater treatment plants. The formation of four types of chlorinated THMs and HAAs were investigated during the pilot effort by applying 1 mg L^{-1} of free chlorine and incubation at 25 ^{o}C for one hour of contact time. Chlorinated THM and HAA formations in spent GAC treatment train effluents with and without ozonation are shown in Figure 2.4 which indicates that ozonation reduced the formation of the four chlorinated THMs and the HAAs. Similar results were also observed in previous literature (Mao et al., 2018), and are expected as DBP precursors were likely oxidized through the ozone BAF process. It is known that the precursors of chlorination by-products are mainly humic and fulvic acids (Rebelo et al., 2016; von Gunten, 2003; Wang et al., 2016). As a matter of fact, ozone is good at reducing humic and fulvic substances by transforming them to simple non-humic forms with small molecules that are less recalcitrant to biodegradation (Akcay et al., 2016; Glaze, 1986). FEEM is a very effective method to examine the presence of humic-like and fulvic-like compounds (Chen et al., 2003), and intensity reduction of the fluorescence peaks has often been used to indicate the removal of humic-like and fulvic-like compounds (Zhang et al., 2008; Liu et al., 2011). By comparing Figures 2.5a and b, it was estimated that ozonation approximately decreased the peak fluorescence intensities of humic-like and fulvic-like compounds by 70-80%, which indicated that substances with humic and fulvic signatures in the FEEM plots were effectively removed or transformed by ozone. This observation matches up well with reduced chlorinated THMs and HAAs formations in ozonated treatment trains as shown in Figure 2.4 and is likely a result of DBP precursor transformation through oxidation by ozone.

By comparing Figures 2.5a and c, it can be seen that although biodegradation by spent GAC can remove some humic and fulvic substances, a substantial amount still remained. It is known that humic and fulvic substances can be resistant to biodegradation due to their recalcitrant structure and high molecular weight (Akcay et al., 2016). Thus, BAF without pre-ozonation was the least effective treatment investigated and yielded the highest chlorinated THM and HAA formations

(Figure 2.4). Figure 2.5d shows a FEEM plot for the effluent of regenerated GAC treatment train without ozonation. By comparing Figures 2. 5a and d, it can be seen that adsorption can effectively remove humic and fulvic substances while active adsorptive capacity is still available. This is attributed to the high hydrophobicity of humic and fulvic substances (Matilainen et al., 2010), and is supported by the data in Figure 2.4 which shows lower chlorinated THM and HAA formations in the effluent from regenerated GAC than that from spent GAC without ozonation. This observation suggests that adsorption by recently regenerated GAC effectively removed chlorinated THM and HAA precursors by adsorbing most of the humic and fulvic substances that would contribute to its formation upon free chlorination. Although regenerated GAC adsorption is initially very effective for chlorinated THM and HAA precursor control, long-term effectiveness can be expected to degrade (Figure 2.3); thus requiring repeated thermal regenerations to periodically restore treatment efficiency.

Given the fact that humic and fulvic substances are not readily biodegradable (Akcay et al., 2016) and adsorptive removal requires frequent periodic regenerations, ozone oxidation begins to look very favorable as an important pathway to control chlorinated THMs and HAAs formations. Furthermore, since neither ozone oxidation nor biodegradation can effectively remove chlorinated THMs and HAAs once they are formed (Allard et al., 2013; Nunes-Halldorson et al., 2004; Rajagopal et al., 2012), a proactive approach using ozone BAF to remove DBP precursors, followed by free chlorination for disinfection was determined to be the optimum process to employ at this potable reuse facility.

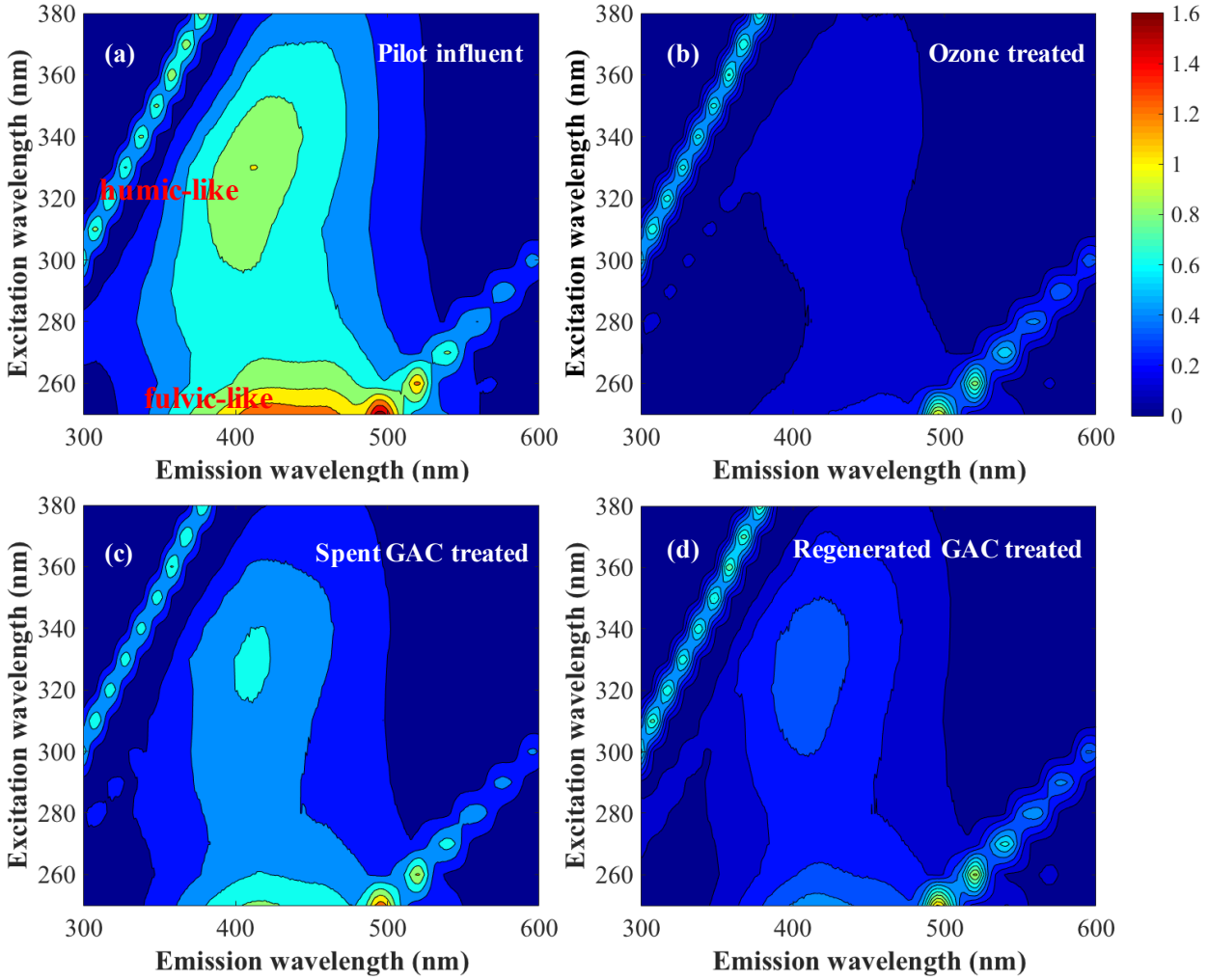

Figure 2.5 FEEM fingerprints of (a) pilot influent and (b) effluent from ozone contactor operated at the ozone:DOC ratio of 0.65 mg O_3 mg^{-1} DOC; (c) effluent from spent GAC treatment train without ozonation; and (d) effluent from regenerated GAC treatment train without ozonation. The regions of humic- and fulvic-like matters are labeled according to the information from the work by Chen et al. (2003)

2.5.4 Nitrosamines removal and formations

Nitrosamines are by-products of several industrial processes and typically present at very low levels in certain foodstuffs, especially those that are cooked, smoked, or cured (Newcombe, 2013). Nitrosamines can be measured in water; one of which, N-nitrosodimethylamine (NDMA) is a known byproduct resulting from ozonation and chloramination of certain waters. California

Department of Public Health (CDPH) and the National Water Research Institute's (NWRI) Expert Panel on Direct Potable Reuse (DPR) have published an NDMA health-based advisory level of 10 ng L^{-1} (NWRI, 2013). NDMA is a compound listed on EPA's Unregulated Contaminant Monitoring Rule for possible consideration of future regulation under the Safe Drinking Water Act. Therefore, nitrosamines and particularly NDMA are compounds of interest to the water treatment industry. Nine types of nitrosamines were analyzed in this study and NDMA was primarily detected. The presence of NDMA and its precursors is of particular interest where membrane or ozone treatment of wastewater effluent is used for potable reuse because these processes can lead to the formation of significant concentrations of NDMA (Mitch et al., 2003).

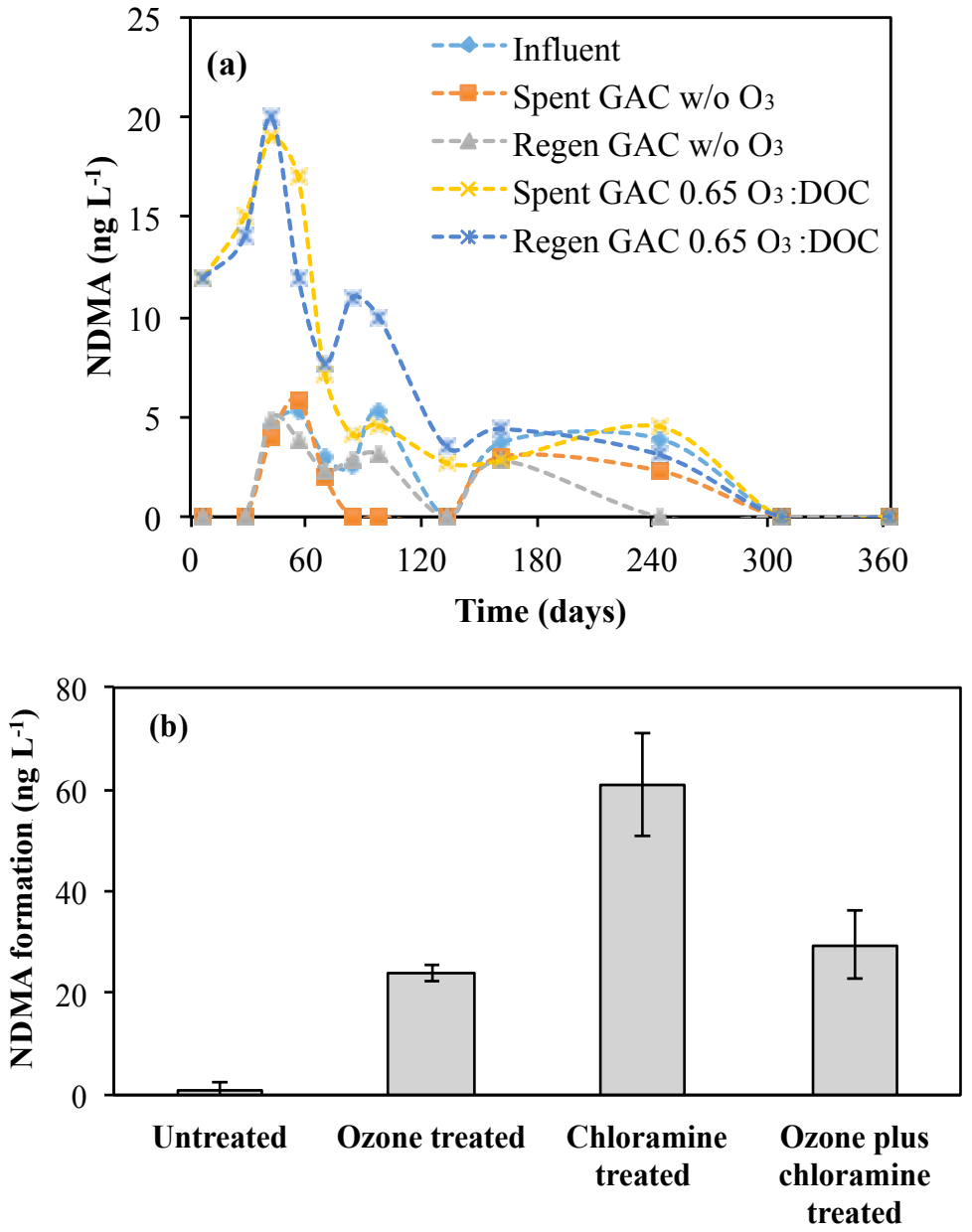

Figure 2.6 (a) Influent and effluent NDMA concentrations from spent and regenerated GAC treatment trains with or without (w/o) ozonation; (b) Effect of ozonation and chloramination on NDMA formation. "Untreated" represents the pilot influent; "ozone treated" represents the effluent from ozone contactor with ozone:DOC ratio of 0.65 mg O_3 mg^{-1} DOC prior to BAF and not subject to chloramination; "chloramine treated" represents the pilot influent incubated with 3 mg L^{-1} of chloramine for 24 hours at 25 ^{o}C; "ozone plus chloramine treated" represents the effluent from the ozone contactor with ozone:DOC ratio of 0.65 mg O_3 mg^{-1} DOC and incubated with 3 mg L^{-1} of chloramine for 24 hours at 25 ^{o}C

2.5.4.1 NDMA formation from ozonation and subsequent degradation through BAF

Figure 2.6a shows that NDMA levels detected in the pilot influent were always below 5 ng L^{-1}. However, the biofilter treatment trains that were pre-ozonated showed dramatic increases in biofilter effluent NDMA concentration during the first three-months of the pilot test. So it is quite clear that ozonation of the pilot influent resulted in NDMA formation. The same phenomenon has been observed previously (Hollender et al., 2009; Pisarenko et al., 2015), which is attributed to the ozone oxidation of NDMA precursors. *N,N*-dimethylsulfamide (DMS) has been identified as one such precursor in water from other studies (Schmidt and Brauch, 2008). Figure 2.6a also demonstrates that the high NDMA concentration resulting from pre-ozonation of the biofilter influent decreased over time after the first 90 days of operation and was eventually reduced to a level close to that of the non-ozonated influent. This gradual NDMA concentration decrease can be explained by biodegradation. The biodegradability of NDMA has been reported previously (Bradley et al., 2005; Kaplan and Kaplan, 1985; Schmidt and Brauch, 2008) and is particularly amenable to co-metabolic biodegradation (Fournier et al., 2009; Hatzinger et al., 2017). The similar NDMA profiles between spent and regenerated GAC, particularly early on in the study when adsorptive capacity of the regenerated GAC was observed, also confirms that adsorption of NDMA was ineffective and is likely due to its low hydrophobicity. Usually, compounds with log K_{OW} values greater than 1 are regarded as hydrophobic (Calow, 1997). According to the study by Mitch et al. (2003), the log K_{OW} value for NDMA is only -0.57. Hence, it was not surprising to observe that regenerated GAC was not effective in adsorbing it.

2.5.4.2 Examination of precursors to NDMA formation resulting from ozonation and chloramination

Figure 2.6b shows that incubating the untreated pilot influent with 3 mg L^{-1} chloramine for 24 hours at 25 ^{o}C formed NDMA concentrations around 60 ng L^{-1} which is significantly higher than the NDMA concentration resulting from simply pre-ozonating the same water with 2.6 mg L^{-1} of applied ozone dose (equivalent to the ozone:DOC ratio of 0.65 mg O_3 mg^{-1} DOC) and five minutes of contact time. However, when pre-ozonated biofilter influent samples were then chloraminated

and incubated as described above, NDMA concentrations only increased to around 30 ng L^{-1} which is a level of treatment similar to that of the ozone treatment alone (Figure 2.6b). This interesting phenomenon confirms the observation that different precursor compounds may be responsible for NDMA formation during ozonation and chloramination (Park et al., 2015). It should also be pointed out that many of these precursors are only reactive with just one of the two oxidants examined in this study (Marti et al., 2015). Thus, NDMA precursors can be classified into two groups, namely ozone-reactive NDMA precursors and chloramine-reactive NDMA precursors (Marti et al., 2017). For example, precursors containing hydrazine (e.g., unsymmetrical dimethyl-hydrazine and semicarbazides) or sulfamide (e.g., N,N-dimethylsulfamide functionalities) are ozone-reactive NDMA precursors, and most secondary amines (e.g., dimethylamine) are chloramine-reactive NDMA precursors (Krasner et al., 2013). Figure 2.6b indicates that although both ozone and chloramine trigger NDMA formation, the quantity of ozone-reactive precursors and level of NDMA formation from ozonation was substantially lower than the NDMA formation resulting from chloramination of the chloramine-reactive precursors in the same water. This was also observed for NDMA formations in the biofilter influent studied by previouse studies (Andrzejewski et al., 2008; Kosaka et al., 2009). Previous research also indicated that pre-oxidation with chlorine, ozone, hydrogen peroxide, and even sunlight were able to reduce NDMA formation during subsequent chloramination by deactivating chloramine-reactive NDMA precursors, and ozone turned out to be the most effective among all these oxidants (Krasner et al., 2013). Figure 2.7 shows the effluent NDMA concentrations from treatment trains with ozone contactors operated at ozone:DOC ratio of 0.65 mg O_3 mg^{-1} DOC followed by spent and regenerated GAC biofilters with and without chloramination from month 5 to 12. It can be seen that effluent NDMA concentrations from biofilters were all far below the 10 ng L^{-1} advisory level after biofilters were acclimated to co-metabolize NDMA as a substrate, which indicated that combination of ozone with subsequent BAF turned out to be a very promising technique to reduce NDMA formation during ozonation and chloramination. Similar conclusions were also drawn by Pisarenko et al. (2012).

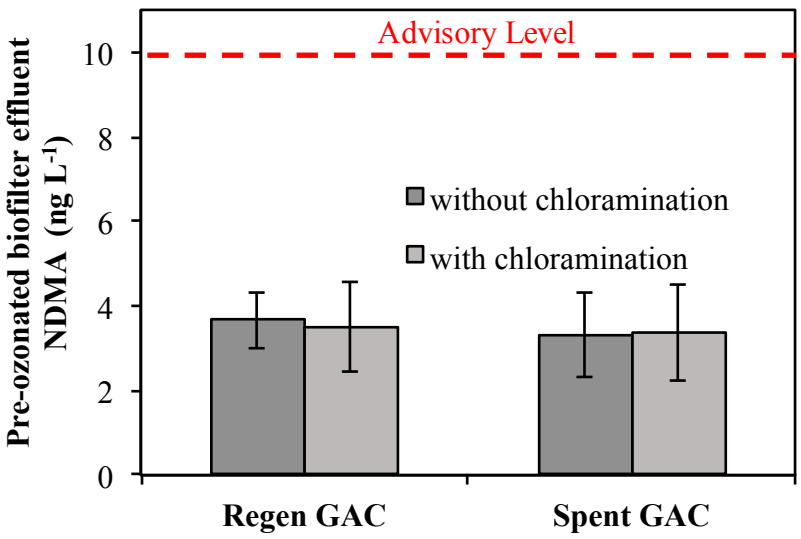

Figure 2.7 Effluent NDMA concentrations from the treatment trains with ozone reactor operated at ozone:DOC ratio of 0.65 mg O_3 mg^{-1} DOC followed by spent and regenerated GAC biofilters with and without chloraminaton between month 5 to 12

2.5.5 PFAS removal

PFASs may occur in wastewater in service areas where industrial surfactants, surface coating agents, firefighting foams, and other additives have been used (Pisarenko et al., 2015). Several PFASs are on EPA's Unregulated Contaminant Monitoring Rule (UCMR) list for potential future regulation under the SDWA. Two of these, perfluoro-octanoic acid (PFOA) and perfluoro-octanoic sulfonate (PFOS) are subjects of an EPA drinking water health advisory set at 70 ng L^{-1} for the sum of these two compounds (EPA, 2016). Therefore, six PFASs were analyzed in this study, namely perfluorobutanesulfonic acid (PFBS), perfluoroheptanoic acid (PFHpA), perfluorohexanesulfonic acid (PFHxS), perfluorononanoic acid (PFNA), PFOS and PFOA. Out of the six PFASs, PFHxS was the only one undetected in the pilot influent. However, all samples analyzed for PFAS resulted in the sum of both PFOS and PFOA concentrations significantly below EPA's 70 ng L^{-1} health-based advisory level. In addition, the detection limit of PFOS (4 ng L^{-1}) was always very close to its influent level (5 ng L^{-1}), while the detection limit of PFBS (9 ng L^{-1}), PFHpA (1 ng L^{-1}), PFNA (2 ng L^{-1}), and PFOA (2 ng L^{-1}) was much lower than their influent

levels (PFBS: 32 ng L^{-1}, PFHpA: 27 ng L^{-1}, PFNA: 7 ng L^{-1}, and PFOA: 26 ng L^{-1}). Thus, PFOS was excluded from the process performance data presented in Figure 2.8.

2.5.5.1 Effects of ozonation on PFASs

Observation of the triplicate average of PFAS removal efficiencies by spent and regenerated GAC treatment trains with and without ozonation are shown in Figure 2.8. Comparison between spent GAC with and without ozonation indicates that the effect of ozonation on PFAS degradation was actually very poor. Numerous previous research studies reported that ozone-based oxidation failed to degrade PFASs (Shivakoti et al., 2010; Tabe et al., 2010; Takagi et al., 2011; Thompson et al., 2011). In the study by Takagi et al. (2011), it was reported that even at a very high ozone dose (5 mg L^{-1}) and contact time (120 min), PFOA and PFOS cannot be effectively degraded. This observation has been attributed to the presence of the strong carbon-fluorine bond together with -COOH or -SO_3H features in the molecular structures of PFASs (Rahman et al., 2014). Rahman et al. (2014) pointed out that fluorine is the most electronegative element, so it resists oxidation to retain its electrons. It is also known that -COOH and -SO_3H are electron-withdrawing groups that reduce the reactivity of such compounds with ozone (Gunten, 2003).

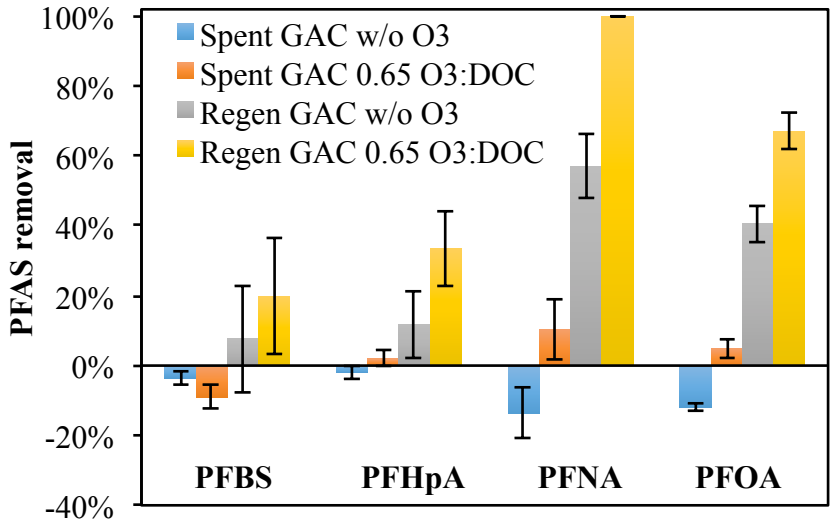

Figure 2.8 PFAS removal efficiency in spent and regenerated GAC treatment trains with or without ozonation between month 3 to 5

2.5.5.2 PFAS removal by adsorption

One note is that the assessment of PFAS removal performance is based on data gathered after three months of operation and after detection limits for these analyses were optimized. So, the initial period of GAC biofilter operation, and the time of operation with the highest adsorption capacity, was not captured in the data shown herein. By comparing the removal efficiency of PFNA and PFOA in the regenerated GAC treatment train without ozonation in Figure 2.8, it can be inferred that adsorption is an effective technique for removing PFNA and PFOA (about 60% and 40% removal). Previous literature reported that adsorption is good at removing longer chain PFASs (e.g., PFNA and PFOA in Figure 2.8). For example, the removal of PFOA was found to be about 40 to 50% (Eschauzier et al., 2012; Flores et al., 2013), which is close to the efficiency measured in this study (Figure 2.8).

Conversely, the adsorption of short chain PFASs was quite poor. For example, when looking at the removal of both PFBS and PFHpA in the regenerated GAC treatment train without ozonation in Figure 2.8, removals were only 10% or less. This lines up with observations from others which demonstrated that shorter chain PFASs (e.g., PFBA, PFBS, PFPA, PFHxA and PFHpA) are more resistant to adsorption (Eschauzier et al., 2012; Flores et al., 2013) than the longer chained ones. One may anticipate that the hydrophobicity of PFASs would increase with their molecular chain length. For example, the relatively longer chained PFOA has a high enough log K_{OW} value of 6.28 to yield good adsorption (Ahrens et al., 2010; Higgins and Luthy, 2006; Sanderson et al., 2003).

Another observation apparent from Figure 2.8 is that PFASs removal by regenerated GAC was improved when pre-ozonation was applied but the same improvement was not observed when pre-ozonation was applied on spent GAC. This suggests that although ozone cannot oxidize PFASs, adsorption of PFASs may be improved through the oxidation of other organic compounds that would otherwise compete for adsorption sites on the GAC if they were not otherwise oxidized by ozone. Therefore, more active sites became available for PFAS adsorption in the pre-ozonated regenerated GAC biofilter than in the regenerated GAC biofilter that did not receive pre-ozonation.

2.5.5.3 Effects of desorption and biological activities on PFASs

Figure 2.8 shows that the PFAS removal efficiencies of the spent GAC treatment train without ozonation were slightly negative. The low removal efficiency agrees with others that found PFASs to be non-biodegradable in aerobic environments (Rahman et al., 2014). However, negative removals would suggest that either some desorption was occurring or that bacteria on the GAC surface may have formed some small amounts of PFASs through microbial metabolization of PFAS precursors. For example, microbial metabolization of fluorotelomer alcohols (FTOHs) and the FTOH-based products, FASAs, FASEs, as well as other PFAS precursors have been reported to occur during wastewater treatment in aerobic environment (Martin et al., 2010; Rhoads et al., 2008; Wang et al., 2005), which may eventually lead to the formation of PFASs (e.g. PFOS, PFOA) in Figure 2.8. Pilot influent PFAS concentrations decreased during the course of the study suggesting that desorption could possibly be a mechanism contributing to the increase in PFAS concentrations at the biofilter effluents.

2.5.6 Flame retardants removal

Two flame retardants were analyzed in this study, namely Tris (2-chloroethyl) phosphine (TCEP) and Tris (1-chloro-2-propyl) phosphate (TCPP). Some flame retardants have been included in EPA's UCMR lists, and TCEP is a flame retardant identified for monitoring by an NWRI expert panel on DPR. The DPR expert panel selected a 5 $\mu g\ L^{-1}$ TCEP concentration to be the level that poses a de-minimus risk to public health (NWRI, 2013). It can be seen in Figure 2.9 that ozonation promoted very little flame retardant degradation because there was almost no difference between the removal efficiency of TCEP and TCPP in spent GAC treatment trains with and without ozonation. Both TCEP and TCPP molecules have fully oxidized structures (Stapleton et al., 2011), so it is reasonably difficult to further oxidize them with ozone.

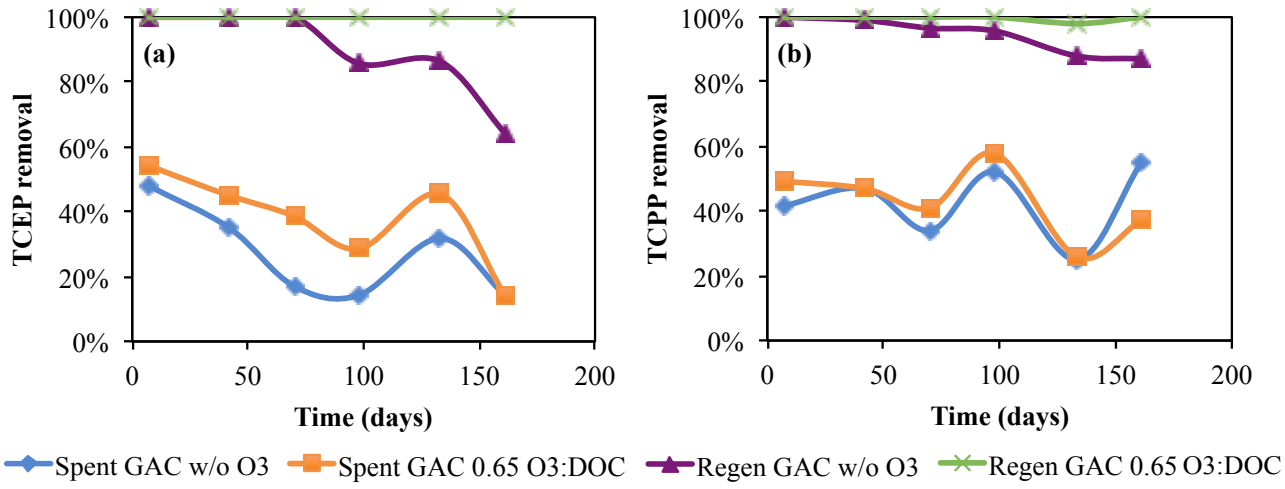

Figure 2.9 Removal efficiency of (a) TCEP and (b) TCPP in spent and regenerated GAC treatment trains with or without ozonation

Since the removal efficiency of TCEP and TCPP in regenerated GAC treatment trains was much higher than those in spent GAC treatment trains, it can be concluded that adsorption is the dominant pathway for their removal (Figure 2.9). This can be explained by the relative high log K_{OW} value of these flame retardants (e.g., 2.6 for TCPP, 1.7 for TCEP) (Regnery and Püttmann, 2009). It should also be noted from Figure 2.9 that there was some TCEP and TCPP removal in the spent GAC treatment trains regardless of whether the contactor was ozonated or not. This may be explained by either biodegradation or perhaps because there was still some adsorption capacity for these flame retardants left on the spent GAC. Zhang et al. (2017) reported that flame retardants are moderately biodegradable (removal of 50% to 75%), which may imply that degradation contributed although it is known that adsorption is the dominant removal pathway for these compounds.

Although ozone was unable to remove flame retardants through oxidation, one can see from Figure 2.9 that there are distinct advantages to pre-ozonating the regenerated GAC biofilters. As described earlier for the readily adsorbable PFAS compounds, similar behavior is observed for the flame retardants. Looking at the removal efficiency for regenerated GAC treatment trains with and without ozonation in Figure 2.9, pre-ozonation actually extended excellent performance of the GAC by transforming or oxidizing other contaminants that compete for adsorption sites on the

carbon. This phenomenon appears to have increased flame retardant adsorption capacities of the regenerated GAC (Li et al., 2013).

2.5.7 PPCPs removal

During this study, 66 PPCPs were investigated in nine sampling campaigns. Interestingly, only 31 of those compounds were actually detected in the pilot influent. Detectable concentrations of PPCPs allow for the assessment of the percent removals shown in Figure 2.10. It presents a side-by-side comparison of the removal efficiency of PPCPs between using ozonation alone (without biofilter) and using the spent or regenerated GAC treatment train (without pre-ozonation). This comparison clarifies the role that ozonation, biodegradation, and adsorption played in removal of the various PPCPs detected (Figure 2.10). It can be seen that ozone alone was capable of achieving 95% to 100% removal efficiency for 25 out of the 31 PPCPs detected. Three other PPCPs, namely dilantin, primidone, and N,N-diethyl-meta-toluamide (DEET) achieved 80% to 90% removal efficiency through ozone treatment alone. Meprobamate, nicotine, and cotinine were the only three PPCPs that were not as effectively degraded by ozonation and demonstrated removal efficiency less than 60%. The removal efficiency of various PPCPs shown in Figure 2.10 by ozonation can be explained by their ozone reaction rate constants (K_{O_3}), which represents the reactivity a compound has with ozone. Compounds that have high ozone reactivity usually have very large K_{O_3} values. For example, naproxen, atenolol, and trimethoprim possess large K_{O_3} values of 2×10^5, 1.69×10^3, and 2.71×10^5 M^{-1} s^{-1} at neutral pH, respectively (Benitez et al., 2009; Rodriguez et al., 2013), and their high ozonation removal efficiencies were verified experimentally in Figure 2.10 and also have been reported previously (Gerrity et al., 2011; Yao et al., 2018). For dilantin, primidone, and DEET, their removal efficiency was not as high and can be classified as compounds having moderate reactivity with ozone (Gerrity et al., 2012). Such compounds usually have K_{O_3} values between 1 and 10 M^{-1} s^{-1}. For example, K_{O_3} values for primidone and DEET are both < 10 M^{-1} s^{-1} (Gerrity et al., 2012). It should be pointed out that the three PPCPs with less than 60% removal, namely meprobamate, nicotine, and cotinine, were not as effectively degraded by ozonation and have low reactivities with ozone as evidenced by their K_{O_3} < 1 M^{-1} s^{-1} (Gerrity et al., 2012).

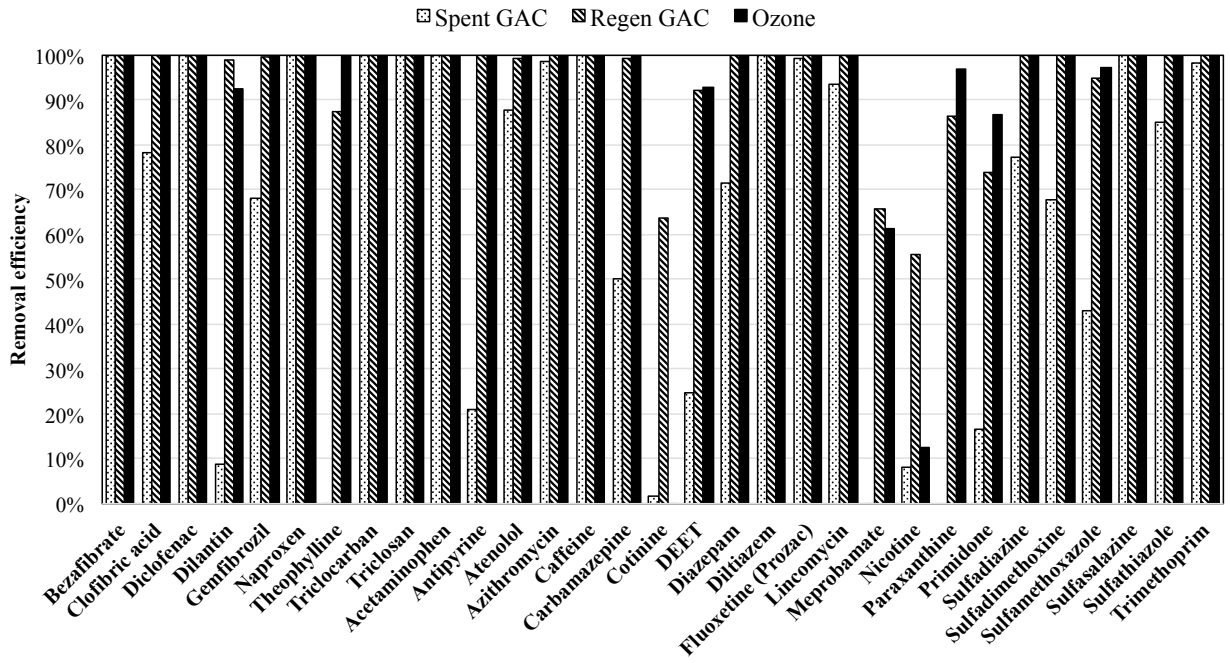

Figure 2.10 Removal efficiency of PPCPs in ozone contactors as well as spent and regenerated GAC treatment trains without ozonation. "Spent GAC" represents spent GAC biofilter effluent without ozone; "Regen GAC" represents regenerated GAC biofilter effluent without ozone; "Ozone" represents effluent from ozone contactor with ozone:DOC ratio of 0.65 mg O_3 mg^{-1} DOC

Figure 2.10 also can be used to observe how well the detected PPCPs can be removed simply through activated carbon adsorption. It is evident that only four of 31 PPCPs detected were not well removed by adsorption on regenerated GAC, namely primidone, meprobamate, nicotine, and cotinine. This can be explained by their hydrophilic nature. For example, log K_{OW} for primidone and meprobamate are only 0.83 (Wijekoon et al., 2013) and 0.70 (Yoon et al., 2007), respectively. Other than these four PPCPs, most of the other 27 PPCPs are relatively hydrophobic and thus more readily adsorbed onto regenerated GAC media.

Biodegradation of the various detected PPCPs was investigated by observing the removal through spent GAC biofilters that were not pre-ozonated. Figure 2.10 indicates that nine PPCPs were not readily biodegraded. These included primidone, paraxanthine, meprobamate, dilantin, nicotine, theophylline, DEET, antipyrine, and cotinine. Zhang et al. (2017) reported that DEET and cotinine are recalcitrant to biodegradation, and Guo and Krasner (2009) reported that primidone is usually

stable in natural environments. Another study by Benotti and Brownawell (2009) compared the half-lives ($t_{1/2}$) of different PPCPs. They concluded that: 1) biodegradability of nicotine is quite different under different environments ($t_{1/2}$ = 0.68 to 9.7 days); 2) paraxanthine exhibits intermediate resistance to biodegradation; and 3) antipyrine and cotinine are some of the most environmentally persistent pharmaceuticals ($t_{1/2}$ > 40 days).

Although it is difficult to remove all the detected PPCPs through a single removal pathway, the synergy provided by ozonation, adsorption, and biodegradation present in the treatment processes tested has reduced PPCP concentrations to between non-detectable and 0.01 μg L^{-1}. Thus, it was concluded that pre-ozonation followed by BAF on GAC media is a very effective treatment for the PPCPs observed at this facility.

2.6 Conclusions

The effects of ozone oxidation, adsorption, and biodegradation on the removal of contaminants through the pre-ozonated biofilters filled with either adsorptive phase or biologically activated carbon analyzed in this study are tabulated in Table 2.3 and summarized below.

- THM and HAA formation resulting from free chlorination of biofilter effluents decreased with increasing ozone dose and ozone:DOC ratio (mg O_3 mg^{-1} DOC). Therefore, ozonation did a good job in reducing the precursor compounds that form these regulated DBPs after free chlorination.
- Ozonation increased NDMA concentrations, but the NDMA formed through the ozone reactors was fully biodegraded once the microbial community in the downstream biofilters became acclimated to it.
- Most of the 31 PPCPs detected in this study were effectively degraded by ozonation with meprobamate, nicotine, and cotinine being some exceptions. Only nine out of the 31 detected PPCPs were found resistant to biodegradation in spent GAC biofilters that were not pre-ozonated. The measurable concentrations of PPCPs observed after any of the treatments applied were orders of magnitude lower than concentrations previously identified as posing de Minimus risk.

- Although, oxidation by ozone had little effect on the four PFASs and two flame retardants detected in this study, pre-ozonation of biofilters containing regenerated GAC improved the adsorptive life/capacity of the regenerated GAC for the PFASs and flame retardants by removing organic compounds that compete for adsorption sites on the GAC surface.
- Adsorption played a very important role in the removal of chlorinated THM and HAA precursors, PFASs, flame retardants, and most PPCPs. However, NDMA was not removed by adsorption because of its low hydrophobicity. In addition, flame retardants and PFASs were the groups of compounds removed primarily by adsorption but were also found to be resistant to treatment by oxidation and biodegradation.
- This work provides some insight into selecting spent or regenerated GAC as an appropriate BAF media to pair with ozonation for potable water reuse. Certainly if the only goal is to achieve the highest product water quality, then incorporating a configuration that provides oxidation, biodegradation and an adsorptive phase component to the GAC media would be preferred. However, potable reuse applications often include multiple significant barriers such as source control, reverse osmosis, nanofiltration, surface or groundwater buffers, soil aquifer treatment or a downstream potable water treatment facility that produces high purity water. In cases like these, the water quality obtained from ozone BAF using spent GAC media may be a perfectly acceptable, yet a more economical and sustainable choice than adsorptive phase GAC. Therefore, the selection of spent or regenerated GAC in practice should be tailored to process water quality goals that achieve acceptable target contaminant concentrations and viewed holistically with respect to the intended role that ozone BAF will play in the overall potable reuse scenario being applied.

Table 2.1 Experimental design for six ozone-BAF trains operating at the 23 minute EBCT.

Train	O_3:DOC (mg O_3 mg^{-1} DOC)	Type of GAC
1	0	Spent
2	0	Regenerated
3	0.33	Spent
4	0.65	Spent
5	0.65	Regenerated
6	1.10	Spent

Table 2.2 Methods or instruments for the analyses performed in this study

Analysis	**Methods/Instruments**
Ozone	IN USA, Mini-Hicon Ozone Analyzer
DOC	SM* 53108
TTHM and HAA5 formation potentials	SM 57108-D; EPA 524.2; EPA 552.2
pH	SM 4500-H
Bromide	EPA** 300.0
Bromate	EPA 300.1
Nitrosamines (formation)	EPA 521
PFASs	EPA 537
Flame retardants	UR*** L220
PPCPs	UR L220, L221
FEEM	Horiba Scientific, Aqualog-UV-800-C

*SM: Standard Methods (APAH, 2005)

**EPA: Environmental Protection Agency (Telliard et al., 1999)

***UR: Underwriters Laboratory (now Eurofins Eaton Analytical, Indiana, USA)

Table 2.3 A summary of the roles of ozone oxidation, adsorption, and biodegradation: "+" increase; "–" decrease; "×" no effect (less than 60%~70% removal for PPCPs); "~" unclear

Contaminants		**Ozone Oxidation**	**Adsorption**	**Biodegradation**
Chlorinated THMs & HAAs (formation)	Chloroform	–	–	–
	Bromodichloromethane	–	–	–
	Trichloroacetic Acid	–	–	–
	Dichloroacetic Acid	–	–	–
Nitrosamines	NDMA	+	×	–
Perfluoro Alkyl Acids**	PFBS	×	–	~
	PFHpA	×	–	~
	PFNA	×	–	~
	PFOA	×	–	~
Flame Retardants*	TCEP	×	–	–
	TCPP	×	–	–
Pharmaceuticals (66 analyzed, 31 detected)	Primidone	–	×	×
	Paraxanthine	–	–	×
	Meprobamate	–	×	×
	Dilantin	–	–	×
	Nicotine	×	×	×
	Theophylline	–	–	×
	Cotinine	×	×	×
	DEET	–	–	×
	Antipyrine	–	–	×
	22 Others…	–	–	–

*Ozone oxidation could improve the adsorptive life/capacity of regenerated GAC for the PFASs and flame retardants.

- **Need further experiments to determine if the increase effluent PFASs are due to desorption or biological activities.

2.7 References

Ahrens, L., Taniyasu, S., Yeung, L. W., Yamashita, N., Lam, P. K., Ebinghaus, R, 2010. Distribution of polyfluoroalkyl compounds in water, suspended particulate matter and sediment from Tokyo Bay, Japan. Chemosphere, 79, 266-272.

Akcay, M. U., Avdan, Z. Y., Inan, H, 2016. Effect of biofiltration process on the control of THMs and HAAs in drinking water. Desalin Water Treat, 57, 2546-2554.

Allard, S., Nottle, C. E., Chan, A., Joll, C., von Gunten, U, 2013. Ozonation of iodide-containing waters: selective oxidation of iodide to iodate with simultaneous minimization of bromate and I-THMs. Water Res, 47, 1953-1960.

Andrzejewski, P., Kasprzyk-Hordern, B., Nawrocki, J, 2008. N-nitrosodimethylamine (NDMA) formation during ozonation of dimethylamine-containing waters. Water Res, 42, 863-870.

Basu, O. D., Dhawan, S., Black, K, 2016. Applications of biofiltration in drinking water treatment–a review. J Chem Technol Biot, 91, 585-595.

Benitez, F. J., Acero, J. L., Real, F. J., Roldan, G, 2009. Ozonation of pharmaceutical compounds: Rate constants and elimination in various water matrices. Chemosphere, 77, 53-59.

Benotti, M. J., Brownawell, B. J, 2009. Microbial degradation of pharmaceuticals in estuarine and coastal seawater. Environ Pollut, 157, 994-1002.

Bradley, P. M., Carr, S. A., Baird, R. B., Chapelle, F. H, 2005. Biodegradation of N-nitrosodimethylamine in soil from a water reclamation facility. Bioremediation Journal, 9, 115-120.

Calow, P, 1997. The Octanol‐Water Partition Coefficient. Oxford, UK: Blackwell Publishing Ltd.

Chang, E. E., Lin, Y. P., Chiang, P. C., 2001. Effects of bromide on the formation of THMs and HAAs. Chemosphere, 43, 1029-1034.

Chen, W., Westerhoff, P., Leenheer, J. A., Booksh, K, 2003. Fluorescence excitation− emission matrix regional integration to quantify spectra for dissolved organic matter. Environ Sci Technol, 37, 5701-5710.

EPA, 2012. Guidelines for water reuse. Washington, DC: EPA Office of Research and Development.

EPA, 2016. Lifetime health advisories and health effects support documents for perfluorooctanoic acid and perfluorooctane sulfonate. Federal Register, 81.

Eschauzier, C., Beerendonk, E., Scholte-Veenendaal, P., De Voogt, P, 2012. Impact of treatment processes on the removal of perfluoroalkyl acids from the drinking water production chain. Environ Sci Technol, 46, 1708-1715.

Farré, M. J., Reungoat, J., Argaud, F. X., Rattier, M., Keller, J., Gernjak, W, 2011. Fate of N-nitrosodimethylamine, trihalomethane and haloacetic acid precursors in tertiary treatment including biofiltration. Water Res, 45, 5695-5704.

APAH, 2005. Standard methods for the examination of water and wastewater. American Public Health Association (APHA): Washington, DC, USA.

Flores, C., Ventura, F., Martin-Alonso, J., Caixach, J, 2013. Occurrence of perfluorooctane sulfonate (PFOS) and perfluorooctanoate (PFOA) in NE Spanish surface waters and their removal in a drinking water treatment plant that combines conventional and advanced treatments in parallel lines. Sci Total Environ, 461, 618-626.

Fournier, D., Hawari, J., Halasz, A., Streger, S. H., McClay, K. R., Masuda, H., Hatzinger, P. B, 2009. Aerobic biodegradation of N-nitrosodimethylamine by the propanotroph Rhodococcus ruber ENV425. Appl Environ Microbiol, 75, 5088-5093.

Gerrity, D., Gamage, S., Holady, J. C., Mawhinney, D. B., Quiñones, O., Trenholm, R. A., Snyder, S. A, 2011. Pilot-scale evaluation of ozone and biological activated carbon for trace organic contaminant mitigation and disinfection. Water Res, 45, 2155-2165.

Gerrity, D., Gamage, S., Jones, D., Korshin, G.V., Lee, Y., Pisarenko, A., Trenholm, R.A., Von Gunten, U., Wert, E.C., Snyder, S.A, 2012. Development of surrogate correlation models to predict trace organic contaminant oxidation and microbial inactivation during ozonation. Water Res, 46, 6257-6272.

Glaze, W. H, 1986. Reaction products of ozone: a review. Environmental Health Perspectives, 69, 151.

Griffini, O., Bao, M., Barbieri, K., Burrini, D., Santianni, D., Pantani, F, 1999. Formation and removal of biodegradable ozonation by-products during ozonation-biofiltration treatment: pilot-scale evaluation. Ozone Sci Eng, 21 , 79–98.

Gunten, v, 2003. Ozonation of drinking water: Part I. Oxidation kinetics and product formation. Water Res, 37, 1443-1467.

Guo, Y. C., Krasner, S. W, 2009. Occurrence of primidone, carbamazepine, caffeine, and precursors for N-nitrosodimethylamine in drinking water sources impacted by wastewater. JAWRA Journal of the American Water Resources Association, 45, 58-67.

Hatzinger, P. B., Lewis, C., Webster, T. S, 2017. Biological treatment of N-nitrosodimethylamine (NDMA) and N-nitrodimethylamine (NTDMA) in a field-scale fluidized bed bioreactor. Water Res, 126, 361-371.

Higgins, C. P., Luthy, R. G, 2006. Sorption of perfluorinated surfactants on sediments. Environ Sci Technol, 40, 7251-7256.

Hollender, J., Zimmermann, S.G., Koepke, S., Krauss, M., Mcardell, C.S., Ort, C., Singer, H., von Gunten, U., Siegrist, H, 2009. Elimination of organic micropollutants in a municipal wastewater treatment plant upgraded with a full-scale post-ozonation followed by sand filtration. Environ Sci Technol, 43, 7862-7869.

Huang, J. Y., Wang, X., Pan, Z. Q., Li, X. K., Ling, Y., Li, L. S, 2016. Efficient degradation of perfluorooctanoic acid (PFOA) by photocatalytic ozonation. Chem Eng J, 296, 329-334.

Kaplan, D. L., Kaplan, A. M, 1985. Biodegradation of N-nitrosodimethylamine in aqueous and soil systems. Appl Environ Microb, 50, 1077-1086.

Kosaka, K., Asami, M., Konno, Y., Oya, M., Kunikane, S, 2009. Identification of antiyellowing agents as precursors of N-nitrosodimethylamine production on ozonation from sewage treatment plant influent. Environ Sci Technol, 43, 5236-5241.

Krasner, S. W., Mitch, W. A., McCurry, D. L., Hanigan, D., Westerhoff, P, 2013. Formation, precursors, control, and occurrence of nitrosamines in drinking water: a review. Water Res, 47, 4433-4450.

Li, D., Stanford, B., Dickenson, E., Khunjar, W. O., Homme, C. L., Rosenfeldt, E. J., Sharp, J. O, 2017. Effect of advanced oxidation on N-nitrosodimethylamine (NDMA) formation and microbial ecology during pilot-scale biological activated carbon filtration. Water Res, 113, 160-170.

Li, S., Lv, Y., Zhao, N, 2013. Research on phthalic acid esters removal and its health risk evaluation by combined process for secondary effluent of wastewater treatment plant. The Scientific World Journal, 2013.

Liao, X., Wang, C., Wang, J., Zhang, X., Chen, C., Krasner, S. W., SUFFET, I. M, 2014. Nitrosamine precursor and DOM control in an effluent-affected drinking water. J Am Water Works Ass, 106.

Lin, A. Y. C., Panchangam, S. C., Chang, C. Y., Hong, P. K. A., Hsueh, H. F, 2012. Removal of perfluorooctanoic acid and perfluorooctane sulfonate via ozonation under alkaline condition. J Hazard Mater, 243, 272-277.

Liu, P., Wagner, N, 1985. Thermal regeneration of granular activated carbon. Environ Prog Sustain, 4, 136-141.

Liu, T., Chen, Z. L., Yu, W. Z., You, S. J, 2011. Characterization of organic membrane foulants in a submerged membrane bioreactor with pre-ozonation using three-dimensional excitation–emission matrix fluorescence spectroscopy. Water Res, 45, 2111-2121.

Mao, Y., Guo, D., Yao, W., Wang, X., Yang, H., Xie, Y.F., Komarneni, S., Yu, G., Wang, Y, 2018. Effects of conventional ozonation and electro-peroxone pretreatment of surface water on disinfection by-product formation during subsequent chlorination. Water Res, 130, 322-332.

Marti, E. J., Dickenson, E. R., Trenholm, R. A., Batista, J. R, 2017. Treatment of specific NDMA precursors by biofiltration. J Am Water Works Ass, 109, E273-E286.

Marti, E. J., Pisarenko, A. N., Peller, J. R., Dickenson, E. R, 2015. N-nitrosodimethylamine (NDMA) formation from the ozonation of model compounds. Water Res, 72, 262-270.

Martin, J. W., Asher, B. J., Beesoon, S., Benskin, J. P., Ross, M. S, 2010. PFOS or PreFOS? Are perfluorooctane sulfonate precursors (PreFOS) important determinants of human and environmental perfluorooctane sulfonate (PFOS) exposure? Journal of Environmental Monitoring, 12, 1979-2004.

Matilainen, A., Vepsäläinen, M., Sillanpää, M, 2010. Natural organic matter removal by coagulation during drinking water treatment: a review. Advances in Colloid and Interface Science, 159, 189-197.

McKie, M. J., Taylor-Edmonds, L., Andrews, S. A., Andrews, R. C, 2015. Engineered biofiltration for the removal of disinfection by-product precursors and genotoxicity. Water Res, 81, 196-207.

Mitch, W. A., Gerecke, A. C., Sedlak, D. L, 2003. A N-nitrosodimethylamine (NDMA) precursor analysis for chlorination of water and wastewater. Water Res, 37, 3733-3741.

Mitch, W. A., Sharp, J. O., Trussell, R. R., Valentine, R. L., Alvarez-Cohen, L., Sedlak, D. L, 2003. N-nitrosodimethylamine (NDMA) as a drinking water contaminant: a review. Environ Eng Sci, 20, 389-404.

Nagel, R, 2015. Making direct potable reuse a reality. J Am Water Works Ass, 107, 76-82.

Newcombe, G, 2013. Generic management plan for nitrosamines in drinking water. London, UK: IWA Publishing.

Nunes-Halldorson, V. D., Steiner, R. L., Smith, G. B, 2004. Residual toxicity after biodegradation: interactions among benzene, toluene, and chloroform. Ecotox Environ Safe, 57, 162-167.

NWRI, 2013. Examining the criteria for direct potable reuse: recommendations of an NWRI Independent Advisory Panel. Alexandria, VA: W. R. Foundation

Park, S. H., Padhye, L. P., Wang, P., Cho, M., Kim, J.-H., Huang, C.-H, 2015. N-nitrosodimethylamine (NDMA) formation potential of amine-based water treatment polymers: Effects of in situ chloramination, breakpoint chlorination, and pre-oxidation. J Hazard Mater, 282, 133-140.

Pharand, L., Van Dyke, M. I., Anderson, W. B., Yohannes, Y., Huck, P. M, 2015. Full-Scale Ozone Biofiltration: Seasonally Related Effects on NOM Removal. J Am Water Works Ass, 107, 81-81.

Pisarenko, A. N., Marti, E. J., Gerrity, D., Peller, J. R., Dickenson, E. R. V, 2015. Effects of molecular ozone and hydroxyl radical on formation of N-nitrosamines and perfluoroalkyl acids during ozonation of treated wastewaters. Environ Sci-Wat Res, 1, 668-678.

Pisarenko, A. N., Stanford, B. D., Yan, D., Gerrity, D., Snyder, S. A, 2012. Effects of ozone and ozone/peroxide on trace organic contaminants and NDMA in drinking water and water reuse applications. Water Res, 46, 316-326.

Rahman, M. F., Peldszus, S., Anderson, W. B, 2014. Behaviour and fate of perfluoroalkyl and polyfluoroalkyl substances (PFASs) in drinking water treatment: a review. Water Res, 50, 318-340.

Rajagopal, S., Jenner, H. A., Venugopalan, V. P, 2012. Operational and Environmental Consequences of Large Industrial Cooling Water Systems: Springer US.

Rebelo, A., Ferra, I., Marques, A., Silva, M. M, 2016. Wastewater reuse: modeling chloroform formation. Environ Sci Pollut R, 23, 24560-24566.

Regnery, J., Püttmann, W, 2009. Organophosphorus flame retardants and plasticizers in rain and snow from middle Germany. CLEAN–Soil, Air, Water, 37, 334-342.

Rennecker, J. L., Marinas, B. J., Owens, J. H., Rice, E. W, 1999. Inactivation of Cryptosporidium parvum oocysts with ozone. Water Res, 33, 2481-2488.

Rhoads, K. R., Janssen, E. M.-L., Luthy, R. G., Criddle, C. S, 2008. Aerobic biotransformation and fate of N-ethyl perfluorooctane sulfonamidoethanol (N-EtFOSE) in activated sludge. Environ Sci Technol, 42, 2873-2878.

Richardson, S. D., Thruston, A. D., Caughran, T. V., Chen, P. H., Collette, T. W., Floyd, T. L, 1999. Identification of new drinking water disinfection byproducts formed in the presence of bromide. Environ Sci Technol, 33, 3378-3383.

Rittmann, B. E., Stilwell, D., Garside, J. C., Amy, G. L., Spangenberg, C., Kalinsky, A., Akiyoshi, E, 2002. Treatment of a colored groundwater by ozone-biofiltration: pilot studies and modeling interpretation. Water Res, 36, 3387-3397.

Rodriguez, E. M., Marquez, G., Leon, E. A., Alvarez, P. M., Amat, A. M., Beltran, F. J, 2013. Mechanism considerations for photocatalytic oxidation, ozonation and photocatalytic ozonation of some pharmaceutical compounds in water. J Environ Manage, 127, 114-124.

Sanderson, H., Boudreau, T. M., Mabury, S. A., Solomon, K. R, 2003. Impact of perfluorooctanoic acid on the structure of the zooplankton community in indoor microcosms. Aquatic Toxicology, 62, 227-234.

Schmidt, C. K., Brauch, H.-J, 2008. N,N-dimethylsulfamide as precursor for N-nitrosodimethylamine (NDMA) formation upon ozonation and its fate during drinking water treatment. Environ Sci Technol, 42, 6340-6346.

Shivakoti, B., Fujii, S., Nozoe, M., Tanaka, S., Kunacheva, C, 2010. Perfluorinated chemicals (PFCs) in water purification plants (WPPs) with advanced treatment processes. Water Science and Technology: Water Supply, 10, 87-95.

Siddiqui, M. S., 1992. Ozone-Bromide Interactions in Water Treatment. (Dissertation/Thesis), The University of Arizona.

Stapleton, H.M., Klosterhaus, S., Keller, A., Ferguson, P.L., van Bergen, S., Cooper, E., Webster, T.F., Blum, A, 2011. Identification of flame retardants in polyurethane foam collected from baby products. Environ Sci Technol, 45, 5323-5331.

Sundaram, V., Emerick, R. W., Shumaker, S. E, 2014. Advanced treatment process for pharmaceuticals, endocrine disruptors, and flame retardants removal. Water Environ Res, 86, 111-122.

Swietlik, J., Sikorska, E, 2004. Application of fluorescence spectroscopy in the studies of natural organic matter fractions reactivity with chlorine dioxide and ozone. Water Res, 38, 3791-3799.

Tabe, S., Yang, P., Zhao, X., Hao, C., Seth, R., Schweitzer, L., Jamal, T, 2010. Occurrence and removal of PPCPs and EDCs in the Detroit River watershed. Water practice and technology, 5, wpt2010015.

Takagi, S., Adachi, F., Miyano, K., Koizumi, Y., Tanaka, H., Watanabe, I., Tanabe, S., Kannan, K, 2011. Fate of perfluorooctanesulfonate and perfluorooctanoate in drinking water treatment processes. Water Res, 45, 3925-3932.

Telliard, W. A., United States. Environmental Protection Agency. Office of Water, 1999. EPA methods and guidance for analysis of water

Thompson, J., Eaglesham, G., Mueller, J, 2011. Concentrations of PFOS, PFOA and other perfluorinated alkyl acids in Australian drinking water. Chemosphere, 83, 1320-1325.

Volk, C. J., Lechevallier, M. W, 2002. Effects of conventional treatment on AOC and BDOC levels. J Am Water Works Ass, 94, 112-123.

von Gunten, U, 2003. Ozonation of drinking water: Part II. Disinfection and by-product formation in presence of bromide, iodide or chlorine. Water Res, 37, 1469-1487.

Wang, H. W., Wang, Y. N., Li, X. Y., Sun, Y. J., Wu, H., Chen, D. L, 2016. Removal of humic substances from reverse osmosis (RO) and nanofiltration (NF) concentrated leachate using continudusly ozone generation-reaction treatment equipment. Waste Manage, 56, 271-279.

Wang, N., Szostek, B., Buck, R.C., Folsom, P.W., Sulecki, L.M., Capka, V., Berti, W.R., Gannon, J.T, 2005. Fluorotelomer alcohol biodegradation direct evidence that perfluorinated carbon chains breakdown. Environ Sci Technol, 39, 7516-7528.

Wijekoon, K. C., Hai, F. I., Kang, J., Price, W. E., Guo, W., Ngo, H. H., Nghiem, L. D, 2013. The fate of pharmaceuticals, steroid hormones, phytoestrogens, UV-filters and pesticides during MBR treatment. Bioresource Technol, 144, 247-254.

World Health Organization, 2009. Bromide in drinking-water: background document for development of WHO guidelines for drinking-water quality.

Yan, M. Q., Wang, D. S., Ma, X. N., Ni, J. R., Zhang, H. S, 2010. THMs precursor removal by an integrated process of ozonation and biological granular activated carbon for typical Northern China water. Sep Purif Technol, 72, 263-268.

Yao, W., Rehman, S. W. U., Wang, H., Yang, H., Yu, G., Wang, Y, 2018. Pilot-scale evaluation of micropollutant abatements by conventional ozonation, UV/O3, and an electro-peroxone process. Water Res, 138, 106-117.

Yoon, Y., Westerhoff, P., Snyder, S. A., Wert, E. C., Yoon, J, 2007. Removal of endocrine disrupting compounds and pharmaceuticals by nanofiltration and ultrafiltration membranes. Desalination, 202, 16-23.

Zhang, S., Gitungo, S. W., Axe, L., Raczko, R. F., Dyksen, J. E, 2017. Biologically active filters–An advanced water treatment process for contaminants of emerging concern. Water Res, 114, 31-41.

Zhang, T., Lu, J., Ma, J., Qiang, Z, 2008. Fluorescence spectroscopic characterization of DOM fractions isolated from a filtered river water after ozonation and catalytic ozonation. Chemosphere, 71, 911-921.

Chapter 3 Mathematical Modeling of Biologically Active Filtration (BAF) for Potable Water Production Applications

(This chapter has been published as "Sun Y.W., Vaidya R., Khunjar W.O., Rosenfeldt E., Selbes M., Wilson C., Bott C.B., Titcomb M., Wang Z.W. (2019) Mathematical Modeling of Biologically Active Filtration (BAF) for Potable Water Production Applications, Water Research, 167, 115128")

3.1 Abstract

In this study, a modeling framework was developed to simulate biologically active filtration (BAF) headloss buildup in response to organic removal and nitrification. This model considered not only the biofilm growth on the BAF media but also the particle deposition in the BAF bed. In addition, the model also took temperature effect into consideration. It was calibrated and validated with data collected from a pilot-scale study used for potable water reuse and a full-scale facility used for potable water treatment. The model prediction provided insights that biofilm growth rather than particle deposition primarily contributes to the headloss buildup. Therefore, biofilm control is essential for managing headloss buildup and reducing the backwash frequency. Model simulation indicated that the BAF performance in terms of pollutant removal per unit headloss is insensitive to the BAF bed depth but can be effectively improved by increasing the media size. The partial biofilm coverage of the media was confirmed in this study and mathematically verified to be a prerequisite for the model fitness.

3.2 Keywords

BAF; granular activated carbon; headloss; backwash; biofilm;

3.3 Graphic Abstract

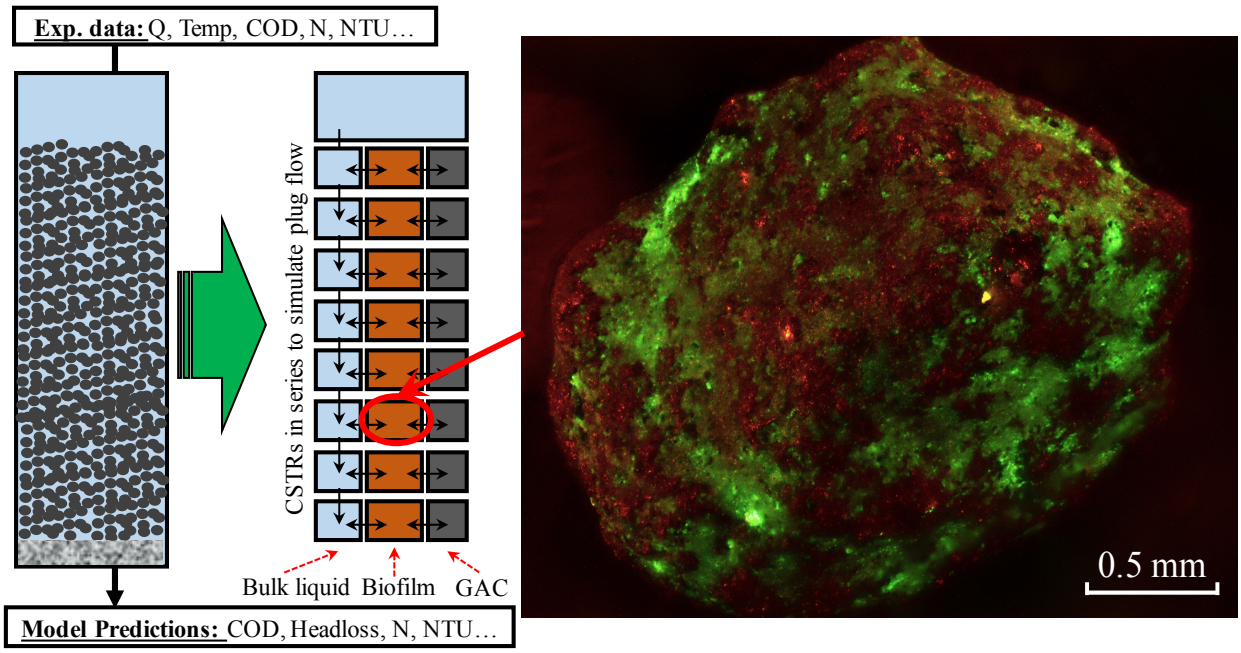

3.4 Introduction

Potable water production from water resource recovery facility effluent can employ two main approaches. The first approach relies on membrane technologies, namely microfiltration (MF), reverse osmosis (RO), ultraviolet (UV), and advanced oxidation process (AOP) in sequence (MF-RO-UV-AOP) while the second approach minimizes the use of membranes and instead uses a combination of flocculation, sedimentation, ozonation, biologically active filtration (or biologically active filter, BAF), granular activated carbon (GAC), and ultraviolet irradiation (UV) (O_3-BAF-GAC-UV) (Schimmoller et al., 2014). The O_3-BAF-GAC-UV approach has recently found significant interest with practitioners because it has the potential to generate high quality potable water at a reduced energy and chemical demand versus the MF-RO-UV-AOP approach. Further, O_3-BAF-GAC-UV configuration does not require management and disposal of brines with high total dissolved solids content (Schimmoller et al., 2014).

The BAFs within the O_3-BAF-GAC-UV configuration are important to overall treatment train performance as they utilize a combination of physical, chemical and biological processes to remove particulate, colloidal and soluble organic and nutrient materials (Bouwer et al., 1995; Evans et al., 2016; Ottengraf et al., 1983; Simpson, 2008). Although BAF is an emerging technique for potable water reuse applications, it has been an integral part of potable water treatment processes for decades (Simpson, 2008), in that it provides added benefits to polish residual organics and nutrients (Dussert et al., 1994; Zhang et al., 1996), reduce disinfectant demand (Dussert et al., 1994), and in turn diminish the undesirable disinfection by-products formation (Scholz et al., 1997). Also, potable water treatment BAF might contribute to the elimination of some contaminants of emerging concern, as well (Gerrity et al., 2011; Scholz et al., 1997; Zhang et al., 2017).

For the BAFs to function properly, it is necessary for bacteria to colonize the filtration media (often spent GAC) as biofilms (Sun et al., 2018; Takeuchi et al., 1997). During a filter run, growth of biofilm as well as removal of particulate material decrease the porosity of the BAFs, resulting in headloss buildup across the filters (Leverenz et al., 2009; Snowball, 2006). Headloss buildup in this manner decreases filter run-time, which can increase the number of filters required as well as

backwashing frequency in order to meet production demands (Amburgey et al., 2005; Moore et al., 2001; Slavik et al., 2013; Snowball, 2006). Increased backwash frequency increases energy consumption of BAF (Adams et al., 1989; Simpson, 2008) and requires between 2-5% of finished water to be reused for backwashing, therefore reducing the system productivity (Vigneswaran et al., 1996). Reduced porosity can also reduce hydraulic retention time within the filters, which can increase the potential of contaminant breakthrough in the BAF (Leverenz et al., 2009; Snowball, 2006).

Optimization of BAF therefore requires a comprehensive understanding of what impacts the physical, chemical, and biological processes as these processes are intrinsically linked to the overall treatment goals for the BAFs. Significant work has been performed to characterize particulate material removal on abiotic and biotic filters (Bablon et al., 1988; Boller et al., 1995; Davidson et al., 1978; O'Melia et al., 1979; Payatakes et al., 1974). Similarly, much work has been performed to investigate how to control the biofilm growth on BAF media surfaces by manipulating water temperature, dissolved oxygen (DO), organic content, nutrients, and pH (Brown et al., 2006; Nishijima et al., 1992; Scholz et al., 1998; Wang et al., 1995). Research has also been performed to investigate how chemical disinfectants (e.g. chlorine) can be used to manipulate biofilm growth, with varying degrees of success (Simpson, 2008).

Despite these works being performed and the fact that BAFs are widely utilized in other aspects of the water industry (e.g., wastewater denitrification, odor control scrubbers), sizing and optimization of BAFs for potable water production currently still rely on industry rules of thumbs and site-specific piloting. Technically, mathematical model can be used as an effective tool for BAF optimization, however few mechanistic modeling studies exist that link physical, chemical, and biological processes in BAFs. For instance, some previous modeling efforts focused on abiotic GAC filters (Al-Naseri et al., 2009; Clark, 1987; Han et al., 2008; Sperlich et al., 2005). Other BAF modeling work has utilized empirical models (Mann et al., 1997; Wang et al., 2006) or simplified Monod model based on single type of biomass or substrate (Chang et al., 1987; Liang et al., 2007; Shim et al., 2004). Although Rittmann et al. (2002) and Sun et al. (2017) included multiple species in their BAF model, the model did not consider headloss buildup during BAF operation and ignored plug flow pattern in bulk liquid. To the authors' knowledge, Bi et al. (2014)

and Bernier et al. (2014), are the only modeling works known to correlate BAF headloss to bacterial growth. Yet, these studies had limited datasets for model verification and also ignored both mass diffusion in the biofilms and particle deposition in the BAF bed. Consequently, the suitability of these models for describing BAF performance, both water quality and hydraulics, under dynamic operating conditions is unclear, which limits their use as an optimization tool.

This study seeks to fill this gap by developing a model that accounts for mass diffusion-governed biofilm growth kinetics, temperature effects, transformation of organics and inorganic nitrogen species, as well as the particle deposition kinetics. The model was calibrated and validated with long-term seasonal experimental data from both pilot-scale potable water reuse and full-scale potable water treatment BAFs. It was demonstrated that the model could effectively predict water quality and hydraulic performance of BAFs used to produce potable water. The model was then used to develop some insight into how BAF design and operating parameters can impact water quality and headloss development. It is envisioned that the approach undertaken in this work can help inform future engineering and scientific endeavors related to improving the design and operation of BAFs for maximizing performance and productivity within potable water and potable water reuse BAF treatment.

3.5 Materials and Methods

A combination of experimental and modeling work was performed to develop, calibrate and validate the BAF model. Data from a pilot-scale BAF employed in a potable water reuse application as well as from a full-scale potable water BAF were used in this work.

3.5.1 Model Development

As shown in Figure 3.1, for mathematical modeling purposes, the depth of the BAF bed was divided into eight continuous stirred-tank reactors (CSTRs) in this study to simulate the processes impacting soluble substrate removal, biomass growth, and turbidity removal. In each CSTR, three compartments were modeled, namely bulk liquid, biofilms, and GAC (Figure 3.1). The dissolved contaminants are assumed to transport from the bulk liquid compartment to the biofilm and GAC

compartments in each CSTR via mass diffusion in the course of their porous flow (Deshusses et al., 1995). The particulate contaminants can be removed through physical deposition in the course of porous flow through the BAF bed height. The adsorption of contaminants by BAF is ignored from this model because the spent GAC media used in BAF has exhausted almost all adsorption capacity (Sun et al., 2018; Vaidya et al., 2017). Inside the biofilm compartment, the dissolved contaminants are transformed along a diffusion gradient by attached microorganisms growing in the form of biofilms. The biofilm model is divided into nine layers to simulate the profiles of biomass growth and substrate utilization along the mass diffusion direction. The eight CSTRs are connected via bulk liquid flowing through the BAF bed between CSTRs.

3.5.2 Biological Kinetics Model

The biological kinetics model includes four types of substrates, three functional bacterial groups, as well as the production of extracellular polymeric substances (EPSs). The four types of substrates include ammonium (NH_4^+), nitrite (NO_2^-), nitrate (NO_3^-), and biodegradable organic carbon expressed as chemical oxygen demand (COD). The three functional bacterial groups comprise aerobic ammonia-oxidizing bacteria (AOB), aerobic nitrite-oxidizing bacteria (NOB), and ordinary heterotrophic organisms (OHO). The kinetic model was set up with Monod-type equations commonly used in activated sludge model No. 1 (Henze et al., 2000). The stoichiometric matrix, expressions, and parameter values used in the model are listed in Tables 3.1, 3.2, and 3.3, respectively. Since the bulk liquid in the O_3-BAF-GAC-UV treatment train is usually supersaturated with dissolved oxygen (DO > 10 mg L^{-1}), DO concentration is not considered as a limiting factor for bacterial growth and was excluded from the model for simplification. Similarly, it was assumed that denitrification and deammonification would not occur under oxygen saturated conditions. Nitrification was modeled as a two-step process; i) oxidation of NH_4^+ to NO_2^- by AOB, and ii) NO_2^- oxidation to NO_3^- by NOB, which are defined in Eq 16 and 17 presented in Table 3.2. Heterotrophic growth in this model is expressed as COD oxidation by OHO which is defined in Eq. 3.18. EPSs are formed during the growth of OHO as defined in Eq. 3.22. The temperature effect on all rate coefficients used in this study was modeled using the van't Hoff-Arrhenius relationship (Metcalf & Eddy. et al., 1979). It should be noted that both attached growth and suspended growth bacteria were modeled using similar stoichmetric and kinetic coefficients.

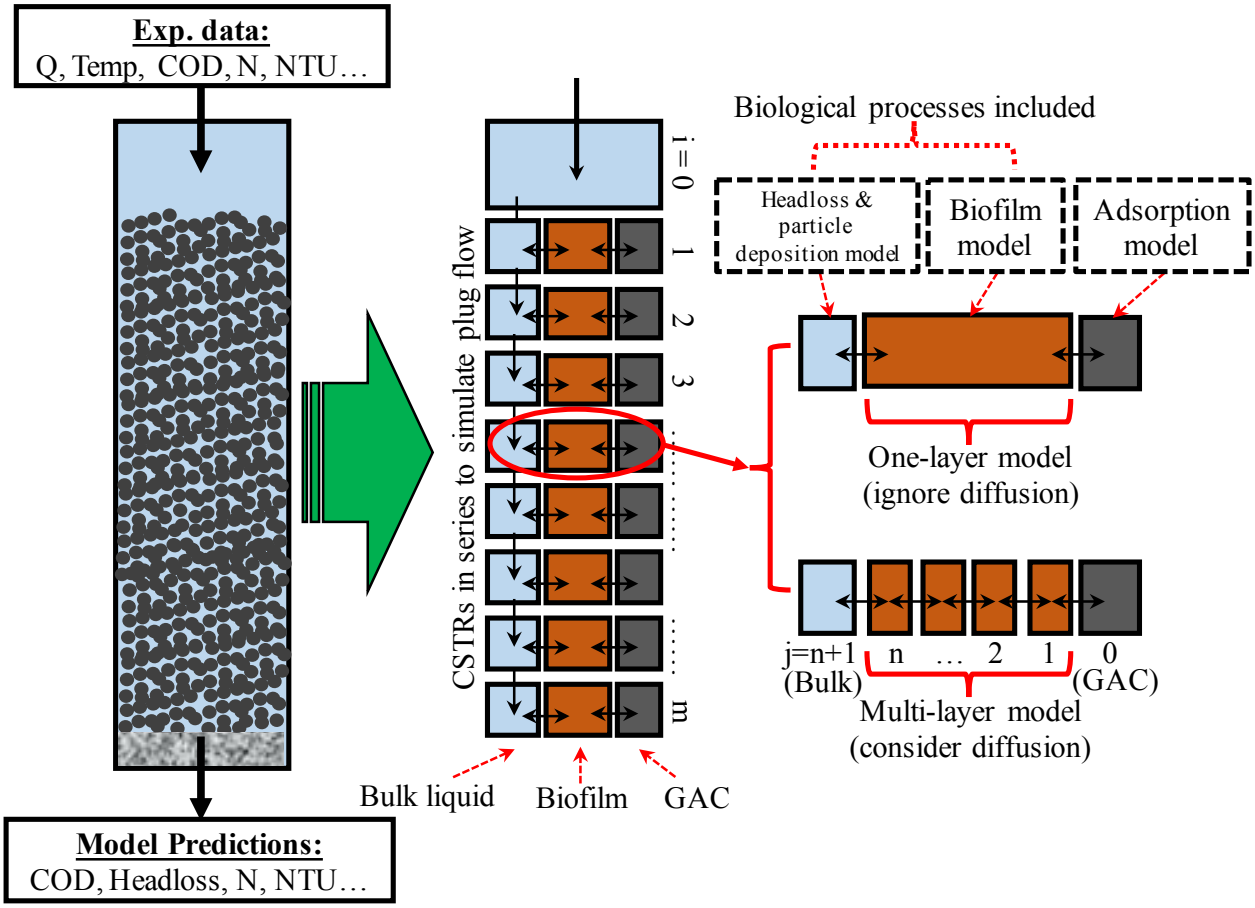

Figure 3.1 Schematic illustration of BAF model setup

3.5.2.1 Biofilm Model

The biofilm model framework is adapted from the work by Li et al. (2019). There are two substrate mass balances considered in the biofilm model, namely bulk and biofilm substrate mass balances. The bulk substrate mass balance in the i^{th} CSTR in Figure 3.1 is defined as:

$$\frac{dS_{i,bulk}}{dt} \cdot V_{R,i} = Q \cdot \left(S_{i-1,bulk} - S_{i,bulk}\right) - J_i \cdot A_f \quad \textbf{(3.1)}$$

in which $S_{i,bulk} = S_{i,n+1}$ is the bulk concentration of a substrate in CSTR i (g m^{-3}) as shown in Figure 3.1; $V_{R,i}$ is the volume of CSTR i (m^3); Q is the influent flow rate (m^3 d^{-1}); J_i is the substrate flux into the biofilms in the CSTR i (g m^{-2} d^{-1}); and A_f is biofilm surface area in CSTR i (m^2). When i = 1, $S_{i-1,bulk}$ in Eq. 3.1 becomes $S_{0,1}$ which represents the influent concentration of a given substrate.

The substrate mass balance in the biofilms of CSTR i can be defined with the differential equations in Eq. 3.2 by assuming the biofilm boundary layer thickness is negligible due to the fast, porous flow velocity in BAF.

$$\frac{dS_{i,j}}{dt} = \frac{D_f(S_{i,j-1} - S_{i,j})}{(\frac{L_i}{n})^2} - \frac{D_f(S_{i,j} - S_{i,j+1})}{(\frac{L_i}{n})^2} - r_{i,j} \quad \textbf{(3.2)}$$

in which $S_{i,j}$ (g m^{-3}) and $r_{i,j}$ (g m^{-3} d^{-1}) are the substrate concentration and the utilization rate in the layer j of the biofilm in CSTR i; L_i is the biofilm thickness in CSTR i (μm); n represents the total number of layers divided in the biofilm, and n = 9 is used in this model. When j = n, $S_{i,n+1} = S_{i,bulk}$, and when j = 1, Eq. 3.2 becomes:

$$\frac{dS_{i,1}}{dt} = -\frac{D_f(S_{i,1} - S_{i,2})}{(\frac{L_i}{n})^2} - r_{i,1} \quad \textbf{(3.3)}$$

The growth of biofilm thickness is modeled by Eq. 3.4:

$$\frac{dL_i}{dt} = \sum_{j=1}^{n} \left(\frac{dX_{i,j}}{X_f dt} - D_e\right) \cdot \frac{L_i}{n} \quad \textbf{(3.4)}$$

in which L_i is the biofilm thickness in the CSTR i (μm); $dX_{i,j}$ represents the transient biofilm density change during dt within the layer j of biofilm in the CSTR i due to biofilm growth (g COD m^{-3}); X_f denotes the biofilm density which is usually assumed as a constant (g COD m^{-3}), D_e represents the biofilm detachment rate (d^{-1}). The initial biofilm thickness right after each backwash is expressed as $L_{initial}$ and was determined using experimental data as shown in Table 3.3.

3.5.2.2 Particle Deposition Model

As noted previously, one of the main function of the BAF is the removal of particulate and colloidal material through particle deposition. The particle deposition rate ($\frac{\partial \sigma}{\partial t}$) in the BAF can be expressed according to the study by Ives (1980) as:

$$\frac{d\sigma_i}{dt} = \frac{Q}{A_R} \cdot \frac{X_{p,i-1} - X_{p,i}}{h_i} \quad \textbf{(3.5)}$$

in which Q is the inflow rate of the BAF (m^3 d^{-1}); A_R is the cross-section area of the BAF; σ_i is the specific deposit in the CSTR i (g m^{-3}) which quantifies the amount of particles deposited in unit

volume of BAF bed; h_i is the BAF bed depth in the CSTR i (m), and $X_{p,i}$ represents the total suspended solid concentration (TSS) contained in the bulk liquid of the CSTR i (g m^{-3}). $\frac{X_{p,i+1}-X_{p,i}}{h_i}$ can be expressed by using Eq. 3.6,

$$\frac{X_{p,i+1}-X_{p,i}}{h_i} = -\lambda_i \cdot X_{p,i} \quad \textbf{(3.6)}$$

in which λ_i is a filtration coefficient of the CSTR i (m^{-1}) which, according to the study by Ives (1980), can be written as:

$$\lambda_i = \lambda_0 + a_1 \cdot \sigma_i - \frac{a_2.{\sigma_i}^2}{\varepsilon_i} \quad \textbf{(3.7)}$$

in which λ_0 is the initial filtration coefficient (m^{-1}), a_1 and a_2 are fitted empirical parameters, and ε_i is the porosity of the CSTR i.

Typically, data collected from BAFs assume a correlation between turbidity (τ) and TSS. In this work, τ translation to TSS was performed by using the following relationship described in previous literatures (Hannouche et al., 2011; Packman et al., 1999):

$$X_{p,i} = c \cdot \tau_i + e \quad \textbf{(3.8)}$$

in which c and e are unique coefficients that need to be calibrated from the experimental datasets.

3.5.2.3 Headloss Model

Both the biofilm growth and particle deposition within BAF bed lead to the porosity decrease, which increases headloss. According to previous studies (Bi et al., 2014; Page et al., 2006; Pushnov, 2006), the decrease of porosity caused by the biofilm growth and particle deposition can be expressed in Eq. 3.9:

$$\varepsilon_i = \varepsilon_0 - \frac{A_{f,i} \cdot L_i}{V_{R,i}} - \sigma_i \cdot b_p \quad \textbf{(3.9)}$$

in which ε_0 and ε_i represent the initial and current BAF bed porosities in the CSTR i with volume $V_{R,i}$ (m^3); $A_{f,i}$ is the biofilm surface area of the CSTR i (m^2); b_p is a bulk factor (m^3 g^{-1}) that measures the possible deposit volume after the deposition (Ojha et al., 1993). According to Pushnov (2006), ε_0 can be estimated by using Eq. 3.10,

$$\varepsilon_0 = \frac{1}{\left(\frac{1000 \cdot D}{d}\right)^2} + 0.375 \quad \textbf{(3.10)}$$

in which D denotes the cross-section diameter of the BAF (m), and d represents the effective size of BAF media in diameter (mm). Both D and d values are listed Table 3.4. Thereby, headloss (H) can be expressed with Kozeny-Carman equation as:

$$H_i = \frac{180 \cdot \mu_{s,i} \cdot (1 - \varepsilon_i)^2 \cdot Q \cdot V_{R,i}}{\phi^2 \cdot d^2 \cdot {\varepsilon_i}^3 \cdot {A_R}^2} \quad \textbf{(3.11)}$$

in which $\mu_{s,i}$ represents the viscosity of the bulk liquid in the CSTR i, which can be corrected with the viscosity of water (μ_w) as $\mu_{s,i} = \mu_w \cdot 1.05 \cdot e^{0.08 \cdot X_{p,i}}$ as reported by Bi et al. (2014); and ϕ is the sphericity of the BAF media.

3.5.2.4 Biofilm Coverage

In this model, we assumed that BAF media is only partially covered by biofilms, which can be described by a coverage factor (η) in Eq. 3.12:

$$A_{f,i} = \eta \cdot \alpha_B \cdot V_{B,i} \quad \textbf{(3.12)}$$

in which α_B is specific surface area of BAF media ($m^2\ m^{-3}$) estimated in Eq. 3.13 by using ϕ, and $V_{B,i}$ is the total volume of the BAF bed in CSTR i excluding the porous space as expressed in Eq. 3.14 (m^3):

$$\alpha_B = \frac{3}{d \cdot \phi} \quad \textbf{(3.13)}$$

$$V_{B,i} = V_{R,i} \cdot (1 - \varepsilon_0) \quad \textbf{(3.14)}$$

Table 3.1 Stoichiometric matrix of the multipopulation biofilm model

Processes	Components								
	S_S gCOD m^{-3}	S_{NH4} g N m^{-3}	S_{NO2} g N m^{-3}	S_{NO3} g N m^{-3}	X_I gCOD m^{-3}	X_{AOB} gCOD m^{-3}	X_{NOB} gCOD m^{-3}	X_{OHO} gCOD m^{-3}	X_{EPS} gCOD m^{-3}
Growth									
X_{AOB}		$-i_{NXB} - 1/Y_{AOB}$	$1/Y_{AOB}$			1			
X_{NOB}		$-i_{NXB}$	$-1/Y_{NOB}$	$1/Y_{NOB}$			1		
X_{OHO}	$-1/Y_{OHO}$	$-i_{NXB}$						1	Y_{EPS}
Decay									
X_{AOB}					1	-1			
X_{NOB}					1		-1		
X_{OHO}					1			-1	
X_{EPS}									-1

Table 3.2 Process rates of the multipopulation biofilm model (corresponding to Table 3.1)

Process	**Process Rate r**	
	Biomass growth	
X_{AOB}	$\mu_{max,AOB} X_{AOB} \frac{S_{NH_4^+}}{K_{NH_4^+,AOB} + S_{NH_4^+}}$	(**3.15**)
X_{NOB}	$\mu_{max,NOB} X_{NOB} \frac{S_{NO_2^-}}{K_{NO_2^-,NOB} + S_{NO_2^-}}$	(**3.16**)
X_{OHO}	$\mu_{max,OHO} X_{OHO} \frac{S_S}{K_{S,OHO} + S_S}$	(**3.17**)
	Biomass decay	
X_{AOB}	$b_{AOB} X_{AOB}$	(**3.18**)
X_{NOB}	$b_{NOB} X_{NOB}$	(**3.19**)
X_{OHO}	$b_{OHO} X_{OHO}$	(**3.20**)
	EPS	
Growth	$Y_{EPS} \mu_{max,OHO} X_{OHO} \frac{S_S}{K_{S,OHO} + S_S}$	(**3.21**)
Decay	$b_{EPS} X_{EPS}$	(**3.22**)

Table 3.3 Model parameters

Symbol	Unit	Description	Value	Source
		Biological kinetics process		
Ammonium oxidizing bacteria (AOB)				
$\mu_{max,AOB}$	d^{-1}	maximum specific growth rate of AOB	2.05	(Wiesmann, 1994)
Y_{AOB}	gCOD gN^{-1}	growth yield of AOB	0.15	(Wiesmann, 1994)
$K_{NH_4^+,AOB}$	gN m^{-3}	half saturation constant for AOB	2.40	(Wiesmann, 1994)
b_{AOB}	d^{-1}	decay rate of AOB	0.13	(Wiesmann, 1994)
i_{NXB}	gN $gCOD^{-1}$	ammonium yield for cell synthesis	0.092	(Henze et al., 2000)
Nitrite oxidizing bacteria (NOB)				
$\mu_{max,NOB}$	d^{-1}	maximum specific growth rate of NOB	1.45	(Wiesmann, 1994)
Y_{NOB}	gCOD gN^{-1}	growth yield of NOB	0.041	(Wiesmann, 1994)
$K_{NO_2^-,NOB}$	gN m^{-3}	half saturation constant for NOB	5.5	(Koch et al., 2000)
b_{NOB}	d^{-1}	decay rate of NOB	0.06	(Koch et al., 2000)
Ordinary heterotrophic organisms (OHO)				
$\mu_{max,OHO}$	d^{-1}	maximum specific growth rate of OHO	6.0	(Henze et al., 2000)
Y_{OHO}	gCOD $gCOD^{-1}$	growth yield of OHO	0.67	(Henze et al., 2000)
$K_{S,OHO}$	gCOD m^{-3}	half saturation constant for OHO	20	(Henze et al., 2000)
b_{OHO}	d^{-1}	decay rate of OHO	0.62	(Henze et al., 2000)
Extracellular polymeric substance (EPS)				
Y_{EPS}	gCOD $gCOD^{-1}$	yield of EPS	0.289	(Lee et al., 2007)
b_{EPS}	d^{-1}	decay rate of EPS	0.336	(Lee et al., 2007)
		Biofilm model		
$D_{NH_4^+}$	m^2 d^{-1}	diffusivity of NH_4^+ in water	1.5×10^{-4}	(Williamson et al., 1976)
$D_{NO_2^-}$	m^2 d^{-1}	diffusivity of NO_2^- in water	1.4×10^{-4}	(Williamson et al., 1976)
$D_{NO_3^-}$	m^2 d^{-1}	diffusivity of NO_3^- in water	1.4×10^{-4}	(Williamson et al., 1976)
D_S	m^2 d^{-1}	diffusivity of COD in water	1.0×10^{-4}	(Hao et al., 2004)
X_T	kgCOD m^{-3}	biofilm density	60	(Alonso et al., 2001)
$L_{initial}$	μm	biofilm thickness after backwash	38[1]; 86[2]	Regressed
D_e	d^{-1}	biofilm detachment rate	7.5×10^{-8}[1] ;0[2]	Regressed
η	N/A	BAF media biofilm coverage factor	30%[1]; 45%[2]	Regressed
		Particle deposition model		
λ_0	d^{-1}	initial filtration coefficient	6.3×10^{-4}[1]	Regressed
a_1	N/A	fitted empirical parameters	300[1]	Regressed
a_2	N/A	fitted empirical parameters	1000[1]	Regressed
		Headloss model		
b_p	m^3 g^{-1}	bulk factor of particle deposition	10^{-5}	(Ojha et al., 1993)
ϕ	N/A	sphericity of the BAF media	0.7[1,2]	Regressed

1: regressed based on pilot-scale potable water reuse BAFs data; 2: regressed based on full-scale potable water treatment plant BAF data

3.5.3 Experimental Design and Datasets

3.5.3.1 Potable Water Reuse Dataset

BAFs in two pilot-scale treatment trains consisting of coagulation/flocculation/sedimentation, O_3-BAF-GAC-UV were operated at Hampton Roads Sanitation District (HRSD) York River Plant (Seaford, VA, USA) and were used to generate experimental data for model calibration and validation for this study. The influent to the pilot system is tertiary treated (TN < 3 g N m^{-3}, TP < 0.3 g P m^{-3}) effluent from an existing full-scale biological nitrogen removal treatment plant. The basic design and operation information of the two BAFs such as dimension, flow rates, empty bed contact times (EBCTs), and media sizes can be referred to Table 3.4. The biologically activated carbon (BAC) (Calgon F816, Moon Township, PA, USA) used in the two BAFs was pre-exhausted using membrane bioreactor effluent offsite to the point of steady state total organic carbon (TOC) removal (30% TOC removal) prior to pilot operation (Vaidya et al., 2017). This helped exhausting the adsorptive capacity of the activated carbon media and ensured that TOC removal was largely due to biological growth on the media. The BAFs are backwashed when either the turbidity is above 0.1 NTU or the headloss is above 0.3 m. The effluent from GAC filtration columns of the pilot is used as the backwash water for the BAFs.

3.5.3.2 Potable Water Treatment Dataset

To verify the general predictability of the model developed in this study, the experimental data from one of the BAFs in a full-scale potable water treatment plant (Newport News, VA, USA) were also used this study (Table 3.4). The source water of this potable water treatment plant is reservoir surface water, and the upstream processes of BAF include coagulation/flocculation, dissolved air floatation, and ozonation. The basic design and operational parameters of the full-scale BAFs such as dimension, flow rates, EBCTs, and the media sizes can be referred to Table 3.4. BAFs are backwashed when (i) the turbidity is above 0.1 NTU in two consecutive recorded values at 15-min intervals, or (ii) the headloss is above 2.0 m, or the filter run time has reached 120 hours. The finished water (effluent of BAFs) is used as the backwash water for the BAFs.

Table 3.4 BAF design and operational parameters, and model verification strategies

Datasets	BAF design and operational parameters						Model verification strategy	
	EBCT (min)	**Bed depth (m)**	**Surface dimensions**	**Surface loading rate ($m\ d^{-1}$)**	**Flowrate ($m^3\ d^{-1}$)**	**Effective media size (mm)****	**Calibration**	**Validation**
Pilot-scale potable water reuse treatment	5	1.52	0.15 m diameter	440	8	1.40	Headloss & TSS (summer)	Headloss (winter) and COD, nitrogen profiles (summer and winter)
	10			220	4		N/A	Headloss (summer) and COD, nitrogen profiles (summer)
Full-scale potable water treatment	20	0.71	6.17 m×5.18 m×2*	59	3754	0.95	Headloss (summer)	Headloss (winter)

* One filter basin has two (2) cells each with dimensions of 6.17 m and 5.18 m

** Biologically active media, e.g. BAC or anthracite

3.5.4 Analytical Methods

TOC, dissolved organic carbon (DOC), NH_4^+-N, NO_3^--N, and NO_2^--N were measured according to the standard methods (APHA, 1998). Pilot-scale BAFs were purchased from Intuitech™ (Salt Lake City, UT, USA). Headloss, temperature, and turbidity were real-time monitored by using pressure transmitters (IFM Efector PX3227, Malvern, PA, USA), thermometers (Thermo Scientific PH21A1A2, Waltham, MA, USA), and turbidimeters (HACH, Loveland, CO, USA) every 5 min in the pilot-scale study. These parameters were also monitored in real-time in the full-scale study but recorded every 15 min. The BAC samples for fluorescent imaging were collected from the inlet and outlet of the pilot-scale potable water reuse BAFs and fixed with 4% paraformaldehyde solution immediately following the sample collection. Then, the BAC samples were stained with the cell permeable nucleic acid dye, SYTO 9 (Grand Island, NY, USA), for visualizing the microbial distribution. The fluorescent images were visualized by using a Nikon Eclipse E200 microscope (Melville, NY, USA).

3.5.5 Influent Organic Composition

The model framework uses COD as the basis for tracking organic carbon behavior. This approach is consistent with biological process modeling used within the activated sludge field. In this work, and at many facilities operating BAFs, TOC but not COD is routinely measured to address permit requirements. In this work, the correlation between TOC (mg L^{-1}) and COD (mg L^{-1}) was expressed by using Eq. 3.23. This linear correlation was developed from experimental data utilized in this work.

$$\mathrm{COD} = 2.91 \cdot \mathrm{TOC} + 0.2249 \quad \textbf{(3.23)}$$

The COD in Eq. 3.1 includes both particulate and soluble COD. Based on the experimental data used for model calibration, the differences between TOC and DOC are less than 5%, hence the particulate COD can be approximately regarded as less than 5% of the total COD. The removal of particulate COD was ascribed to the particle deposition in this study because the EBCT and backwash interval used in this study are assumed to be too short for appreciable particulate COD hydrolysis by bacteria (Veeken et al., 1999). The soluble COD is further categorized into both biodegradable and non-biodegradable fractions. Soluble COD transformation is assumed to be

relevant to the biodegradable fraction only in this study. Because ultimate biodegradability tests were not performed, it was necessary to make an assumption of the biodegradable fraction of the soluble COD. In this study, we assumed that the soluble COD present in the effluent of the BAF operating at an EBCT of 10 min under summer condition is not readily biodegradable. Further refinement of this assumption is necessary in future work through direct experimentation and measurement.

3.5.6 Model Calibration and Validation

The model was framed with equations in appendix by using MATLAB 8.6 (MathWorks, Inc., Natick, MA). Parameters without values were regressed by minimizing the sum of squares of the deviations between the measured and the simulated data. The model was calibrated and validated by using separate datasets. The design and operational parameters as well as the model calibration and validation strategies are summarized in Table 3.4.

As shown in Table 3.4, the model calibration of potable water reuse data was performed by using the headloss data from the summer operation of the pilot BAF operated at 5 min EBCT. Out of over 250,000 total data points collected, 8,314 data points of headloss and turbidity within 12 consecutive days during summer were used to regress seven unknown parameters listed in Table 3.3 to calibrate the model. In order to validate the accuracy of the calibrated model, and determine its sensitivity to temperature and EBCT effects, model validation was performed using three separate datasets. The first validation effort was performed by using headloss data from the summer operation of the potable water reuse pilot BAF operated at 10 min EBCT. The second validation effort used headloss data from winter operation of a BAF operated at 5 min EBCT. The third validation effort used water quality data from summer and winter operation and focused on matching TOC removal and nitrogen turnover along the BAF bed depth as well as in the effluent from the BAF.

The model was also calibrated and validated by using data collected from the full-scale BAF treatment train from the potable water treatment plant. A similar calibration and validation procedure was performed as described above and summarized in Table 3.4. Briefly, data collected

during 11 consecutive summer days were used for model calibration, while 16 consecutive days of winter headloss profiles were utilized for model validation. In the full-scale facility, only influent and effluent contaminant concentrations were available for use.

3.6 Results

3.6.1 Model prediction of headloss is sensitive to the biofilm coverage of BAF media

Calibration of the model required regression fitting of seven parameters linked to the biofilm component (biofilm thickness after backwash, biofilm detachment rate, biofilm coverage factor), particle deposition component (initial filtration coefficient, two empirical parameters), and headloss component (sphericity of BAF media) as shown in Table 3.3. Once these parameters were regressed, the model predicted headloss profiles and turbidity removal very well for the 5 min EBCT potable water reuse pilot data ($R^2 = 0.96$, Figure 3.2a and b). When applied to the full-scale potable water treatment BAF, the calibrated model also described summer headloss data similarly well ($R^2 = 0.94$, Figure 3.2e). It is noteworthy that, out of the seven regressed parameters in Table 3.3, four share exactly the same values between the potable water reuse pilot-scale and the potable water treatment full-scale model while the remaining three, namely biofilm thickness after backwash, biofilm coverage factor, and biofilm detachment rate, are slightly different (Table 3.3), which indicates there is no fundamental difference between the BAFs used for producing potable reuse water and potable water.

During calibration, it was initially assumed that the biofilm coverage factor was equal to 100%. This was consistent with prior work documented by Shen et al. (2012). However, assuming 100% coverage resulted in the model overpredicting the rate of headloss development versus the experimental data profiles. It was necessary to reduce the biofilm coverage factor to 30% and 45% for the potable water reuse pilot- and the potable water treatment full-scale calibration efforts, respectively. To confirm this hypothesis, BAF media from the inlet and outlet of the potable water reuse pilot BAF was microscopically visualized. The fluorescent images in Figure 3.3 revealed that those BAF media were indeed partially covered by biofilms, which is in line with the model prediction in this works and supports a previous report by Weber et al. (1978). Further, it can be

seen from Figure 3.3 that biofilm coverage was higher at the BAFs inlet than at the outlet. This further supports the biofilm thickness profiles predicted by the model and illustrated in Figure 3.4.

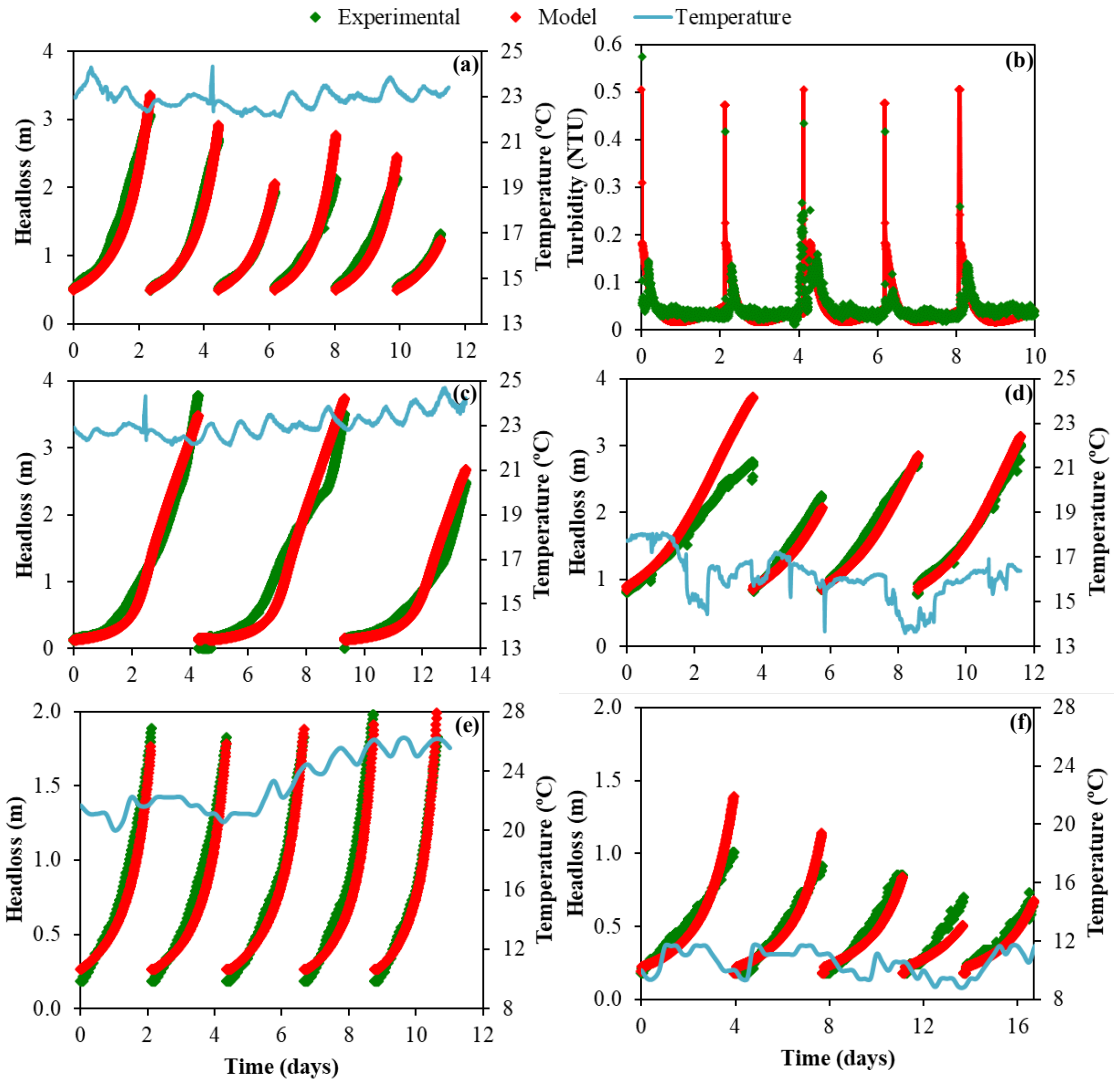

Figure 3.2 Model calibration with (a) headloss and (b) turbidity data from the BAF in a pilot-scale O_3-BAF-GAC treatment train operated with 5 min EBCT in summer; and model validation with headloss data collected from the same pilot BAF operated with (c) 10 min EBCT in summer and (d) 5 min EBCT in winter, respectively. Model calibration with (e) summer headloss data from a full-scale BAF operated with 20 min EBCT in a local water treatment plant, and model validation with (f) headloss data from the same full-scale BAF operated in the winter.

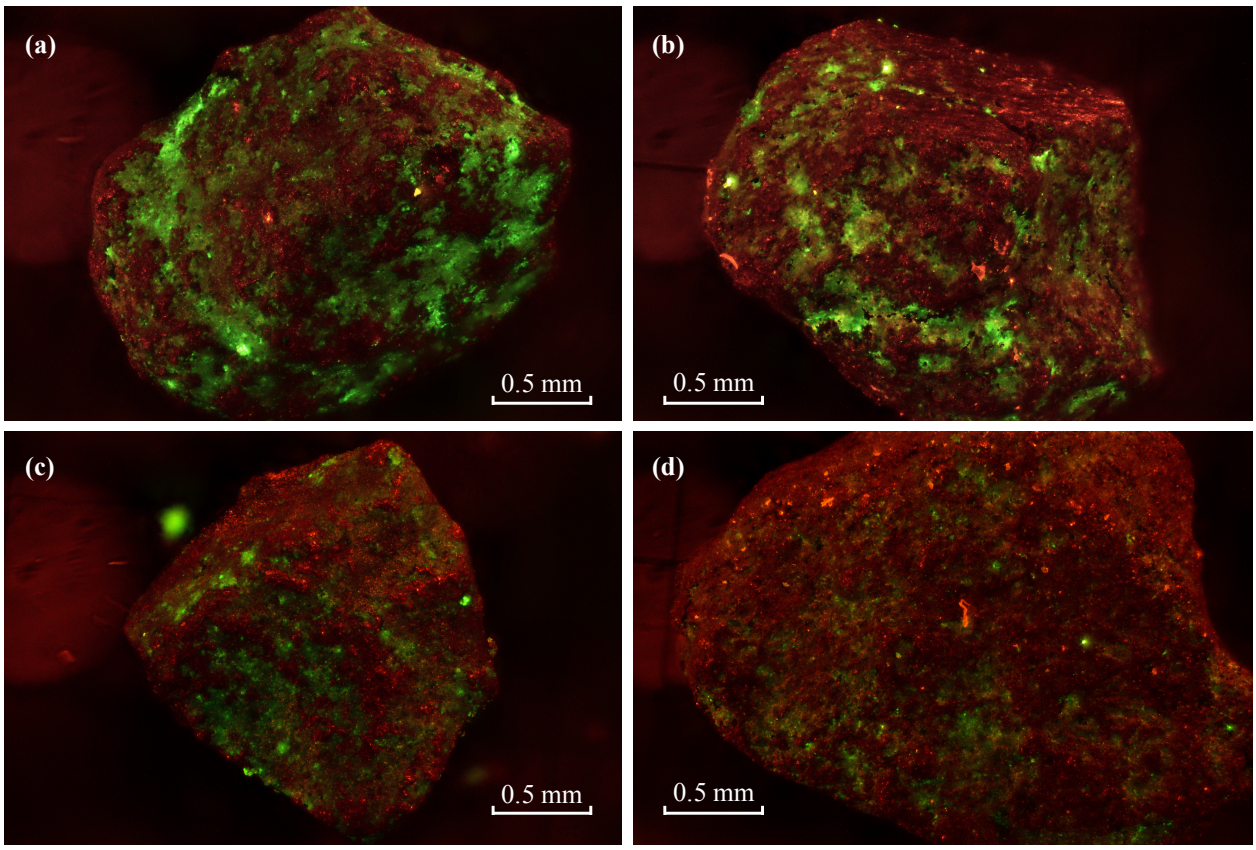

Figure 3.3 Microscopic visualization of the biofilm coverage (green) on pilot-scale potable water reuse BAF media (red) collected from the inlet of BAFs operated with (a) 5 and (b) 10 min EBCTs and the outlet with (c) 5 min and (d) 10 min EBCTs, respectively

3.6.2 Model prediction of the EBCT and temperature effects on headloss, TOC, and nitrogen profiles

To validate the model prediction, the calibrated models were then used to predict headloss development and water quality for: i) winter operation of the pilot BAF at 5 min EBCT and ii) summer operation of a BAF operated at 10 min EBCT (Figure 3.2c and d). No further adjustments were made to regressed values from the calibration effort in Table 3.3. Results indicate that the model calibrated to the potable water reuse pilot readily predicts both headloss development in the BAF (R^2 = 0.96 and 0.92). The model calibrated using the full-scale BAF was also validated by using the winter headloss data. Again, very good agreement was reached between the model prediction and actual experimental data in Figure 3.2f (R^2 = 0.95). The good fitness in Figure 3.2c,

d, and f confirms that the calibrated models are effective for predicting headloss development at different EBCTs and temperatures.

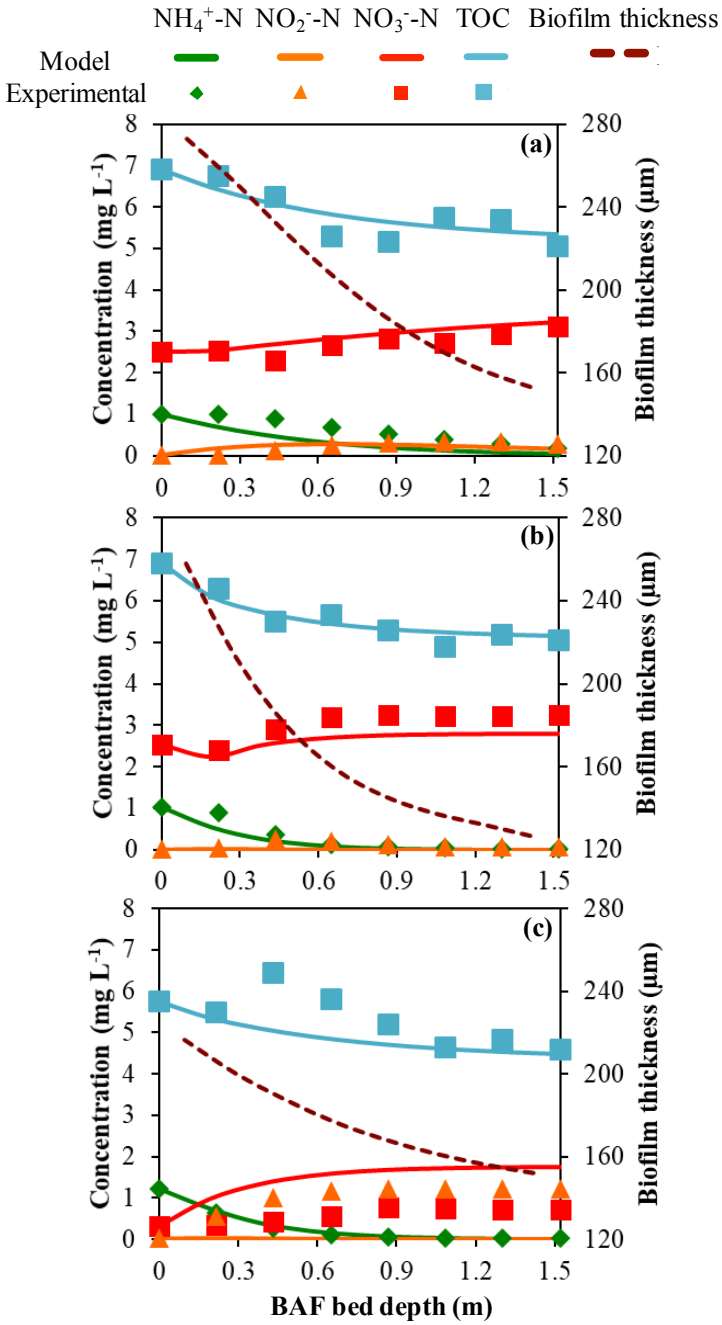

Figure 3.4 Model predicted biofilm thickness and model validation by comparing simulated TOC and nitrogen profiles to those of the experimental data collected from the pilot-scale potable water reuse BAFs operated with (a) 5 and (b) 10 min EBCTs in summer, as well as (c) 5 min EBCT in winter.

The model outputs of organic and nutrient removal were also compared with the TOC and nitrogen transformation profiles measured along the BAF bed depth at different EBCTs for the potable water reuse pilot in Figure 3.4. It can be seen that the model predicted summer TOC and nutrient profiles fit the experimental data very well in Figure 3.4a and b (e.g. R^2 for TOC, NH_4^+, and NO_3^- are 0.83, 0.85, and 0.81 when EBCT = 5 min, and 0.96, 0.91, and 0.89 when EBCT = 10 min, respectively). For winter data, both predicted and measured TOC and NH_4^+ data matched well in Figure 3.4c (R^2 for TOC and NH_4^+ are 0.70 and 0.99, respectively). However, predicted profiles of NO_2^- and NO_3^- did not match for the winter condition. This is because NO_2^- accumulation was observed in the potable water reuse pilot (Figure 3.4c); however, the current model did not adequately describe this transient nitrite accumulation. Despite this limitation, it was determined that the current models were suitable for examining how design and operational parameters may impact BAF performance as related to headloss development, as well as TOC and NH_4^+ removal.

3.7 Discussion

The calibrated and validated models were used to investigate how design and operational parameters can be optimized to enhance BAF performance as related to headloss development, organics (COD or TOC) and NH_4^+ removal. For this investigation, the model influent was set as following according to the average influent composition of the potable water reuse pilot BAFs in HRSD: total soluble organics: 15.48 mg L^{-1} COD (5.24 mg L^{-1} TOC); biodegradable soluble organics: 4.49 mg L^{-1} COD; NH_4^+: 1.05 mg N L^{-1}; NO_2^-: 0.01 mg N L^{-1}; NO_3^-: 1.56 mg N L^{-1}; turbidity: 0.5 NTU (except section 4.1). A BAF surface loading rate of 220 m^3 d^{-1} m^{-2} and the temperature of 25˚C was adhered to in the optimization simulations.

3.7.1 Biofilm growth is a significant contributor to headloss development in BAFs treating low turbidity water

It is known that the headloss buildup can be attributed to both biofilm growth and particle deposition as described in Eqs. 3.9 to 3.11 (Moore et al., 2001; Shen et al., 2012; Simpson, 2008); however, the respective contribution of these two factors is still unknown. According to Eq. 3.9,

even if all the influent particles, corresponding to a turbidity of 0.5 NTU, were trapped by the BAF bed as reflected in the specific deposit (σ_i), they can only lower the bed porosity by 0.5%. This suggests that particle deposition is likely a minor contributor to headloss in the potable water reuse pilot- and potable water treatment full-scale BAFs investigated in this study. We hypothesize that this phenomenon is attributed to the low influent turbidity of the potable reuse water and potable water. To validate this hypothesis, the validated model was used to predict the contribution of biofilm growth and particle deposition to the headloss at different influent turbidities after 72-hour of BAF run time as described in Figure 3.5. Results indicate that particle deposition can contribute between 1% and 15% of the overall headloss development when influent turbidity ranges from 0.5 to 15 NTU. This seems to suggest that biofilm growth can be a significant contributor to headloss development in BAF especially when the influent turbidity is low (Figure 3.5).

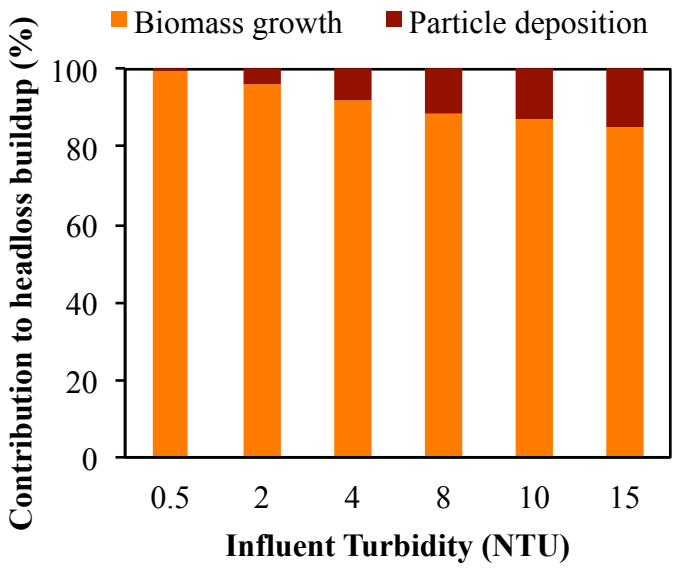

Figure 3.5 Model predicted contribution of biofilm growth and particle deposition to headloss buildup at different influent turbidity after 72-hour of BAF run time. Surface loading rate: 220 $m^3\ d^{-1}\ m^{-2}$; BAF bed depth: 2.2 m; BAF media size: 1.4 mm; and influent characteristics: 15.48 mg L^{-1} total soluble COD, 4.49 mg L^{-1} biodegradable soluble COD, 1.05 mg NH_4^+-N L^{-1}, 0.01 mg NO_2^--N L^{-1}, 1.56 mg NO_3^--N L^{-1}, temperature = 25˚C

3.7.2 Effects of the BAF media size and bed depth on BAF performance

Media size and bed depth are two parameters that can be manipulated in the design of a BAF. The typical effective media size is usually between 0.9 to 1.4 mm for potable water treatment (Page et al., 2006) and from 1.5 to 6 mm for potable water reuse and wastewater treatment (Moore et al., 2001). The typical BAF bed depth is usually from 0.9 to 1.5 m. Thus, effects of these two parameters on some important indicators of the BAF performance were investigated.

3.7.2.1 Effect of the BAF media size on headloss buildup

As shown in Figure 3.6a, headloss will drop over 90% after 72-hour BAF run time as the BAF media size increases from 0.9 to 2.8 mm. This indicates that using larger BAF media can help slow headloss development. The experimental results from the study by Moore et al. (2001) support this model prediction as they measured that when the organic loading rate is 8.1 kg COD m^{-3} d^{-1}, the headloss development in small medium (1.5-3.5 mm) filter is two times faster than that in large medium (2.5-4.5 mm) filter. This phenomenon can be explained by the effect of BAF media size on empty bed porosity and biofilm thickness. According to Eq. 3.10, the empty bed porosity will increase as the BAF media size increase, and thus the headloss will decrease accordingly (Eq. 3.11). As shown in Figure 3.7, the surface area available for biofilm coverage, namely A_f, should decrease as the BAF media size increases. This should increase influent substrate availability, namely biofilm surface loading rate. A higher biofilm surface loading rate may then result in faster development of biofilm thickness ($\frac{dL}{dt}$; Eq. 3.4). Interestingly, simulations indicate that the growth rate of total biofilm volume in the filtration bed, $\frac{dL}{dt} \cdot A_f$, decreases as the BAF media size increases. This is because the surface area available for biofilm coverage (A_f) decreases more rapidly than the increase of biofilm thickness ($\frac{dL}{dt}$). This helps to explain the headloss reduction observed as media size increase (Figure 3.6a).

3.7.2.2 Effect of the BAF bed depth on headloss buildup

Results in Figure 3.6a indicated that increasing BAF bed depth will only slightly increase the headloss. For example, the headloss only increases from 2 to 2.5 m after 72-hour BAF run time as BAF bed depth increases from 0.9 to 1.5 m when 1.4 mm BAF media is used. This phenomenon

can be ascribed to the fact that biofilms primarily grow at the inlet side of the BAF (i.e., top layers of the BAF media) as visualized in the Figure 3.3 and model predicted in Figure 3.4. For this reason, further increasing bed depth of the BAF bed has very limited effect on the headloss due to the lack of biofilm growth in the deeper sections of the bed (Figure 3.6a).

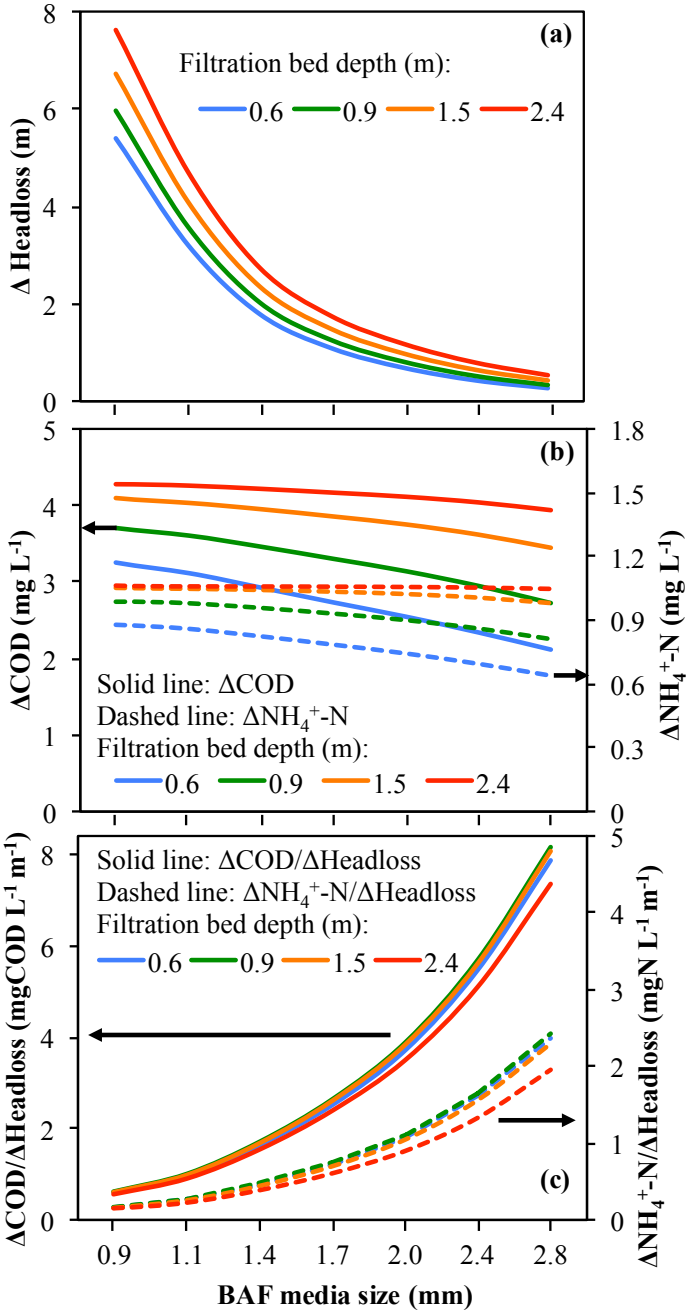

Figure 3.6 Model predicted effects of BAF media size and bed depth on (a) headloss buildup (Δheadloss); (b) average COD removal (ΔCOD) and nitrification (ΔN); and (c) ΔCOD/Δheadloss and ΔN/Δheadloss after 72-hour of BAF run time. Surface loading rate: 220 m^3 d^{-1} m^{-2}; Influent

characteristics: 15.48 mg L^{-1} total soluble COD, 4.49 mg L^{-1} biodegradable soluble COD, turbidity: 0.5 NTU, 1.05 mg NH_4^+-N L^{-1}, 0.01 mg NO_2^--N L^{-1}, and 1.56 mg NO_3^--N L^{-1}, temperature = 25°C

3.7.2.3 Effects of BAF media size and bed depth on organic removal and nitrification

As shown in Figure 3.6b, increasing BAF media size tends to decrease the efficiencies of COD removal (ΔCOD) and ammonium removal (ΔNH_4^+-N), which concurs with the experimental observation by Moore et al. (2001). A primary reason lies in the reduction of biofilm surface area, A_f, as BAF media size increases. This acts to reduce the biological reaction rates as shown in Figure 3.7. The increases in the ΔCOD and ΔNH_4^+-N with greater BAF bed depth can also be seen from the Figure 3.6b and have been observed in practice by numerous prior studies (LeChevallier et al., 1992; McDowell et al., 2006). When examining impacts on nitrification, it can be seen that increasing BAF bed depth beyond 1.5 m did not appear to further increase ΔNH_4^+-N under the loading conditions used in this study. This finding is important in that it implies that nitrifiers (AOB or NOB) can outcompete OHOs in water treated for potable water reuse, which usually comes with extremely low COD/N ratios, e.g. 1.7 in this study.

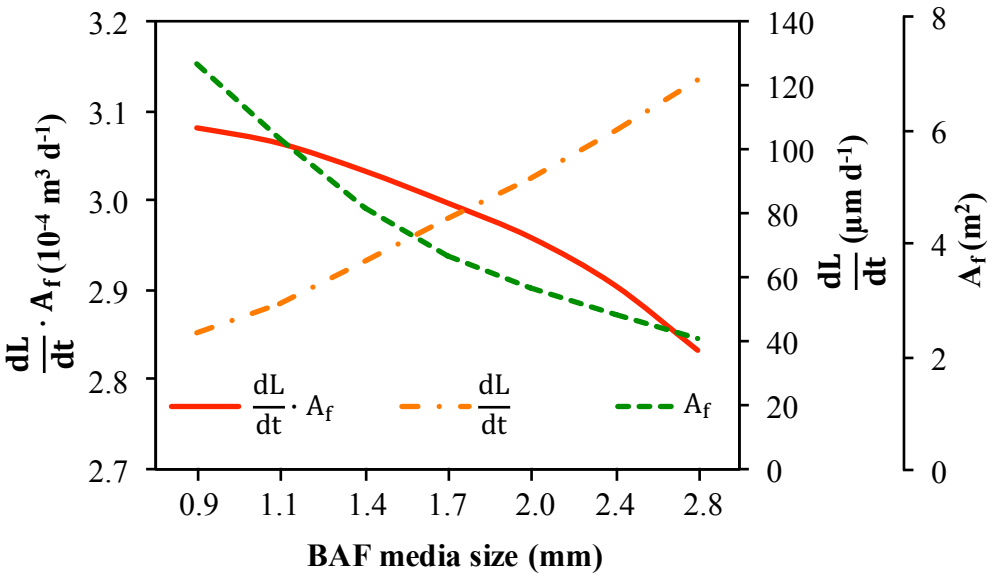

Figure 3.7 Model predicted BAF media size-dependent growth rates of biofilm volume ($\frac{dL}{dt} \cdot A_f$) and thickness ($\frac{dL}{dt}$), as well as the biofilm coverage (available surface area for biofilm, A_f) during

72-hour of BAF run time. Influent total soluble organic: 15.48 mg L^{-1} COD, biodegradable soluble organic: 4.49 mg L^{-1} COD, turbidity: 0.5 NTU, NH_4^+: 1.05 mg N L^{-1}, NO_2^-: 0.01 mg N L^{-1}, NO_3^-: 1.56 mg N L^{-1}, surface loading rate = 220 m^3 d^{-1} m^{-2}, BAF bed depth: 2.4 m, temperature = 25˚

3.7.2.4 Balancing contaminant removal and headloss buildup

In practical BAF operation, it is desired to achieve high contaminant removal with low headloss. Thus, the COD and ammonia removal per unit headloss, namely ΔCOD/Δheadloss and ΔNH_4^+-N/Δheadloss, are adopted in this study to evaluate BAF performance relative to changes in operational and design parameters. Higher ratios indicate superior performance. As shown in Figure 3.6c, both ΔCOD/Δheadloss and ΔNH_4^+-N/Δheadloss increase as the BAF media size increase; meanwhile, it also can be seen that neither of these two ratios is highly sensitive to the BAF bed depth. The significant increase of ΔCOD/Δheadloss and ΔNH_4^+-N/Δheadloss in response to the BAF media size increase can be attributed to the fact that biological performance of BAF does not deteriorate too much when the media size increases.

3.7.3 Implications on BAF design

It is believed that finding the optimal BAF media size is the key to achieve qualified effluent standard at minimized operating cost (Moore et al., 2001). Therefore, a BAF should be capable of removing particulates (i.e., turbidity) and contaminants (COD, NH_4^+, etc.) while minimizing the headloss. The model simulations in this study provide theoretical evidence demonstrating that increasing BAF media size may be a very effective strategy to improve the BAF performance (Figure 3.6c). However, according to Figure 3.6b, as the BAF media size increase, there is still deterioration in COD and NH_4^+ removal due to the reduction of available surface area for biofilm. In addition, larger size BAF media may raise the concern of possible turbidity removal failure, as well. For instance, Moore et al. (2001) found that when BAF media size range increased from 1.5-3.5 mm to 2.5-4.5 mm, turbidity (suspended particle) removal decreased from 92% to 85%.

To accommodate for lower removal of these constituents, increasing BAF bed depth should be considered as a strategy when using larger media in BAFs. As documented in Figure 3.5, the source waters in this study had low influent turbidity. However, if the influent turbidity was higher, the deterioration of effluent turbidity could have been distinct. Once again, to accommodate for lower removal of turbidity, increasing BAF bed depth should be considered. The number that is used to avoid a breakthrough of a particle in BAF is expressed as the ratio of BAF bed depth (L in mm) to effective size of media (d in mm), namely L/d ratio. While L/d ratio is not an absolute concept, it has been derived based on the BAF design and operation (Logsdon, 2008). Increasing the media depth while keeping the media size constant increases the L/d ratio. Therefore, a particle is more likely to be captured by the media. In general, an L/d ratio of 1200 or greater is recommended (Logsdon, 2008). The L/d ratio for the system investigated in this study are in the range of 860 to 2,600. Further work is certainly needed to validate the model whether these assumptions are appropriate for BAFs treating high turbidity water.

3.8 Conclusions

A BAF modeling framework established in this study can be calibrated and validated to describe headloss buildup as a result of both biofilm growth and particle deposition in response to contaminant removal. The model prediction turned out to be sensitive to the biofilm coverage of BAF media and revealed that the particle deposition makes marginal contribution to the headloss in potable reuse water and potable water treatment when influent turbidity is low. Increasing the BAF media size appears to be an effective strategy for reducing headloss buildup while minimally impacting contaminant removal. The slight deterioration of contaminant removal as a result of larger BAF media size increase can be compensated by a moderate increase in BAF bed depth.

3.9 References

Adams, J. Q., and Clark, R. M. (1989). Cost estimates for GAC treatment systems. *Journal-American Water Works Association, 81*(1), 35-42.

Al-Naseri, S. K., and Abbas, T. R. (2009). Predicting NOM removal by fixed-bed GAC adsorbers. *Jordan Journal of Civil Engineering, 3*(2), 172-183.

Alonso, C., Zhu, X., Suidan, M. T., Kim, B. R., and Kim, B. J. (2001). Mathematical model of biofiltration of VOCs: effect of nitrate concentration and backwashing. *J Environ Eng, 127*(7), 655-664.

Amburgey, J. E., and Amirtharajah, A. (2005). Strategic filter backwashing techniques and resulting particle passage. *J Environ Eng, 131*(4), 535-547.

APHA. (1998). *Standard methods for the examination of water and wastewater*. Washington, DC: American Public Health Association.

Bablon, G. P., Ventresque, C., and Aïm, R. B. (1988). Developing a Sand-GAC Filter to Achieve High-Rate Biological Filtration. *Journal-American Water Works Association, 80*(12), 47-53.

Bernier, J., Lessard, P., and Rocher, V. (2014). Modelling headloss and two-step denitrification in a full-scale wastewater post-denitrifying biofiltration plant. *Journal of Environmental Engineering and Science, 9*, 171-180.

Bi, D. S., He, C. D., and Wu, J. (2014). Modeling head losses in biological aerated filters including active biomass, inert biomass and extracellular polymeric substances. *Environ Eng Manag J, 13*(4), 929-938.

Boller, M. A., and Kavanaugh, M. C. (1995). Particle characteristics and headloss increase in granular media filtration. *Water Res, 29*(4), 1139-1149.

Bouwer, E. J., Goel, S., and Hozalski, R. M. (1995). *Removal of Natural Organic Matter in Biofilters* (631). WRF Report.

Brown, J. C., and Lauderdale, C. V. (2006). Efficient, simultaneous destruction of multiple drinking water contaminants using biological filtration. *Florida Water Resources Journal, 3*, 28.

Chang, H. T., and Rittmann, B. E. (1987). Mathematical modeling of biofilm on activated carbon. *Environ Sci Technol, 21*(3), 273-280.

Clark, R. M. (1987). Modeling TOC removal by GAC: The general logistic function. *Journal - American Water Works Association, 79*(1), 33-37.

Davidson, C. I., and Friedlander, S. K. (1978). A filtration model for aerosol dry deposition: Application to trace metal deposition from the atmosphere. *Journal of Geophysical Research: Oceans, 83*(C5), 2343-2352.

Deshusses, M. A., Hamer, G., and Dunn, I. J. (1995). Behavior of biofilters for waste air biotreatment. 1. Dynamic model development. *Environ Sci Technol, 29*(4), 1048-1058.

Dussert, B., and R. Van Stone, G. (1994). *Biological activated carbon process for water purification* (Vol. 141). Water Engineering and Management.

Evans, P. J., Hooper, J. L., Amador, J. C., Metz, D. H., Kashinkunti, R. D., Hong, Y., and Meyer, M. (2016). *Chemically Enhanced Biological Filtration to Enhance Water Quality and Minimize Costs* (4429). WRF Report.

Gerrity, D., Gamage, S., Holady, J. C., Mawhinney, D. B., Quiñones, O., Trenholm, R. A., and Snyder, S. A. (2011). Pilot-scale evaluation of ozone and biological activated carbon for trace organic contaminant mitigation and disinfection. *Water Res, 45*(5), 2155-2165.

Han, S., Fitzpatrick, C. S., and Wetherill, A. (2008). Mathematical modelling of particle removal and head loss in rapid gravity filtration. *Separ Sci Technol, 43*(7), 1798-1812.

Hannouche, A., Chebbo, G., Ruban, G., Tassin, B., Lemaire, B. J., and Joannis, C. (2011). Relationship between turbidity and total suspended solids concentration within a combined sewer system. *Water Sci Technol, 64*(12), 2445-2452.

Hao, X.-D., and van Loosdrecht, M. C. M. (2004). Model-based evaluation of COD influence on a partial nitrification-Anammox biofilm (CANON) process. *Water Sci. Technol., 49*(11-12), 83-90.

Henze, M., Gujer, W., Mino, T., and van Loosdrecht, M. C. M. (2000). *Activated Sludge Models ASM1, ASM2, ASM2d and ASM3* (Vol. No.9). London: IWA Publishing.

Ives, K. (1980). Deep bed filtration: theory and practice. *Filtration and separation, 17*(2), 157-166.

Koch, G., Egli, K., van der Meer, J. R., and Siegrist, H. (2000). Mathematical modeling of autotrophic denitrification in nitrifying biofilm of a rotating biological contactor. *Water Sci. Technol., 41*(4-5), 191-198.

LeChevallier, M. W., Becker, W. C., Schorr, P., and Lee, R. G. (1992). Evaluating the performance of biologically active rapid filters. *Journal - American Water Works Association, 84*(4), 136-146.

Lee, M. W., and Park, J. M. (2007). One-dimensional mixed-culture biofilm model considering different space occupancies of particulate components. *Water Res, 41*(19), 4317-4328.

Leverenz, H. L., Tchobanoglous, G., and Darby, J. L. (2009). Clogging in intermittently dosed sand filters used for wastewater treatment. *Water Res, 43*(3), 695-705.

Li, X., Sun, Y., Wang, Z. W., and He, Z. (2019). Theoretical understanding of the optimum conditions for a mainstream granular nitritation-anammox reactor coupled with anaerobic pretreatment. *Sci Total Environ, 669*, 683-691.

Liang, C.-H., and Chiang, P.-C. (2007). Mathematical model of the non-steady-state adsorption and biodegradation capacities of BAC filters. *J Hazard Mater, 139*(2), 316-322.

Logsdon, G. S. (2008). *Water Filtration Practices: Including Slow Sand Filters and Precoat Filtration*: American Water Works Association.

Mann, A. T., and Stephenson, T. (1997). Modelling biological aerated filters for wastewater treatment. *Water Res, 31*(10), 2443-2448.

McDowell, W. H., Zsolnay, A., Aitkenhead-Peterson, J. A., Gregorich, E., Jones, D. L., Jödemann, D., Kalbitz, K., Marschner, B., and Schwesig, D. (2006). A comparison of methods to determine the biodegradable dissolved organic carbon from different terrestrial sources. *Soil Biology and Biochemistry, 38*(7), 1933-1942.

Metcalf & Eddy., and Tchobanoglous, G. (1979). *Wastewater engineering: treatment disposal reuse* (2d ed.). New York: McGraw-Hill.

Moore, R., Quarmby, J., and Stephenson, T. (2001). The effects of media size on the performance of biological aerated filters. *Water Res, 35*(10), 2514-2522.

Nishijima, W., Tojo, M., Okada, M., and Murakami, A. (1992). Biodegradation of organic substances by biological activated carbon–simulation of bacterial activity on granular activated carbon. *Water Sci Technol, 26*(9-11), 2031-2034.

O'Melia, C. R., and Ali, W. (1979). *The role of retained particles in deep bed filtration.* Paper presented at the Ninth International Conference on Water Pollution Research, Stockholm, Sweden.

Ojha, C., and Graham, N. (1993). Theoretical estimates of bulk specific deposit in deep bed filters. *Water Res, 27*(3), 377-387.

Ottengraf, S. P. P., and Van Den Oever, A. H. C. (1983). Kinetics of organic compound removal from waste gases with a biological filter. *Biotechnol Bioeng, 25*(12), 3089-3102.

Packman, J., Comings, K., and Booth, D. (1999). Using turbidity to determine total suspended solids in urbanizing streams in the Puget Lowlands. *Canadian Water Resources Association Annual Meeting, 27–29* pp. 158–165.

Page, D., Wakelin, S., Van Leeuwen, J., and Dillon, P. (2006). *Review of biofiltration processes relevant to water reclamation via aquifers.* SA Water Center for Water Science and Systems, University of South Australia, Adelaide, SA, AUS.

Payatakes, A. C., Tien, C., and Turian, R. M. (1974). Trajectory calculation of particle deposition in deep bed filtration: Part I. Model formulation. *AIChE Journal, 20*(5), 889-900.

Pushnov, A. S. (2006). Calculation of average bed porosity. *Chemical and Petroleum Engineering, 42*(1), 14-17.

Rittmann, B. E., Stilwell, D., and Ohashi, A. (2002). The transient-state, multiple-species biofilm model for biofiltration processes. *Water Res, 36*(9), 2342-2356.

Schimmoller, L., and Foundation, W. (2014). *Fit for purpose water: The cost of overtreating reclaimed water*: WateReuse Research Foundation.

Scholz, M., and Martin, R. J. (1997). Ecological equilibrium on biological activated carbon. *Water Res, 31*(12), 2959-2968.

Scholz, M., and Martin, R. J. (1998). Control of bio‐regenerated granular activated carbon by spreadsheet modelling. *Journal of Chemical Technology & Biotechnology: International Research in Process, Environmental AND Clean Technology, 71*(3), 253-261.

Shen, L., Lu, Y., and Liu, Y. (2012). Mathematical modeling of biofilm‐covered granular activated carbon: a review. *Journal of Chemical Technology & Biotechnology, 87*(11), 1513-1520.

Shim, W. G., Chaudhary, D. S., Vigneswaran, S., Ngo, H. H., Lee, J. W., and Moon, H. (2004). Mathematical modeling of granular activated carbon (GAC) biofiltration system. *Korean J Chem Eng, 21*(1), 212-220.

Simpson, D. R. (2008). Biofilm processes in biologically active carbon water purification. *Water Res, 42*(12), 2839-2848.

Slavik, I., Jehmlich, A., and Uhl, W. (2013). Impact of backwashing procedures on deep bed filtration productivity in drinking water treatment. *Water Res, 47*(16), 6348-6357.

Snowball, M. (2006). Water treatment: Reducing backwash with air scouring. *Filtration & separation, 43*(10), 39-40.

Sperlich, A., Werner, A., Genz, A., Amy, G., Worch, E., and Jekel, M. (2005). Breakthrough behavior of granular ferric hydroxide (GFH) fixed-bed adsorption filters: modeling and experimental approaches. *Water Res, 39*(6), 1190-1198.

Sun, Y., Angelotti, B., Brooks, M., Dowbiggin, B., Evans, P. J., Devins, B., and Wang, Z. W. (2018). A pilot-scale investigation of disinfection by-product precursors and trace organic removal mechanisms in ozone-biologically activated carbon treatment for potable reuse. *Chemosphere, 210*, 539-549.

Sun, Y., Zhang, D., and Wang, Z. W. (2017). The potential of using biological nitrogen removal technique for stormwater treatment. *Ecol Eng, 106*, 482-495.

Takeuchi, Y., Mochidzuki, K., Matsunobu, N., Kojima, R., Motohashi, H., and Yoshimoto, S. (1997). Removal of organic substances from water by ozone treatment followed by biological activated carbon treatment. *Water Sci Technol, 35*(7), 171-178.

Vaidya, R., Buehlmann, P., Bott, C., Salazar-Benites, G., Schimmoller, L., and Nading, T. (2017). *Pilot Plant Performance of Carbon-Based and Membrane-Based Potable Reuse Processes.* Paper presented at the 11th IWA International Conference on Water Reclamation and Reuse, Long Beach, CA.

Veeken, A., and Hamelers, B. (1999). Effect of temperature on hydrolysis rates of selected biowaste components. *Bioresource Technol, 69*(3), 249-254.

Vigneswaran, S., Boonthanon, S., and Prasanthi, H. (1996). Filter backwash water recycling using crossflow microfiltration. *Desalination, 106*(1-3), 31-38.

Wang, C., Li, J., Wang, B., and Zhang, G. (2006). Development of an empirical model for domestic wastewater treatment by biological aerated filter. *Process Biochem, 41*(4), 778-782.

Wang, J. Z., Summers, R. S., and Miltner, R. J. (1995). Biofiltration performance: part 1, relationship to biomass. *Journal-American Water Works Association, 87*(12), 55-63.

Weber, J., Walter, Pirbazari, M., and Melson, G. (1978). Biological growth on activated carbon: an investigation by scanning electron microscopy. *Environ Sci Technol, 12*(7), 817-819.

Wiesmann, U. (1994). Biological Nitrogen Removal from Wastewater. *Advances in Biochemical Engineering Biotechnology, 51*, 113-154.

Williamson, K., and McCarty, P. L. (1976). Verification Studies of the Biofilm Model for Bacterial Substrate Utilization. *Journal of Water Pollution Control Federation, 48*(2), 281-296.

Zhang, S., Gitungo, S. W., Axe, L., Raczko, R. F., and Dyksen, J. E. (2017). Biologically active filters – An advanced water treatment process for contaminants of emerging concern. *Water Res, 114*, 31-41.

Zhang, S., and Huck, P. M. (1996). Parameter estimation for biofilm processes in biological water treatment. *Water Res, 30*(2), 456-464.

Chapter 4 The Potential of Using Biological Nitrogen Removal Technique for Stormwater Treatment

(This chapter has been published as "Sun, Y.W., Zhang, D., & Wang, Z. W. (2017). The potential of using biological nitrogen removal technique for stormwater treatment. *Ecological Engineering*, *106*, 482-495")

4.1 Abstract

Biological nitrogen removal (BNR) may provide permanent elimination of nitrogen pollutants by conversion to nitrogen gas. However, few studies have explored the potential of BNR for the removal of nitrogen from stormwater even though this technique has been broadly applied for wastewater purification. Urban runoff is characterized by its low strength and high dissolved oxygen content, which poses multiple challenges to effective BNR. In this study, mathematical modeling indicated that for most runoff input concentrations, complete nitrogen removal within a 0.5-day hydraulic retention time could be achieved if a critical organic carbon concentration is provided in the influent of steady-state bioretention systems. An appropriate amount of organic carbon is required to simultaneously create spatial aerobic and anoxic conditions for successful stormwater BNR in the layered structures of biofilms that are formed on bioretention media and inhabited with syntrophic BNR communities. Because organic carbon is normally limiting in stormwater denitrification processes, anammox becomes an especially important pathway for stormwater BNR. An analysis of influent runoff concentrations from the National Stormwater Quality Database suggested that 71.1% runoff could have nitrogen pollutant removed via partial nitritation followed by anammox. The adequacy of dissolved oxygen, ammonia, and alkalinity in stormwater for successful BNR was also evaluated. It was concluded that adjusting influent organic content to a critical value determined in this study should suffice the stormwater BNR requirement of steady-state bioretention systems. Bioaugmentation is required to expedite the bioretention system startup.

4.2 Keywords

Stormwater; BNR; Anammox; Nitritation; Biofilms; Alkalinity

4.3 Graphical Abstract

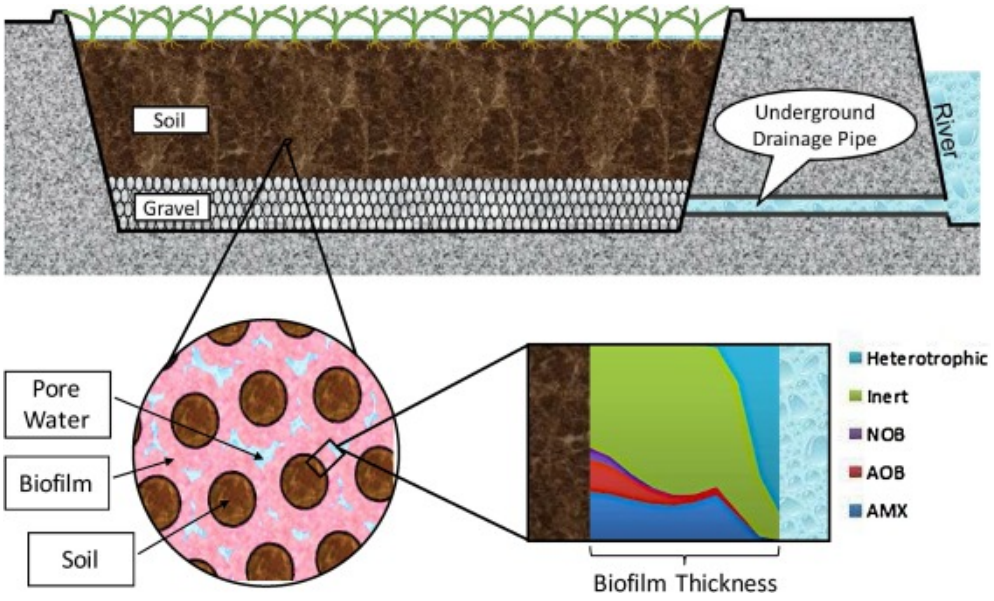

4.4 Introduction

A large portion of waterways across the world has been identified with excessive nitrogen pollution, a known cause for the water body "dead zone" formation (Dybas 2005). For example, a study of the Chesapeake Bay showed that increases in reactive nitrogen contributed to excessive growth of phytoplankton, which eventually die, resulting in consumption of available oxygen, and increasing the anoxic and hypoxic waters within the Bay (Galloway et al. 2003). The number of those oxygen-starved "dead zones" has doubled over the past decade and was projected to become the greatest threat to marine ecosystems (Pelley 2004). Climate change may lead to an increase in nitrogen pollution and a decrease in the time of concentration with the increase of rainfall and thence runoff, which is exacerbated with urbanization (Jennings and Jarnagin 2002, Makepeace et al. 1995, Davidson et al. 2010). Thus, having a purification technique capable of nitrogen removal from stormwater is imperative in improving water quality of affected surface waters. Out of all existing removal mechanisms, biological nitrogen removal (BNR) is the only one that allows for permanent nitrogen removal, as plant uptake or soil adsorption only temporarily stores and relocates nitrogen pollutants (Valero et al. 2010). BNR transforms nitrogen pollutants into harmless nitrogen gas through bacterial nitrification, denitrification and/or anammox (Cao 2008). However, the potential of BNR to provide stormwater nitrogen removal is largely unknown, as only limited research on this topic has been conducted. In contrast, much work has been conducted on nitrogen pollutant removal in wastewater treatment. The influent nitrogen concentrations of wastewater are orders of magnitude higher than stormwater. The National Stormwater Quality Database (NSQD) is an urban runoff characterization database developed by Maestre and Morquecho (2005) containing information on runoff water quality for many U.S. sites. As indicated by information summarized from NSQD in Figures 4.1a and b (Maestre and Morquecho 2005), most of the Total Kjehldahl Nitrogen (TKN) and Total Nitrogen (TN) contained in urban stormwater actually falls within very low ranges of 0-2 g TKN m^{-3} (95%) and 1-3 g TN m^{-3} (75%), respectively. It is recognized that even low TN concentrations, possibly around 1-2 g N m^{-3}, may trigger eutrophication in nutrient poor (oligotrophic) surface waters (James et al. 2005).

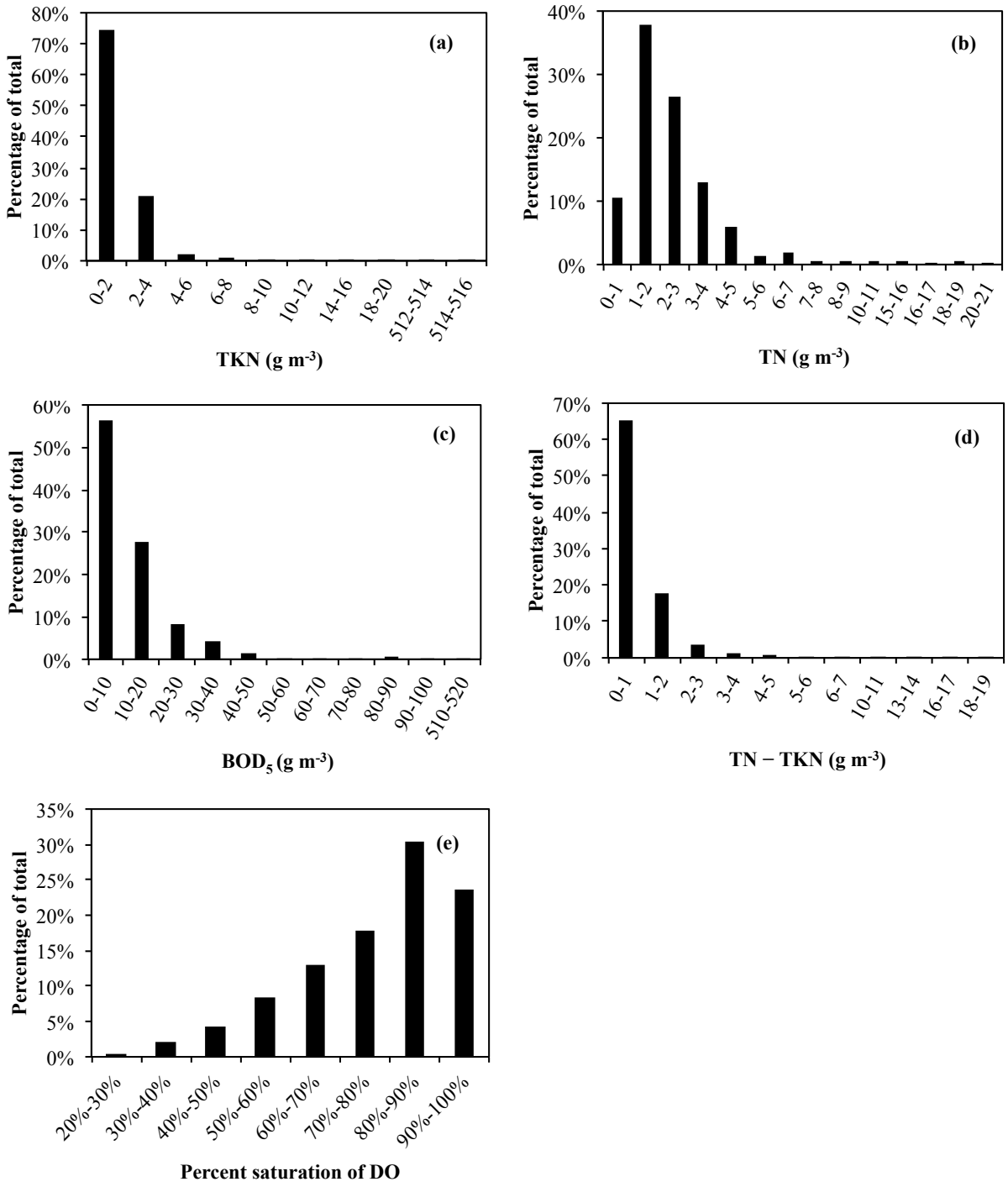

Figure 4.1 Probability density of (a) TKN, (b) TN, (c) BOD_5, (d) TKN − TN, and (e) Percent saturation of DO of stormwater reported in NSQD.

BNR communities usually possess a very high affinity to nitrogen pollutants (half-saturation constant K_s = 0.005 ~ 1.1 g N m^{-3} as shown in Table 4.3 and the study by De Clippeleir et al. (2011), which enables quick microbial uptake of these pollutants at low concentration (Hao et al. 1983). However, it is unknown whether BNR communities are able to adapt to the task of stormwater treatment. Mathematical models are a powerful tool that can be used to explore the applicability of BNR. The aim of this study is to provide a thorough and systematic assessment of the potential of BNR for the removal of nitrogen from stormwater using a mathematical modeling approach.

Several members of the BNR microbial communities are extremely slow growing microorganisms, especially in the low strength environment of stormwater. For example, anammox has doubling time of 14 to 21 days (Strous and Jetten 2004), in contrast to nitrite-oxidizing bacteria who has doubling time of only 10 to 13 hours (Rodriguez-Sanchez et al., 2014). To sustain those BNR communities with longer retention times but still provide a reasonable processing time for the massive flow of stormwater, system designs that can uncouple solids retention time (SRT) from the hydraulic retention time (HRT) should be considered. Stormwater treatment systems like bioretention (also called biofiltration) immobilize bacterial cells in the form of biofilms in filter media and thus can be used to fulfill this role. As illustrated in Figure 4.2, contaminants are removed in bioretention while stormwater passes through the height of the filter media area consisting of soil and vegetated groundcover (Davis et al. 2009). Bioretention has been regarded as one of the most effective designs for stormwater treatment. It is effective in retaining large volumes of runoff and pollutants on site (County 1999, Dietz 2007). Bioretention systems have been shown to remove nitrogen via several different pathways including plant assimilation, two-step nitrification and denitrification, and a shortcut that transfer ammonium and nitrite directly into nitrogen gas with the absence of oxygen, namely anammox (Li et al. 2008). Previous bioretention studies have been carried out in long-term (Lucas and Greenway 2011) and short-term experiments (Fan et al. 2013, Henderson et al. 2007) for the removal of nitrogen from stormwater and found that plant assimilation, rather than BNR, played a primary role (Zinger et al. 2013, Payne et al. 2014). It should be noted that plant assimilation only temporarily stores nitrogen during growth, and will eventually release stored nitrogen back to the downstream water at their death and decay, unless the systems are periodically harvested, which opens up a maintenance and disposal issue.

Enhancing BNR in bioretention systems to permanently remove and transform nitrogen pollutant into nitrogen gas (Payne 1981) would potentially provide a game changer. Therefore, this study focused upon bioretention systems as a model object to explore the potential of BNR for the removal of nitrogen from stormwater.

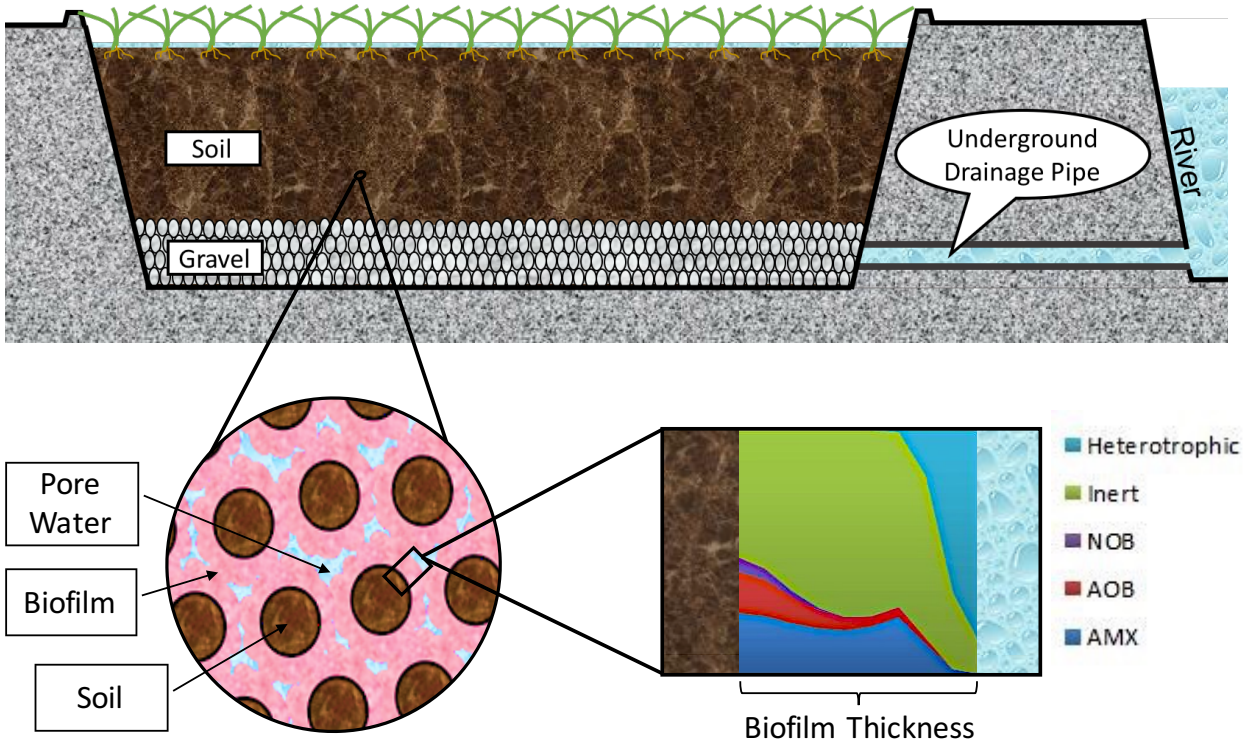

Figure 4.2 Illustration of the biofilm composition and distribution in bioretention systems.

4.5 Materials and Methods

4.5.1 Model assumptions

In this exploratory study, we assume a homogenous environment within the bioretention system for the ease of model development and solution. We believe this simplification is acceptable because the depths of bioretention cells are usually shallow (0.6 to 1.2 m) (Brown et al., 2011), and biofiltration system like that usually can be approximated as homogenous (Rittmann et al., 2002, Almenglo et al., 2016). Pollutant turnovers in the mass diffusion gradient of BNR biofilms growing on the surfaces of bioretention media were considered in the development of this model, a novel approach. A comprehensive BNR mathematical model specifically tailored for the

stormwater BNR was developed with knowledge built upon a review of existing modeling systems summarized in Table 4.1. Table 4.1 summarized statistical, empirical, and structured models currently used in literature with regard to nitrogen removal in bioretention treatment systems. As can be seen, those statistical models only predicted the removal efficiencies of nitrogen pollutant without consideration of the removal kinetics and mechanistic pathways (Daly et al., 2012; Guerra, Park, & Kim, 2013; Guerra, Park, Niu, et al., 2013), and those empirical models simply applied first-order kinetics to all nitrogen removal pathways ignoring the effects of the key deterministic parameters such as dissolved oxygen (DO), plant density, microbial concentration, and organic carbon availability (Masi, 2011; Xuan et al., 2013). In comparison, structured models have much more superior extrapolative abilities as it consists of structural relationships between multiple elements contributing to the system performance (Henderson et al., 2007). However, there is only one structured model developed for stormwater nitrogen removal (Deng, 2012), and that model only simulated the biological denitrification, one of the four primary nitrogen turnover pathways. To achieve a better stormwater nitrogen removal modeling, this study developed a structured model capable of simulating the turnover of stormwater nitrogen through two-step nitrification, denitrification, deammonification, and plant nitrogen uptake.

4.5.2 Model development

4.5.2.1 Bacterial model

The components of this bioretention BNR model include: five substrates in the liquid phase, i.e., dissolved oxygen (DO), nitrate (NO_3^-), nitrite (NO_2^-), ammonium (NH_4^+), and biodegradable organic carbon source expressed as chemical oxygen demand (COD); three types of autotrophic bacteria, namely ammonia-oxidizing bacteria (AOB), nitrite-oxidizing bacteria (NOB), and anammox bacteria (AMX); three types of heterotrophic bacteria, namely oxygen-respiring heterotroph (ORH), nitrite denitrifier (NID), and nitrate denitrifier (NAD), and the inert and plant biomass. The mathematical model was set up based upon equations commonly used in active sludge model No. 1 (ASM1) (Henze et al. 2000) and constructed wetland model No.1 (CWM1) (Mburu et al. 2012) with simplified kinetic expressions listed in Table 4.2, parameter values listed

in Table 4.3 and stoichiometric matrix provided in Table 4.4. Nitrification in this model consisted of oxidation of NH_4^+ to NO_2^- by AOB and oxidation of NO_2^- to NO_3^- by NOB, which are defined in Eqs. 4.1 and 3, respectively (Jubany et al. 2008). Denitrification was defined in Eqs. 4.9 and 10 for NID and NAD to reduce NO_3^- to NO_2^- and then to nitrogen gas, respectively (Henze et al. 2000, Alpkvist et al. 2006). Deammonification was defined in Eq. 4.5 for AMX (Volcke et al. 2010), which utilizes NO_2^- to oxidize NH_4^+ to nitrogen gas. It is important to note that the distinction among the three types of heterotrophic bacteria (ORH, NID and NAD), which can only be specified in the mathematical model for tracing the flow of electron acceptors used for heterotrophic growth. However, as there is no way to distinguish the three types of heterotrophic bacteria experimentally, reliance must be on the model concept and subsequent calibration. All related equations and parameters used in this study were based on published data in the literature. Since most of the bioretention systems are operated during mild season or in temperature zones (Fan et al. 2013, Payne et al. 2014), all rate coefficients used in this study were adjusted to the values at 20 $^{\circ}$C by using the van't Hoff-Arrhenius relationship (Metcalf & Eddy. and Tchobanoglous 1979).

Table 4.1 A summary of stormwater BNR models reported in literature

Basis	Influent ($g\ TN\ m^{-3}$)	Model type				Literature	Limitation
		Based on pollutant type					
		TN	**TKN**	**NH_4^+-N**	**NO_3^--N**		
Statistical	6.3~20.0	Linear regression	Linear regression	Linear regression	Linear regression	(Guerra et al. 2013a)	Only modeled pollutant removal efficiencies, the specific removal pathway cannot be tracked
	3.41~21.08	Linear regression	Linear regression	Linear regression	N/A	(Guerra et al. 2013b)	
	N/A	PDF*	N/A	N/A	N/A	(Daly et al. 2012)	
		Based on removal pathway					
		Nitrification	**Denitrification**	**Deammonification**	**Plant Uptake**		
Empirical	0.87~48.6	First-order kinetic	First-order kinetic	N/A	First-order kinetic	(Xuan et al. 2013)	Assumed first-order reaction, not suitable for stormwater with low nutrient concentration
	1.30~1.70	First-order kinetic	First-order kinetic	N/A	N/A	(Masi 2011)	
Structured	2.00~11.59	N/A	VART**	N/A	N/A	(Deng et al. 2012)	Some BNR pathways are not included (the model developed in this study considered all of them)
	44	CWM1***	CWM1	N/A	Monod-type kinetic	(Mburu et al. 2012) ****	
	1.00~44.69	ASM1	ASM1	ASM1-like	Logistic & Monod-type kinetic	This study	

*Probability density function (PDF). TN_{out} is determined via PDF of soil water content. For more detail please see reference paper.

**The Variable Residence Time model, originally developed for simulation of longitudinal dispersion and transport of solutes in natural streams by the author of this literature.

***Constructed wetland model No.1 (CWM1)

****Mburu et al. (2012) is the constructed wetland model.

Table 4.2 Model kinetic processes

Process	Process Rate		Reference
	Autotrophic Bacteria		
Growth of X_{AOB}	$\mu_{max,AOB} X_{AOB} \frac{S_{NH_4^+}}{K_{NH_4^+,AOB} + S_{NH_4^+}} \frac{S_{O_2}}{K_{O_2,AOB} + S_{O_2}}$	**(4.1)**	(Jubany et al. 2008)
Decay of X_{AOB}	$b_{AOB} X_{AOB} \frac{S_{O_2}}{K_{O_2,AOB} + S_{O_2}}$	**(4.2)**	(Volcke et al. 2010)
Growth of X_{NOB}	$\mu_{max,NOB} X_{NOB} \frac{S_{NO_2^-}}{K_{NO_2^-,NOB} + S_{NO_2^-}} \frac{S_{O_2}}{K_{O_2,NOB} + S_{O_2}}$	**(4.3)**	(Jubany et al. 2008)
Decay of X_{NOB}	$b_{NOB} X_{NOB} \frac{S_{O_2}}{K_{O_2,NOB} + S_{O_2}}$	**(4.4)**	(Volcke et al. 2010)
Growth of X_{AMX}	$\mu_{max,AMX} X_{AMX} \frac{S_{NH_4^+}}{K_{NH_4^+,AMX} + S_{NH_4^+}} \frac{S_{NO_2^-}}{K_{NO_2^-,AMX} + S_{NO_2^-}} \frac{K_{O_2,AMX}}{K_{O_2,AMX} + S_{O_2}}$	**(4.5)**	(Volcke et al. 2010)
Decay of X_{AMX}	$b_{AMX} X_{AMX} \frac{S_{O_2}}{K_{O_2,AMX} + S_{O_2}}$	**(4.6)**	(Volcke et al. 2010)
	Heterotopic Bacteria		
OB Growth	$\mu_{max,H} X_H \frac{S_S}{K_{S,H} + S_S} \frac{S_{O_2}}{K_{O_2,H} + S_{O_2}}$	**(4.7)**	(Henze et al. 2000)
Decay of X_H	$b_H X_H$	**(4.8)**	(Henze et al. 2000)
DEN_3 Growth	$\mu_{max,N} X_N \frac{S_{NH_4^+}}{K_{NH_4^+,N} + S_{NH_4^+}} \frac{S_{NO_3^-}}{K_{NO_X^-,N} + S_{NO_3^-}} \frac{K_{O_2,N}}{K_{O_2,N} + S_{O_2}} \frac{S_S}{K_{S,N} + S_S}$	**(4.9)**	(Henze et al. 2000)
DEN_2 Growth	$\mu_{max,N} X_N \frac{S_{NH_4^+}}{K_{NH_4^+,N} + S_{NH_4^+}} \frac{S_{NO_2^-}}{K_{NO_X^-,N} + S_{NO_2^-}} \frac{K_{O_2,N}}{K_{O_2,N} + S_{O_2}} \frac{S_S}{K_{S,N} + S_S}$	**(4.10)**	(Alpkvist et al. 2006)
	Plant		
Uptake of NH_4^+	$\mu_{max,pl,NH_4^+} X_{N,pl} (1 - \frac{X_{N,pl}}{X_{max,N,pl}/d}) \frac{S_{NH_4^+}}{K_{NH_4^+,pl} + S_{NH_4^+}}$	**(4.11)**	(van Dam et al. 2007)
Uptake of NO_3^-	$\mu_{max,pl,NO_3^-} X_{N,pl} (1 - \frac{X_{N,pl}}{X_{max,N,pl}/d}) \frac{S_{NO_3^-}}{K_{NO_3^-,pl} + S_{NO_3^-}}$	**(4.12)**	(van Dam et al. 2007)
Decay of X_{pl}	$b_{pl} X_{pl}$	**(4.13)**	(Mburu et al. 2012)
Degradation of $X_{dead,pl}$	$b_{degrade} X_{dead,pl}$	**(4.14)**	(Mburu et al. 2012)
Root Oxygen Leaching	$k_{ol} X_{pl} (e^{S_{sat,O_2} - S_{O_2}} - 1)$	**(4.15)**	(Mburu et al. 2012)
	Biofilm		
Detachment	DeL_f	**(4.16)**	(Henze 2008)

Table 4.3 Model parameters (20 °C), for bacteria plant, and biofilm

Variables	Variables meaning	Value	Unit	Reference
X_i	Concentrations of bacteria i	N/A	gCOD m^{-3}	N/A
S_i	Concentrations of liquid compartment i	N/A	gCOD m^{-3}	N/A
$\mu_{max,AOB}$	Max specific growth rates of AOB	0.75*	d^{-1}	(Jubany et al. 2008)
$\mu_{max,NOB}$	Max specific growth rates of NOB	1.072*	d^{-1}	(Jubany et al. 2008)
$\mu_{max,AMX}$	Max specific growth rates of AMX	0.026*	d^{-1}	(Strous et al. 1998)
$\mu_{max,H}$	Max specific growth rates of OB	6	d^{-1}	(Henze et al. 2000)
$\mu_{max,N}$	Max specific growth rates of DEN	4.8	d^{-1}	(Henze et al. 2000)
b_{AOB}	Decay rate of AOB	0.037*	d^{-1}	(Volcke et al. 2010)
b_{NOB}	Decay rate of NOB	0.054*	d^{-1}	(Volcke et al. 2010)
b_{AMX}	Decay rate of AMX	0.0013*	d^{-1}	(Volcke et al. 2010)
b_H	Decay rate of OB	0.0025	d^{-1}	(Henze et al. 2000)
b_N	Decay rate of DEN	0.003	d^{-1}	(Henze et al. 2000)
Y_{AOB}	Growth yields of AOB	0.18	gCOD gN^{-1}	(Jubany et al. 2008)
Y_{NOB}	Growth yields of NOB	0.08	gCOD gN^{-1}	(Jubany et al. 2008)
Y_{AMX}	Growth yields of AMX	0.17	gCOD gN^{-1}	(Strous et al. 1998)
Y_H	Growth yields of OB	0.33	gCOD $gCOD^{-1}$	(Henze et al. 2000)
Y_N	Growth yields of DEN	0.33	gCOD $gCOD^{-1}$	(Henze et al. 2000)
Y_{NO}	Nitrate yields	0.42	gN $gCOD^{-1}$	(Henze et al. 2000)
Y_{NH}	Ammonium yields	0.092	gN $gCOD^{-1}$	(Henze et al. 2000)
$K_{O_2,AOB}$	AOB half-saturation coefficients for O_2	0.2	g m^{-3}	(Manser et al. 2005)
$K_{NH_4^+,AOB}$	AOB half-saturation coefficients for NH_4^+	1.1	gN m^{-3}	(Wiesmann 1994)
$K_{O_2,NOB}$	NOB half-saturation coefficients for O_2	0.4	g m^{-3}	(Perez et al. 2014)
$K_{NO_2^-,NOB}$	NOB half-saturation coefficients for NO_2^-	0.5	gN m^{-3}	(Wiesmann 1994)
$K_{O_2,AMX}$	AMX half-saturation coefficients for O_2	0.01	g m^{-3}	(Hao et al. 2002)
$K_{NO_2^-,AMX}$	AMX half-saturation coefficients for NO_2^-	0.005	gN m^{-3}	(Volcke et al. 2010)
$K_{NH_4^+,AMX}$	AMX half-saturation coefficients for NH_4^+	0.03	gN m^{-3}	(Volcke et al. 2010)
$K_{S,H}$	OB half-saturation coefficients for substrate	4	gCOD m^{-3}	(Henze et al. 2000)
$K_{O_2,H}$	OB half-saturation coefficients for O_2	0.2	g m^{-3}	(Henze et al. 2000)
$K_{NH_4^+,N}$	DEN_X half-saturation coefficients for NH_4^+	0.05	gN m^{-3}	(Henze et al. 2000)
$K_{NO_X^-,N}$	DEN_X half-saturation coefficients for NO_X^-	0.5	gN m^{-3}	(Henze et al. 2000)
$K_{O_2,N}$	DEN_X half-saturation coefficients for O_2	0.2	g m^{-3}	(Henze et al. 2000)
$K_{S,N}$	DEN_X half-saturation coefficients for substrate	2	gCOD m^{-3}	(Henze et al. 2000)
μ_{max,pl,NH_4^+}	Max specific plant uptake rates of NH_4^+	0.05	d^{-1}	(van Dam et al. 2007)
μ_{max,pl,NO_3^-}	Max specific plant uptake rates of NO_3^-	0.05	d^{-1}	(van Dam et al. 2007)

b_{pl}	Decay rate of plant	0.0015	d^{-1}	(Mburu et al. 2012)
$b_{degrade}$	Degradation rate of dead plant	0.01	d^{-1}	(Mburu et al. 2012)
$K_{NH_4^+,pl}$	Plant half-saturation coefficients for NH_4^+	0.7	gN m^{-3}	(van Dam et al. 2007)
$K_{NO_3^-,pl}$	Plant half-saturation coefficients for NO_3^-	0.1	gN m^{-3}	(van Dam et al. 2007)
$X_{max,N,pl}$	Maximum plant nitrogen biomass	150	gN m^{-3}	(van Dam et al. 2007)
k_{ol}	Oxygen releasing coefficient	N/A	d^{-1}	N/A
p_n	Plant nitrogen content	1.5%	N/A	(van Dam et al. 2007)
d_{root}	Root depth	N/A	m	N/A
L_f	Biofilm thickness	N/A	μm	N/A
De	Biofilm detachment coefficient	N/A	d^{-1}	N/A
A_s	Specific area	N/A	$m^2 m^{-3}$	N/A
$D_{NO_X^-}$	Diffusion coefficient of NO_x^-	0.00017	$m^2 d^{-1}$	(Picioreanu et al. 1997)
$D_{NH_4^+}$	Diffusion coefficient of NH_4^+	0.00019	$m^2 d^{-1}$	(Picioreanu et al. 1997)
D_{O_2}	Diffusion coefficient of O_2	0.00022	$m^2 d^{-1}$	(Picioreanu et al. 1997)
D_S	Diffusion coefficient of substrate	0.0001	$m^2 d^{-1}$	(IWA 2006)

*Parameters were converted from the original data in the paper to values at 20 °C

Table 4.4 Stoichiometric matrix

Process	O_2	NH_4^+	NO_2^-	$^{14}NO_3^-$	$^{15}NO_3^-$	NO_3^-	COD	X_{AOB}	X_{NOB}	X_{AMX}	X_H	X_{Inert}	X_{pl}	$X_{dead,pl}$
Growth of X_{AOB}	-(3.43-Y_{AOB}) /Y_{AOB}	-1/ Y_{AOB}	1/ Y_{AOB}					1						
Decay of X_{AOB}								-1				1		
Growth of X_{NOB}	-(1.14-Y_{NOB}) /Y_{NOB}		-1/ Y_{NOB}	1/ Y_{NOB}		1/ Y_{NOB}			1					
Decay of X_{NOB}									-1			1		
Growth of X_{AMX}		-1/ Y_{AMX}	-1/ Y_{AMX}-1/1.14	1/1.14		1/1.14				1				
Decay of X_{AMX}										-1		1		
Growth of X_{OB}	-(1-Y_H) /Y_H						-1/ Y_H				1			
Decay of X_H											-1	1		
Growth of X_{DEN3}		-Y_{NH}	Y_{NO}	($^{14}NO_3^-/NO_3^-$)* (-Y_{NO})	($^{15}NO_3^-/NO_3^-$)* (- Y_{NO})	- Y_{NO}	-1/ Y_N				1			
Growth of X_{DEN2}		-Y_{NH}	-Y_{NO}				-1/ Y_N				1			
Uptake of $X_{NH_4^+,pl}$		-1											1/p_N	
Uptake of $X_{NO_3^-,pl}$				-$^{14}NO_3^-/NO_3^-$	-$^{15}NO_3^-/NO_3^-$	-1							1/p_N	
Decay of X_{pl}													-1	1
Degradation of $X_{dead,pl}$							1							-1
Root Oxygen leaching	1													

4.5.2.2 Plant model:

Plants in bioretention systems are capable of assimilating both NH_4^+ and NO_3^-. However, this nitrogen is only temporarily stored in plant tissues and will be eventually released back to the downstream water at their death and decay (Payne 1981), unless a harvesting schedule is implemented, which leads to additional maintenance and material disposal. More importantly, it is known that microbes in bioretention systems utilize nutrients quicker than plants, and plants are thus only able to utilize nutrients that exceed microbial demands (Hodge et al. 2000). As the goal of this study is to explore the potential of permanent nitrogen removal at steady sate, we considered plant assimilation in simulation of initial conditions of the bioretention system but not in long-term performance simulation. However, most plant models used in wastewater treatment (e.g. wetland systems) are simply empirical models that simulate the process rate as a constant (Liu et al. 2005), as a first-order kinetics (Sonavane and Munavalli 2009), or as a complicated model with too many unknown empirical parameters (Sagehashi et al. 2009). In the study by van Dam et al. (2007), a plant model was formulated with maximum uptake rate depending on the concentration of nitrogen in the form of a Monod-type equation and a maximum plant density in the form of a logistic equation. This plant nitrogen uptake model not only has a simple structure, but also has taken into consideration the plant uptake ability limited by both of its own growth stage and NO_3^- and NH_4^+ concentrations in the soil pore water. For these reasons, we adopted this plant nitrogen uptake model in Eqs. 4.11 and 12. As shown in Table 4.4, plant decay and degradation in this model were only considered to provide a carbon source but not a nitrogen source for the bioretention system. This is because the plant nitrogen uptake expressed in this equation is indeed a net uptake rate in which the nitrogen that diffused into the roots but not utilized has been subtracted (Charles-Edwards et al. 1986).

All equations were programed and solved in AQUASIM (Reichert 1994) by using the biofilm reactor module. The density of biofilm was considered constant and set as 10 kg COD m^{-3} (IWA 2006). The specific surface area, initial biofilm thickness and its initial bacteria composition was calibrated by using the literature data. Biofilm detachment rate was modeled by using Eq. 4.16 in Table 4.2, and the detachment coefficient (De) was calibrated by using literature data. The suspended bacteria detached from biofilms were considered still active and followed the same growth kinetics as the bacteria in the biofilms.

4.5.3 Model calibration and validation

The advantage of this model is that it not only macroscopically predicts nitrogen removal performance, but also provides theoretical explanations for the mechanism and pathways behind the phenomenon. Traditional validation methods that only compare model output against the influent and effluent nitrogen data is insufficient to verify the pathways of nitrogen transformation in a bioretention system. To our knowledge, the study by Payne et al. (2014) is the only work that has experimentally determined the nitrogen transformation pathways in bioretention systems. A nitrogen isotope pairing method proposed by Nielsen (1992) was employed in the experiment to track the amount of nitrogen flowing through nitrification, denitrification, and plant assimilations, respectively. Briefly, this method directly measures the amount of nitrogen denitrified and remained. The amount of plant assimilation was determined from nitrogen mass balance. Apparently, the study by Payne et al. (2014) provides suitable experimental data for the validation of the bioretention model developed in this study. A cross-verification approach was taken in this study to provide added confidence towards the model validation. Firstly, two sets of data (NH_4^+ and NO_3^-) collected from the study by Payne et al. (2014) were used to calibrate the model parameters (Figure 4.4). After that, the model prediction was compared against another two individual sets of data (denitrified nitrogen and nitrogen pathways under different influent nitrogen loading) to verify the model accuracy (Figures 4.5 and 4.6). The calibration process and results are described below.

4.5.3.1 Model calibration with effluent ammonium and nitrate concentrations

In the study by Payne et al. (2014), the batch operation adopted is shown in Figure 4.3, and influent nitrogen concentration of 20 g N m^{-3} was dosed into bioretention system with 1:1 concentration ratio of NH_3^+-N to NO_3^--N. The effluent nitrogen concentrations were used to calibrate those unknown parameters in Table 4.5. The unknown parameters include initial values of COD, biofilm thickness (L_f), plant nitrogen content, and the initial concentrations of all BNR communities, i.e., ammonia-oxidizing bacteria (AOB), nitrite-oxidizing bacteria (NOB), anammox bacteria (AMX); oxygen-respiring heterotroph (ORH), nitrite denitrifier (NID), and nitrate denitrifier (NAD); root oxygen leaching rate constant (K_{ol}), specific surface area (A_s), and root depth (d_{root}). The initial values of all the bacteria were regressed in this model because the exact amount of bacteria in the bioretention system is not measurable. K_{ol} is regressed in this model because K_{ol} is different for different plants and there is no typical value available (Mburu et al. 2012).

Table 4.5 Calibrated model parameters by using data from Payne et al. (2014)

AOB ($gCOD\ m^{-3}$)	NOB ($gCOD\ m^{-3}$)	AMX ($gCOD\ m^{-3}$)	N-Plant ($gN\ m^{-3}$)	Heterotrophic ($gCOD\ m^{-3}$)	K_{ol} (d^{-1})	COD ($g\ m^{-3}$)	d_{root} (m)	A_s ($m^2\ m^{-3}$)	Lf (μm)
5295.2	3082.3	300	70	9.1	9.6×10^{-8}	17.0	0.18	986.7	81

As can be seen in Figure 4.4, the calibrated model fit the experimental data very well with R^2 values of 0.99 and 0.98 for effluent ammonia and nitrate, respectively. AMX is a type of autotrophic bacteria that can directly convert ammonium and nitrite into N_2, but it is noteworthy that the model calibration process actually predicted an extremely small initial AMX value. It is known that AMX ubiquitously exists in natural environments and has been broadly cultivated for wastewater treatment (Terada et al. 2011), but it is highly sensitive to oxygen (Li et al. 2008), and can only prosper in low DO environments (Li et al. 2008).

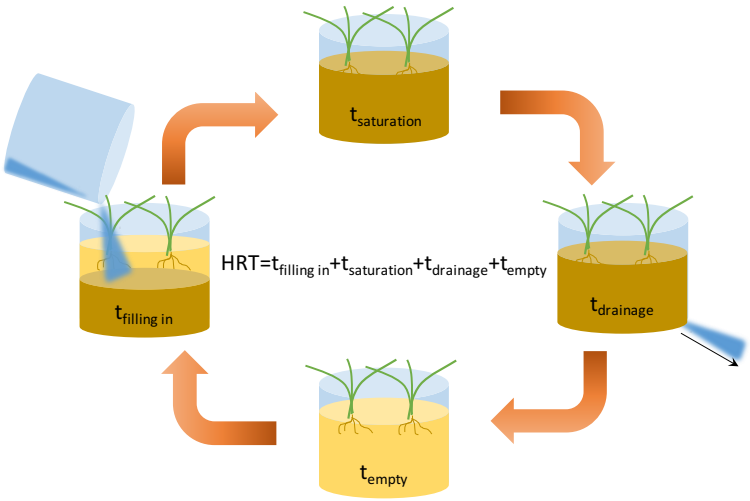

Figure 4.3 Batch operation of bioretention systems, in which light yellow indicates soil, dark yellow indicates saturated soil, and cycle duration equals hydrolytic retention time (HRT)

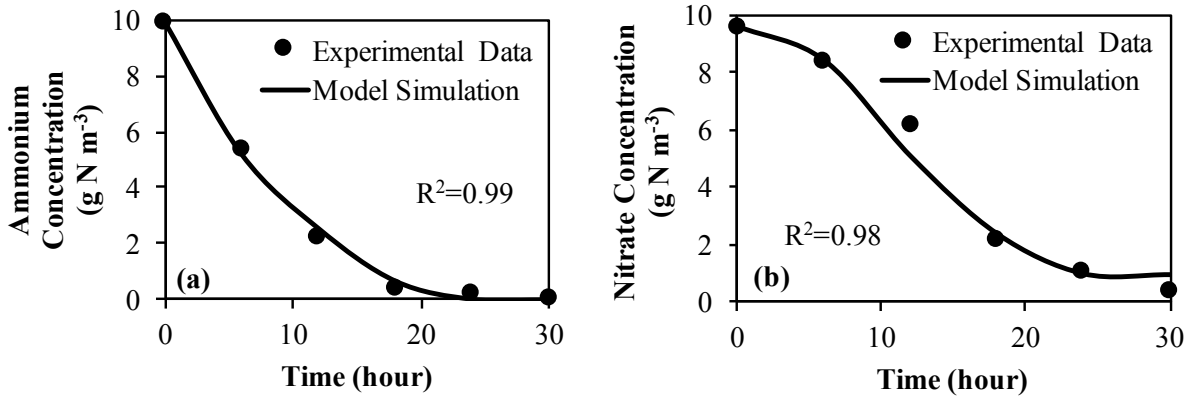

Figure 4.4 Determination of model parameters in Table 4.5 using least square regression of the a) ammonia; and b) nitrate data from a previous study (Payne et al. 2014) using influent 20 g N m^{-3} with model equations in Table 4.2.

4.5.3.2 Model validation with denitrified nitrogen concentration

The study by Payne et al. (2014) has experimentally determined the amount of influent nitrogen removed through denitrification pathway at a six-hour interval. This information is taken advantage in this study to verify the model accuracy. As shown in Figure 4.5, using calibrated parameters in Table 4.5, the model made a prediction of the denitrified nitrogen concentration in close correlation with experimental measruement with an $R^2 = 0.98$.

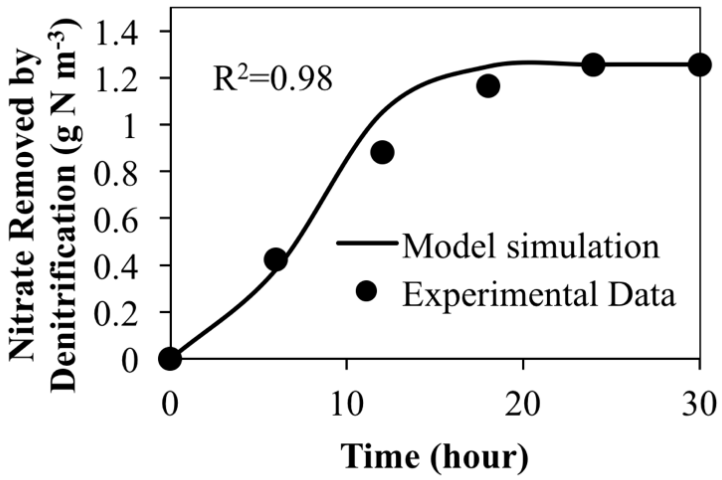

Figure 4.5 Model simulation of the denitrified nitrogen using model equations in Table 4.2 with parameters determined in Table 4.5 at an influent concentration of 20 g N m^{-3}

4.5.3.3 Model validation under different nitrogen loading

In order to further confirm the validity of the model developed in this study, the model calibrated above was also employed to predict the nitrate that was denitrified, assimilated by plant and remained within the pore water after 12 hours when influent total nitrogen concentration was 1 g N m^{-3}, 10 g N m^{-3}, and 20 g N m^{-3}, respectively. As designed in the study by Payne et al. (2014), all the vegetated reactors are the same size, and the same amount of vegetation was planted into each reactor, which means the calibrated initial values in Table 4.5 can be applied to bioretention reactors operated at the other nitrogen loading. Model predicted results are presented in Figure 4.6. As can be seen, the model prediction agreed very well with experimental data determined by Payne et al. (2014) using the nitrogen isotope pairing method proposed by Nielsen (1992).

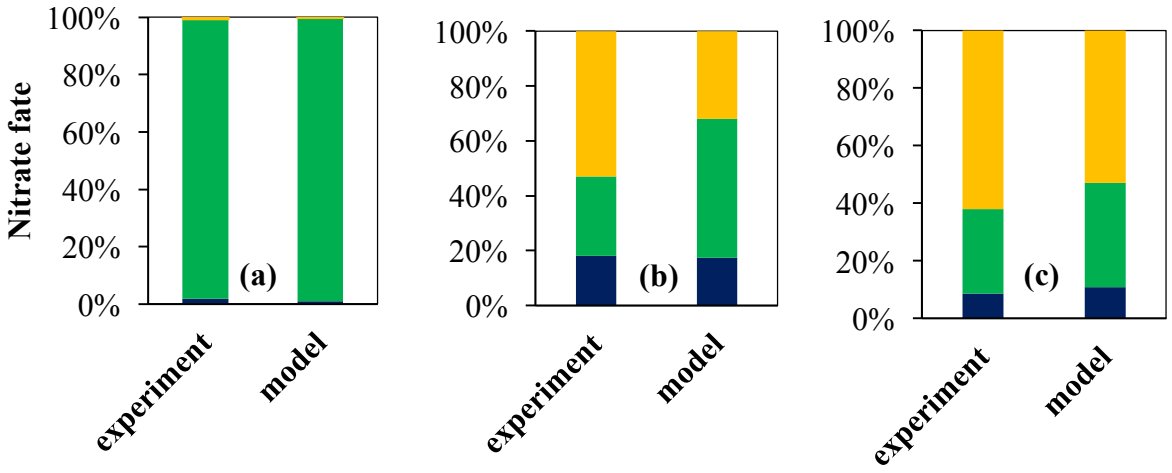

Figure 4.6 A comparison between model simulation and experimental results from the study by Payne et al. (2014) in terms of the fraction of influent nitrate being denitrified, assimilated by plant and remained within the pore water after 12 hours at different influent loading: (a) 1 g N m^{-3}, (b) 10 g N m^{-3}, (c) 20 g N m^{-3}; orange: remained, green: assimilated, navy blue: denitrified

4.5.4 Model stormwater composition

According to the NSQD (Maestre and Morquecho 2005) summarized in Figure 4.1, most of the TKN values fall within the low range of 0-2 g N m^{-3} (Figure 4.1a). It is known that anoxic condition (without oxygen) is a must for successful BNR to occur via either denitrification and/or anammox reactions. In other words, both aerobic and anoxic conditions need to co-exist in one bioretention system for successful BNR. However, the percent saturation of DO analyzed in Figure 4.1e reveals that majority of stormwater comes with 70%-100% saturated DO, hence excellent environment exists in stormwater for nitrification but not for denitrification/anammox to occur. To create an anoxic local condition, sufficient electron donors (e.g. COD or NH_4^+) need to be present in stormwater for depletion of the excessive DO. Theoretically, the minimum COD or NH_4^+ necessary for DO depletion can be estimated via stoichiometry matrix in Table 4.4 under the assumption that they are the primary electron donors in stormwater. Based on the stoichiometric matrix in Table 4.3, anoxic condition can be created in stormwater only when the reducing power in terms of oxygen consumption capacity contributed from COD and NH_4^+ concentrations is greater than stormwater DO. According to the stoichiometric relations

in Table 4.4, the reducing power, namely the amount of DO that can be reduced, can be expressed by Eq. 4.17,

$$\mathrm{COD}\,(1 - \mathrm{Y_H}) + \mathrm{S_{NH_4^+-in}}(3.43 - \mathrm{Y_{AOB}}) = 0.67\mathrm{COD} + 3.25\mathrm{S_{NH_4^+-in}} \quad \textbf{(4.17)}$$

in which, COD and $S_{NH_4^+-in}$ are influent COD and NH_4^+ nitrogen concentrations. Assuming the stormwater at 20 °C contains 90% saturated DO (Figure 4.1e), namely 8 g m^{-3}, then at least either COD = 11.94 g m^{-3} or $S_{NH_4^+-in}$ = 2.46 g N m^{-3} is required for DO depletion and anoxic environment establishment. For the convenience of the model interpretation and comparison of results, we regard BOD_5 reported in NSQD as the biodegradable fraction of the stormwater COD, which is equivalent to the substrate COD used in this model. In view of the high oxidation state of stormwater, we simplify TKN value as NH_4^+ concentration and TN – TKN value as NO_3^- concentration, respectively. As illustrated in Figures 4.1a and c, BOD_5 and TKN contained in most stormwater fall within the equivalent ranges COD < 11.94 g m^{-3} and $S_{NH_4^+-in}$< 2.46 g N m^{-3}. In other words, most of the stormwater BNR is deficient in reducing power and thus needs external organic carbon supplementation. To understand the influence of stormwater composition on the potential of BNR, we selected four combinations of influent COD and NH_4^+ concentrations, namely COD = 10 g m^{-3} and $S_{NH_4^+-in}$ = 0.5 g N m^{-3}; COD = 10 g m^{-3} and $S_{NH_4^+-in}$ = 2.5 g N m^{-3}; COD = 2.5 g m^{-3} and $S_{NH_4^+-in}$ = 0.5 g N m^{-3}; and COD = 2.5 g m^{-3} and $S_{NH_4^+-in}$ = 2.5 g N m^{-3}, as four example types of stormwater in this modeling effort to explore the potential and challenges of stormwater BNR. Given the prominent popularity observed in Figure 4.1e, 90% saturation of DO at 20 °C, namely as 8 g m^{-3}, was chosen as a representative influent DO value in this study. As for the influent NO_3^- concentration, a typical value of 1 g NO_3^--N m^{-3} was adopted from Figure 4.1d.

4.6 Results

4.6.1 Effect of HRT on steady-state NH_4^+ and TN removal efficiencies

Since HRT determines the size and cost of a stormwater treatment system, the system design capable of achieving maximum TN removal at a minimum HRT is desired. The steady-state NH_4^+ removal was simulated within a wide range of HRTs from 0.125 day to 2 days in Figure 4.7. As can be seen from profiles in Figure 4.7, steady-state NH_4^+ removal in all four types of stormwater reached maximum when HRT exceeds 0.5 days, indicating 0.5 days HRT should be sufficient for stormwater NH_4^+ removal.

Similarly, Hsieh et al. (2007) has reported that, for stormwater with 4 g m^{-3} influent nitrogen, about 85% NH_4^+ can be removed with 6 hours (0.25 day) HRT at steady state, which is in line with the result simulated in Figure 4.7b (3.5 g m^{-3} influent TN). Comparing to the typical HRT (24 to 72 hours) used for stormwater treatment (Becciu and Raimondi 2015, Wong and Somes 1995), the HRT for complete NH_4^+ removal is much shorter (Figure 4.7), which indicates that HRT should not be a limiting factor for NH_4^+ removal in stormwater treatment.

Although NH_4^+ removal was high, the TN removal efficiencies were found to be lower than 4% when $S_{NH_4^+-in}$ is as low as 0.5 g N m^{-3} regardless of the COD level at 2.5 or 10 g m^{-3}. It is significantly improved to 12% when $S_{NH_4^+-in}$ increased from 0.5 to 2.5 g N m^{-3} at COD = 2.5 g m^{-3}, and then to over 15% when COD is increased to COD = 10 g m^{-3}. Such an improvement in TN removal efficiency along with the increase of elector donors (COD and NH_4^+) concentration was related to the oxidation state of the stormwater. As calculated in Eq. 4.17, the total reducing power of NH_4^+ and COD in Figures 4.7a, b, c and d are equivalent to 8.32, 14.78, 3.29, and 9.74 g DO m^{-3}, respectively. Apparently, this trend is in line with the BNR efficiency profile in Figure 4.7, i.e., the more reducing power provided (COD and NH_4^+), the more fraction of nitrogen could be reduced to nitrogen gas.

The contribution of AMX to BNR was also investigated in the scenarios with or without AMX inoculation. Results in Figures 4.7 and c show that AMX does not contribute to BNR when NH_4^+ and reducing power are low (e.g. $S_{NH_4^+-in}$ = 0.5 g N m^{-3}, reducing power is 3.29 or 8.32 g DO m^{-3}) as the growth of AMX requires NH_4^+ and anoxic conditions. As NH_4^+ and reducing power increased, the contribution of AMX to TN removal started to manifest. As shown in Figures 4.7b and d, significant portions of TN removal can be ascribed to AMX. AMX has been found ubiquitously existing in natural environment such as soil, sediment, sludge, etc. (Terada et al. 2011). The contribution of AMX can be attributed to its ability to use NH_4^+ as a reducer to carry out BNR, which substantially mitigated the limitation of COD availability in stormwater (this is explained in a later section). Thus, analysis of simulation results in Figure 4.7 implies that AMX should be exploited as an important pathway for stormwater BNR. The essential role of AMX in stormwater BNR is further discussed in the later section of this paper.

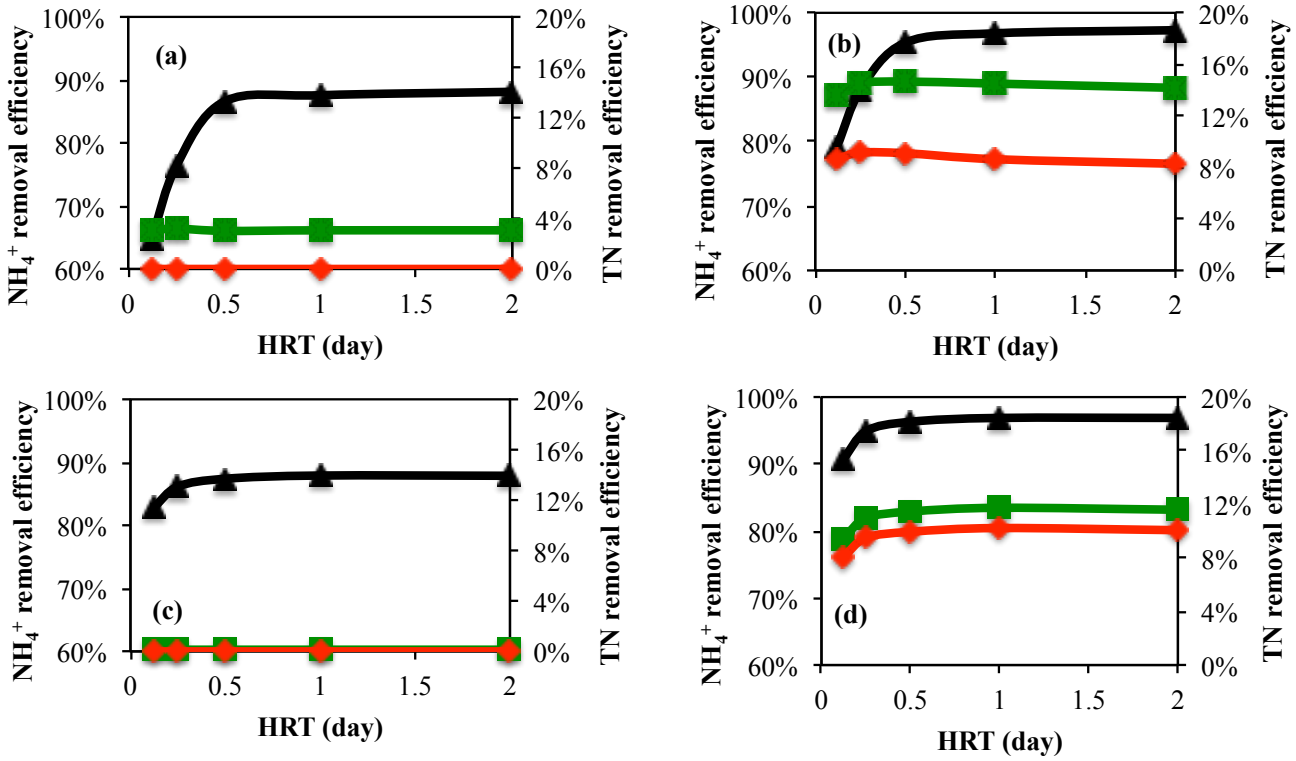

Figure 4.7 Effect of HRT on steady-state NH_4^+ and TN removal of stormwater with $S_{NO_3^- -in}$ = 1 g N m^{-3} and: a) COD =10 g m^{-3}, $S_{NH_4^+ -in}$ = 0.5 g N m^{-3}; b) COD =10 g m^{-3}, $S_{NH_4^+ -in}$ = 2.5 g N m^{-3}; c) COD = 2.5 g m^{-3}, $S_{NH_4^+ -in}$ = 0.5 g N m^{-3}; and d) COD = 2.5 g m^{-3}, $S_{NH_4^+ -in}$ = 2.5 g N m^{-3}, in which black triangle stands for NH_4^+ removal efficiency; green square for TN removal efficiency; red diamond for TN removal efficiency by AMX.

4.6.2 Effect of HRT on biofilm thickness

It should be realized that the possibility of TN removal in the homogenous bioretention system modeled in this study depends upon the existence of local anoxic zone deep inside biofilms as a result of the mass diffusion gradient (Figure 4.9). Certainly, thicker biofilms are more likely to create anoxic conditions than thinner biofilms. Figure 4.8 shows that the steady-state biofilm thickness tends to increase with the decrease of HRT. Hence, a short HRT, e.g. 0.5 day, is not only favorable for minimizing the treatment system size and cost but also is conducive to cultivating thicker biofilms with higher microbial retention

for faster bioreaction. Moreover, the layered structure in thicker biofilms tends to cultivate better aerobic and anoxic local conditions in favor of the more efficient BNR.

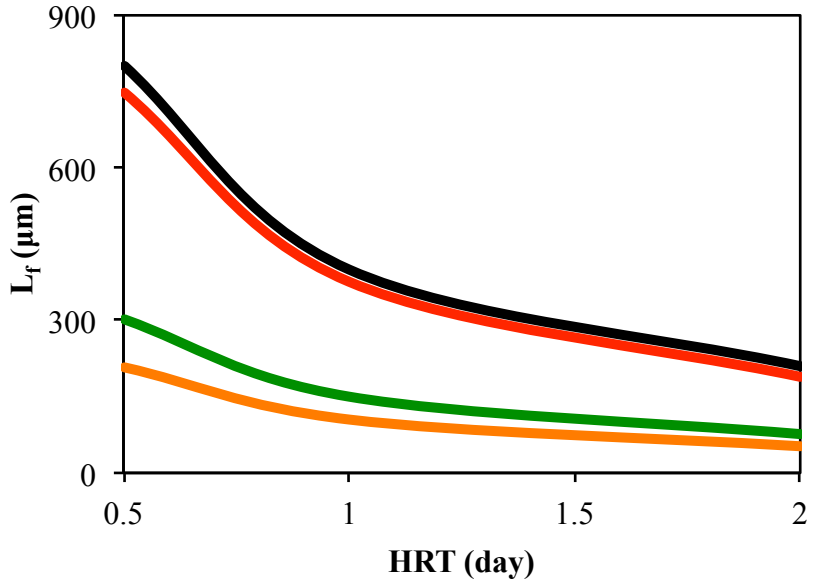

Figure 4.8 Effect of HRT on steady-state biofilm thicknesses in stormwater with $S_{NO_3^- - in}$ = 1 g N m^{-3} and COD =10 g m^{-3}, $S_{NH_4^+ - in}$ = 0.5 g N m^{-3} (red); COD =10 g m^{-3}, $S_{NH_4^+ - in}$ = 2.5 g N m^{-3} (black); COD = 2.5 g m^{-3}, $S_{NH_4^+ - in}$ = 0.5 g N m^{-3} (orange); and COD = 2.5 g m^{-3}, $S_{NH_4^+ - in}$ = 2.5 g N m^{-3} (green).

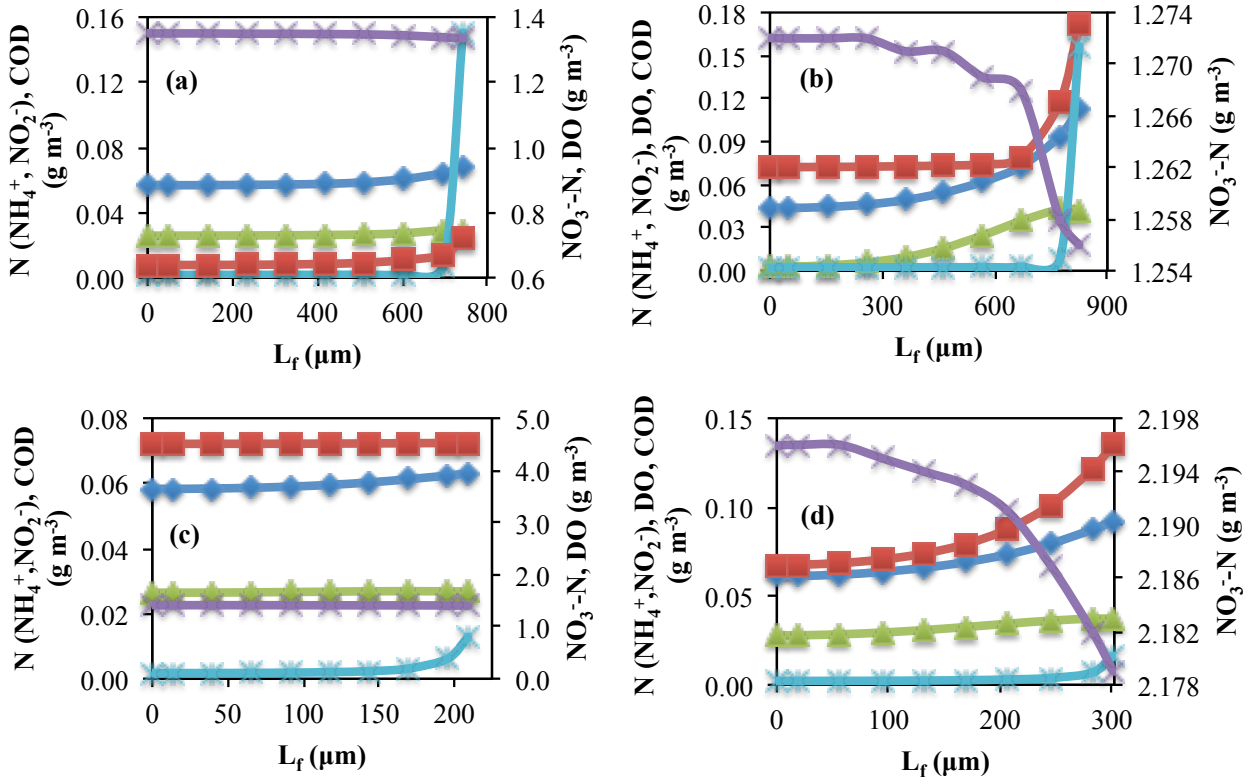

Figure 4.9 Steady-state mass distribution within biofilms treating stormwater with $S_{NO_3^- - in}$ = 1 g N m^{-3} and a) COD=10 g m^{-3}, $S_{NH_4^+ - in}$=0.5 g N m^{-3}; b) COD=10 g m^{-3}, $S_{NH_4^+ - in}$=2.5 g N m^{-3}; c) COD=2.5 g m^{-3}, $S_{NH_4^+ - in}$=0.5 g N m^{-3}; and d) COD=2.5 g m^{-3}, $S_{NH_4^+ - in}$=2.5 g N m^{-3} in which dark blue diamond stands for NH_4^+, green triangle for NO_2^-, purple X for NO_3^-, light blue asterisk for COD, and red square for DO. HRT = 0.5 days.

4.6.3 Mass distributions in biofilms

Simulation with HRT = 0.5 days in Figure 4.9 shows that all COD (e.g. 2.5 or 10 g m^{-3}) can be oxidized within the top 50 µm layer immediately after their diffusion into the biofilms. While, NH_4^+ oxidation occurs further inside biofilm beneath the layer where COD oxidation occurs. The extent of NH_4^+ oxidation depends on the penetration of the remaining DO. When $S_{NH_4^+ - in}$ = 0.5 g N m^{-3}, about 0.7 and 4.5 g m^{-3} of DO remains at COD = 10 and 2.5 g m^{-3}, respectively, due to insufficient reducing power contained in the stormwater, and this residual DO concentration penetrates the entire thickness of the biofilm. As a consequence, significant NH_4^+ oxidation can be achieved with only 0.06 g NH_4^+-N m^{-3} remaining, which

is the minimum NH_4^+ concentration to sustain AOB growth at steady state (Figures 4.9a and c). However, when $S_{NH_4^+-in}$ increases to 2.5 g N m^{-3}, merely 0.07 g m^{-3} DO can access the interior depth of the biofilm while most of the DO is consumed within the top 90-150 µm layer of the biofilm (Figures 4.9b and d). This is the depth in which COD oxidation, NH_4^+ nitrification and NO_2^- oxidation occurs within the biofilm. The coupled NH_4^+ and NO_2^- decrease without DO consumption at the depth further inside the biofilm suggests that AMX must be playing an essential role (Figure 4.9b). Microbial distribution in Figure 4.10 revealed that heterotroph, AOB and NOB predominate the top layers of the biofilm where COD and DO are depleted. AMX can only grow deep inside the biofilm where COD and DO are lean but NO_2^- and NH_4^+ are affluent. As shown in Figure 4.7, only stormwater with a relatively high reducing power offers the possibility to cultivate biofilms with an anoxic local environment for AMX prosperity.

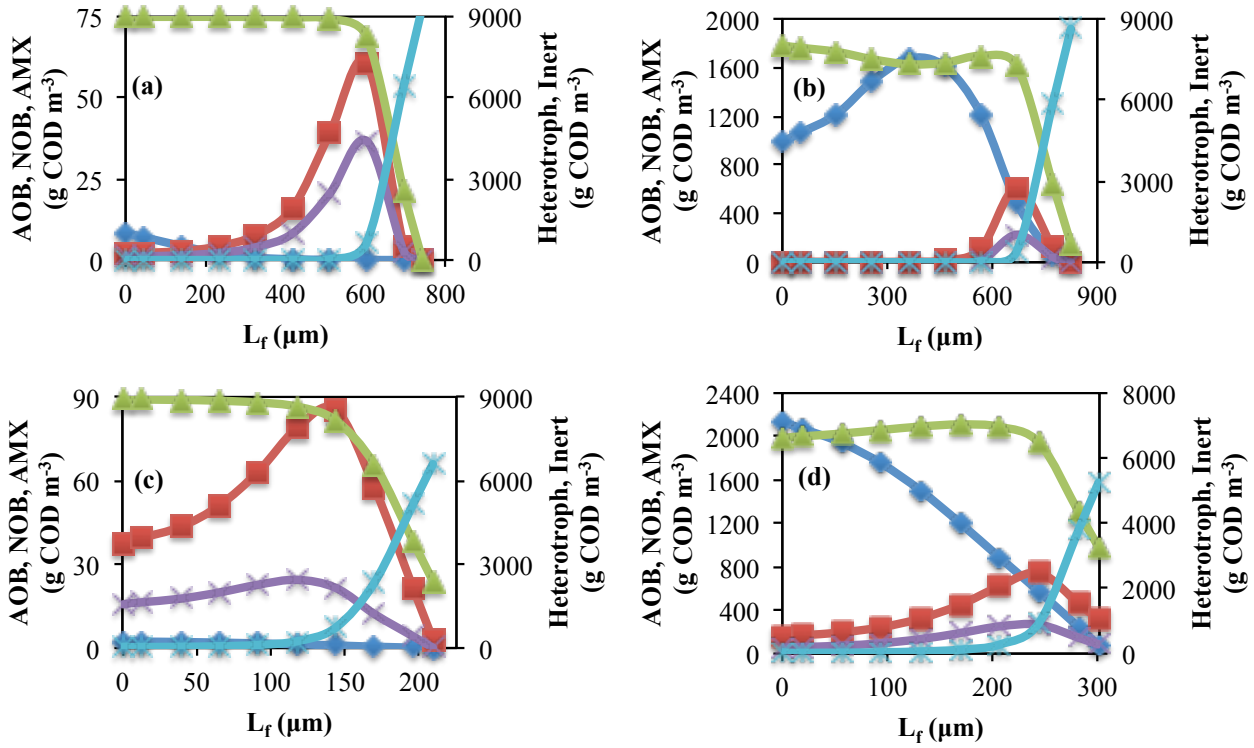

Figure 4.10 Steady-state microbial distributions within biofilms treating stormwater with $S_{NO_3^--in}$ = 1 g N m^{-3} and a) COD=10 g m^{-3}, $S_{NH_4^+-in}$=0.5 g N m^{-3}; b) COD=10 g m^{-3}, $S_{NH_4^+-in}$=2.5 g N m^{-3}; c) COD=2.5 g m^{-3}, $S_{NH_4^+-in}$=0.5 g N m^{-3}; d) COD=2.5 g m^{-3}, $S_{NH_4^+-in}$=2.5 g N m^{-3}, in which dark blue diamond stands for AMX, purple X for NOB, red square for AOB, green triangle for Inert, and light blue asterisk for Heterotroph. HRT = 0.5 days.

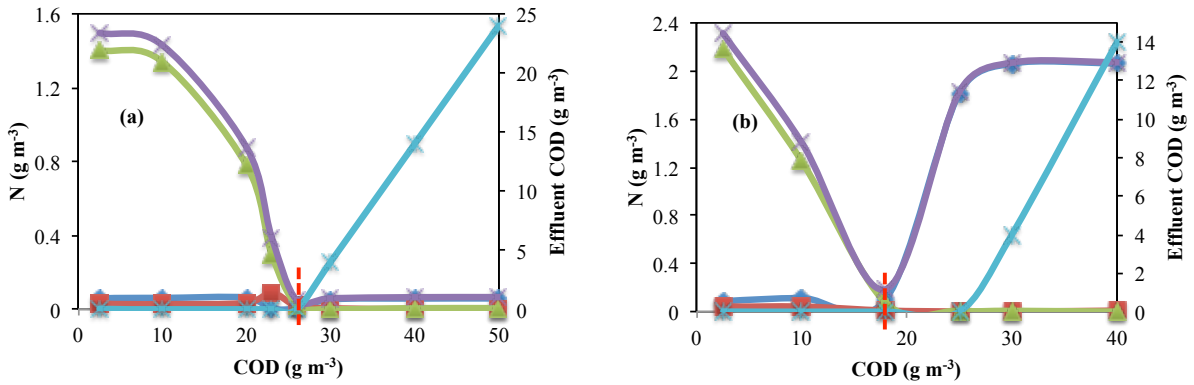

Figure 4.11 Effect of influent COD concentration on BNR of stormwater with $S_{NO_3^- - in}$ = 1 g N m^{-3} and (a) $S_{NH_4^+ - in}$ = 0.5 g N m^{-3}; and (b) $S_{NH_4^+ - in}$ = 2.5 g N m^{-3}, in which dark blue diamond stands for NH_4^+; green triangle for NO_3^-; red square for NO_2^-; purple X for TN, and light blue asterisk for COD. HRT = 0.5 days.

4.6.4 Effect of COD on BNR

It is clear from Figure 4.7 that NH_4^+ removal is easily achievable in stormwater treatment but TN removal efficiency can be improved only when the reducing power (COD and NH_4^+) provided in stormwater exceeded its oxidation power (DO). Nitrogen pollutants exist in both reducing (NH_4^+) and oxidizing (NO_3^-) forms in stormwater (Figures 4.1a and d). Hence, in a flow-through stormwater treatment system, both aerobic and anoxic conditions must be simultaneously provided to accommodate the removal of both pollutants. COD can be manipulated to achieve such an accommodating condition. As shown in Figure 4.11, TN decreased to nearly zero as the influent COD increased to a threshold COD value, namely 26 and 18 g COD m^{-3} when $S_{NH_4^+ - in}$ = 0.5 and 2.5 g N m^{-3}, respectively. Beyond this first critical COD value, effluent TN quickly increased to almost the influent level at a second threshold COD value where residual COD began to appear in the effluent stream. It is noteworthy that TN and NH_4^+ profiles closely overlapped each other beyond the first critical COD value, indicating TN in the effluent mainly consisted of NH_4^+ as a result of unsuccessful nitrification when COD exceeded the first threshold which we define as COD*. This is the COD dose that began to impact AOB activity by favoring ORH over AOB for DO utilization. Since the second COD threshold corresponded to complete breakthrough of influent COD, it indicates the minimum COD level that can deplete all oxidizing power from influent DO and NO_3^-.

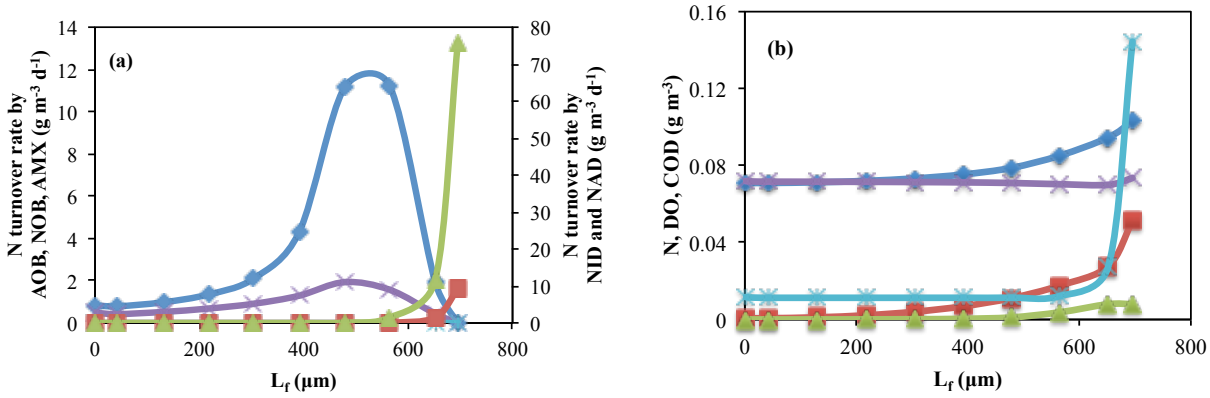

Figure 4.12 a) Distribution of BNR pathways within biofilms in which dark blue diamond stands for AMX, purple X for AOB, light blue asterisk for NOB, red square for NID, and green triangle for NAD; (b) Distribution of substrates within biofilms in which dark blue diamond stands for NH_4^+, green triangle for NO_2^-, purple X for NO_3^-, light blue asterisk for COD, and red square for DO. $S_{NO_3^- - in}$ = 1 g N m^{-3}, $S_{NH_4^+ - in}$= 2.5 g N m-3, COD^* = 18 g m^{-3} and HRT = 0.5 days.

4.6.5 BNR pathway and nitrogen flow in biofilms at COD*

A scrutiny into the BNR pathway distribution inside the biofilms at influent COD = COD* and $S_{NH_4^+ - in}$= 2.5 g N m^{-3} in Figure 4.12a reveals that both NAD and NID reactions occurred only within the top 100µm layer of the biofilm where COD is available (Figure 4.12b). Moreover, NID activity became significantly lower than that of NAD at COD*. While the highest AMX and AOB activities were located further beneath the denitrification layer, it should be noted that NOB activity became negligible throughout the entire biofilm thickness, which is indeed unique at COD*. An integration of the amount of nitrogen removed through each pathway in Figure 4.12a reveals two major characteristics of BNR at COD*: i) Majority (90%) of nitrogen (NH_4^+ or NO_3^-) is removed through AMX while only 10% through NID; and ii) Only partial nitritation occurred with no need of NOB. Therefore, Figure 4.12 implies that the primary BNR pathway at COD* is through partial nitritation and AMX for the least COD consumption.

4.7 Discussion

4.7.1 Mechanism of complete BNR at COD*

Since BNR requires the co-existence of aerobic and anoxic conditions, and biofilms offer both local conditions along the mass diffusion gradient across the biofilm thickness, COD becomes a decisive factor in regulating the oxidation and reduction conditions in stormwater. A threshold COD* must be provided to strike a balance between the two conditions, i.e., allow enough oxygen for NH_4^+ oxidation and sufficient COD for residual oxygen depletion. It can be seen from Figure 4.12a that AMX and NAD dominated nitrogen removal processes, which implies that the essence in providing COD* is to reduce stormwater DO to a critical level that is just enough for the oxidation of an appropriate amount of NH_4^+ to NO_2^- to establish an anoxic condition and an optimum NO_2^--to-NH_4^+ ratio deep inside the biofilms for AMX reaction. COD < COD* leads to BNR failure because of the inadequate reducing power for anoxic condition establishment (Figure 4.11), while COD > COD* causes insufficient NH_4^+ nitrification due to inadequate DO remaining for AOB after COD oxidation.

4.7.2 Stoichiometric estimation of COD*

The value of COD* is indeed governed by the need for bulk DO depletion, NH_4^+ oxidation, and NO_3^-/ NO_2^- denitrification. Theoretically, three scenarios can be generalized for stormwater BNR with regard to COD* demand.

Scenario 1: When influent NH_4^+ nitrogen ($S_{NH_4^+-in}$) to influent NO_3^- nitrogen ($S_{NO_3^--in}$) ratio $S_{NH_4^+-in}$: $S_{NO_3^--in}$ > 1.15 (this value can be determined from a later derivation in Eq. 4.27), NH_4^+ oxidation, NAD, and AMX will become the major pathways for stormwater BNR at minimum COD consumption. In this scenario, COD* is provided to reduce the NO_3^- contained in influent ($S_{NO_3^--in}$) and the NO_3^- produced by AMX ($S_{NO_3^--AMX}$), and also to reduce the DO excessive to AOB utilization. According to the stoichiometry matrix in Table 4.4 and the nitrogen flow in Figure 4.13a, the NH_4^+ consumption for the two steps of denitrification ($S_{NH_4^+-NAD}$ and $S_{NH_4^+-NID}$) of the NO_3^- in influent ($S_{NO_3^--in}$) and the NO_3^- produced by AMX ($S_{NO_3^--AMX}$) can be calculated by Eq. 4.18,

$$S_{NH_4^+-NAD} + S_{NH_4^+-NID} = (S_{NO_3^--in} + 2S_{NO_3^--AMX})\frac{Y_{NH}}{Y_{NO}} \quad \textbf{(4.18)}$$

Defining the NH_4^+ and NO_2^- consumed by AMX as $S_{NH_4^+-AMX}$ and $S_{NO_2^--AMX}$, respectively, NO_3^- produced by AMX can be calculated as,

$$S_{NO_3^--AMX} = \frac{S_{NH_4^+-AMX} + S_{NO_2^--AMX}}{\frac{2}{Y_{AMX}} + \frac{1}{1.14}} \times \frac{1}{1.14} \quad \textbf{(4.19)}$$

Since at COD*, complete TN removal can be achieved without NOB, the NH_4^+ consumption by AOB ($S_{NH_4^+-AOB}$) and AMX can be calculated through mass balance as,

$$S_{NH_4^+-AOB} + S_{NH_4^+-AMX} = S_{NH_4^+-in} - \left(S_{NH_4^+-NAD} + S_{NH_4^+-NID}\right) \quad \textbf{(4.20)}$$

Because AMX is the primary pathway for N_2 production in this scenario (Figure 4.13a), all nitrogen input except the NO_3^- produced by AMX bacteria, namely $S_{NO_3^--in} + S_{NH_4^+-in} - S_{NO_3^--AMX}$ will be removed by AMX. Thereby, the NO_2^- consumed by AMX ($S_{NO_2^--AMX}$) can be estimated by,

$$S_{NO_2^--AMX} = S_{NO_3^--in} + S_{NH_4^+-AOB} \quad \textbf{(4.21)}$$

The relation between NO_2^- and NH_4^+ consumed by AMX is expressed in Eq. 4.22,

$$S_{NO_2^--AMX} = S_{NH_4^+-AMX}\frac{\frac{1}{Y_{AMX}} + \frac{1}{1.14}}{\frac{1}{Y_{AMX}}} \quad \textbf{(4.22)}$$

Likewise, the ratio of DO to NH_4^+ consumption by AOB can be described in Eq. 4.23,

$$S_{O_2-AOB} = S_{NH_4^+-AOB}(3.43 - Y_{AOB}) \quad \textbf{(4.23)}$$

All unknown parameters in Eqs. 4.18 to 23 can be solved. In turn, COD required by ORH (COD_{ORH}) can be estimated as,

$$COD_{ORH} = \frac{S_{O_2-ORH}}{1 - Y_H} = \frac{S_{O_2-in} - S_{O_2-AOB}}{1 - Y_H} \quad \textbf{(4.24)}$$

in which S_{O_2-ORH} is DO consumed by ORH. Likewise, COD required by denitrifier (COD_{DEN}) can be estimated as,

$$COD_{DEN} = \frac{S_{NO_3^--in} + 2S_{NO_3^--AMX}}{Y_N Y_{NO}} \quad \textbf{(4.25)}$$

Thus, COD^* in scenario 1 can be expressed in Eq. 4.26,

$$COD^* = COD_{ORH} + COD_{DEN} = \frac{S_{O_2-in} - S_{O_2-AOB}}{1 - Y_H} + \frac{S_{NO_3^--in} + 2S_{NO_3^--AMX}}{Y_N Y_{NO}} \quad \textbf{(4.26)}$$

Based on the nitrogen flux calculated for scenario 1 in Figure 4.13a, about 91% influent nitrogen can be converted to nitrogen gas, in which 84% is produced by AMX. Obviously, AMX plays an essential role in nitrogen removal in scenario 1.

As the $S_{NH_4^+-in}$: $S_{NO_3^--in}$ ratio decreases in scenario 1, AOB activity decreases accordingly. There is a critical $S_{NH_4^+-in}$: $S_{NO_3^--in}$ ratio in scenario 1 when zero NH_4^+ is available for AOB utilization. This ratio defines the lower boundary of scenario 1 and can be determined as $S_{NH_4^+-in}$: $S_{NO_3^--in}$ = 1.15 in Eq. 4.27,

$$\frac{S_{NH_4^+-in} - \left(S_{NH_4^+-NAD} + S_{NH_4^+-NID}\right)}{S_{NO_3^--in} - S_{NH_4^+-NID}\frac{Y_{NO}}{Y_{NH}}} = \frac{\frac{1}{Y_{AMX}}}{\frac{1}{Y_{AMX}} + \frac{1}{1.14}} \quad \textbf{(4.27)}$$

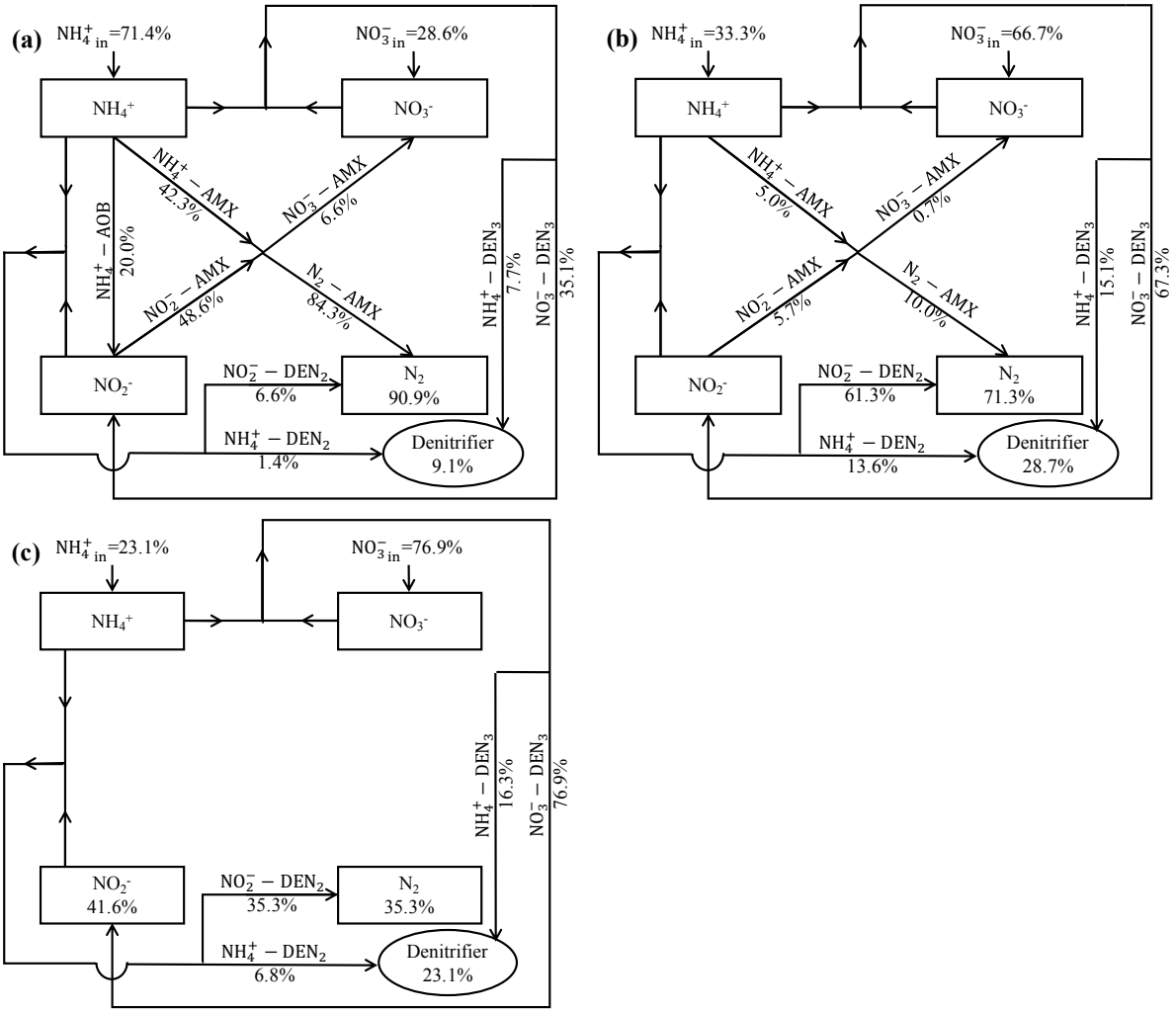

Figure 4.13 Example nitrogen flux in biofilms calculated by stoichiometric equations for a) scenario 1; b) scenario 2; and c) scenario 3.

Scenario 2: When the ratio of influent $S_{NH_4^+-in} : S_{NO_3^--in} \leqslant 1.15$, AOB reaction cannot occur for the lack of influent NH_4^+. In this scenario, COD* needs to be provided to denitrify all influent NO_3^- to NO_2^- and then denitrify the NO_2^- that cannot be processed by AMX to nitrogen gas. Because $S_{NH_4^+-AOB} = 0$ in this scenario, Eq. 4.20 can be simplified as Eq. 4.28,

$$S_{NH_4^+-AMX} = S_{NH_4^+-in} - \left(S_{NH_4^+-NAD} + S_{NH_4^+-NID}\right) \quad \textbf{(4.28)}$$

The amount of NH_4^+ that needs to be used for denitrification can be estimated from the stoichiometry in Table 4.4 as,

$$S_{NH_4^+-NAD} + S_{NH_4^+-NID} = \left(S_{NO_3^--NAD} + S_{NO_2^--NID}\right)\frac{Y_{NH}}{Y_{NO}} \quad \textbf{(4.29)}$$

The mass balance for nitrogen flow through denitrification can be expressed in Eq. 4.30,

$$S_{NO_3^--NAD} + S_{NO_2^--NID} = 2S_{NO_3^--in} - S_{NO_2^--AMX} + 2S_{NO_3^--AMX} \quad \textbf{(4.30)}$$

Substituting Eq. 4.28 into Eq. 4.22 gives Eq. 4.31,

$$S_{NO_2^--AMX} = \frac{S_{NH_4^+-in} - \left(S_{NH_4^+-NAD} + S_{NH_4^+-NID}\right)}{\frac{1}{Y_{AMX}}}\left(\frac{1}{Y_{AMX}} + \frac{1}{1.14}\right) \quad \textbf{(4.31)}$$

Likewise, the NO_3^- produced by AMX can be estimated in Eq. 4.32,

$$S_{NO_3^--AMX} = \frac{S_{NH_4^+-in} - \left(S_{NH_4^+-NAD} + S_{NH_4^+-NID}\right)}{\frac{1}{Y_{AMX}}}\frac{1}{1.14} \quad \textbf{(4.32)}$$

$S_{NH_4^+-NAD} + S_{NH_4^+-NID}$ can be solved from Eqs. 4.29 to 32 as Eq. 4.33,

$$S_{NH_4^+-NAD} + S_{NH_4^+-NID} = \frac{2S_{NO_3^--in} - S_{NH_4^+-in}\left(1 - \frac{Y_{AMX}}{1.14}\right)}{\frac{Y_{NO}}{Y_{NH}} - \left(1 - \frac{Y_{AMX}}{1.14}\right)} \quad \textbf{(4.33)}$$

Hence, Eqs. 4.34 and 35 can be derived,

$$COD_{DEN} = \frac{S_{NO_3^--NAD} + S_{NO_2^--NID}}{Y_N Y_{NO}} = \frac{2S_{NO_3^--in} - S_{NO_2^--AMX} + 2S_{NO_3^--AMX}}{Y_N Y_{NO}} \quad \textbf{(4.34)}$$

$$COD^* = COD_{ORH} + COD_{DEN} = \frac{S_{O_2-in}}{1 - Y_H} + \frac{2S_{NO_3^--in} - S_{NO_2^--AMX} + 2S_{NO_3^--AMX}}{Y_N Y_{NO}} \quad \textbf{(4.35)}$$

An example calculation of the nitrogen flux in scenario 2 is shown in Figure 4.13b. As can be seen, about 71% influent nitrogen can be removed as nitrogen gas in this scenario, of which majority (61%) is removed by NID while only 10% by AMX. Again, the insufficient NH_4^+ for AMX accounts for it.

Scenario 3: When influent NH_4^+ is so low that it is even insufficient for two-step denitrification, namely $S_{NH_4^+-in} : S_{NO_3^--in} < \frac{2Y_{NH}}{Y_{NO}} = 0.44$, only incomplete BNR can be possibly achieved. Hence, COD_{DEN} can be expressed in Eq. 4.36,

$$COD_{DEN} = \frac{S_{NH_4^+-in}}{Y_N Y_{NH}} \quad \textbf{(4.36)}$$

In this case, the maximum BNR efficiency can be estimated as,

$$BNR\% = \frac{S_{NH_4^+-in}}{S_{NO_3^--in} + S_{NH_4^+-in}} \cdot \frac{Y_{NO}}{2Y_{NH}} \quad \textbf{(4.37)}$$

Hence, COD demand in this scenario can be estimated in Eq. 4.38,

$$COD^* = COD_{ORH} + COD_{DEN} = \frac{S_{O_2-in}}{1 - Y_H} + \frac{S_{NH_4^+-in}}{Y_N Y_{NH}} \quad \textbf{(4.38)}$$

As illustrated in an example calculation in Figure 4.13c, denitrification is the only pathway that contributes to BNR in this scenario, and only about 35.3% influent nitrogen can be effective removed in the form of nitrogen gas.

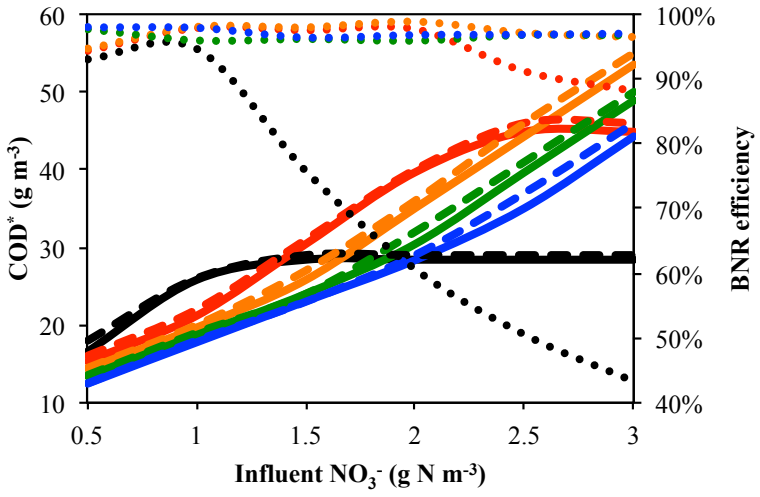

Figure 4.14 Effect of $S_{NO_3^--in}$ and $S_{NH_4^+-in}$ on COD^* and BNR efficiency, in which $S_{NH_4^+-in}$= 0.5 (black), 1 (red), 1.5 (orange), 2 (green), and 2.5 (blue) g N m^{-3}. Solid lines represent calculated COD* using Eqs.

4.26, 35 and 38; long dashed lines represent model simulated COD*; and short dashed lines represent BNR efficiency.

4.7.3 NH_4^+ availability for BNR

As explained in previous section, the COD* value for maximum stormwater BNR is closely related to the ratio of NH_4^+ to NO_3^- in stormwater and can be estimated with stoichiometric equations (Eqs. 4.26, 35 and 38). The accuracy of these equations in predicting COD* was compared with the kinetic model prediction in Figure 4.14. As can be seen, the results of stoichiometric calculation closely followed that of the kinetic model simulation, indicating the adequacy of using Eqs. 4.26, 35 and 38 for quick COD* estimation. Moreover, Figure 4.14 also demonstrates that COD* significantly increases with the influent NO_3^- concentration for increased reducer needs, while COD* tends to decrease with the increase of influent NH_4^+ concentration for the opposite reason. As for the BNR efficiency, when sufficient COD* is provided, the NH_4^+ availability becomes a major limiting factor, as it is a required substrate for both AMX and denitrification. Such an NH_4^+ limitation becomes especially prominent as the influent NH_4^+-to-NO_3^- ratio falls below 0.44 as discussed in scenario 3. For example, BNR efficiencies of stormwater with low $S_{NH_4^+-Ha}$ (0.5 or 1.0 g N m^{-3}) quickly plunged to minimum once $S_{NO_3^--Oc}$ exceeds 1 and 2 g N m^{-3}, respectively (Figure 4.14). Thus can be seen, the NH_4^+ availability is essential for successful stormwater BNR, as well. An analysis of NSQD in Figure 4.15 shows that about 9.6% stormwater are subjected to NH_4^+ limitation (scenario 3). While, it is encouraging to see that 71% of the stormwater contains sufficient NH_4^+ for AMX-predominated scenario 1 and 19% for denitrification-predominated scenario 2 (Figure 4.15).

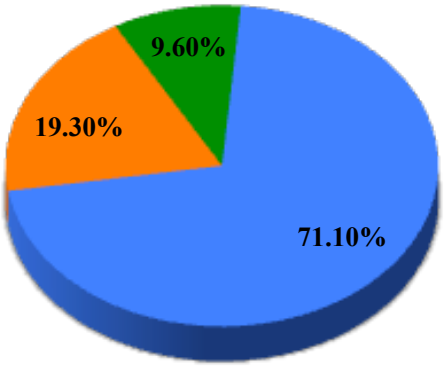

Figure 4.15 Fraction of U.S. stormwater in NSQD with NH_4^+-N to NO_3^--N ratio under scenario 1 (blue), scenario 2 (orange), and scenario 3 (green).

4.7.4 COD availability for BNR

A comparison of COD* with the actual BOD_5 contents in stormwater at corresponding NH_4^+ and NO_3^- levels were plotted in Figure 4.16a. It is further estimated from Figure 4.16b that about 82.6% U.S. stormwater contains BOD_5 lower than COD* required for complete BNR, which implies that external carbon source needs to be supplemented for most of the stormwater BNR facilities. Vegetation planted in the topsoil of bioretention system may release some COD (Table 4.4). For example, plant roots exude small organic molecules including sugars, amino acids, organic acids and amides (Neff and Asner 2001). However, it has been reported that denitrification is controlled by the limited translocation of organic carbon to the soils by crop roots. Moreover, COD in the agricultural soils have been found not to be bioavailable and thus contributed negligibly to the denitrification process (Siemens et al. 2003). The slow COD-releasing biofilm carriers developed in recent years may be applied as an alternative for COD supplementation (Liu et al. 2012, Zhang et al. 2015).

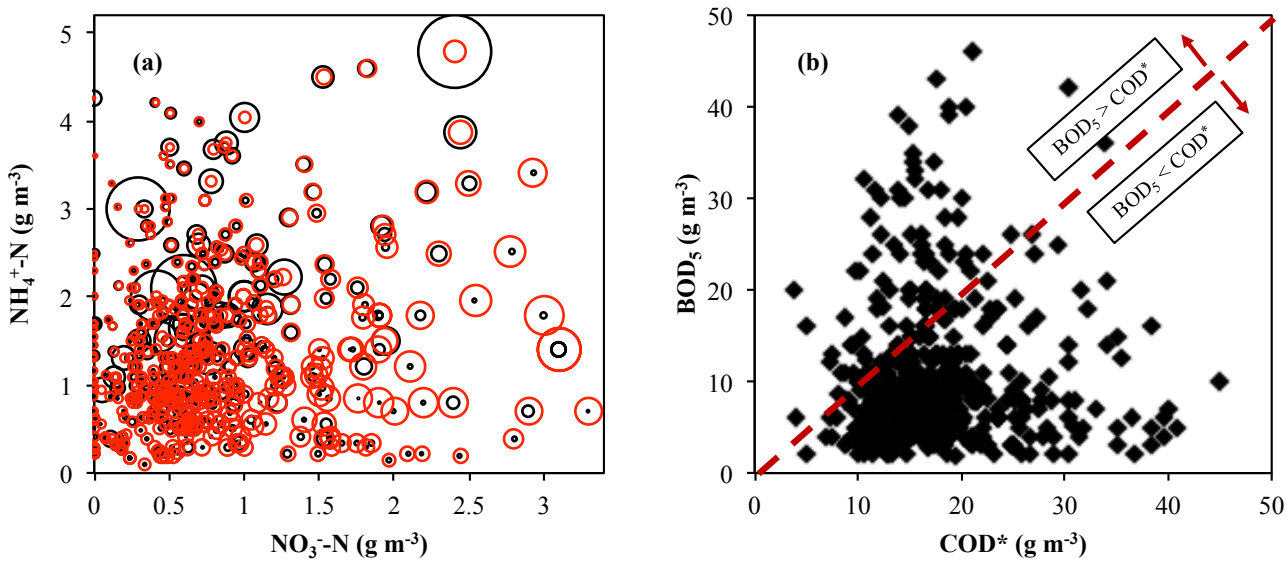

Figure 4.16 (a) BOD_5 concentration (black circle size) and COD* concentration (red circle size) calculated at corresponding influent NH_4^+-N and NO_3^--N concentrations in NSQD; (b) BOD_5 vs COD^* plot.

4.7.5 Importance of AMX for stormwater BNR

According to kinetic model simulation and stoichiometric estimation presented previously, 71% of the stormwater in the U.S. contains NH_4^+-to-NO_3^- ratios suitable for nitrogen removal via AMX pathway (Figure 4.15 and Scenario 1). To elucidate the importance of AMX in stormwater BNR, simulation was performed with and without AMX for stormwater with $S_{NH_4^+-in}$ ranging from 0.5 to 2.5 g N m^{-3} and $S_{NO_3^--in}$ from 0.5 to 3 g N m^{-3}, and results are shown in Figure 4.17. As can be seen in Figure 4.17a, the COD* without AMX can be two-fold higher than the COD* with AMX, which indicates the essential role of AMX in mitigating the carbon source limitation in stormwater BNR. Figure 4.17b demonstrates that the BNR efficiency can be significantly compromised without AMX, which is true especially at higher $S_{NH_4^+-in}$: $S_{NO_3^--in}$ ratio.

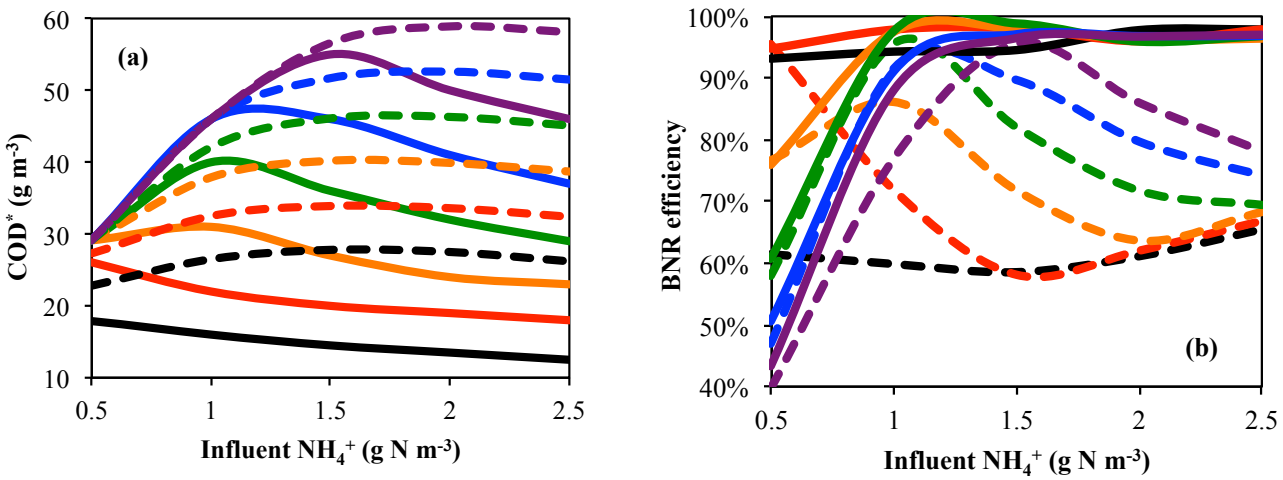

Figure 4.17 Effect of influent NH_4^+ on a) COD* and b) BNR efficiency with (solid line) and without (dashed line) AMX at $S_{NO_3^- - in}$ = 0.5 (black), 1 (red), 1.5 (orange), 2 (green), 2.5 (blue), 3 (purple) g N m^{-3}. HRT = 0.5 days.

4.7.6 Alkalinity availability for stormwater BNR

Given the essential role of autotrophic bacteria (e.g. AOB and AMX) in stormwater BNR, it is important to know the alkalinity availability in stormwater as alkalinity provides inorganic carbon source for AOB an AMX growth (Paredes et al. 2007). Eqs. 4.39 and 40 are stoichiometric equations in description of AOB and AMX growth according to their growth yield values listed in Table 4.3 (Henze 2002, van Dongen et al. 2001),

$$NH_4^+ + 1.4035O_2 + 1.9852HCO_3^- + 0.07425CO_2 \rightarrow 0.01485C_5H_7NO_2 + 0.9852NO_2^- + 1.9852CO_2 + 2.9406H_2O \quad \textbf{(4.39)}$$

$$NH_4^+ + 1.32NO_2^- + 0.066HCO_3^- + 0.13H^+ \rightarrow 1.02N_2 + 0.26NO_3^- + 0.66CH_2O_{0.5}N_{0.15} + 2.03H_2O \quad \textbf{(4.40)}$$

According to Eqs. 4.39 and 40, the molar ratio of HCO_3^-: NH_4^+ for AOB and AMX growth is 1.99 and 0.07, respectively, suggesting that AOB is a major consumer of alkalinity in stormwater BNR. The scenario 1 described in Figure 4.13a has the highest alkalinity demand because of the intensive NH_4^+ oxidation and

significant nitrogen gas production via AMX. The stoichiometry of such a partial nitritation and AMX process can be expressed by Eq. 4.41 as derived from Eqs. 4.39 and 40,

$$NH_4^+ + 1.165HCO_3^- + 0.556H^+ + 0.0425CO_2 + 0.8037O_2 \rightarrow 0.4359N_2 + 0.2821CH_2O_{0.5}N_{0.15} + 2.5515H_2O + 0.0085C_5H_7NO_2 + 1.1368CO_2 + 0.1111NO_3^- \quad \textbf{(4.41)}$$

According to Eq. 4.41, the molar ratio of HCO_3^-: NH_4^+ for an integrated partial nitritation and AMX process in scenario 1 is 1.17, and this ratio also indicates that 4.16 g alkalinity ($CaCO_3$) is required for 1 g NH_4^+-N consumption. Hence, as long as the mass ratio of influent alkalinity to NH_4^+ ($S_{Alk(CaCO_3)-in}: S_{NH_4^+-N-in}$) is greater 4.16, the alkalinity for AOB and AMX growth in scenario 1 should be adequate. According to NSQD analyzed in Figure 4.18, at least 95% of the stormwater in the U.S. contains $S_{Alk(CaCO_3)-in}: S_{NH_4^+-N-in} \geq 4.16$. Hence, it is a reasonable consideration that the alkalinity content of most stormwater should be sufficient for BNR, which justifies the negligence of alkalinity effect from the model development in this study.

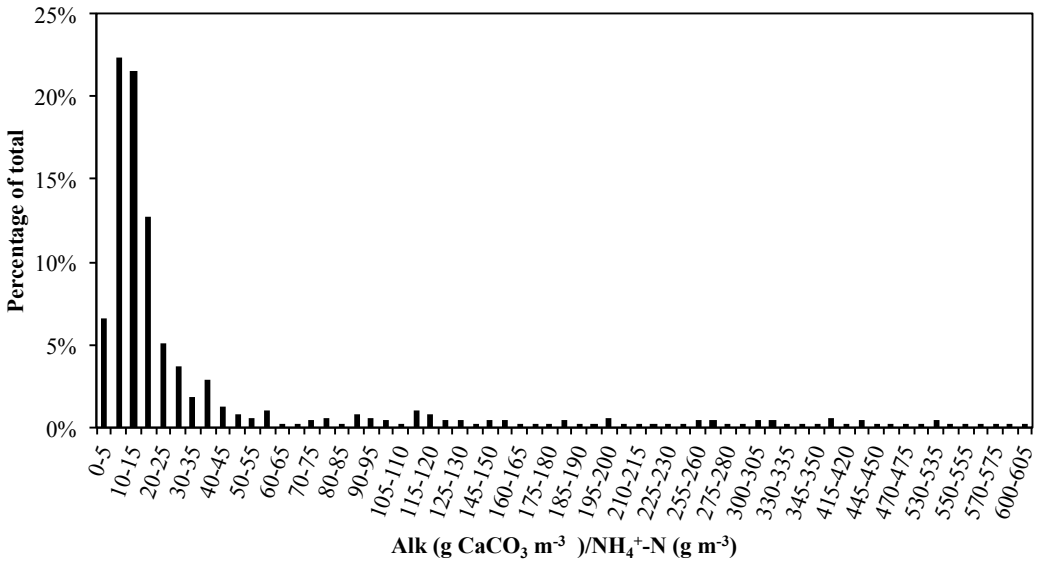

Figure 4.18 Probability density of alkalinity to NH_4^+-N ratio calculated with data from NSQD.

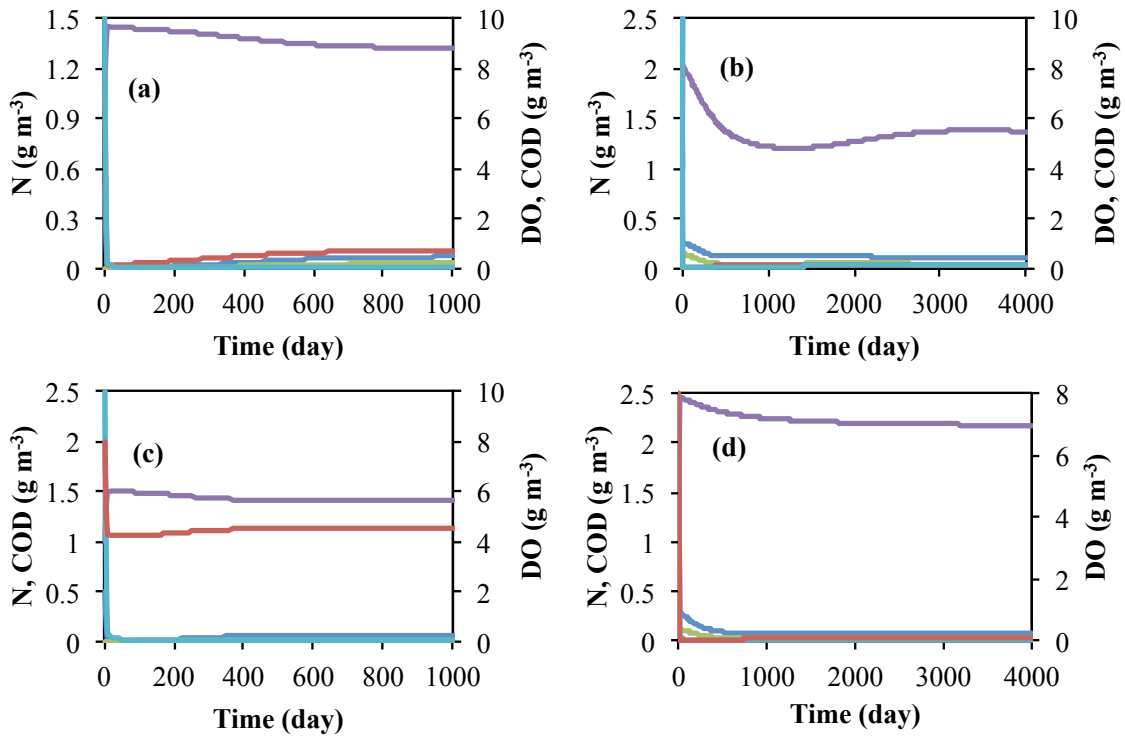

Figure 4.19 Variation of the effluent COD, DO, and N along with the operation duration of bioretention treating stormwater with $S_{NO_3^- - in}$ = 1 g N m^{-3} and a) COD = 10 g m^{-3}, $S_{NH_4^+ - in}$ = 0.5 g N m^{-3}; b) COD = 10 g m^{-3}, $S_{NH_4^+ - in}$ = 2.5 g N m^{-3}; c) COD = 2.5 g m^{-3}, $S_{NH_4^+ - in}$ = 0.5 g N m^{-3}; d) COD = 2.5 g m^{-3}, $S_{NH_4^+ - in}$ = 2.5 g N m^{-3}. Dark blue stands for NH_4^+, green for NO_2^-, purple for NO_3^-, light blue for COD, and red for DO. HRT = 0.5 days.

4.7.7 Importance of bioaugmentation for stormwater BNR

Although excellent stormwater BNR is achievable at steady state with influent COD optimization, the actual duration it takes for a natural bioretention system to reach such a steady state deserves investigation. By using the initial microbial concentrations determined from the model simulation of the study by Payne et al. (2014) (Table 4.5), it can be seen from Figure 4.19 that extremely long startup duration is needed to achieve steady-state performance. Apparently, the startup duration of a biological system is highly dependent on the inoculum concentration, especially for the bioprocesses that rely on slow growing microbes such as AMX. Therefore, seed incubators should be developed in service for future stormwater BNR application.

4.7.8 Model limitations and future work

The mathematical model developed in this study is designated to access the BNR potential of various stormwater, which limits its applicability in predicting the dynamic performance of bioretention systems. For example, homogeneous environment is assumed to exist in the bioretention that is continuously fed with constant quality stormwater in this study. While, stormwater quality is known to vary with time and space. As a matter of fact, the kinetic expressions listed in Tables 4.2 provide a mechanistic framework for simulating the dynamic processes of bioretention systems, and practitioners may have the freedom to apply the same modeling framework towards specific scenarios in the real world. The major unknown component of the modeling framework actually lies in the simulation of the BNR community response to the dry season interval between storm events, which is another important aspect in need of further investigation. Accumulated evidence shows that BNR communities are rather resilient to periodic starvation. Studies by Reeve et al. (2016) and Wu et al. (2015) show that the AMX communities were able to quickly resume to normal activity within one day after about two-month starvation. AOB activity decreased slowly during starvation up to 10 days. Yet, within 10 min after the addition of fresh NH_4^+, 100% activity was regained (Bollmann et al. 2005). The recovery of AOB and NOB activities was also reported by Ma et al. (2015) within four and seven days after about a month starvation, and the better recovery ability of AOB comparing to NOB is actually favorable for stormwater BNR in that NOB has very limited involvement in the three scenarios described above. It is a reasonable speculation that the BNR system for stormwater treatment may share similar resilience in handling dry periods between storm events. Experimental verification is definitely needed in the future to evaluate the model accuracy and such a dry period effect.

4.8 Conclusions

Following concluding remarks can be made from this study:

1. A mathematical model was for the first time developed to simulate the spatial distribution of BNR activity in the structure of biofilms formed on bioretention media for stormwater treatment.
2. At the steady state of the bioretention operation, 0.5 days turn out to be the minimum HRT for maximum stormwater BNR.

3. Model simulation showed that biofilm thickness increased with decreasing HRT, and all heterotrophs (ORH, NAD, and NID) are distributed in the top layer of the biofilm due to the COD limitation. Beneath that, AOB and NOB are inhabited with the latter being mostly outcompeted by the former for DO limitation. AMX grows in the bottom layer of biofilms where both DO and COD are limited but NH_4^+ and NO_2^- are present as a result of partial nitritation by AOB.
4. A comparison of the modeled results to NSQD information shows that 82.6% of urban stormwater is deficient in influent organic carbon source for the lack of reducing power to create necessary anoxic conditions for BNR. Hence, an appropriate amount of external carbon source needs to be supplemented in most urban runoff influent to meet a threshold reducing power demand (COD*) for complete BNR.
5. COD* values increased with the increasing stormwater NO_3^- content but decreased with the NH_4^+ content. Application of AMX can significantly reduce COD* and enhance BNR efficiency.
6. The availability of NH_4^+ is another limiting factor for stormwater BNR as it is a required substrate for AMX and denitrification. It was estimated in this study that 71.1% urban stormwater contains adequate NH_4^+ for both AMX and denitrification, 19.3% contains adequate NH_4^+ for denitrification but inadequate for AMX, while the NH_4^+ content in 9.6% urban stormwater is inadequate for neither AMX nor denitrification.
7. When the ratio of influent NH_4^+-N to NO_3^--N > 1.15, most stormwater nitrogen can be removed through AMX pathway to nitrogen gas. When this ratio ≤ 1.15 but > 0.44, denitrification becomes a major nitrogen removal pathway. When this ratio ≤ 0.44, NH_4^+ becomes a limiting substrate for both denitrifier and AMX, and in turn only incomplete nitrogen removal can be achieved through denitrification.
8. 95% urban stormwater was found to contain sufficient alkalinity as inorganic carbon source for autotropic growth of the BNR community.
9. Although this study demonstrated that the steady-state performance of stormwater bioretention systems is sufficient for BNR removal, the time it takes to reach such a steady state is very long. For this reason, bioaugmentation should be considered as a necessary means in future stormwater treatment system development and application.

4.9 References

Almenglo, F., Ramírez, M., Gómez, J. M., Cantero, D., Gamisans, X., & Dorado, A. D. (2016). Modeling and control strategies for anoxic biotrickling filtration in biogas purification. Journal of Chemical Technology & Biotechnology, 91(6), 1782-1793.

Alpkvist, E., Picioreanu, C., van Loosdrecht, M. C. M., & Heyden, A. (2006). Three-dimensional biofilm model with individual cells and continuum EPS matrix. Biotechnology and Bioengineering, 94(5), 961-979.

Becciu, G., & Raimondi, A. (2015). Probabilistic analysis of the retention time in stormwater detention facilities. Procedia Engineering, 119, 1299-1307.

Bollmann, A., Schmidt, I., Saunders, A. M., & Nicolaisen, M. H. (2005). Influence of starvation on potential ammonia-oxidizing activity and amoA mRNA levels of Nitrosospira briensis. Applied and Environmental Microbiology, 71(3), 1276-1282.

Brown, R. A., & Hunt, W. F. (2011). Impacts of media depth on effluent water quality and hydrologic performance of undersized bioretention cells. Journal of Irrigation and Drainage Engineering-Asce, 137(3), 132-143.

Cao, Y. S. (2008). Biological nitrogen removal activated sludge process in warm climates: full-scale process investigation, scaled-down laboratory experimentation and mathematical modelling. London: IWA Pub.

Charles-Edwards, D. A., Doley, D., & Rimmington, G. M. (1986). Modelling plant growth and development. Orlando;Sydney;: Academic Press.

County, P. G. s. (1999). Low-impact development design strategies: an integrated design approach. Department of Environmental Resources, Programs and Planning Division, Prince George's County, Maryland.

Daly, E., Deletic, A., Hatt, B. E., & Fletcher, T. D. (2012). Modelling of stormwater biofilters under random hydrologic variability: a case study of a car park at Monash University, Victoria (Australia). Hydrological Processes, 26(22), 3416-3424.

Davidson, E. A., Savage, K. E., Bettez, N. D., Marino, R., & Howarth, R. W. (2010). Nitrogen in runoff from residential roads in a coastal area. Water, Air, & Soil Pollution, 210(1), 3-13.

Davis, A. P., Hunt, W. F., Traver, R. G., & Clar, M. (2009). Bioretention technology: overview of current practice and future needs. Journal of Environmental Engineering-Asce, 135(3), 109-117.

De Clippeleir, H., Yan, X. G., Verstraete, W., & Vlaeminck, S. E. (2011). OLAND is feasible to treat sewage-like nitrogen concentrations at low hydraulic residence times. Applied Microbiology and Biotechnology, 90(4), 1537-1545.

Deng, Z. Q., Sun, S. W., & Gang, D. D. (2012). Modeling nitrate-nitrogen removal process in first-flush reactor for stormwater treatment. Bioprocess and Biosystems Engineering, 35(6), 865-874.

Dietz, M. E. (2007). Low impact development practices: A review of current research and recommendations for future directions. Water Air and Soil Pollution, 186(1-4), 351-363.

Dybas, C. L. (2005). Dead zones spreading in world oceans. Bioscience, 55(7), 552-557.

Fan, J. L., Wang, W. G., Zhang, B., Guo, Y. Y., Ngo, H. H., Guo, W. S., . . . Wu, H. M. (2013). Nitrogen removal in intermittently aerated vertical flow constructed wetlands: Impact of influent COD/N ratios. Bioresource Technology, 143, 461-466.

Galloway, J. N., Aber, J. D., Erisman, J. W., Seitzinger, S. P., Howarth, R. W., Cowling, E. B., & Cosby, B. J. (2003). The nitrogen cascade. Bioscience, 53(4), 341-356.

Guerra, H. B., Park, K., & Kim, Y. (2013). Empirical regression models for estimating nitrogen removal in a stormwater wetland during dry and wet days. Water Science and Technology, 68(7), 1641-1649.

Guerra, H. B., Park, K., Niu, S., & Kim, Y. (2013). Adaptability of wastewater wetland models in estimating nutrient removal in a stormwater wetland on dry days. Desalination and Water Treatment, 51(19-21), 4035-4043.

Hao, O. J., Richard, M. G., Jenkins, D., & Blanch, H. W. (1983). The half-saturation coefficient for dissolved oxygen: a dynamic method for its determination and its effect on dual species competition. Biotechnology and Bioengineering, 25(2), 403-416.

Hao, X. D., Heijnen, J. J., & van Loosdrecht, M. C. M. (2002). Sensitivity analysis of a biofilm model describing a one-stage completely autotrophic nitrogen removal (CANON) process. Biotechnology and Bioengineering, 77(3), 266-277.

Henderson, C., Greenway, M., & Phillips, I. (2007). Removal of dissolved nitrogen, phosphorus and carbon from stormwater by biofiltration mesocosms. Water Science and Technology, 55(4), 183-191.

Henze, M. (2002). Wastewater treatment: biological and chemical processes (3rd ed.). Berlin ; New York: Springer.

Henze, M., Gujer, W., Mino, T., & van Loosdrecht, M. (2000). Activated sludge models ASM1, ASM2, ASM2d and ASM3, IWA task group on mathematical modelling for design and operation of biological wastewater treatment. IWA Scientific and Technical Report.

Hodge, A., Robinson, D., & Fitter, A. (2000). Are microorganisms more effective than plants at competing for nitrogen? Trends in Plant Science, 5(7), 304-308.

Hsieh, C. H., Davis, A. P., & Needelman, B. A. (2007). Nitrogen removal from urban stormwater runoff through layered bioretention columns. Water Environment Research, 79(12), 2404-2411.

IWA. (2006). Mathematical Modeling of Biofilms (I. publishing Ed.). London: IWA Publishing.

James, C., Fisher, J., Russell, V., Collings, S., & Moss, B. (2005). Nitrate availability and hydrophyte species richness in shallow lakes. Freshwater Biology, 50(6), 1049-1063.

Jennings, D. B., & Jarnagin, S. T. (2002). Changes in anthropogenic impervious surfaces, precipitation and daily streamflow discharge: a historical perspective in a mid-atlantic subwatershed. Landscape Ecology, 17(5), 471-489.

Jubany, I., Carrera, J., Lafuente, J., & Baeza, J. A. (2008). Start-up of a nitrification system with automatic control to treat highly concentrated ammonium wastewater: experimental results and modeling. Chemical Engineering Journal, 144(3), 407-419.

Li, A., Sun, G., & Xu, M. (2008). Recent patents on anammox process. Recent Patents on Engineering, 2(3), 189-194.

Liu, G. Y., Zhang, H. Z., Li, W., & Zhang, X. (2012). Advances of external carbon source in denitrification. Advances in Environmental Science and Engineering, Pts 1-6, 518-523, 2319-2323.

Liu, W. X., Dahab, M. F., & Surampalli, R. Y. (2005). Nitrogen transformations modeling in subsurface-flow constructed wetlands. Water Environment Research, 77(3), 246-258.

Lucas, W. C., & Greenway, M. (2011). Hydraulic Response and Nitrogen Retention in Bioretention Mesocosms with Regulated Outlets: Part II-Nitrogen Retention. Water Environment Research, 83(8), 703-713.

Ma, F. S., Li, A. D., Li, B. Y., Cui, Z. B., Shi, C. H., & Zhou, B. H. (2015). Prolonged starvation and subsequent recovery of nitrification process in a simulated photovoltaic aeration SBR. Environmental Science and Pollution Research, 22(14), 10778-10787.

Maestre, A., & Morquecho, R. (2005). The national stormwater quality database (NSQD, version 1.1). Paper presented at the 1st Annual Stormwater Management Research Symposium Proceedings.

Makepeace, D. K., Smith, D. W., & Stanley, S. J. (1995). Urban stormwater suality: summary of contaminant data. Critical Reviews in Environmental Science and Technology, 25(2), 93-139.

Manser, R., Gujer, W., & Siegrist, H. (2005). Consequences of mass transfer effects on the kinetics of nitrifiers. Water Research, 39(19), 4633-4642.

Masi, M. (2011). A SWMM-5 model of a denitrifying bioretention system to estimate nitrogen removal from stormwater runoff. (Dissertation/Thesis), ProQuest Dissertations Publishing.

Mburu, N., Sanchez-Ramos, D., Rousseau, D. P. L., van Bruggen, J. J. A., Thumbi, G., Stein, O. R., . . . Lens, P. N. L. (2012). Simulation of carbon, nitrogen and sulphur conversion in batch-operated experimental wetland mesocosms. Ecological Engineering, 42, 304-315.

Metcalf & Eddy., & Tchobanoglous, G. (1979). Wastewater engineering: treatment disposal reuse (2d ed.). New York: McGraw-Hill.

Neff, J. C., & Asner, G. P. (2001). Dissolved organic carbon in terrestrial ecosystems: synthesis and a model. Ecosystems, 4(1), 29-48.

Nielsen, L. P. (1992). Denitrification in sediment determined from nitrogen isotope pairing. Fems Microbiology Ecology, 86(4), 357-362.

Palfy, T. G., & Langergraber, G. (2014). The verification of the Constructed Wetland Model No. 1 implementation in HYDRUS using column experiment data. Ecological Engineering, 68, 105-115.

Paredes, D., Kuschk, P., Mbwette, T. S. A., Stange, F., Muller, R. A., & Koser, H. (2007). New aspects of microbial nitrogen transformations in the context of wastewater treatment—A review. Engineering in Life Sciences, 7(1), 13-25.

Payne, E. G. I., Fletcher, T. D., Russell, D. G., Grace, M. R., Cavagnaro, T. R., Evrard, V., . . . Cook, P. L. M. (2014). Temporary storage or permanent removal? The division of nitrogen between biotic assimilation and denitrification in stormwater biofiltration systems. Plos One, 9(3).

Payne, W. J. (1981). Denitrification. New York: Wiley.

Pelley, J. (2004). "Dead zones" on the rise. Environmental Science & Technology, 38(11), 193a-194a.

Perez, J., Lotti, T., Kleerebezem, R., Picioreanu, C., & van Loosdrecht, M. C. M. (2014). Outcompeting nitrite-oxidizing bacteria in single-stage nitrogen removal in sewage treatment plants: a model-based study. Water Research, 66, 208-218.

Picioreanu, C., vanLoosdrecht, M. C. M., & Heijnen, J. J. (1997). Modelling the effect of oxygen concentration on nitrite accumulation in a biofilm airlift suspension reactor. Water Science and Technology, 36(1), 147-156.

Reeve, P. J., Mouilleron, I., Chuang, H. P., Thwaites, B., Hyde, K., Dinesh, N., . . . van den Akker, B. (2016). Effect of feed starvation on side-stream anammox activity and key microbial populations. Journal of Environmental Management, 171, 121-127.

Reichert, P. (1994). AQUASIM—A tool for simulation and data analysis of aquatic systems. Water Science and Technology, 30(2), 21-30.

Rittmann, B. E., Stilwell, D., & Ohashi, A. (2002). The transient-state, multiple-species biofilm model for biofiltration processes. Water Research, 36(9), 2342-2356.

Rodriguez-Sanchez, A., Gonzalez-Martinez, A., Martinez-Toledo, M. V., Garcia-Ruiz, M. J., Osorio, F., & Gonzalez-Lopez, J. (2014). The effect of influent characteristics and operational conditions over the performance and microbial community structure of partial nitritation reactors. Water*, 6*(7), 1905-1924.

Sagehashi, M., Zhou, S., Naruse, T., Osada, M., & Hosomi, M. (2009). Nitrogen dynamics and biomass production in a vertical flow constructed wetland cultivated with forage rice and their mathematical modeling. Journal of Water and Environment Technology, 7(4), 251-266.

Siemens, J., Haas, M., & Kaupenjohann, M. (2003). Dissolved organic matter induced denitrification in subsoils and aquifers? Geoderma, 113(3), 253-271.

Sonavane, P. G., & Munavalli, G. R. (2009). Modeling nitrogen removal in a constructed wetland treatment system. Water Science and Technology, 60(2), 301-309.

Strous, M., Heijnen, J. J., Kuenen, J. G., & Jetten, M. S. M. (1998). The sequencing batch reactor as a powerful tool for the study of slowly growing anaerobic ammonium-oxidizing microorganisms. Applied Microbiology and Biotechnology, 50(5), 589-596.

Strous, M., & Jetten, M. S. M. (2004). Anaerobic oxidation of methane and ammonium. Annual Review of Microbiology, 58, 99-117.

Terada, A., Zhou, S., & Hosomi, M. (2011). Presence and detection of anaerobic ammonium-oxidizing (anammox) bacteria and appraisal of anammox process for high-strength nitrogenous wastewater treatment: a review. Clean Technologies and Environmental Policy, 13(6), 759-781.

Valero, M. A. C., Read, L. F., Mara, D. D., Newton, R. J., Curtis, T. P., & Davenport, R. J. (2010). Nitrification-denitrification in waste stabilisation ponds: a mechanism for permanent nitrogen removal in maturation ponds. Water Science and Technology, 61(5), 1137-1146.

van Dam, A. A., Dardona, A., Kelderman, P., & Kansiime, F. (2007). A simulation model for nitrogen retention in a papyrus wetland near Lake Victoria, Uganda (East Africa). Wetlands Ecology and Management, 15(6), 469-480.

van Dongen, U., Jetten, M. S. M., & van Loosdrecht, M. C. M. (2001). The SHARON®-Anammox® process for treatment of ammonium rich wastewater. Water Science and Technology, 44(1), 153-160.

Volcke, E. I. P., Picioreanu, C., De Baets, B., & van Loosdrecht, M. C. M. (2010). Effect of granule size on autotrophic nitrogen removal in a granular sludge reactor. Environmental Technology, 31(11), 1271-1280.

Wiesmann, U. (1994). Biological nitrogen removal from wastewater. Biotechnics/wastewater, 113-154.

Wong, T. H. F., & Somes, N. L. G. (1995). A stochastic approach to designing wetlands for stormwater pollution-control. Water Science and Technology, 32(1), 145-151.

Wu, X., Liu, S. T., Dong, G. L., & Hou, X. L. (2015). The starvation tolerance of anammox bacteria culture at 35°C. Journal of Bioscience and Bioengineering, 120(4), 450-455.

Xuan, Z. M., Chang, N. B., Wanielista, M. P., & Williams, E. S. (2013). System dynamics modeling of nitrogen removal in a stormwater infiltration basin with biosorption-activated media. Journal of Environmental Quality, 42(4), 1086-1099.

Zhang, D. Y., Zhang, X., Wang, Y., Zhou, G. Z., & Li, G. H. (2015). Innovative slow-release organic carbon-source material for groundwater in situ denitrification. Environmental Technology, 36(7), 909-919.

Zhao, Y. W., Liu, Y. X., Wu, S. R., Li, Z. M., Zhang, Y., Qin, Y., & Yin, X. A. (2016). Construction and application of an aquatic ecological model for an emergent-macrophyte-dominated wetland: A case of Hanshiqiao wetland. Ecological Engineering, 96, 214-223.

Zinger, Y., Blecken, G. T., Fletcher, T. D., Viklander, M., & Deletic, A. (2013). Optimising nitrogen removal in existing stormwater biofilters: benefits and tradeoffs of a retrofitted saturated zone. Ecological Engineering, 51, 75-82.

Chapter 5 Continuous-Flow Aerobic Granulation in Plug-Flow Bioreactors Fed with Real Domestic Wastewater

(This chapter has been published as "Sun Y.W., Angelotti B., Wang Z.W. (2019) Continuous-flow aerobic granulation in plug-flow bioreactors fed with real domestic wastewater, Science of The Total Environment, 688 (20): 762-770")

5.1 Abstract

This pilot study was designed to explore the feasibility of achieving successful aerobic granulation in continuous flow infrastructure used in modern wastewater treatment plants (WWTPs). Results demonstrated that aerobic granulation of activated sludge can be achieved in plug-flow reactors (PFRs) fed with primary effluent from a domestic WWTP with seasonal temperature variation between 10 and 22.5 °C. It took about 90 days during the reactor startup to reach a state of sustained aerobic granulation. The characteristics of aerobic granules formed were comparable to those measured in sequential batch reactors (SBRs). The feast-to-famine concentration profiles measured in the plug-flow pilot reactors were found to be in line with those present in the full-scale treatment trains, lending support to the feasibility of converting existing infrastructure to continuous flow aerobic granulation systems. A selection pressure based on settling velocity (V_s) was applied in a V_s selector to retain bioparticles with V_s greater than ~9–9.75 m h^{-1}. It was theorized that an external V_s selection pressure would be necessary but would not be the sole condition sufficient to drive aerobic granulation. The alternating feast-to-famine internal selection provided by the PFRs is also believed to be a required condition to transform biomass from flocs toward dense and compact aerobic granules. While the pilot-scale Plug-flow Aerobic Granulation (PAG) reactor achieved similar COD and NH_3 removal efficiencies as the full-scale WWTP treatment train, its effluent from V_s selector contained an average of 138 mg L^{-1} total suspended solids (TSS) as a result of the biomass 'wash-out" by the V_s selection pressure. Pilot results suggest a second clarifier for polishing, in addition to the V_s selector, may be needed in a full-scale application of the technique unless other downstream processes (flocculation, sedimentation, filtration) are provided to reach final water quality goals.

5.2 Keywords

Aerobic granule; Plug flow reactor; Sequential batch rector; Completely stirred tank reactor; Selection pressure; Settleability

5.3 Graphical Abstract

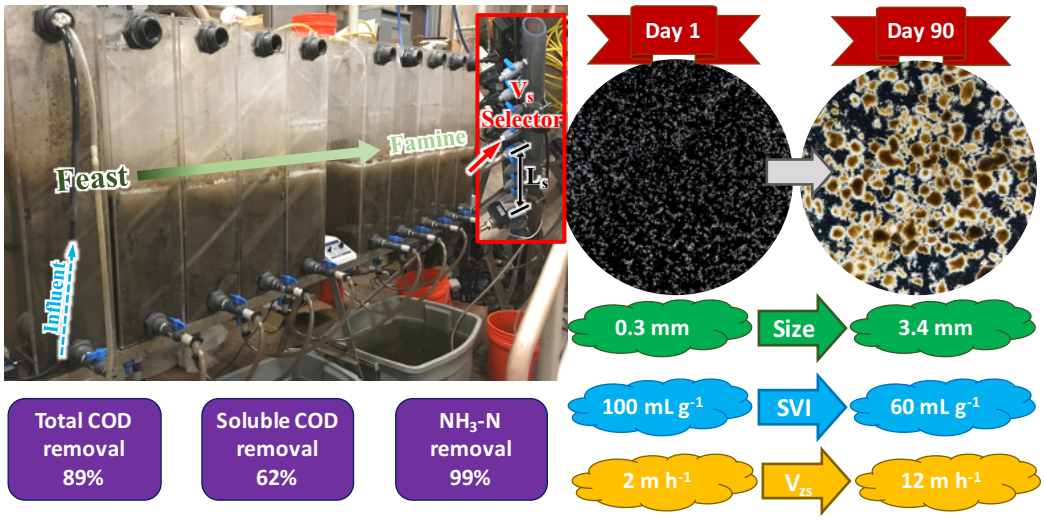

5.4 Introduction

Aerobic granular sludge offers advantages over conventional activated sludge such as high biomass retention, easy sludge-water separation, multiple biological processes integrated within the granule structure, resistance to shock loading, and general process intensification (Gao et al., 2011; Hasebe et al., 2017), which make aerobic granulation a promising technique for domestic and industrial wastewater treatment (De Kreuk et al., 2007; Morgenroth et al., 1997; Pronk et al., 2015). In recent years, two full-scale demonstration wastewater treatment plants (WWTPs) using the Nereda® aerobic granulation technique have been constructed and operated in Gansbaai, South Africa and Frielas, Portugal in 2006 and 2008 (Niermans et al., 2014). Later on, based on the experience gained from these two demonstration plants, two full-scale aerobic granulation WWTPs treating mixture of industrial and domestic were constructed in Epe, the Netherlands and Haining, China in 2010 (Giesen et al., 2013; Li et al., 2014). In 2013, the first full-scale domestic WWTP using the aerobic granulation technique was constructed in Garmerwolde, the Netherlands (Pronk et al., 2015). In spite of these full-scale demonstrations, it is noteworthy that the application of aerobic granulation technique is still only limited to sequential batch reactors (SBRs) after its about twenty years of development (Kent et al., 2018; Pronk et al., 2015), which is inconsistent with the continuous flow nature of the majority of existing domestic WWTPs. Continuous flow reactors (CFRs) provide advantages over SBRs in terms of simple process operation and control while accommodating larger treatment capacities (Chen et al., 2017; Juang et al., 2010; Kent et al., 2018; Li et al., 2016b). Hence, the development of a continuous flow aerobic granulation technique is highly desired for promoting the application of aerobic granular sludge in large-scale WWTPs (Kent et al., 2018).

A critical recent review of the state of the art for continuous flow aerobic granulation techniques described three major limitations requiring additional research (Kent et al., 2018). First, real aerobic granules have rarely been transformed from conventional, floc type activated sludge mixed liquors within CFRs. Most previous studies initially inoculated aerobic granules that were pre-formed in SBRs into CFRs to study the subsequent stability of the seeded granules (Corsino et al., 2016; Li et al., 2016b; Liu et al., 2012). Second, tall airlift or bubble-column type reactors, similar in shape to those applied for SBR aerobic granulation, have been overwhelmingly used for CFR granulation studies (Liu et al., 2015; Ramos et al., 2016; Xin et al., 2017). However, this type of reactor is seldom employed in the mainstream of existing domestic WWTPs. This presents questions about whether existing WWTP infrastructure could be

effectively modified to include aerobic sludge granulation systems into full-scale CFR infrastructure for purposes of process intensification. Third, carefully prepared and controlled synthetic wastewater has been predominantly used in previous studies rather than feeding reactors with a community's indigenous wastewater with its naturally occurring variability (Corsino et al., 2016; Li et al., 2016a). In addition, most granular CFR studies were also carried out at relatively constant room temperatures (e.g., 20 to 30 °C). Therefore, the applicability of continuous flow aerobic granulation to real wastewater treatment plant conditions is still largely undemonstrated. This study was specially tailored to address these research needs by investigating whether aerobic granules can actually be formed from conventional floc type activated sludge inoculated into a plug-flow reactor (PFR) and fed continuously with real wastewater directly from a domestic WWTP with seasonal temperature and influent quality variations.

According to a previous literature review (Kent et al., 2018), it is hypothesized that an alternating feast/famine condition and an effective settling velocity (V_s) selection pressure are two essential factors required to promote successful aerobic granulation in SBRs. Thus, a Plug-flow Aerobic Granulation (PAG) technique was tested in this study to demonstrate the feasibility of the aerobic granulation of activated sludge in CFRs. This hypothesis was considered based on the fact that aerobic granulation has not been achieved in completely stirred tank reactors (CSTRs) even with sufficient V_s selection pressure incorporated (Corsino et al., 2016), even though V_s selection pressure has been long regarded as the ultimate driving force for aerobic granulation (Liu et al., 2005). CSTRs obviously lack the alternating feast/famine conditions provided in SBRs and have no zone, or period, of high initial food/micro-organism ratio (F:M). Since the feast/famine concentration profiles along the space vector of plug-flow reactors is equivalent to those along the time vector of SBRs, there should be theoretically no reason why the same SBR aerobic granulation success cannot be reproduced in PFRs when the appropriate effective selection pressures are provided. So, the PAG reactor to be tested in this study, very importantly, was intentionally designed to mimic the plug-flow nature of full-scale WWTPs and was fed with primary effluent (PE) as substrate for this continuous-flow aerobic granulation study. The purpose was to demonstrate the applicability of PAG in a more real-world scenario, and also to help develop an aerobic granulation technique that could best be compared with existing WWTP infrastructure. Therefore, the outcome from this study should be appealing to both researchers and practitioners interested in continuous-flow aerobic granulation based bioprocesses to intensify treatment in existing WWTPs taking advantage of major infrastructure that has already been constructed.

5.5 Materials and Methods

5.5.1 Reactor design

5.5.1.1 Pilot-scale configuration

The pilot-scale reactor depicted in Figures 5.1a and c is a plug-flow reactor built and operated at the Upper Occoquan Service Authority (UOSA), a WWTP in Centreville, VA, USA. The study was intentionally conducted during autumn and winter seasons from October 2018 to February 2019 to include the lower temperature effects. The reactor influent was continuously pumped directly from UOSA's PE, without additional pretreatment or conditioning for the pilot feed. The average temperature of PE for the period was around 15.9 °C as shown in Table 5.1, with the highest temperature of 22.5 °C and the lowest temperature of 10.0 °C. The temperature measurements show that the temperature difference between the influent and effluent of the PFR was less than 1.9%, thus PE temperatures were used to represent the operating temperature of the reactor. The other characteristics of UOSA's domestic wastewater are also shown in Table 5.1, including pH, total COD (tCOD), soluble COD (sCOD), 5-day biochemical oxygen demand (BOD_5), alkalinity, total suspended solid (TSS), Total Kjeldahl Nitrogen (TKN), ammonia nitrogen (NH_3-N), and total phosphorus (TP). tCOD includes colloidal COD and sCOD. The PFR consists of ten CSTRs in series with 128 L total working volume to approximate a plug-flow condition. The hydraulic retention time (HRT) of the reactor was controlled at 6.5 hours. All of the ten chambers were continuously aerated with micro bubble air diffuser rings (EcoPlus®, Vancouver, WA, Canada) from the bottom of each chamber at a total aeration rate 32 L min^{-1} to ensure dissolved oxygen (DO) concentrations greater than 3 mg L^{-1}. As shown in Figures 5.1a and c, two external settling selectors, each with internal diameter of 5 cm and total height of 120 cm, was placed at the end of the PFR to apply a V_s selection pressure to drive aerobic granulation. The selective retention of bioparticles with fast V_s was achieved by operating the settling selector column as an intermittent clarifier with each cycle consisting of 1 minute of feed, 4 minutes of discrete settling, and 1 minute of effluent discharge. This intermittent clarifier only caused about 1.8% of the total working volume fluctuation in the PAG. The critical settling velocities (V_c) were set at ~ 9 - 9.75 m h^{-1} by settling time of 4 minutes and the effluent discharge heights of ~ 60 - 65 cm to selectively retain bioparticles with V_s greater than V_c according to a previous study (Wang et al.,

2006). During initial testing to configure this study's pilot plant, peristaltic pumping of return sludge was found to crush granules pre-formed in UOSA's bench-scale, onsite SBRs. Therefore, an air-driven transfer strategy was employed to return the selectively retained granular sludge back to the inlet of the PFR by using an air compressor (Bostitch 6 Gallon 150 PSI Oil-Free Compressor, Towson, MD, USA) and several timer-controlled motorized valves (BACOENG CR04).

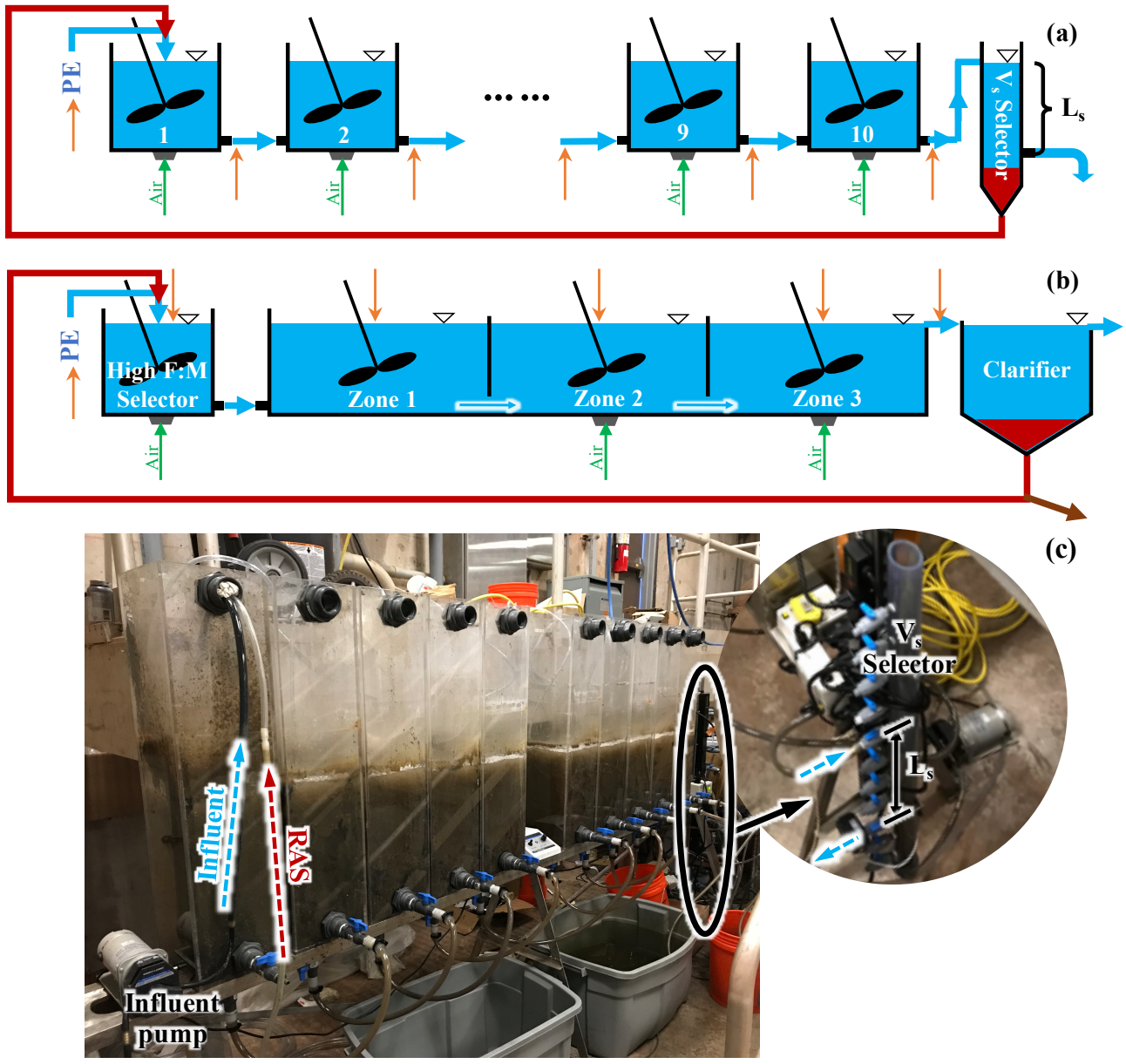

Figure 5.1 Schematic illustration of the (a) pilot- and (b) full-scale reactors, and (c) photo of the pilot-scale reactors. Dark red: return activated sludge (RAS); Brown: wasted activated sludge (WAS); Green: Air; Blue: Water flow; Orange arrows: sampling locations.

Table 5.1 Characteristics of the domestic wastewater*

Parameters	Unit	Raw influent	Primary effluent
Temperature	°C	N/A	15.9 ± 2.9
pH	N/A	7.3 ± 0.2	7.2 ± 0.1
tCOD	mg L^{-1}	415 ± 171	326 ± 97
sCOD	mg L^{-1}	N/A	89 ± 20
BOD_5	mg L^{-1}	170 ± 51	107 ± 20
Alkalinity	mg L^{-1}	187.6 ± 26.8	199.3 ± 24.1
TSS	mg L^{-1}	210 ± 164	88 ± 19
TKN	mg L^{-1}	39.5 ± 7.6	40.8 ± 7.7
NH_3-N	mg L^{-1}	27.1 ± 4.8	27.8 ± 5.4
TP	mg L^{-1}	3.7 ± 0.9	4.2 ± 0.8

*N/A: not applicable; ±: standard deviation

5.5.1.2 Full-scale configuration

The flowrate of UOSA's full-scale secondary treatment process is about 1.7×10^5 m^3 d^{-1} (Table 5.1). The entire secondary treatment process has been divided into two parallel treatment trains. The schematic design of one of the treatment trains is shown in Figure 5.1b. The full-scale secondary treatment process includes a high food-to-microorganism ratio (F:M) selector with very short 7 min HRT followed by one anoxic zone (zone 1) and two aerobic zones (zones 2 and 3) of the same HRT (2.1 hours) with total HRT of 6.5 hours. The clarifier is operated with HRT of 1.5 hour and a surface overflow rate (SOR) of 1 m h^{-1}.

5.5.2 Analytical methods

Sludge characteristics such as sludge volume index (SVI), zone settling velocity (V_{zs}), total suspended solid (TSS), volatile suspended solid (VSS), and specific oxygen utilization rate (SOUR) are all analyzed by using standard methods (APHA, 1998). Mixed liquor samples were collected weekly from every other

chambers of the pilot-scale reactor to calculate the average mixed liquor suspended solids (MLSS) and mixed liquor volatile suspended solids (MLVSS) values, while mixed liquor samples for the full-scale treatment trains were collected in the middle of zone 3 in Figure 5.1b. Samples for SVI, V_{zs}, and SOUR analyses were collected from the last chamber of pilot-scale PAG reactor and the effluent side of zone 3 of the full-scale treatment train. For SVI measurement, both 5 min and 30 min SVI tests were performed and recorded as SVI_5 and SVI_{30}, respectively. SVI measurements for the full-scale reactors were performed using a standard 2 L stirred settleometer. For the pilot-scale reactor, SVI was measured in an unstirred 2 L settleometer. Since MLSS concentration greatly impacts sludge bed V_{zs} (Vanderhasselt et al., 2000), full-scale return activated sludge (RAS) was diluted to the MLSS concentration of the pilot-scale PAG reactor prior to V_{zs} measurement for a fair comparison. solid retention time (SRT) was estimated based on the effluent TSS and average MLSS in the plug flow reactor. PE temperatures and pH were monitored using an online Liquiline M CM42 transmitter (Endress+Hauser, Greenwood, IN, USA). The mixed liquor temperature in the first and last chambers of the pilot-sale reactor were monitored by using RC-4 temperature data logger (Elitech®, Milpitas, CA, USA). Dissolved oxygen was measured in each chamber of the pilot-scale reactor by using a HQ40D BOD meter (Hach, Loveland, CO, USA). COD was analyzed using COD TNTplus® 820 vials and a spectrophotometer (Hach, Loveland, CO, USA), in which sCOD samples were filtered using 0.45 μm syringe filters (EZFlow®, Old Saybrook, CT, USA), and pilot-scale effluent tCOD was measured by using supernatant after 30-minute settling to exclude washed-out sludge for a fair comparison with the tCOD measured on the effluent from full-scale clarifiers. BOD_5 and alkalinity were both analyzed using standard methods (APHA, 1998). TKN, TP, NH_3-N, NO_2^--N, NO_3^--N, and orthophosphate (OP) were analyzed using a QuikChem® 8500 series 2 flow injection analysis system (Lachat, Loveland, CO, USA), in which NH_3-N, NO_2^--N, NO_3^--N, and OP samples were filtered through 0.45 μm syringe filters (EZFlow®, Old Saybrook, CT, USA) before being analyzed. Samples for COD and nutrient analyses were collected at different locations across the pilot- and full-scale treatment trains. For the pilot-scale reactor, the samples were collected from the influent and the effluent of each chamber. For full-scale treatment trains, the samples were collected from the influent, the the high F:M selector and each zone (zones 1, 2, and 3 as shown in Figure 5.1b), as well as the effluent from zone 3. Mix liquor samples were collected from the last chamber of the pilot-scale PAG reactor for particle sizes distribution analysis using image processing software (ImageJ 2.0.0). Extracellular polymeric substances (EPSs) extraction was performed based on the method described in Liu et al. (2002) in duplicate by using sludge samples from the last chamber of the pilot-scale reactor and zone 3 of the

full-scale treatment train. Briefly, 2% EDTA was used as the chemical extractant. Dialysis Kits (Spectrum™ Labs Spectra/Por™ 3500 D MWCO Standard RC Pre-Treated, Waltham, MA USA) were utilized to separate polymers with molecular weight greater than 3500 Dalton. A phenol-sulfuric acid method was adopted for carbohydrates (PS) analysis (Nielsen, 2010), and Pierce™ modified Lowry protein assays were used for the protein (PN) analysis (Thermo Scientific™, Waltham, MA, USA).

5.6 Results

5.6.1 Morphology of the sludge

After 90 days of continuous operation, granular sludge with the morphology shown in Figure 5.2a was formed within the pilot-scale PAG reactor which was originally inoculated with floc type conventional activated sludge from UOSA's full-scale bio-reactors. As can be seen, near spherical and compact microbial aggregates with median diameter (d_{50}) of 3.4 mm were dominating the mixed liquor. The biomass morphology was distinctly different from the morphology of the initially inoculated activated sludge as well as that cultivated in the full-scale plant with the same wastewater and HRT (Figure 5.2b). It is noteworthy that the morphology of the granular sludge developed in the pilot-scale PAG reactor was similar to that reported to be formed in SBRs fed with real domestic wastewater (Liu et al., 2010; Pronk et al., 2015; van der Roest et al., 2011). Particularly, the fluffy surfaces of these PAG granules look very much like those formed in full-scale SBRs (Pronk et al., 2015). The particle size evolution in the course of PAG is exhibited in Figure 5.2c. It displays that 50% of the seed sludge were tiny bioflocs with particle size smaller than 0.3 mm, namely d_{50} = 0.3 mm, and the most abundant fraction (38%) was distributed in the range of 0.2-0.4 mm. With 61 days of PAG, d_{50} increased significantly to 2 mm, and the most abundant fraction (38%) of the sludge was distributed within the range of 1-2 mm. 90 days later, d_{50} was stabilized around 3.4 mm with the most abundant fraction (35%) of sludge distributed within the size range of 2-3 mm. The feast-famine internal reactor selection pressure due to substrate concentration gradients along the flow direction were determined to be similar when comparing the pilot- and full-scale reactors (see section 3.4), likely suggesting that the major driver towards granular morphology transformation was the external V_s selector applied only to the pilot-scale reactors but not to the full-scale reactors.

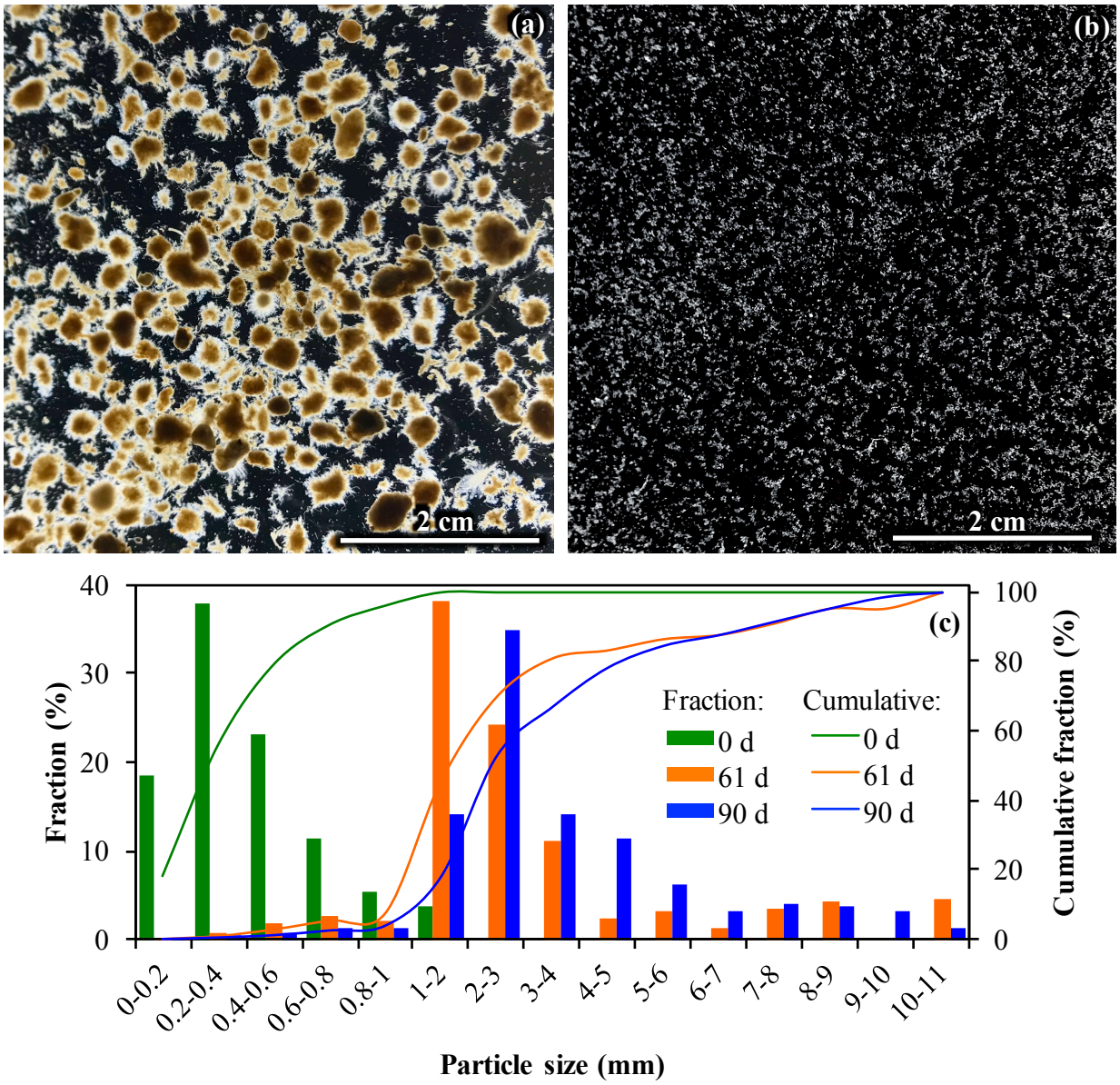

Figure 5.2 Morphology of the sludge stabilized in the (a) pilot- and (b) full-scale reactors after 90 days of operation, and (c) particle size distribution in the pilot-scale reactor in the course of Plug-flow Aerobic Granulation (PAG) (d represent days).

5.6.2 Settleability and concentration of the sludge

Both 5 and 30 min SVI values were measured during the course of PAG operation. Figure 5.3(a) shows that the seed sludge had SVI_{30} around 100 mL g^{-1}. As a result of the quick washout during the reactor

startup, only 16% of inoculated sludge remained in the pilot-scale PAG reactor on the 14th day of the startup (Figure 5.3c), and the retained sludge showed much lower SVI_{30} around 50 mL g^{-1}. However, as biomass growth continued under selection pressures, the retained sludge adapted to the limiting V_s conditions needed to remain in the reactor system and the biomass concentration steadily increased (Figure 5.3c). With another 76 days of PAG, the TSS accumulated to and stabilized around 2400 mg L^{-1} (Figure 5.3c). The VSS accumulation along with the TSS buildup during the whole PAG duration is shown in Figure 5.3c. SVI_{30} of the pilot-scale PAG reactor gradually decreased to and stabilized around 64 mL g^{-1} which indicated that very good settling sludge was established as a result of the PAG. According to a survey conducted by Martin et al. (2016) on 39 WWTPs in North America, four facilities having favorable conditions for aerobic granulation in SBRs reported that their best settleability occurred during summer months and the annual average SVI_{30} values were around 60 mL g^{-1}. This study shows that the steady-state SVI_{30} values of the pilot PAG reactor were in the same range in spite of the cold season (Figure 5.3a). On the contrary, the SVI_{30} profiles measured in the full-scale treatment train started from an initial value of 92 mL g^{-1}, and then slightly increased to and stabilized around 120 mL g^{-1} (Figure 5.3a). This phenomenon is closely correlated with the decreasing PE temperature during the experimental period (Figure 5.S1), and the worsening settleability is probably due to higher populations of filamentous bacteria (Guo et al., 2012; Knoop et al., 1998; Martins et al., 2004), which typically appear at the UOSA WWTP under lower temperature and lower F:M ratios. It is noteworthy that the full-scale SVI was actually measured under the stirred condition which should have produced lower values than those measured under the unstirred condition in which the pilot-sludge SVI was measured (Rachwal et al., 1982). It is broadly accepted that SVI_{30} values and SVI_5/SVI_{30} ratios are two major indicators of the successful aerobic granulation (Kent et al., 2018; Pronk et al., 2015). Profiles in Figure 5.3b revealed that the SVI_5/SVI_{30} ratio gradually dropped from 1.7 to 1.1 over the 51-day startup period and then was stabilized around 1.1, indicating that the 5 min settleability of the PAG sludge bed was almost same as that of the 30 min test, which demonstrates very good and rapid initial sludge settling. On the contrary, the SVI_5/SVI_{30} ratio of the full-scale sludge was as high as 1.8 (Figure 5.3b), which is typical for conventional activated sludge (Świątczak et al., 2018; Wan et al., 2009). Table 5.2 shows that there was an average of 138 mg L^{-1} TSS in the effluent of the pilot-scale reactor while the value in the full-scale treatment train was only 5.2 mg L^{-1}. Thus, a subsequent clarifier for effluent polishing, in addition to the settling selector in Figure 5.1a, may be needed to apply the PAG technique unless other downstream processes

such as chemical flocculation-sedimentation-filtration are provided to reach final product water quality goals.

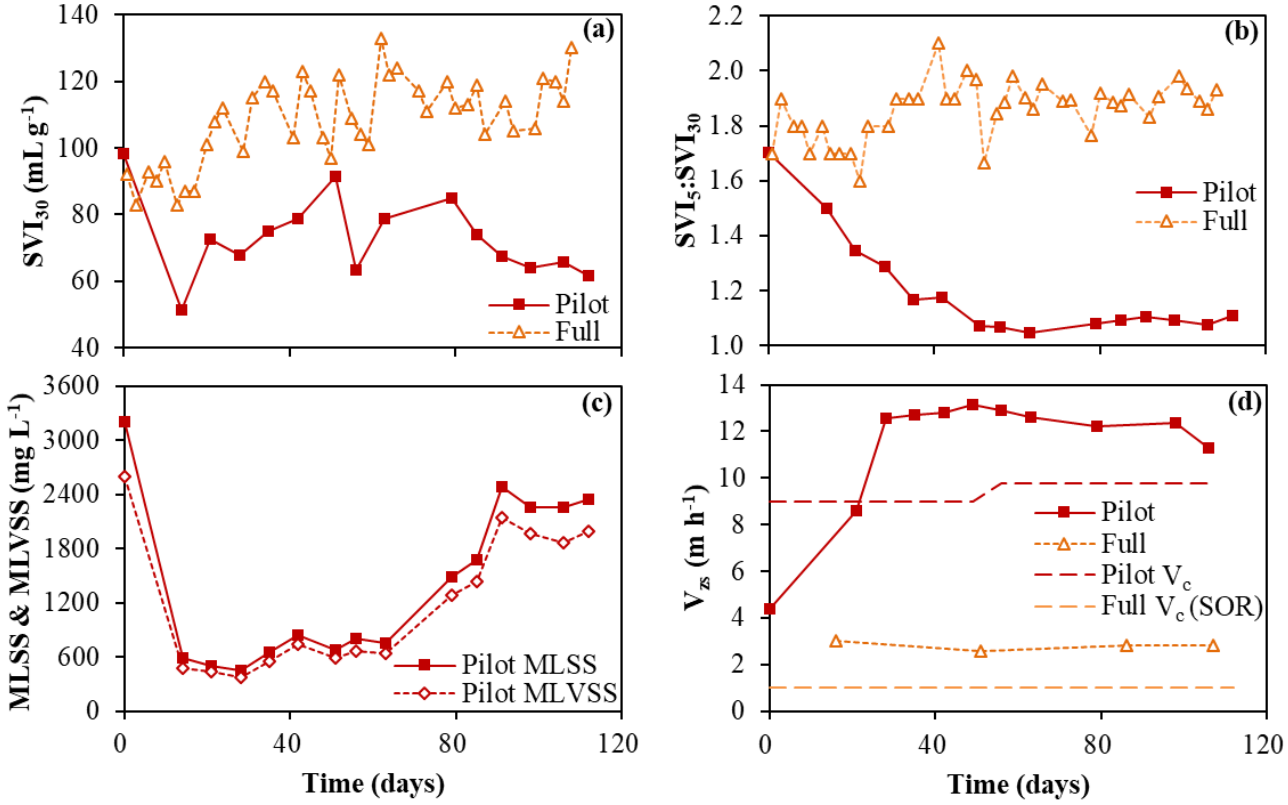

Figure 5.3 (a) SVI_{30}, (b) SVI_5:SVI_{30}, (c) MLSS and MLVSS, and (d) V_{zs} profiles in pilot- and full-scale reactors in the course of PAG.

5.6.3 Sludge bed zone settling velocity (V_{zs})

While V_s of a single floc or granule is only determined by their own physical characteristics (e.g., density, size, shape, etc.), zone settling velocity of the sludge/water interface, V_{zs}, is also highly impacted by the MLSS concentration. In general, V_{zs} is smaller than V_s, and higher MLSS leads to smaller V_{zs} (Vanderhasselt et al., 2000). As shown in Figure 5.3d, V_{zs} of the pilot-scale PAG reactor was as low as 4.4 m h^{-1} at the beginning of the reactor startup, and then gradually increased to 8.6 m h^{-1} over the following 20 days, which may be attributed to the decreased MLSS as a result of the quick washout caused by V_s selection pressure (Figure 5.3c). However, while MLSS remained similar in the subsequent 10 days (Figure 5.3c), V_{zs} continued to rise to above 12 m h^{-1}, which may suggest the onset of sludge adaption to V_s selection pressure. During the following 80 days, V_{zs} was basically stabilized at values above 11 m h^{-1}

while MLSS continuously increased to 2400 mg L^{-1} (Figure 5.3c). In contrast, the V_{zs} of the sludge bed in the full-scale treatment train was six times lower because its V_c, equivalent to the SOR used in the full-scale clarifier, was only about 1 m h^{-1} (Figure 5.3d and Table 5.2). It is noteworthy that the actual V_{zs} of the pilot PAG sludge bed was faster than the V_c of the selector which was set at 9 m h^{-1} for the first 50 days and then increased to 9.75 m h^{-1} for the rest of the startup period (Figure 5.3d), indicating that the sludge biomass has fully adapted to the pilot PAG reactor's V_s selection pressure. Since V_c set for the pilot reactor is a comparable parameter to the SOR parameter used in conventional clarifiers, the V_c used in the PAG V_s selector translates to a clarifier size that is almost 10 times smaller than that of the full-scale conventional clarifiers with SOR = 1 m h^{-1} (Table 5.2).

5.6.4 COD removal performance

Figure 5.4a shows that the sCOD removal performance quickly deteriorated from 76% to 30% in the first seven days of the pilot reactor startup due to dramatic sludge washout by the V_s selection pressure (Figure 5.3c). However, the sCOD removal quickly resumed to around 60% once the granular sludge bed was formed and stabilized (Figure 5.4a). However, the steady-state sCOD removal of the granular sludge was not as good as that of the activated sludge in the full-scale treatment train (Figure 5.4a and Table 5.2). The sCOD removal in the pilot-scale PAG system effluent was about 20% lower than that in the full-scale activated sludge system (Figure 5.4a). This might be attributable to the better sCOD adsorption capacity and treatment efficiency of activated sludge floc by virtue of its high specific surface area when compared to granular sludge (Tan et al., 1997). The profiles of sCOD removal in each chamber of the pilot reactor revealed that most of the sCOD was actually removed in the first chamber within only 0.7 h HRT (Figures 5.5b, c, and d). The remaining nine chambers of the PAG were actually functioning as the starvation or famine phases for the granules without significant sCOD substrate available in the liquid and insignificant further sCOD removal from the liquid portion of the mixed liquor. Further analysis of the values in Table 5.2 showed that, while sCOD removal efficiency of the granular sludge was 20% less than that of the activated sludge, the removal efficiency of tCOD, measured in supernatant after 30-minute settling, by the granular sludge was very close to that of the activated sludge (only 5% difference). This phenomenon may suggest that the granular sludge is slightly better at removing the colloidal COD. Accumulated evidence has shown that high contents of EPS are positively correlated with sorption capacity (Jorand et al., 1995; Wang et al., 2017; Zhang et al., 2018), and EPS contents of the sludge were also positively correlated with

removal efficiency of particulate and colloidal COD (Miller et al., 2013; Modin et al., 2016). Thus, one possible explanation is that the colloidal COD removal by granules was facilitated by the increased EPS production, resulting in better flocculation/adsorption of this COD fraction, because the EPS contents (e.g. PS and PN) in the granular sludge were twice that observed in the conventional activated sludge (Table 5.2). It should also be noticed that the steady-state profiles of sCOD were comparable in the pilot- and full-scale reactors (Figures 5.5c and d), which suggested that major driver of aerobic granulation was the external V_s selector applied only to the pilot-scale reactors but not to the full-scale reactors.

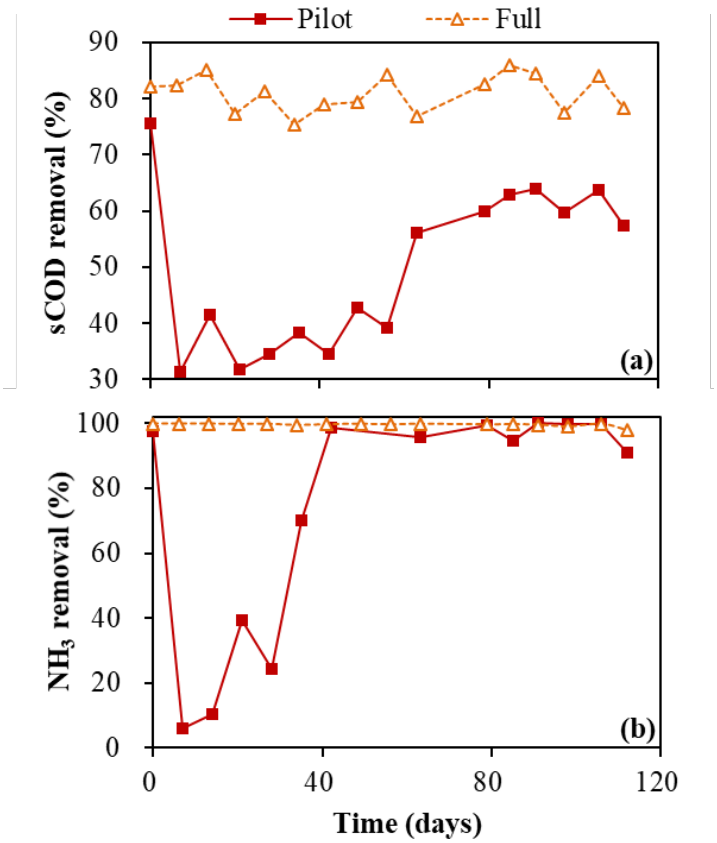

Figure 5.4 Removal of (a) sCOD and (b) NH_3 in pilot- and full-scale reactors in the course of PAG.

5.6.5 Nitrification performance

As observed for COD removal, ammonia removal initially deteriorated from 99% to 6% during the first seven days of the reactor startup as a consequence of biomass washout, and then gradually recovered as the granular sludge accumulated (Figures 5.4b). The steady-state ammonia profile suggests that five

chambers, namely 3.3 h HRT, were needed to fully oxidize all influent ammonia at the loading, MLSS concentration, temperature and dissolved oxygen conditions in this study (Figure 5.5h). Obviously, ammonia oxidizing bacteria (AOB) require much longer reaction time to completely remove influent ammonia than ordinary heterotrophic organisms (OHOs) need for COD removal. The growth and retention of nitrite oxidizing bacteria (NOB) within the granule community lagged behind that of the AOB, which is evident from the transient accumulation of nitrite shown in Figure 5.5f, particularly 42 days after the startup. Complete nitrification was achieved in the pilot reactor 63 days after startup (Figure 5.5g). As shown in Figure 5.5h, it took 6.5 h HRT in the full-scale reactor to complete the nitrification of 24 mg L^{-1} ammonia while the granular sludge only took 3.3 h HRT to achieve the same removal efficiency, which can be attribute to two aspects. On the one hand, there should be very limited nitrification in the anoxic zone 1 for the full-scale treatment trains (Figure 5.2b), thus longer HRT are required. On the other hand, PAG granular sludge may possess much better load withstanding capacity over the suspended activated sludge flocs in terms of ammonia oxidation. Actually, Hasebe et al. (2017) found that the ammonia oxidation rate of aerobic granules is 2.5- to 5-fold higher than that of traditional activated sludge.

5.6.6 Other performance comparisons

The overall performance comparison between the full- and pilot-scale reactors are summarized in Table 5.2. As can be seen, the SRT of the pilot-scale PAG reactor was actually smaller than the full-scale activated sludge system because the latter was intentionally controlled at a high value to ensure sufficient nitrification and denitrification. It is noteworthy that the same nitrification efficiency was actually achieved in the pilot-scale PAG reactor even though it was running at a much lower SRT (Table 5.2). This probably can be explained by the different SRTs between granule and floc portions of the biomass in the pilot-scale reactor. Theoretically, the granular sludge portion has a much longer SRT as the granules are retained and not wasted while much of the floc portion is washed out by loss through the settling selector. The overall biomass SRT is based on the total sludge amount wasted/lost out of the system, and it is influenced highly by the wash-out selection imposed which results in a lower calculated SRT than is expected for the granular fraction. Such a difference in the bulk SRT might explain the much greater carbonaceous and nitrogenous SOUR values of the sludge in the pilot-scale reactor than those in the full-scale treatment train (Table 5.2). It is known that EPSs play very important roles in the structural stability of aerobic granules (Adav et al., 2008; Lee et al., 2010). PS binds small flocs into larger aggregates and

PN reduces surface charge repulsion and increases hydrophobicity (Gao et al., 2011). As shown in Table 5.2, the PS and PN content of the granular sludge was twice that of the activated sludge from the full-scale treatment train.

Table 5.2 Steady-state comparison of pilot- and full-scale reactors*

Parameters	**Unit**	**Pilot-scale**	**Full-scale**
Flowrate	$m^3\ d^{-1}$	0.48	1.7×10^5
V_c	$m\ h^{-1}$	9 ~ 9.75	1.01**
HRT	hours	6.5	6.5
SRT	days	4	9
MLSS	$mg\ L^{-1}$	2,341 ± 108	4,131 ± 535
d_{50}	mm	3.4	0.3
SVI_5	$mL\ g^{-1}$	70.9 ± 2.6	201.6 ± 28.3
SVI_{30}		63.9 ± 2.0	108.5 ± 12.8
SVI_5 / SVI_{30}	N/A	1.1 ± 0.0	1.9 ± 0.1
$SOUR_{COD}$	$mg\ O_2\ g\ VSS^{-1}\ h^{-1}$	15.2 ± 2.0	7.7 ± 0.9
$SOUR_{NH_3}$		26.5 ± 0.2	17.6 ± 4.4
PS	$mg\ g\ VSS^{-1}$	14.9 ± 0.1	6.3 ± 0.4
PN		58.9 ± 2.3	33.1 ± 1.1
Effluent TSS	$mg\ L^{-1}$	138 ± 22***	5 ± 4
Effluent tCOD	$mg\ L^{-1}$	36 ± 5****	19 ± 5
Effluent sCOD	$mg\ L^{-1}$	34 ± 9	18 ± 3
tCOD removal	%	88.9 ± 1.5	94.1 ± 1.4
sCOD removal	%	61.6 ± 10.0	80.9 ± 3.3
NH_3-N removal	%	99.7 ± 0.2	99.5 ± 0.5

*N/A: not applicable; ±: standard deviation

**V_c of full-scale clarifier is equivalent to its SOR

***Settling velocity selector effluent

****Settling velocity selector supernatant after 30 minutes of settling

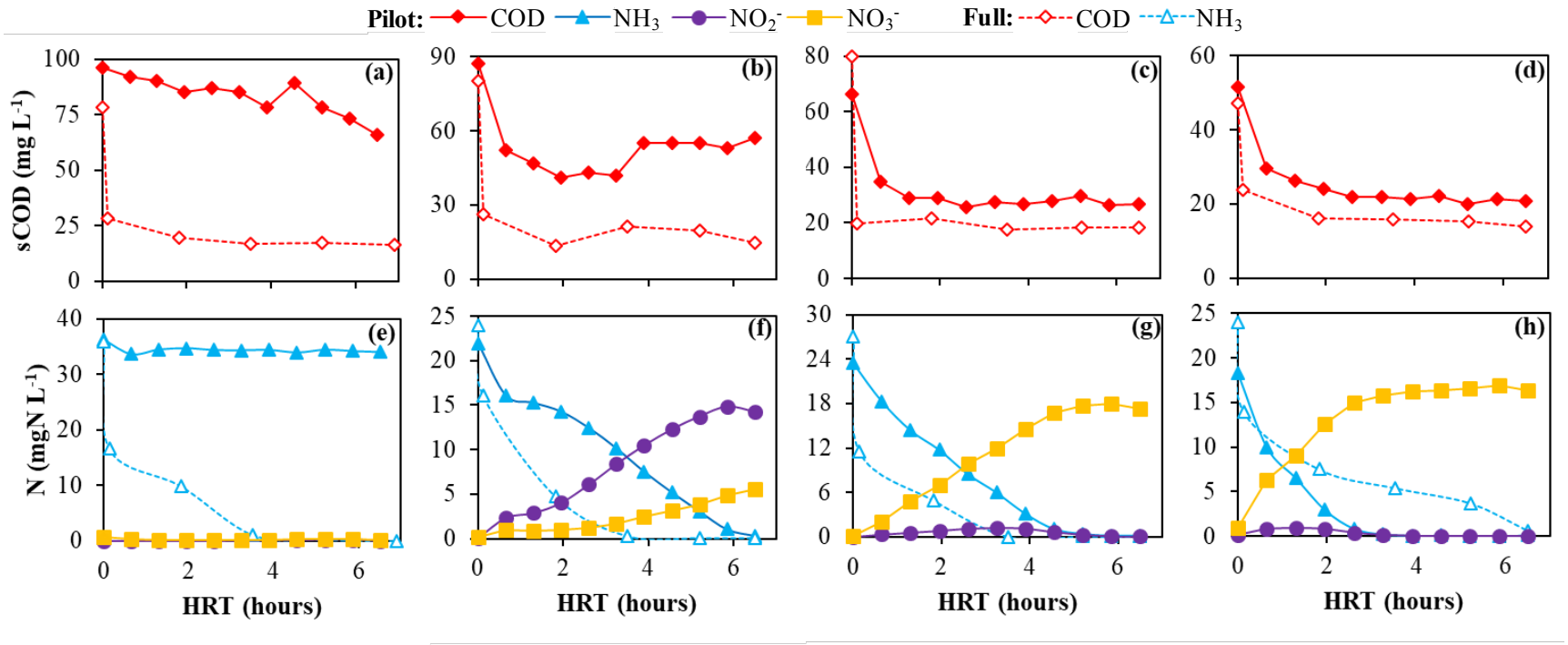

Figure 5.5 Substrate profiles of sCOD (a, b, c, d), NH_3, NO_2^-, and NO_3^- (e, f, g, h) on days 7 (a, e), 42 (c, f), 63 (d, g), and 98 (d, h), respectively, in pilot- and full-scale reactors in the course of PAG. HRT values correspond to sampling locations along the pilot- and full-scale reactors, and the temperature on days 7, 42, 63, and 98 are shown in Figure 5.S1 as 20.5 °C, 17.0 °C, 14.8 °C, and 12.3 °C.

5.7 Discussion

5.7.1 Mechanism of continuous flow aerobic granulation in the PAG reactor

Similar to SBRs, PFRs have been applied for wastewater treatment for decades. However, before the present study, the authors are not aware of documented cases where aerobic granular sludge has been transformed from flocculent sludge in a PFR using an external V_s selector (Figure 5.2a). It is noteworthy that the characteristics of aerobic granules formed in this study in terms of morphology, particle size, SVIs, SOURs, EPS contents, etc., are all comparable to those formed in SBRs (Tay et al., 2001; Wang et al., 2006; Xuan et al., 2010; Yang et al., 2005). The critical role of V_s selection has been repeatedly proven in SBR studies (Gao et al., 2011; Liu et al., 2005). The performance comparison between the full- and pilot-scale studies with and without this selection pressure further strengthens the validity of this selection pressure-driven aerobic granulation theory (Qin et al., 2004; Wang et al., 2006). Moreover, the intensity of the selection pressure (~ 9 - 9.75 m h^{-1}) needed for granulation based on SBR studies was proven to also be effective in the PFR used for this study. Although it is readily recognized that V_s selection is often a needed condition for successful aerobic granulation, it alone is likely not sufficient because aerobic granular sludge was not formed in CSTRs with integrated V_s selection (Corsino et al., 2016; Kent et al., 2018). This observation may explain the hindered development of continuous flow aerobic granulation in the past. This study, together with the accumulated understanding derived from SBR experiments, suggests that alternating feast-to-famine conditions, namely high-to-low substrate concentration profiles, are required for successful aerobic granulation, and the strength of domestic wastewater is high enough to establish such a required concentration gradient in PFRs (Figure 5.5). Future research is expected to focus on different feast-to-famine conditions (e.g., different duration and patterns) and V_s selection selection pressures to provide more insight into the mechanism of continuous flow aerobic granulation.

5.7.2 Full-scale application potential

Comparison between the full- and pilot-scale studies in Figure 5.3 indicates that continuous flow aerobic granulation should be achievable as long as a selector with about 10 m h^{-1} SOR is employed

for sludge V_s selection. However, the results in Table 5.2 also reveal that over 100 mg L^{-1} of suspended solids could be continuously washed out of the 10 m h^{-1} SOR clarifier as a result of the continuous V_s selection pressure. Therefore, a second downstream clarifier or polishing treatment techniques will definitely be needed in the full-scale application of the PAG technique. Given that the existing clarifier infrastructure is usually designed with a SOR around 1 m h^{-1}, a conservative estimate is that the addition of a V_s selector with the surface area less than 10% of the existing clarifiers may enable the successful continuous flow aerobic granulation in full-scale applications. The depth of the clarifier could be also minimized because granular sludge mainly displays discrete settling and thus requires less time for thickening. Certainly, the addition of hydrocyclones discussed in previous literature cited may also prove successful in meeting the needs of granule selection pressure required for full-scale CFRs. Hydrocyclones may provide greater advantages over settling selectors in full-scale applications because of their more compact design and affordable construction (Ford et al., 2016; Shi et al., 2016). This hypothesis is being tested in an ongoing full-scale study at UOSA and the updated findings will be reported in the near future.

5.8 Conclusions

The following concluding remarks can be drawn from this study:

1. Aerobic granulation of the activated sludge can be achieved in PFRs fed with real domestic wastewater with seasonal temperature variation between 10 and 22.5 ^{o}C.
2. The characteristics of aerobic granules formed in PFRs are comparable to those formed in SBRs.
3. Sludge settling velocity selection was once again proven to be a critical selection pressure driving aerobic granulation.
4. The typical strength of domestic wastewater is high enough to provide a feast-to-famine substrate concentration gradient required for continuous flow aerobic granulation in PFRs.
5. The COD and ammonia concentration profiles in the PFRs are in line with those in existing full-scale wastewater treatment trains, suggesting the possibility to convert existing full-scale treatment trains to aerobic granulation reactors with some minor infrastructure additions or alternations.

6. The effluent from the pilot plug-flow aerobic granulation reactor and settling selector still contained more than 100 mg L^{-1} TSS and too high levels of particulate COD. This suggests the need for further effluent polishing by a secondary clarifier or additional downstream treatment such as addition of chemicals followed by flocculation/sedimentation/filtration.
7. The addition of a settling selector with an area less than 10% of the existing clarifier area may hold the potential promise of intensifying floc-based biological wastewater treatment trains in existing WWTPs, converting them to continuous flow, aerobic granulation bioreactors.

5.9 References

Adav, S. S., Lee, D. J., and Tay, J. H. (2008). Extracellular polymeric substances and structural stability of aerobic granule. *Water Res, 42*(6), 1644-1650.

APHA. (1998). Standard methods for the examination of water and wastewater.

Chen, C., Bin, L., Tang, B., Huang, S., Fu, F., Chen, Q., Wu, L., and Wu, C. (2017). Cultivating granular sludge directly in a continuous-flow membrane bioreactor with internal circulation. *Chem Eng J, 309*, 108-117.

Corsino, S., Campo, R., Di Bella, G., Torregrossa, M., and Viviani, G. (2016). Study of aerobic granular sludge stability in a continuous-flow membrane bioreactor. *Bioresource Technol, 200*, 1055-1059.

De Kreuk, M., Kishida, N., and Van Loosdrecht, M. (2007). Aerobic granular sludge–state of the art. *Water Sci Technol, 55*(8-9), 75-81.

Ford, A., Rutherford, B., Wett, B., and Bott, C. (2016). Implementing hydrocyclones in mainstream process for enhancing biological phosphorus removal and increasing settleability through aerobic granulation. *Proceedings of WEFTEC 2016*, 2809-2822.

Gao, D., Liu, L., Liang, H., and Wu, W. M. (2011). Aerobic granular sludge: characterization, mechanism of granulation and application to wastewater treatment. *Critical Reviews in Biotechnology, 31*(2), 137-152.

Giesen, A., De Bruin, L., Niermans, R., and Van der Roest, H. (2013). Advancements in the application of aerobic granular biomass technology for sustainable treatment of wastewater. *Water Practice and Technology, 8*(1), 47-54.

Guo, J., Peng, Y., Wang, Z., Yuan, Z., Yang, X., and Wang, S. (2012). Control filamentous bulking caused by chlorine-resistant Type 021N bacteria through adding a biocide CTAB. *Water Res, 46*(19), 6531-6542.

Hasebe, Y., Meguro, H., Kanai, Y., Eguchi, M., Osaka, T., and Tsuneda, S. (2017). High-rate nitrification of electronic industry wastewater by using nitrifying granules. *Water Sci Technol, 76*(11), 3171-3180.

Jorand, F., Palmgren, R., Block, J., Urbain, V., and Manem, J. (1995). Biosorption of wastewater organics by activated sludges. *Récents Progrés En Génie Des Procédés, 9*(44), 61-67.

Juang, Y. C., Adav, S. S., Lee, D. J., and Tay, J. H. (2010). Stable aerobic granules for continuous-flow reactors: precipitating calcium and iron salts in granular interiors. *Bioresource Technol, 101*(21), 8051-8057.

Kent, T. R., Bott, C. B., and Wang, Z. W. (2018). State of the art of aerobic granulation in continuous flow bioreactors. *Biotechnol. Adv., 36*(4), 1139-1166.

Knoop, S., and Kunst, S. (1998). Influence of temperature and sludge loading on activated sludge settling, especially on Microthrix parvicella. *Water Sci Technol, 37*(4), 27-35.

Lee, D. J., Chen, Y. Y., Show, K. Y., Whiteley, C. G., and Tay, J. H. (2010). Advances in aerobic granule formation and granule stability in the course of storage and reactor operation. *Biotechnology Advances, 28*(6), 919-934.

Li, D., Lv, Y., Cao, M., Zeng, H., and Zhang, J. (2016a). Optimized hydraulic retention time for phosphorus and COD removal from synthetic domestic sewage with granules in a continuous-flow reactor. *Bioresource Technol, 216*, 1083-1087.

Li, D., Lv, Y., Zeng, H., and Zhang, J. (2016b). Startup and long term operation of enhanced biological phosphorus removal in continuous-flow reactor with granules. *Bioresource Technol, 212*, 92-99.

Li, J., Ding, L.-B., Cai, A., Huang, G.-X., and Horn, H. (2014). Aerobic sludge granulation in a full-scale sequencing batch reactor. *Biomed Res Int, 2014*.

Liu, H., and Fang, H. H. (2002). Extraction of extracellular polymeric substances (EPS) of sludges. *J Biotechnol, 95*(3), 249-256.

Liu, H., Li, Y., Yang, C., Pu, W., He, L., and Bo, F. (2012). Stable aerobic granules in continuous-flow bioreactor with self-forming dynamic membrane. *Bioresource Technol, 121*, 111-118.

Liu, Y., Wang, Z. W., Qin, L., Liu, Y. Q., and Tay, J. H. (2005). Selection pressure-driven aerobic granulation in a sequencing batch reactor. *Applied Microbiology and Biotechnology, 67*(1), 26-32.

Liu, Y. Q., Lan, G. H., and Zeng, P. (2015). Excessive precipitation of CaCO 3 as aragonite in a continuous aerobic granular sludge reactor. *Appl Microbiol Biot, 99*(19), 8225-8234.

Liu, Y. Q., Moy, B., Kong, Y. H., and Tay, J. H. (2010). Formation, physical characteristics and microbial community structure of aerobic granules in a pilot-scale sequencing batch reactor for real wastewater treatment. *Enzyme and Microbial Technol, 46*(6), 520-525.

Martin, K., Shaw, A., de Clippeleir, H., and Sturm, B. (2016). "Accidental Granular Sludge?": Understanding process design and operational conditions that lead to low SVI-30 values through a survey of full scale facilities in North America. *Proceedings of the Water Environment Federation, 2016*(9), 3385-3394.

Martins, A. M., Pagilla, K., Heijnen, J. J., and van Loosdrecht, M. C. (2004). Filamentous bulking sludge—a critical review. *Water Res, 38*(4), 793-817.

Miller, M. W., Jimenez, J., Murthy, S., Kinnear, D., Wett, B., and Bott, C. B. (2013). Mechanisms of COD removal in the adsorption stage of the A/B process. *Proceedings of the Water Environment Federation, 2013*(16), 2472-2481.

Modin, O., Persson, F., Wilén, B.-M., and Hermansson, M. (2016). Nonoxidative removal of organics in the activated sludge process. *Crit Rev Env Sci Tec, 46*(7), 635-672.

Morgenroth, E., Sherden, T., Van Loosdrecht, M. C. M., Heijnen, J. J., and Wilderer, P. A. (1997). Aerobic granular sludge in a sequencing batch reactor. *Water Res, 31*(12), 3191-3194.

Nielsen, S. S. (2010). Phenol-sulfuric acid method for total carbohydrates. In S. S. Nielsen (Ed.), *Food Analysis Laboratory Manual* (pp. 47-53). Boston, MA: Springer US.

Niermans, R., Giesen, A., Loosdrecht, M. v., and Buin, B. d. (2014). Full-scale experiences with aerobic granular biomass technology for treatment of urban and industrial wastewater. *Proceedings of the Water Environment Federation, 2014*(19), 2347-2357.

Pronk, M., De Kreuk, M., De Bruin, B., Kamminga, P., Kleerebezem, R. v., and Van Loosdrecht, M. (2015). Full scale performance of the aerobic granular sludge process for sewage treatment. *Water Res, 84*, 207-217.

Qin, L., Liu, Y., and Tay, J. H. (2004). Effect of settling time on aerobic granulation in sequencing batch reactor. *Biochem Eng J, 21*(1), 47-52.

Rachwal, A., Johnstone, D., Hanbury, M., and Critchard, D. (1982). The application of settleability tests for the control of activated sludge plants. *Bulking of Activated Sludge*, 224-244.

Ramos, C., Suárez-Ojeda, M. E., and Carrera, J. (2016). Biodegradation of a high-strength wastewater containing a mixture of ammonium, aromatic compounds and salts with simultaneous nitritation in an aerobic granular reactor. *Process Biochem, 51*(3), 399-407.

Shi, Y., Wells, G., and Morgenroth, E. (2016). Microbial activity balance in size fractionated suspended growth biomass from full-scale sidestream combined nitritation-anammox reactors. *Bioresource Technol, 218*, 38-45.

Świątczak, P., and Cydzik-Kwiatkowska, A. (2018). Performance and microbial characteristics of biomass in a full-scale aerobic granular sludge wastewater treatment plant. *Environmental Science and Pollution Research International, 25*(2), 1655-1669.

Tan, K. N., and Chua, H. (1997). COD adsorption capacity of the activated sludge — Its determination and application in the activated sludge process. *Environ Monit Assess, 44*(1), 211-217.

Tay, J. H., Liu, Q. S., and Liu, Y. (2001). The effects of shear force on the formation, structure and metabolism of aerobic granules. *Appl Microbiol Biot, 57*(1-2), 227-233.

van der Roest, H. F., de Bruin, L. M. M., Gademan, G., and Coelho, F. (2011). Towards sustainable waste water treatment with Dutch Nereda® technology. *Water Practice and Technol, 6*(3).

Vanderhasselt, A., and Vanrolleghem, P. A. (2000). Estimation of sludge sedimentation parameters from single batch settling curves. *Water Res, 34*(2), 395-406.

Wan, J., and Sperandio, M. (2009). Possible role of denitrification on aerobic granular sludge formation in sequencing batch reactor. *Chemosphere, 75*(2), 220-227.

Wang, X., Cheng, B., Ji, C., Zhou, M., and Wang, L. (2017). Effects of hydraulic retention time on adsorption behaviours of EPS in an A/O-MBR: biofouling study with QCM-D. *Sci Rep-Uk, 7*(1), 2895.

Wang, Z. W., Liu, Y., and Tay, J. H. (2006). The role of SBR mixed liquor volume exchange ratio in aerobic granulation. *Chemosphere, 62*(5), 767-771.

Xin, X., Lu, H., Yao, L., Leng, L., and Guan, L. (2017). Rapid formation of aerobic granular sludge and its mechanism in a continuous-flow bioreactor. *Applied Biochemistry and Biotechnology, 181*(1), 424-433.

Xuan, W., Bin, Z., Zhiqiang, S., Zhigang, Q., Zhaoli, C., Min, J., Junwen, L., and Jingfeng, W. (2010). The EPS characteristics of sludge in an aerobic granule membrane bioreactor. *Bioresource Technol, 101*(21), 8046-8050.

Yang, S. F., Tay, J. H., and Liu, Y. (2005). Effect of substrate nitrogen/chemical oxygen demand ratio on the formation of aerobic granules. *J Environ Eng, 131*(1), 86-92.

Zhang, H., Jia, Y., Khanal, S. K., Lu, H., Fang, H., and Zhao, Q. (2018). Understanding the role of extracellular polymeric substances on ciprofloxacin adsorption in aerobic sludge, anaerobic sludge, and sulfate-reducing bacteria sludge systems. *Environ Sci Technol, 52*(11), 6476-6486.

Chapter 6 Feast/Famine Condition is a Prerequisite for Continuous Flow Aerobic Granulation

6.1 Abstract

Plug flow reactors (PFRs) made of multiple completely stirred tank reactors (CSTRs) in series were used to cultivate aerobic granules with real domestic wastewater. Theoretically, changing the number of CSTR chambers in series will change the nature of plug flow, and thus alter the pattern of the feast/famine condition and impact the aerobic granulation. Therefore, the PFRs were operated in 4-, 6-, and 8-chamber modes under the same settling velocity selection pressure (9.75 m h^{-1}) and hydraulic retention time (6.5 hours) until steady states were reached to evaluate the effect of the feast/famine condition on continuous flow aerobic granulation. The correlation of feast/famine conditions to sludge properties such as particle size, circularity, settleability, specific gravity, zone settling velocity, and extracellular polymeric substance contents were analyzed to evaluate its role in aerobic granulation. It was found that aerobic granulation failed whenever the feast/famine ratio was greater than 0.5. Thereby, it was concluded that the feast/famine condition is a prerequisite for continuous flow aerobic granulation.

6.2 Keywords

Feast; Famine; Aerobic granules; Plug flow; Continuous flow

6.3 Introduction

Aerobic granular sludge is spherical aggregates of microbial cells formed by cell-to-cell adhesion, which is advantageous for aqueous pollutant removal over conventional activated sludge in view of their high biomass retention, easy solid-water separation, multispecies synergy in proximity, resilience to shock loading, and low space requirements (Gao et al., 2011; Hasebe et al., 2017; Sehar et al., 2016). Thus, aerobic granulation is a promising technique for domestic and industrial wastewater treatment (De Kreuk et al., 2007; Morgenroth et al., 1997; Pronk et al., 2015). The first aerobic granulation was achieved in sequential batch reactors (SBRs) back in 1997 (Morgenroth et al., 1997). After that, numerous bench- and pilot-scale aerobic granulation studies were performed in SBRs (Beun et al., 2002; Isanta et al., 2012; Liu et al., 2010; Tay et al., 2001a). Recently, some full-scale applications of the aerobic granulation technology in SBRs have been practiced across the world, e.g. South Africa (2006), Portugal (2008), China (2010), and Netherlands (2010 and 2013) (Giesen et al., 2013; Li et al., 2014; Niermans et al., 2014; Pronk et al., 2015). However, it is noteworthy that almost all of these applications are only limited to SBRs (Kent et al., 2018; Pronk et al., 2015). The SBR mode is inconsistent with the continuous flow nature of the most large-scale wastewater treatment plants (WWTPs) (Kent et al., 2018). Hence, the continuous flow reactors (CFRs) are more welcomed than SBRs by utilities for their simple design and easy control without operational interruption (Chen et al., 2017; Juang et al., 2010; Kent et al., 2018; Li et al., 2016). For this reason, the development of a continuous flow aerobic granulation technique is highly desired for promoting the application of aerobic granulation in large-scale WWTPs (Kent et al., 2018). In a previous study, we, for the first time, proved that aerobic granules can actually form from activated sludge inoculated into a continuous-flow plug-flow reactor (PFR) fed with real wastewater directly from a domestic WWTP even with seasonal temperature and influent quality variations (Sun et al., 2019).

According to a previous literature review (Kent et al., 2018), it was hypothesized that the alternating feast/famine condition is an essential factor required to enable successful aerobic granulation in SBRs besides the driving force role of an effective settling velocity (V_s) selection pressure. The critical role of V_s selection in aerobic granulation has been repeatedly proven in SBR studies (Gao et al., 2011; Liu et al., 2005). Basically, V_s selection pressure washed out poorly

settling suspended biomass and retained only well settling granules with a very short settling time (Qin et al., 2004a; Qin et al., 2004b). Thus, V_s selection pressure has been regarded as a driving force towards aerobic granulation (Jiang et al., 2002; Lin et al., 2003; Linlin et al., 2005; Liu et al., 2003; McSwain et al., 2004; Yang et al., 2003). For feast/famine conditions, it was reported by Corsino et al. (2016) that aerobic granulation cannot be achieved in completely stirred tank reactors (CSTRs) which do not offer feast/famine conditions, indicating decent feast/famine conditions might be required for successful aerobic granulation (Lee et al., 2010).

It was observed that periodic feast/famine operation can make bacteria show more hydrophobic surface property, which is a key factor governing the initial cell-to-cell co-aggregation (Bossier et al., 1996; Liu et al., 2004a; López-Palau et al., 2012; Tay et al., 2001b). It was also found that increasing the relative length of the feast period by increasing nutrient availability tended to result in structural dispersal of granules or biofilm (Sauer et al., 2004; Schwarzenbeck et al., 2005), while longer famine period, on the opposite, may result in higher granule structural stability (Reisner et al., 2003). In spite of these observations, rarely any study has been dedicated to elucidating the correlation between feast/famine conditions and the success of aerobic granulation (López-Palau et al., 2012).

For the investigation of feast/famine conditions, the PFR offers an ideal platform because it provides time-independent snapshots of feast/famine conditions along the plug flow direction, which do not change with the sampling time at the steady state. Connecting several CSTRs in series is a common way to approximate the condition of PFRs. Technically, changing the number of CSTRs in series will change the nature of plug flow, and thus alter the pattern of feast/famine condition (e.g. feast/famine ratio). Therefore, this study aims to investigate the effect of periodic feast/famine pattern on continuous flow aerobic granulation by alternating the number of CSTR chambers in series. It should be pointed out that the mechanism revealed from this study should be applicable to aerobic granulation in SBR system, as well.

6.4 Materials and Methods

6.4.1 Reactor design

A bench-scale Plug-flow Aerobic Granulation (PAG) reactor with 128 L total working volume was built and operated at the Upper Occoquan Service Authority (UOSA), a WWTP located in Centreville, VA, USA. Detailed reactor setup information can be found in a previous study by Sun et al. (2019). The bench-scale reactor consists of multiple CSTR chambers connected in series to approximate a PFR in which feast/famine conditions can be created. V_s selection pressure was applied to drive aerobic granulation by using two parallel external settling selectors placed at the end of the PFR. The selective retention of bioparticles with V_s greater than a critical settling velocity (V_c) was achieved by operating the settling selectors as intermittent clarifiers with a short settling time, which was detailed elsewhere (Sun et al., 2019). As shown in Table 6.1, V_c was set at 9 ~ 9.75 m h^{-1} by using a settling time of 4 minutes and a discharge height of 60 ~ 65 cm to selectively retain bioparticles with V_s greater than V_c according to a previous study (Wang et al., 2006). The influent of the bench-scale PFR was UOSA's primary effluent (PE). The characteristics of UOSA's domestic wastewater during the study period are shown in Table 6.2 in terms of temperature, pH, total COD (tCOD), soluble COD (sCOD), 5-day biochemical oxygen demand (BOD_5), alkalinity, total suspended solid (TSS), Total Kjeldahl Nitrogen (TKN), ammonia (NH_3), and total phosphorus (TP). UOSA's full-scale secondary treatment trains share the same influent, plug-flow nature, and hydraulic retention time (HRT) with the bench-scale study, while the major difference is that UOSA's full-scale secondary treatment trains do not have a strong V_c as presented in the previous study by Sun et al. (2019). Basically, V_c of the full-scale treatment train is equivalent to the surface overflow rate (SOR) of its clarifier, which is as low as 1 m h^{-1} (Table 6.1).

6.4.2 Reactor operation

The 416-day operation of the bench-scale PFR was divided into three phases, namely phase I, II, and III (Table 6.1). In this study, the number of CSTR chambers used in these three phases was changed as the only variable to study the effects of feast/famine conditions on continuous flow

aerobic granulation. Phase I lasted 118 days and used 10 CSTR chambers in series to mimic the plug-flow pattern in the bench-scale PFR. Detailed information of the phase I study can be found elsewhere (Sun et al., 2019). On day 118, because of an unexpected clogging and overflow accident, the bench-scale PFR lost more than 80% of its mix liquor suspended solid concentrations (MLSS). Right after that, the phase II operation was initiated on day 133 by reducing the chamber number from 10 to 8 with the other parameters listed in Table 6.1 unchanged. After a three-week steady state was reached, phase III was started on day 253, during which the 10 CSTR chambers were divided into two PFR trains with 4 and 6 chambers in series, respectively. Both bench-scale PFRs were inoculated with UOSA's return activated sludge (RAS). Phase III lasted for 163 days and was terminated on day 416 when no substantial sludge settleability change can be observed for about four weeks. The operational parameters of the full-scale treatment train as shown in in Table 6.1 remained unchanged during the entire study.

Table 6.1 Operational parameters of the bench-scale PFRs and the full-scale treatment train

Phase	Duration	Bench-scale			Full-scale			Study
		Number of chambers	HRT (h^{-1})	V_c ($m\ h^{-1}$)	Number of chambers	HRT (h^{-1})	V_c ($m\ h^{-1}$)	
I	Day 0~ 118	10	6.5	9~9.75				(Sun et al., 2019)
II	Day 133~235	8	6.5	9.75	4	6.5	1	This study
III	Day 253~416	4 & 6	6.5	9.75				

6.4.3 Analytical methods

As described previously (Sun et al., 2019), sludge characteristics such as 5 and 30 minutes sludge volume index (SVI_5 and SVI_{30}), zone settling velocity (V_{zs}), MLSS, mix liquor volatile suspended solid (MLVSS), and specific gravity were all analyzed by using standard methods (APHA, 1998). The samples for sludge characteristics analyses were taken from the last chamber of the PFR. pH was monitored using an online Liquiline M CM42 transmitter (Endress+Hauser, Greenwood, IN, USA), and the temperature was monitored by using RC-4 temperature data logger (Elitech®,

Milpitas, CA, USA). COD was analyzed using COD TNTplus® 820 vials and a spectrophotometer (Hach, Loveland, CO, USA), in which sCOD were filtered using 0.45 μm syringe filters (EZFlow®, Old Saybrook, CT, USA), and tCOD was measured by using supernatant after 30-min settling to separate water and sludge. Hence, tCOD includes particulate, colloidal and soluble COD. BOD_5 and alkalinity were both analyzed using standard methods (APHA, 1998). TKN, TP, NH_3-N, NO_2^--N, and NO_3^--N were analyzed using a QuikChem® 8500 series 2 flow injection analysis system (Lachat, Loveland, CO, USA). Petri dish photos of mix liquor samples were analyzed using image processing software (ImageJ 2.0.0) to determine particle size and circularity distribution. Extracellular polymeric substances (EPSs) extraction and quantification were performed based on the methods described by Liu et al. (2002) and Sun et al. (2019). Briefly, 2% EDTA was used as the chemical extractant. Dialysis Kits (Spectrum™ Labs Spectra/Por™ 3500 D MWCO Standard RC Pre-Treated, Waltham, MA USA) were utilized to separate polymers with molecular weight greater than 3500 Dalton. A phenol-sulfuric acid method was adopted for carbohydrates (PS) analysis (Nielsen, 2010), and Pierce™ modified Lowry protein assays were used for the protein (PN) analysis (Thermo Scientific™, Waltham, MA, USA).

Table 6.2 Characteristics of the domestic wastewater

Parameters	**Unit**	**Raw influent**			**Primary effluent**		
		Max.	**Min.**	**Average**	**Max.**	**Min.**	**Average**
Temperature	°C	N/A	N/A	N/A	23.3	10.1	18.3
pH	N/A	7.7	6.8	7.3	7.7	6.7	7.3
tCOD	mg L^{-1}	1320	219	554	687	150	232
sCOD	mg L^{-1}	N/A	N/A	N/A	160	44	86
BOD_5	mg L^{-1}	344	63	197	148	76	116
Alkalinity	mg L^{-1}	272	103	199	266	119	211
TSS	mg L^{-1}	950	70	252	234	13	97
TKN	mg L^{-1}	67.8	16.9	41.6	53.2	14.0	39.0
NH_3-N	mg L^{-1}	45.8	10.2	28.2	37.3	10.0	27.7
TP	mg L^{-1}	11.3	1.9	5.0	7.2	1.9	4.4

*N/A: not applicable

6.4.4 Determination of the feast and famine conditions

In this study, the feast and famine conditions were defined by whether the substrate concentration is high enough to sustain microbial growth. To be specific, only when the microbial net growth is not negative, namely the theoretical growth rate ≥ theoretical decay rate, can the microbes be deemed growing under the feast condition; otherwise, the condition will be deemed as famine. With that being said, Eq. 6.1 was utilized to measure whether a growth condition is feast; otherwise, it is famine,

$$\frac{dS_S}{dt} \cdot Y_S \geq b \cdot X \cdot Q_{10}^{\frac{T-20}{10}} \quad \textbf{(6.1)}$$

in which S_S is the substrate concentration (mg L^{-1}), t is the time; b is the theoretical decay rate coefficient (h^{-1}) measured at 20 °C; T is the actual temperature (°C) under which the microbes grew; Q_{10} temperature coefficient is a measure of the biological kinetics change as a consequence of the temperature change by 10 °C (Hegarty, 1973), and a value of 1.63 was adopted based on the typical value of activated sludge (Jones et al., 1996); X represents the microbial concentration as quantified by MLVSS values, and a factor of 1.5 mg COD mg VSS^{-1} was used for converting biomass to COD (Bullock et al., 1996); and Y_s represents the theoretical growth yield of the microbes. The typical values of microbial b and Y_s in activated sludge were adapted from Activated Sludge Model No. 1 (ASM1) (Henze et al., 2000), which are 0.6 d^{-1} and 0.67 mg COD mg COD^{-1}, respectively. The $\frac{dS_S}{dt}$ in Eq. 6.1 can be estimated from Eq. 6.2 by assuming the first-order reaction,

$$\frac{dS_S}{dt} = k \cdot S_S \quad \textbf{(6.2)}$$

in which k is the first-order reaction coefficient. Thereby, the steady-state substrate concentration ($S_{S,i}$) in the i^{th} CSTR chamber of the PFR can be estimated by,

$$S_{S,i} = \frac{S_{S,i-1}}{1 + k \cdot \frac{HRT}{n}} \quad \textbf{(6.3)}$$

in which n stands for the total number of chambers used in the PFR; HRT stands for the total HRT of the PFR (Table 6.1); $S_{S,i-1}$ stands for the influent substrate concentration from the previous, namely i-1^{th}, CSTR chamber. Of course, $S_{S,0}$ stands for the PE substrate concentration which is

the influent to the PFR. By fitting substrate concentrations measured in each CSTR chamber along with the HRT and n used in the PFR, k values can be regressed. The fitness of the first-order reaction assumption in description of the measured substrate concentration profile can be evaluated by the correlation coefficient between the regressed and measured data points.

6.5 Results

6.5.1 Effect of chamber numbers on sludge settleability

It is broadly accepted that a SVI_{30} value of 60 mg L^{-1} or lower and a SVI_5:SVI_{30} ratio close to 1 are two major indicators of the successful aerobic granulation in terms of settleability (Kent et al., 2018; Martin et al., 2016; Pronk et al., 2015; Sun et al., 2019), and thus both SVI_5 and SVI_{30} values were measured in the three phases of the study. According to Figure 6.1a and b, SVI_{30} and SVI_5:SVI_{30} ratios of the sludge in the 10-chamber PFR decreased from 100 mL g^{-1} and 1.7 to around 60 mL g^{-1} and 1.1 during the phase I study, which indicated that sludge with good settleability was cultivated and stabilized in the 10-chamber PFR as previously reported (Sun et al., 2019). At the beginning of phase II, SVI_{30} and SVI_5:SVI_{30} of sludge in the 8-chamber PFR were around 80 mg L^{-1} and 1.3 as a result of the accidental clogging and overflow which washed out most of the sludge (Figure 6.1a and b). It took about 60 days for the PFR to regain SVI_{30} and SVI_5:SVI_{30} values as low as 54 mg L^{-1} and 1.2 (Figures 6.1a and b). After SVI_{30} and SVI_5:SVI_{30} values were stabilized around 50 mg L^{-1} and 1.2 for three weeks in the 8-chamber PFR, the phase III study was initiated by dividing the 10-chamber PFR into a 4-chamber and a 6-chamber PFRs and then re-inoculating the two PFRs with the RAS from the full-scale treatment train. As can be seen from Figure 6.1, the initial SVI_{30} and SVI_5:SVI_{30} ratios for 4- and 6-chamber PFRs were as high as 110 ml g^{-1} and 1.8, respectively. The decreasing trends of SVI_{30} and SVI_5:SVI_{30} ratios for 4- and 6-chamber PFRs were generally identical during the first 100 days of phase III operation. However, SVI_{30} of 4-chamber PFR stopped decreasing around the 110^{th} day after the phase III startup and was finally stabilized around 70 mL g^{-1}. On the contrary, SVI_{30} of 6-chamber PFR continued to decrease until reaching around 50 mg L^{-1} at the 360^{th} day and then was stabilized. Likewise, SVI_5:SVI_{30} ratios for 4- and 6-chamber PFRs were stabilized around 1.6 and 1.4, respectively (Figures 6.1). In contrast, the values of SVI_{30} and SVI_5:SVI_{30} in the full-scale

treatment train with the same influent water and HRT but a much lower V_c (1 m h^{-1}, Table 6.1) remained above 110 mg L^{-1} and 1.7 throughout the phase I, II, and III (Figures 6.1), which are not uncommon for conventional activated sludge (Świątczak et al., 2018; Wan et al., 2009). The steady-state values of SVI_{30} and SVI_5:SVI_{30} ratios for 4-, 6-, and 8-chamber PFRs are also summarized in Table 6.3, which indicated that the sludge settleability is positively correlated to the chamber numbers used in the PFR at the same HRT and V_c.

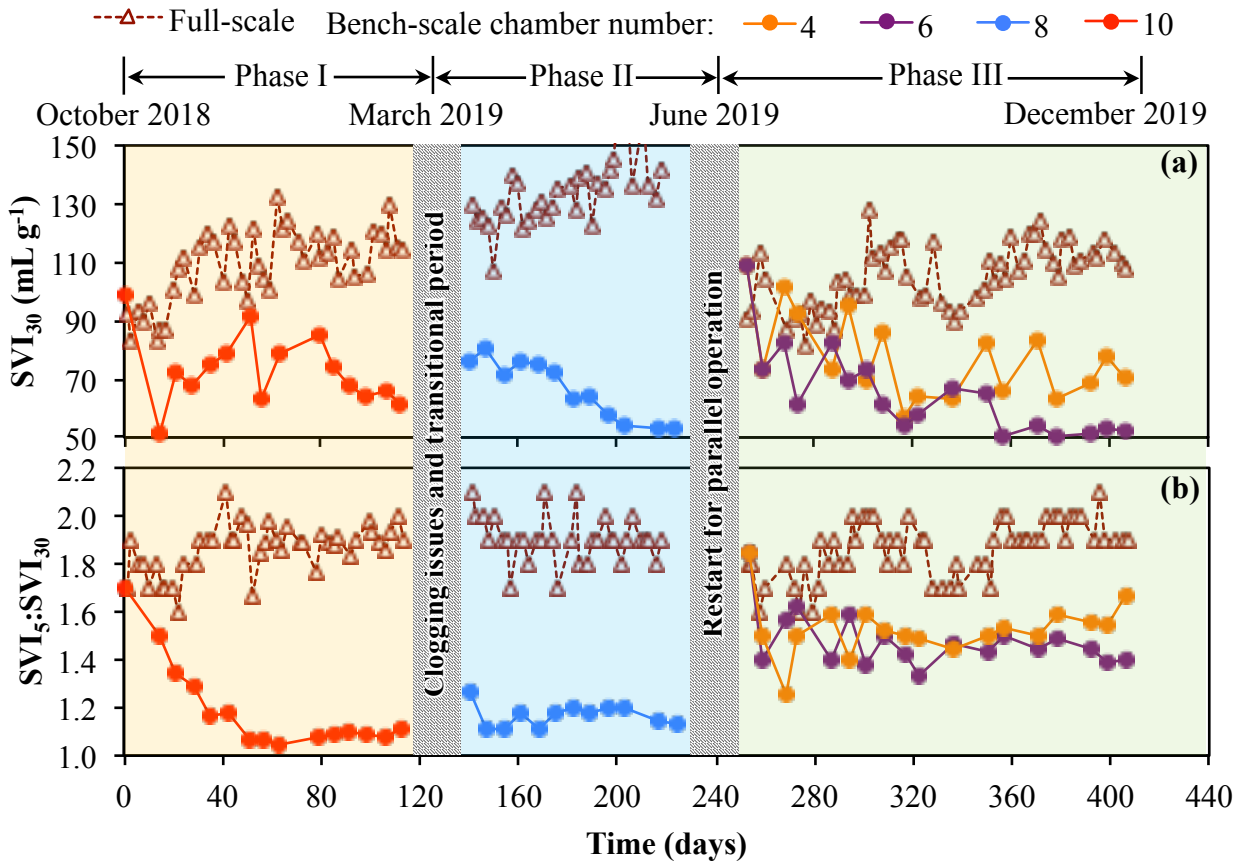

Figure 6.1 Profiles of (a) SVI_{30} and (b) SVI_5/SVI_{30} measured from the last chamber of the bench-scale PFRs and the full-scale treatment train over phase I, phase II, and phase III studies. Phase I

V_{zs} is another indicator of settleability (Sun et al., 2019). As shown in Table 6.3, V_{zs} of the sludge in the 4-chamber PFR was only 7.9 m h^{-1}. It becomes higher, e.g. 11.8 m h^{-1}, in the 6-chamber PFR, and even higher, e.g. 15.0 m h^{-1}, in the 8-chamber PFR. Although it is known that V_{zs} can be impacted by the MLSS concentration, i.e., higher MLSS leads to smaller V_{zs} (Vanderhasselt et al.,

2000). According to Table 6.3, the reactor with high MLSS (e.g., 8-chamber) actually exhibted the high V_{zs}, indicating that the increase of V_{zs} was not due to MLSS. The values of V_{zs} in 6- and 8-chamber PFRs were both greater than the V_c of the selector (9.75 m h^{-1}), indicating that the sludge has adapted to the reactor's V_s selection pressure. On the contrary, the V_{zs} in the 4-chamber reactor was lower than the V_c of the selector, indicating that the sludge was not adapted to the V_s selection pressure in the 4-chamber PFR.

Table 6.3 Comparison of steady-state sludge sludge characteristics in the bench-scale PFRs

Parameters	Units	Chamber number		
		4	**6**	**8**
SVI_{30}	mL g^{-1}	68 ± 9	53 ± 7	52 ± 3
SVI_5:SVI_{30}	N/A	1.56 ± 0.06	1.42 ± 0.04	1.18 ± 0.03
V_{zs}	m h^{-1}	7.9 ± 1.2	11.8 ± 1.5	15.0 ± 0.7
d_{50}	mm	12.4	4.1	2.1
Circularity (median value)	N/A	0.09	0.34	0.55
Specific gravity	N/A	1.03 ± 0.09	1.12 ± 0.07	1.19 ± 0.07
EPS PS	mg g^{-1}	9.5 ± 0.5	9.9 ± 0.7	12.0 ± 0.8
EPS PN	mg g^{-1}	20.4 ± 1.0	22.6 ± 1.5	38.2 ± 2.0
MLSS	mg L^{-1}	942 ±122	2169 ±145	2299 ±177
MLVSS	mg L^{-1}	798 ±102	1857 ±129	2012 ±172
SRT	days	2.0	5.0	6.4

It is commonly known that the sludge with better settleability should possess a higher specific gravity relative to water (Liu et al., 2009). According to literature, the specific gravities of traditional activated sludge are within the range of 1.001 ~ 1.01 (Cassidy et al., 2005; Li et al., 2007; Su et al., 2005), while the granular sludge with good settleability can possess specific

gravities as high as 1.03 ~ 1.2 (Cassidy et al., 2005; Liu et al., 2004b; Tao et al., 2017; Zheng et al., 2005). As shown in Table 6.3, the specific gravities of the sludge in 4-, 6-, and 8-chambers PFRs were all within this high range and increased with the increase of chamber number.

data has been published in Sun et al. (2019). Operational parameters of the bench-scale PFRs and the full-scale treatment train during the three phases are shown in Table 6.1.

6.5.2 Effect of chamber numbers on sludge morphology

The sludge morphology in 4-, 6-, and 8-chamber PFRs at the steady state is shown in Figures 6.2. According to the first petri dish photo in Figure 6.2a, it can be seen that the majority of the sludge in the 4-chamber PFR was in the form of fluffy, large, and irregular bioflocs, and no granular sludge can be found. This is consistent with the particle size and circularity distributions as shown in Figure 6.2b and c. Basically, the size of 60% of the sludge were greater than 8 mm, and more than 80% of the sludge biomass possesses the circularity smaller than 0.2 (Figure 6.2b and c). In the 6-chamber PFR, although most sludge was still fluffy and loose, their shape became more regular, and those large bioflocs that appeared in the 4-chamber PFR did not show up (Figures 6.2a). According to the particle size distribution shown in Figure 6.2b, more than 50% of the particles were within the size range of 4-7 mm. As shown in Figure 6.2c, sludge circularities in the 6-chamber PFR also shifted to larger values. In the 8-chamber PFR, it is noteworthy that dense and spherical granules already became dominant, and about 75% of granules were within the range of 1-3 mm, indicating sizes of granule were more uniform and smaller than those fluffy bioflocs in the 4- and 6-chamber PFRs (Figures 6.2a). Besides, Figure 6.2c showed that the sludge circularities shifted to even higher values in the 8-chamber PFR, which indicates that the granules in the 8-chamber PFR were indeed more spherical as compared to the fluffy bioflocs in the 4- and 6-chamber PFRs. As summarized in Table 6.3, the steady-state sludge median size (d_{50}) was inversely correlated to the chamber number, and vice versa for the circularities.

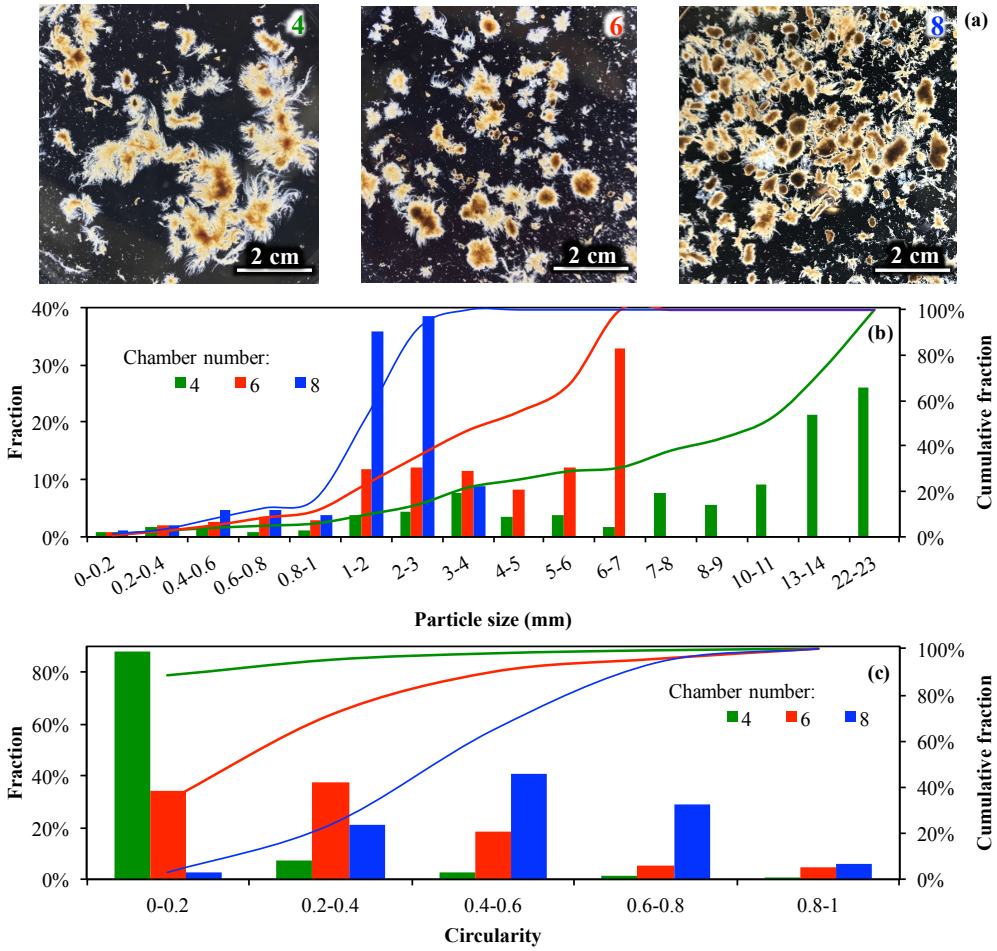

Figure 6.2 Steady-state sludge morphology observed in the last chamber of 4-, 6-, and 8-chamber bench-scale PFRs: (a) petri dish photos, (b) particle size, and (c) circularity distributions.

6.5.3 Effect of chamber numbers on feast/famine ratios

The Eq. 6.3-simulated substrate concentration profiles were plotted against the actual data measured from the experiment with all regressed k and R^2 values presented in Figure 6.3. As can be seen, Eq. 6.3 provided excellent fitness to the substrate profiles in all PFRs with R^2 values greater than 0.9, indicating that the first-order reaction assumption is valid. Most importantly, k values in Eq. 6.3 was found to increase with the PFR chamber numbers at the same HRT, e.g. k = 1.4, 2.0, and 2.2 h^{-1} when n = 4, 6, and 8 (Figure 6.3). This is not difficult to understand in that higher MLVSS were retained in PFRs with more chamber numbers by virtue of the better aerobic granulation (Table 6.3).

The substrate utilization rate ($\frac{dS_S}{dt}$) in each chamber of the in 4-, 6-, and 8-chamber PFRs was calculated by using Eq. 6.2 and then plotted in Figure 6.4 as solid horizontal lines. The minimum $\frac{dS_S}{dt}$ that can sustain microbial growth in each PFR was also calculated using Eq. 6.1 and plotted as dashed horizontal lines in Figure 6.4. The feast and famine phases were differentiated by the last chamber with the growth rate not smaller than the decay rate according to Eq. 6.1. Thereby, the feast and famine phase lengths in 4-, 6-, and 8-chamber PFRs are shown in the three colored boxes on the top of Figure 6.4. According to Figure 6.4, the feast/famine ratios for 4-, 6-, and 8-chamber PFRs were 1, 0.5, and 0.33, respectively.

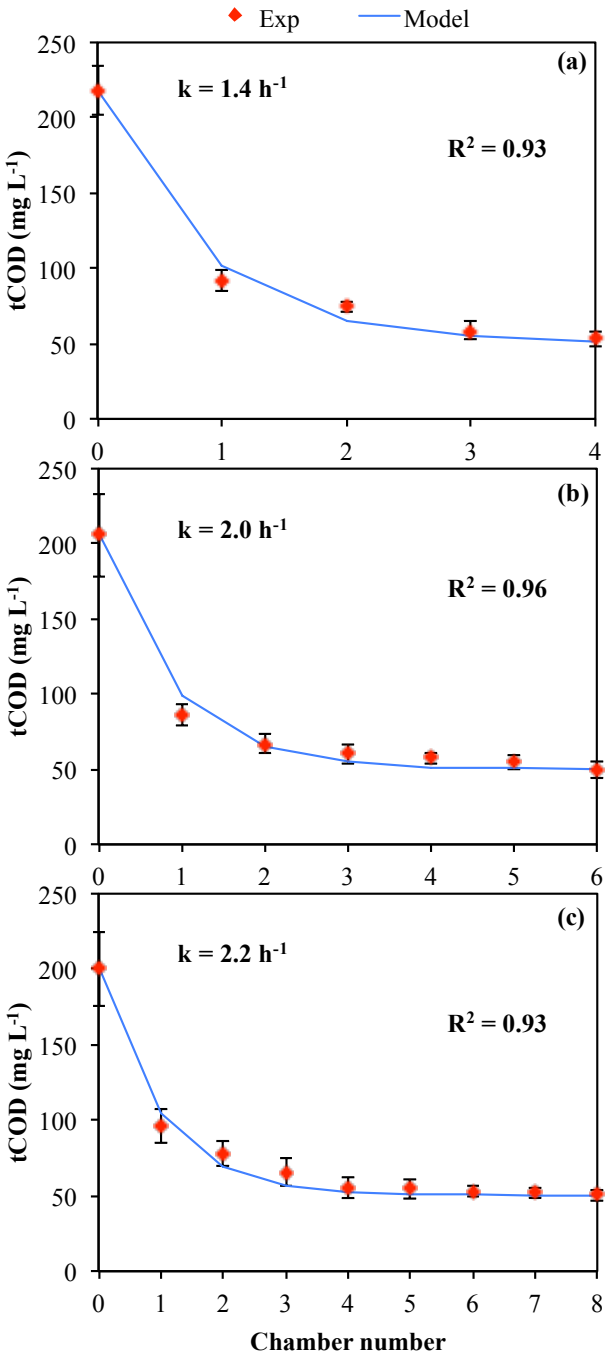

Figure 6.3 Experimental and Eq. 6.3 simulated tCOD profiles at steady state in (a) 4- (b) 6-, and (c) 8-chamber bench-scale PFRs. Chamber number 0 represent the influent concentration

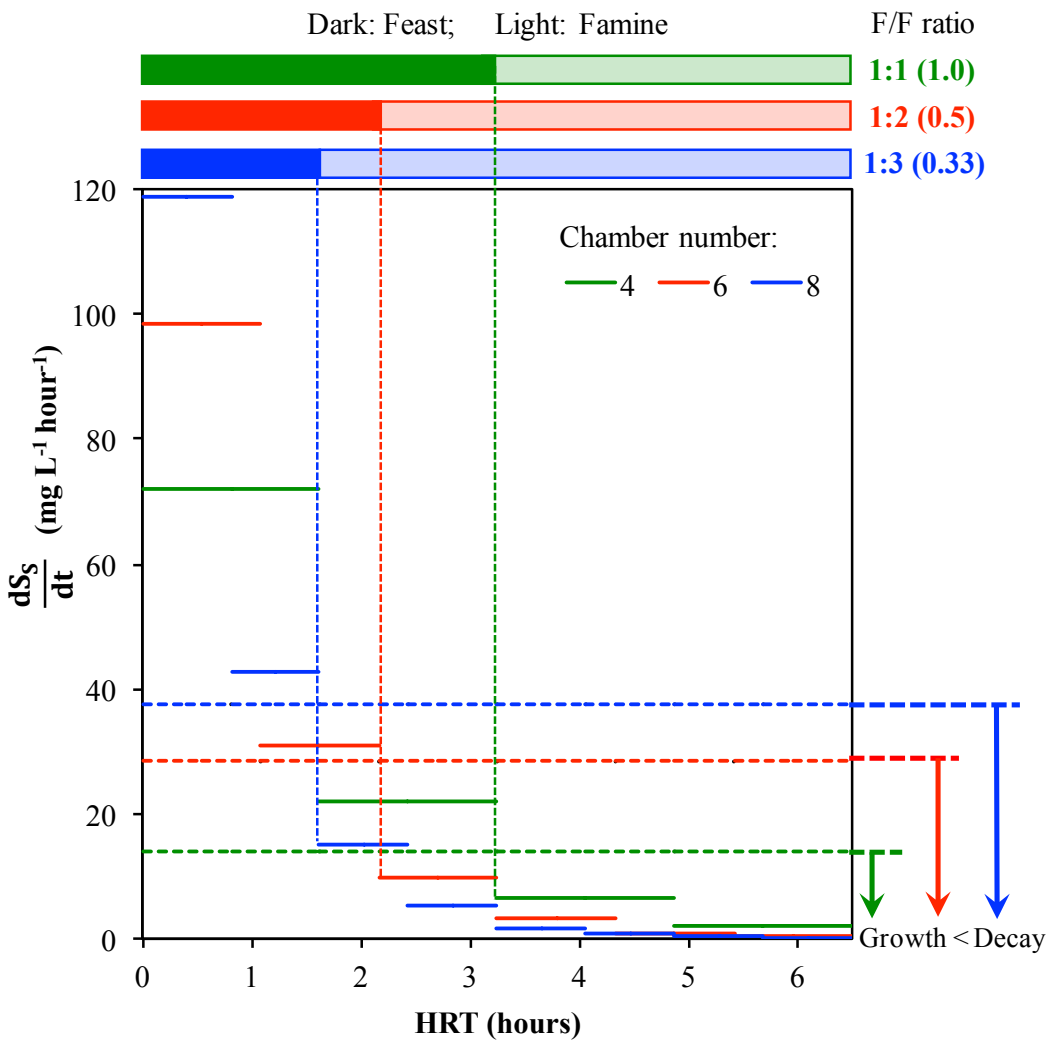

Figure 6.4 Steady-state tCOD utilization rate ($\frac{dS_S}{dt}$, solid horizontal lines) and the minimum $\frac{dS_S}{dt}$ that can sustain microbial growth (dashed horizontal lines) in each chamber of PFRs calculated according to Eq. 6.1, from which the feast/famine (F/F) ratios were determined (colored boxes on the top) in 4- (red), 6- (green), and 8-chamber (blue) bench-scale PFRs

6.6 Discussion

6.6.1 Correlation of feast/famine ratio to sludge characteristics

Figures 6.2 show that the success of aerobic granulation was compromised when the chamber number was reduced from 8 to 6 and then totally failed when further reduced to 4. Figure 6.4

revealed that the number of chambers used in PFRs was actually highly correlated to the feast/famine ratio in PFRs. Therefore, it is a reasonable consideration that the feast/famine ratio might have played essential roles in determining the sludge morphology and settleability. This can be seen from the high correlation ($R^2 > 0.85$) of the feast/famine ratio to almost all the sludge characteristics such as circularity, d_{50}, specific gravity, V_{zs}, SVI_{30}, SVI_5/SVI_{30}, MLVSS, MLSS, and k as shown in Figures 6.5. It is clear from Figures 6.5 that a feast/famine ratio as low as 0.33 can cultivate spherical, dense, and fast settling granular sludge in PFRs. Besides, as the feast/famine ratio increased from 0.33 to 0.5, the sludge morphology and density became worse (Figure 6.5a and b), while the settleability (SVI_{30}) did not change much (Figure 6.5c). This phenomenon implied that the sludge cultivated under the feast/famine ratio of 0.5 did not look like granular sludge but has similar settleability to granular sludge, which makes it more like a transitional form between granular sludge and floc-like sludge. Such a transitional form can also be seen from the second petri dish photo in Figures 6.2a. Hence, 0.5 looks like the critical feast/famine ratio for aerobic granulation, i.e., a feast/famine ratio > 0.5 is very likely to result in aerobic granulation failure, and vice versa. This conclusion can also be supported by many previous findings of aerobic granulation in SBRs. For example, successful aerobic granulation has been reported in SBRs when feast/famine ratios were as low as 0.16, 0.25, 0.33, and 0.42 (Liu et al., 2006, 2008; López-Palau et al., 2012; López–Palau et al., 2009), which are all below the critical feast/famine ratio of 0.5 identified in this study. Besides, López-Palau et al. (2012) and Liu et al. (2008) both reported that aerobic granulation began to fail in SBRs when feast/famine ratios increased from values smaller than 0.5 (e.g., 0.25 and 0.42) to 0.66. Furthermore, Corsino et al. (2016) reported that aerobic granules just cannot form in CSTRs without feast/famine conditions. These facts support that the fact that feast/famine ratio of 0.5 identified in this study is indeed the critical ratio for successful aerobic granulation. It should be also noticed that the abovementioned studies (including this one) were conducted in different kinds of reactors (e.g., SBRs and CFRs) with different operational parameters (e.g., loading rate, cycle time, HRT) and influent sources (e.g., synthetic, municipal, and winery wastewater, etc.) by different research institutes, implying that the necessity of feast/famine ratio should be universal to all aerobic granulation applications.

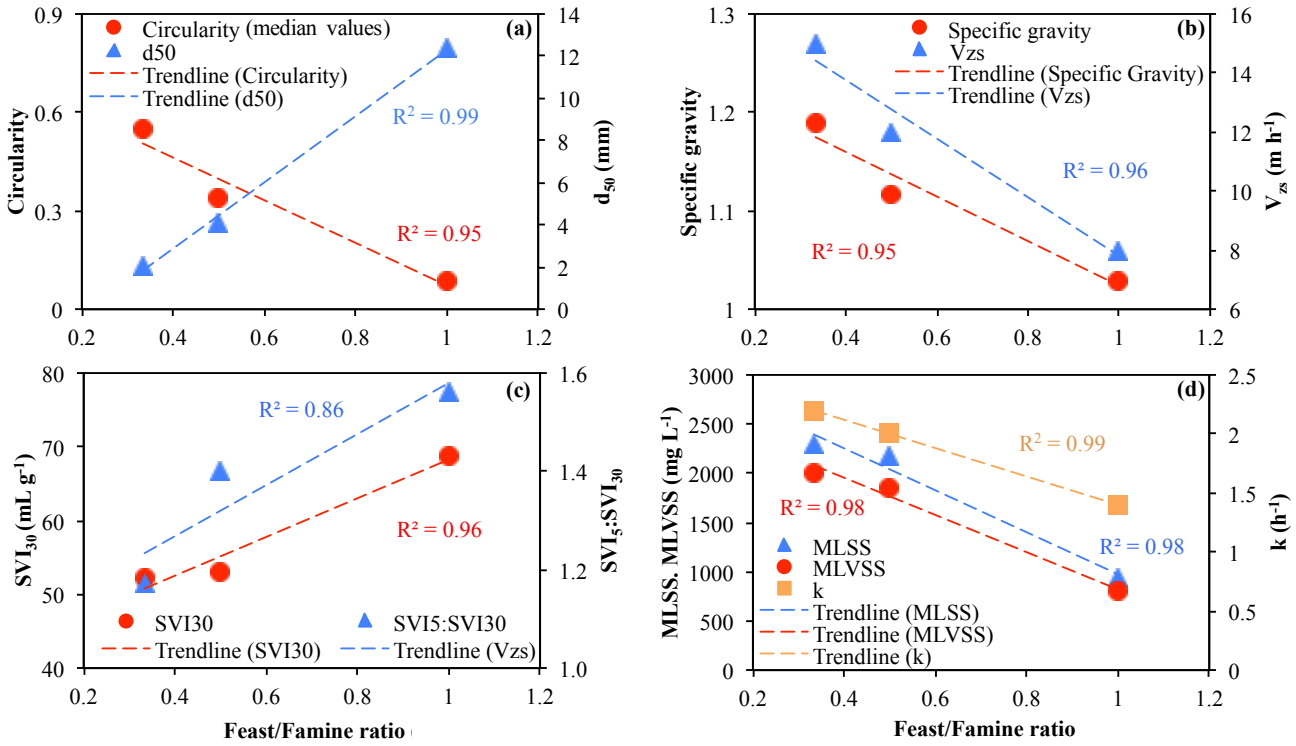

Figure 6.5 Correlation of feast/famine ratios to sludge characteristics such as (a) circularity and d_{50}, (b) specific gravity and V_{zs}, (c) SVI_{30} and SVI_5:SVI_{30} ratios, (d) MLSS, MLVSS, and k at the steady state. Standard deviations for all experimental values are shown in Table 6.3.

6.6.2 Feast/famine condition is a prerequisite for continuous flow aerobic granulation

EPSs have been regarded as the cementing materials excreted by bacteria to bind themselves to each other into the form of aerobic granular sludge or biofilms (Adav et al., 2008; Lee et al., 2010). Table 6.3 shows that the major components of EPSs, namely PS and PN, decreased as the feast/famine ratio increases, especially when the feast/famine ratio is greater than 0.5, i.e., chamber number < 6. Jimenez et al. (2015) revealed that bacteria tended to synthesize and accumulate EPSs during the feast phase, and the EPS production increased with the organic carbon removal rate. It was also recognized that a portion of the EPS is actually biodegradable and thus can be used by bacteria to sustain their lives during the starvation (Wang et al., 2007). Therefore, a decent length of famine phase for bacteria will trigger excessive EPSs production during the feast phase (Rahman et al., 2017), providing the basic materials for granular sludge formation. Other than EPS production, the starvation phase was also reported to increase bacterial surface hydrophobicity

which initiates the reversible cell-to-cell co-aggregation in preparation for irreversible granular sludge formation via EPS binding (Bossier et al., 1996; Liu et al., 2004a; López-Palau et al., 2012; Tay et al., 2001b). That being said, the feast/famine condition must have induced bacteria to prepare the construction materials needed for granular sludge formation.

However, even with all construction materials, e.g. EPSs, are in place, aerobic granules still may not necessarily form unless a selection pressure is provided to confer a growth advantage on bacteria choosing to co-aggregate. It is known that feast/famine alternation may improve sludge settleability to a certain degree but not necessarily lead to granular sludge formation (Rahman et al., 2017). This can be seen from the SVI_{30} and SVI_5:SVI_{30} values of the full-scale treatment train shown in Figure 6.1, i.e., although the full-scale treatment train was also PFRs with feast/famine alternation as described in a previous publication (Sun et al., 2019), granular sludge was not formed because the V_c was too low (Table 6.1). Technically, dispersed cells grow faster than granulated cells due to the increased mass diffusion limitation in denser aggregates, which can be seen from the solids retention time (SRT) values in Table 6.3. Therefore, granulated cells were not able to compete with dispersed cells for limited substrate resources unless a selection pressure, e.g. V_c, is introduced to favor the growth of granulated cells over that of the dispersed cells. This explains the lack of the report of aerobic granules formation in traditional feast/famine offering reactors such as SBRs and PFRs, and also the importance of the driving force role of selection pressure provided by either hydrocyclone or the V_c in SBRs and PFRs (Gao et al., 2011; Kent et al., 2018; Liu et al., 2005; Sun et al., 2019). The similar mechanism was actually also discovered in the research of pure culture responding to feast/famine conditions (Merritt et al., 2018), i.e., alternating feast/famine condition triggered the formation of *E.coli* aggregates which grew at a much lower rate than that of the dispersed *E.coli* cells, so a washout mechanism had to be in place to get rid of the fast-growing, dispersed *E.coli* cells so as to favor the growth of the slow-growing *E.coli* aggregates. Probably, repeatedly experiencing a feast/famine ratio smaller than 0.5 is an environmental factor that can trigger the new phenotype expression for bacteria to switch from suspended to attached growth. Of course, whether such a new phenotype can dominate will depend on the strength of the selection pressure favoring this new phenotype. This mechanism appears to be independent of the microbial species because this phenomenon was observed in both mixed and

pure culture studies fed with a variety of different types of substrates (Liu et al., 2006, 2008; López-Palau et al., 2012; López–Palau et al., 2009; Merritt et al., 2018).

It appears from this study that a feast/famine ratio smaller than 0.5 is required besides the driving force role of V_c around 10 m h^{-1} towards successful continuous flow aerobic granulation as reported in previous studies (Sun et al., 2019; Wang et al., 2006). Therefore, a proper plug flow condition that can provide a feast/famine ratio smaller than 0.5 should be taken into consideration in the future full-scale continuous flow aerobic granulation design. In contrast, CSTRs without feast/famine condition should be avoided. This is especially important in view of the numerous reports of full-scale application without granular sludge formation even though the hydrocyclone has been installed (Ford et al., 2016; Van Winckel et al., 2016; Willoughby et al., 2016). Again, besides the driving force role of selection pressure, the prerequisite role of feast/famine condition is also required.

6.7 Conclusions

Following concluding remarks can be drawn from this study:

1. The formation of aerobic granular sludge was achieved in 8- and 10-chamber PFRs but was compromised when chamber numbers were reduced to 6, and totally failed when the chamber number was further reduced to 4.
2. The feast/famine ratios for 4-, 6-, 8-chamber PFRs were determined by checking whether the bacterial growth rate fell below the decay rate. The characteristics of sludge is closely correlated to the feast/famine ratios established in the PFRs.
3. Feast/famine ratios smaller than a critical value of 0.5 is a prerequisite of continuous flow aerobic granulation and thus should be taken into consideration in full-scale design besides the driving force role of selection pressure.

6.8 References

Adav, S. S., Lee, D. J., and Tay, J. H. (2008). Extracellular polymeric substances and structural stability of aerobic granule. *Water Res, 42*(6), 1644-1650.

APHA. (1998). Standard methods for the examination of water and wastewater.

Beun, J., Van Loosdrecht, M., and Heijnen, J. (2002). Aerobic granulation in a sequencing batch airlift reactor. *Water Res, 36*(3), 702-712.

Bossier, P., and Verstraete, W. (1996). Triggers for microbial aggregation in activated sludge? *Appl Microbiol Biot, 45*(1-2), 1-6.

Bullock, C. M., Bicho, P. A., Zhang, Y., and Saddler, J. N. (1996). A solid chemical oxygen demand (COD) method for determining biomass in waste waters. *Water Res, 30*(5), 1280-1284.

Cassidy, D., and Belia, E. (2005). Nitrogen and phosphorus removal from an abattoir wastewater in a SBR with aerobic granular sludge. *Water Res, 39*(19), 4817-4823.

Chen, C., Bin, L., Tang, B., Huang, S., Fu, F., Chen, Q., Wu, L., and Wu, C. (2017). Cultivating granular sludge directly in a continuous-flow membrane bioreactor with internal circulation. *Chem Eng J, 309*, 108-117.

Corsino, S., Campo, R., Di Bella, G., Torregrossa, M., and Viviani, G. (2016). Study of aerobic granular sludge stability in a continuous-flow membrane bioreactor. *Bioresource Technol, 200*, 1055-1059.

De Kreuk, M., Kishida, N., and Van Loosdrecht, M. (2007). Aerobic granular sludge–state of the art. *Water Sci Technol, 55*(8-9), 75-81.

Ford, A., Rutherford, B., Wett, B., and Bott, C. (2016). Implementing hydrocyclones in mainstream process for enhancing biological phosphorus removal and increasing settleability through aerobic granulation. *Proceedings of the Water Environment Federation*, 2809-2822.

Gao, D., Liu, L., Liang, H., and Wu, W. M. (2011). Aerobic granular sludge: characterization, mechanism of granulation and application to wastewater treatment. *Critical Reviews in Biotechnology, 31*(2), 137-152.

Giesen, A., De Bruin, L., Niermans, R., and Van der Roest, H. (2013). Advancements in the application of aerobic granular biomass technology for sustainable treatment of wastewater. *Water Pract Technol, 8*(1), 47-54.

Hasebe, Y., Meguro, H., Kanai, Y., Eguchi, M., Osaka, T., and Tsuneda, S. (2017). High-rate nitrification of electronic industry wastewater by using nitrifying granules. *Water Sci Technol, 76*(11), 3171-3180.

Hegarty, T. W. (1973). Temperature coefficient (Q10), seed germination and other biological processes. *Nature, 243*(5405), 305-306.

Henze, M., Gujer, W., Mino, T., and van Loosdrecht, M. C. M. (2000). *Activated Sludge Models ASM1, ASM2, ASM2d and ASM3* (Vol. No.9). London: IWA Publishing.

Isanta, E., Suárez-Ojeda, M. E., Val del Río, Á., Morales, N., Pérez, J., and Carrera, J. (2012). Long term operation of a granular sequencing batch reactor at pilot scale treating a low-strength wastewater. *Chem Eng J, 198-199*, 163-170.

Jiang, H. L., Tay, J. H., and Tay, S. L. (2002). Aggregation of immobilized activated sludge cells into aerobically grown microbial granules for the aerobic biodegradation of phenol. *Lett Appl Microbiol, 35*(5), 439-445.

Jimenez, J., Miller, M., Bott, C., Murthy, S., De Clippeleir, H., and Wett, B. (2015). High-rate activated sludge system for carbon management–Evaluation of crucial process mechanisms and design parameters. *Water Res, 87*, 476-482.

Jones, M., and Stephenson, T. (1996). The effects of temperature on enhanced biological phosphate removal. *Environ Technol, 17*(9), 965-976.

Juang, Y. C., Adav, S. S., Lee, D. J., and Tay, J. H. (2010). Stable aerobic granules for continuous-flow reactors: precipitating calcium and iron salts in granular interiors. *Bioresource Technol, 101*(21), 8051-8057.

Kent, T. R., Bott, C. B., and Wang, Z. W. (2018). State of the art of aerobic granulation in continuous flow bioreactors. *Biotechnol. Adv., 36*(4), 1139-1166.

Lee, D. J., Chen, Y. Y., Show, K. Y., Whiteley, C. G., and Tay, J. H. (2010). Advances in aerobic granule formation and granule stability in the course of storage and reactor operation. *Biotechnology Advances, 28*(6), 919-934.

Li, D., Lv, Y., Zeng, H., and Zhang, J. (2016). Startup and long term operation of enhanced biological phosphorus removal in continuous-flow reactor with granules. *Bioresource Technol, 212*, 92-99.

Li, J., Ding, L. B., Cai, A., Huang, G. X., and Horn, H. (2014). Aerobic sludge granulation in a full-scale sequencing batch reactor. *Biomed Res Int, 2014*.

Li, J., Garny, K., Neu, T., He, M., Lindenblatt, C., and Horn, H. (2007). Comparison of some characteristics of aerobic granules and sludge flocs from sequencing batch reactors. *Water Sci Technol, 55*(8-9), 403-411.

Lin, Y. M., Liu, Y., and Tay, J. H. (2003). Development and characteristics of phosphorus-accumulating microbial granules in sequencing batch reactors. *Appl Microbiol Biot, 62*(4), 430-435.

Linlin, H., Jianlong, W., Xianghua, W., and Yi, Q. (2005). The formation and characteristics of aerobic granules in sequencing batch reactor (SBR) by seeding anaerobic granules. *Process Biochem, 40*(1), 5-11.

Liu, H., and Fang, H. H. (2002). Extraction of extracellular polymeric substances (EPS) of sludges. *J Biotechnol, 95*(3), 249-256.

Liu, Q., Tay, J., and Liu, Y. (2003). Substrate concentration‐independent aerobic granulation in sequential aerobic sludge blanket reactor. *Environ Technol, 24*(10), 1235-1242.

Liu, X. W., Sheng, G. P., and Yu, H. Q. (2009). Physicochemical characteristics of microbial granules. *Biotechnology Advances, 27*(6), 1061-1070.

Liu, Y., and Tay, J. H. (2004a). State of the art of biogranulation technology for wastewater treatment. *Biotechnology advances, 22*(7), 533-563.

Liu, Y., Wang, Z. W., Qin, L., Liu, Y. Q., and Tay, J. H. (2005). Selection pressure-driven aerobic granulation in a sequencing batch reactor. *Applied Microbiology and Biotechnology, 67*(1), 26-32.

Liu, Y., Yang, S. F., and Tay, J. H. (2004b). Improved stability of aerobic granules by selecting slow-growing nitrifying bacteria. *J Biotechnol, 108*(2), 161-169.

Liu, Y. Q., Moy, B., Kong, Y. H., and Tay, J. H. (2010). Formation, physical characteristics and microbial community structure of aerobic granules in a pilot-scale sequencing batch reactor for real wastewater treatment. *Enzyme and Microbial Technol, 46*(6), 520-525.

Liu, Y. Q., and Tay, J. H. (2006). Variable aeration in sequencing batch reactor with aerobic granular sludge. *J Biotechnol, 124*(2), 338-346.

Liu, Y. Q., and Tay, J. H. (2008). Influence of starvation time on formation and stability of aerobic granules in sequencing batch reactors. *Bioresource Technol, 99*(5), 980-985.

López-Palau, S., Pinto, A., Basset, N., Dosta, J., and Mata-Álvarez, J. (2012). ORP slope and feast–famine strategy as the basis of the control of a granular sequencing batch reactor treating winery wastewater. *Biochem Eng J, 68*, 190-198.

López–Palau, S., Dosta, J., and Mata-Alvarez, J. (2009). Start-up of an aerobic granular sequencing batch reactor for the treatment of winery wastewater. *Water Sci Technol, 60*(4), 1049-1054.

Martin, K., Shaw, A., de Clippeleir, H., and Sturm, B. (2016). "Accidental Granular Sludge?": Understanding process design and operational conditions that lead to low SVI-30 values through a survey of full scale facilities in North America. *Proceedings of the Water Environment Federation, 2016*(9), 3385-3394.

McSwain, B., Irvine, R., and Wilderer, P. (2004). The influence of settling time on the formation of aerobic granules. *Water Sci Technol, 50*(10), 195-202.

Merritt, J., and Kuehn, S. (2018). Frequency-and amplitude-dependent microbial population dynamics during cycles of feast and famine. *Phys Rev Lett, 121*(9), 098101.

Morgenroth, E., Sherden, T., Van Loosdrecht, M. C. M., Heijnen, J. J., and Wilderer, P. A. (1997). Aerobic granular sludge in a sequencing batch reactor. *Water Res, 31*(12), 3191-3194.

Nielsen, S. S. (2010). Phenol-sulfuric acid method for total carbohydrates. In S. S. Nielsen (Ed.), *Food Analysis Laboratory Manual* (pp. 47-53). Boston, MA: Springer US.

Niermans, R., Giesen, A., Loosdrecht, M. v., and Buin, B. d. (2014). Full-scale experiences with aerobic granular biomass technology for treatment of urban and industrial wastewater. *Proceedings of the Water Environment Federation, 2014*(19), 2347-2357.

Pronk, M., De Kreuk, M., De Bruin, B., Kamminga, P., Kleerebezem, R. v., and Van Loosdrecht, M. (2015). Full scale performance of the aerobic granular sludge process for sewage treatment. *Water Res, 84*, 207-217.

Qin, L., Liu, Y., and Tay, J. H. (2004a). Effect of settling time on aerobic granulation in sequencing batch reactor. *Biochem Eng J, 21*(1), 47-52.

Qin, L., Tay, J. H., and Liu, Y. (2004b). Selection pressure is a driving force of aerobic granulation in sequencing batch reactors. *Process Biochem, 39*(5), 579-584.

Rahman, A., Mosquera, M., Thomas, W., Jimenez, J. A., Bott, C., Wett, B., Al-Omari, A., Murthy, S., Riffat, R., and De Clippeleir, H. (2017). Impact of aerobic famine and feast condition on extracellular polymeric substance production in high-rate contact stabilization systems. *Chem Eng J, 328*, 74-86.

Reisner, A., Haagensen, J. A., Schembri, M. A., Zechner, E. L., and Molin, S. (2003). Development and maturation of Escherichia coli K-12 biofilms. *Molecular microbiology, 48*(4), 933-946.

Sauer, K., Cullen, M., Rickard, A., Zeef, L., Davies, D. G., and Gilbert, P. (2004). Characterization of nutrient-induced dispersion in Pseudomonas aeruginosa PAO1 biofilm. *Journal of bacteriology, 186*(21), 7312-7326.

Schwarzenbeck, N., Borges, J., and Wilderer, P. (2005). Treatment of dairy effluents in an aerobic granular sludge sequencing batch reactor. *Appl Microbiol Biot, 66*(6), 711-718.

Sehar, S., and Naz, I. (2016). Role of the biofilms in wastewater treatment. *Microbial biofilms-importance and applications*, 121-144.

Su, K. Z., and Yu, H. Q. (2005). Formation and characterization of aerobic granules in a sequencing batch reactor treating soybean-processing wastewater. *Environ Sci Technol, 39*(8), 2818-2827.

Sun, Y., Angelotti, B., and Wang, Z. W. (2019). Continuous-flow aerobic granulation in plug-flow bioreactors fed with real domestic wastewater. *Sci Total Environ, 688*, 762-770.

Świątczak, P., and Cydzik-Kwiatkowska, A. (2018). Performance and microbial characteristics of biomass in a full-scale aerobic granular sludge wastewater treatment plant. *Environmental Science and Pollution Research International, 25*(2), 1655-1669.

Tao, J., Qin, L., Liu, X., Li, B., Chen, J., You, J., Shen, Y., and Chen, X. (2017). Effect of granular activated carbon on the aerobic granulation of sludge and its mechanism. *Bioresource Technol, 236*, 60-67.

Tay, J. H., Liu, Q. S., and Liu, Y. (2001a). The effects of shear force on the formation, structure and metabolism of aerobic granules. *Appl Microbiol Biot, 57*(1-2), 227-233.

Tay, J. H., Liu, Q. S., and Liu, Y. (2001b). Microscopic observation of aerobic granulation in sequential aerobic sludge blanket reactor. *Journal of Applied Microbiology, 91*(1), 168-175.

Van Winckel, T., De Clippeleir, H., Mancell-Egala, A., Rahman, A., Wett, B., Bott, C., Sturm, B., Vlaeminck, S. E., Al-Omari, A., and Murthy, S. (2016). Balancing flocs and granules by external selectors to increase capacity in high-rate activated sludge systems. *Screen, 30*, 0.076.

Vanderhasselt, A., and Vanrolleghem, P. A. (2000). Estimation of sludge sedimentation parameters from single batch settling curves. *Water Res, 34*(2), 395-406.

Wan, J., and Sperandio, M. (2009). Possible role of denitrification on aerobic granular sludge formation in sequencing batch reactor. *Chemosphere, 75*(2), 220-227.

Wang, Z. W., Liu, Y., and Tay, J. H. (2006). The role of SBR mixed liquor volume exchange ratio in aerobic granulation. *Chemosphere, 62*(5), 767-771.

Wang, Z. W., Liu, Y., and Tay, J. H. (2007). Biodegradability of extracellular polymeric substances produced by aerobic granules. *Appl Microbiol Biot, 74*(2), 462-466.

Willoughby, A., Houweling, D., Constantine, T., Yin, H., Havsteen, L., Uri, N., Chandran, K., and Li, Z. (2016). Protocols for researching the impact of sludge granulation on BNR processes. *Proceedings of the Water Environment Federation, 2016*(9), 5865-5877.

Yang, S. F., Tay, J. H., and Liu, Y. (2003). A novel granular sludge sequencing batch reactor for removal of organic and nitrogen from wastewater. *J Biotechnol, 106*(1), 77-86.

Zheng, Y. M., Yu, H. Q., and Sheng, G. P. (2005). Physical and chemical characteristics of granular activated sludge from a sequencing batch airlift reactor. *Process Biochem, 40*(2), 645-650.